Heme Synthesis and Acquisition in *Staphylococcus aureus*

by

Jacob Edward Choby

Dissertation

Submitted to the Faculty of the

Graduate School of Vanderbilt University

in partial fulfillment of the requirements

for the degree of

DOCTOR OF PHILOSOPHY

in

Microbiology and Immunology

February 28, 2019

Nashville, Tennessee

Approved:

D. Borden Lacy, Ph.D., Chair

Timothy L. Cover, M.D.

Maria Hadjifrangiskou, Ph.D.

Hassane Mchourab, Ph.D.

Gary Sulikowski, Ph.D.

Eric P. Skaar, M.P.H, Ph.D.

ACKNOWLEDGEMENTS

First and foremost, I acknowledge my advisor Eric Skaar for his support and mentorship during my graduate work. I am the staphylococcologist I am today because of you. Your commitment to my development as an experimenter, writer, and communicator was greater than I ever expected. Thank you for providing me with freedom to explore my research interests, for trusting me to try and fail, for your guidance and input on projects, and critical feedback in all things. Thank you for creating a wonderful laboratory environment in which I could follow Louis Pasteur and say “The more I study nature, the more I stand amazed at the work of the Creator”. Thank you also for treating me as a colleague, valuing my opinion, and setting a high standard. It’s been a good run.

I am grateful to the entire Skaar laboratory, a supportive and scientifically challenging assemblage of talent. All current and many former members have contributed to my graduate education through feedback on presentations, grants, and manuscripts. More specifically, many individuals have impacted my scientific development. I am grateful to Devin Stauff, former lab member and my undergraduate advisor, who was foundational in my development as a bacteriologist and experimentalist and remains an excellent resource and friend. I would not be here without him. Thank you to Neal Hammer for guidance and a thorough education in Staph genetics during my early years in the lab. I benefitted greatly from the mentorship of Laura Anzaldi Mike as an undergraduate and graduate student. Laura (L.A.M.) contributed directly to work in Chapter II and her contributions are noted. Allison Farrand (A.J.F.) laid the foundation for the work in Chapter V and always had a kind word. Vanderbilt undergraduate Matt Reynolds (M.R.) was willing to join me investigating the *gsaM* genes as noted in Chapter III. I thank Andy Weiss and Clare Laut for making room A5101 a great environment and keeping me on my toes. Thank you to Mike Noto for feedback and advice. I am grateful to Andrew Monteith (A.J.M.) for his contributions and feedback regarding work presented in Appendix C. Thank you to Caroline Grunenwald for her friendship, feedback, and contribution to Chapter IV. I thank Lillian Juttukonda, Joe Zackular, and Zach Lonergan for their friendship as well as experimental and intellectual contributions. I am especially grateful to Lauren Palmer for feedback, support, and challenging me to be a better scientist and person. Finally, I am grateful that the laboratory was so well-equipped and supported by Jocelyn Simpson, Jeanette Miller, Billy Burns, Ashley Jordan, Nikesh Dahal, Dennis Horvath, and Audra Fullen under the guidance of Nichole Lobdell and Nichole Maloney, who ensured I had everything I needed to work in the lab.

Outside of the laboratory, my thesis work was made possible by many excellent collaborators. I am grateful for the work contributed to Chapter II by Jeff Boyd (J.M.B) and his student Ameya Mashruwala (A.A.M.). Matt Goff, Tracy Cooper, Erin Gribben and Rob Carnahan of the Vanderbilt Antibody and Protein Resource contributed to experiments in Chapter II as well as efforts towards developing anti-GtrR antibodies. Thank you to Jennifer Dubois and her talented student Arianna Celis (A.I.C), who performed porphyrin quantification in Chapter IV which has led to a fruitful and ongoing collaboration. I acknowledge the support of Hayes McDonald and the Vanderbilt Mass Spectrometry Research Center for quantitative proteomics presented in Chapter IV. I thank Heather Kroh (H.K.) and Borden Lacy for their insights into the GtrR structure. Svetlana Gerdes (S.Y.G.) was an excellent resource for analysis of the conservation of HemX, as shown in Chapter IV. I am thankful for the collaboration with Matt Barber (M.F.B.) presented in Chapter V. The project presented in Appendix C was the result of a collaboration between the Vanderbilt Institute for Clinical and Translational Research, especially Jill Pulley, Jana Shirey-Rice, and Andrea Pruijssers. Thank you to Lauren Himmel (L.H.) and the Vanderbilt Translational Pathology Shared Resource for contributions to Appendix C. Margaret Allaman and the Vanderbilt Digestive Disease Research Center provided technical help with assays in Appendix C. I am grateful to Lars Hederstedt for critical feedback on work presented in Chapter IV. I am additionally thankful to journal editors and anonymous reviewers who have helped improve my manuscripts during the peer-review process.

I also thank the following individuals for providing strains and other reagents: Victor Torres, Chia Lee, Taeok Bae, Douglas Henderson, John Olson, Neal Hammer, Matt Surdel, Alex Horswill, Maria Hadjifrangiskou, and Paris Margaritis. I also used strains provided by the Network on Antimicrobial Resistance in *Staphylococcus aureus* (NARSA) for distribution by BEI Resources, NIAID, NIH (Nebraska Transposon Mutant Library [NTML] Screening Array, NR-48501.

My graduate training has received a great deal of support outside of the laboratory. I am thankful to the Vanderbilt IGP graduate program and the BRET office for support, the Vanderbilt Institute for Chemical Biology and the Chemical Biology Association of Students for scientific edification and training, the Vanderbilt Institute for Infection, Immunology, and Inflammation for increasing the presence and significance of research at the host-pathogen interface, and Lorie Franklin and other administrators for logistical support. I am grateful for the support of my graduate training program and Chris Aiken, Director of Graduate Studies. I

have had an excellent thesis committee who was ever willing to help in the trajectory of my research and career-Borden Lacy, my committee chair, along with Tim Cover, Maria Hadjifrangiskou, Gary Sulikowski, and Hassane Mchaourab.

I am also grateful for the financial support that made these studies possible. Grants awarded to Eric Skaar that directly supported this work, from the NIH: R01AI069233 and R01AI073843, and the Ernest W. Goodpasture Chair in Pathology. I am thankful to support from the NIH Chemical Biology Interface training grant T32GM065086 and a predoctoral fellowship F31AI126662. Immunoassays were performed in the Vanderbilt Digestive Disease Research Center, supported by funding from the NIH P30DK058404.

Finally, I thank my family for their love and support. My budding career as a scientist is based on the foundation set by my parents, and for that I will always be grateful. Thank you to my friends outside of lab, particularly Trevor and Chrissy during graduate school. And a special gratitude to my wonderful wife, Renee. I could not have done it without you at my side.

TABLE OF CONTENTS

LIST OF TABLES

Table Page

LIST OF FIGURES

Figure Page

LIST OF ABBREVIATIONS

ALA	δ-aminolevulinic acid
PBG	porphobilinogen
HMB	hydroxymethylbilane
TCS	two-component system
TSA	tryptic soy agar
TSB	tryptic soy broth
LBA	lysogeny broth agar
LB	lysogeny broth
SDS-PAGE	sodium dodecyl sulfate polyacrylamide gel electrophoresis
RPMI	Roswell Park Memorial Institute medium
PCR	polymerase chain reaction
DNA	deoxyribonucleic acid
CFU	colony forming unit
WT	wildtype
q-RT-PCR	quantitative reverse transcriptase polymerase chain reaction
LC-MRM-MS/MS	liquid chromatography-multiple reaction monitoring-tandem mass spectrometry
LC-qTOF-MS	liquid chromatography-quadrupole time of flight-mass spectrometry
Hb	hemoglobin

CHAPTER I

INTRODUCTION

A portion of the following section was previously published in *Journal of Molecular Biology*
Aug 28;428(17):3408-28. (August 2016)
doi: 10.1016/j.jmb.2016.03.018

Staphylococcus aureus pathogenesis and physiology

"The goal of a bacterium is to become bacteria," stated by Stanley Falkow (1) underscores the critical requirement of replication for the success of a bacterial species. For bacterial pathogens, this replication must occur in the midst of nutrient limitation and the hostile host immune response.

Staphylococcus aureus is an exemplar of sophisticated human bacterial pathogens, because of its global burden, variety of disease manifestations, highly evolved virulence factors, and pace of acquisition of antimicrobial resistance. *S. aureus* asymptomatically colonizes the skin and anterior nares of about a third of the population (2), yet when host barrier defenses are compromised, it is capable of causing a spectrum of invasive diseases. *S. aureus* is a leading cause of osteomyelitis, endocarditis, Gram-positive sepsis, skin and soft tissue infections, and toxic shock syndrome (3). Each of these host infectious niches require staphylococcal replication and the elaboration of virulence factors to cause disease and inhibit the immune response. Clinical treatment for these diseases has been challenged by the rapid expansion of antimicrobial resistance in clinical isolates (4).

Supporting the success of *S. aureus* as a pathogen is a robust host-adapted metabolism. *S. aureus* is a Gram-positive facultative anaerobe capable of performing oxygen-dependent cellular respiration or transitioning to anaerobic metabolism in the absence of oxygen. Cellular respiration can use environmental nitrate, nitrite, or sulfite as terminal electron acceptors for anaerobic respiration. In the absence of terminal electron acceptors, fermentation of a variety of carbon sources support *S. aureus* replication. *S. aureus* has evolved to derive energy from carbon sources (5), acquire divalent cations (6, 7), phosphate (8) and amino acids (9) available in the mammalian host. As such, the physiology of *S. aureus* that supports replication and virulence factor production is key to the success of this organism in both infectious and non-infectious niches. In this dissertation, I probe key aspects of staphylococcal physiology related to iron-sulfur clusters and virulence factor production,

heme-iron acquisition, and heme biosynthesis to further elucidate means by which *S. aureus* replicates in the host.

Heme synthesis, acquisition, and toxicity in bacterial pathogens

Introduction

Heme and iron are essential for life

The tetrapyrrole cofactor heme is important for the cellular processes of most organisms and essential to many lifeforms across domains of life. Heme, a porphyrin ring complexed with iron, serves as a redox active moiety required for the function of many cellular proteins. Heme functions as an electron shuttle in enzymes of the electron transport chain and is required for cellular respiration. Additionally, cells rely on heme for the function of many widely conserved enzymes including catalase, nitric oxide synthase, and hemoglobin. Heme is also an important molecule involved in diverse cellular processes including signaling, gas sensing, microRNA processing, and cellular differentiation (10-13). Thus, nearly all organisms must satisfy the requirement for heme through either synthesis or acquisition.

Heme coordinates an iron atom at its center which is vital for heme's electron transfer abilities and redox activity. Like heme, iron is nearly universally required for life, and only a few exceptions have been identified (14, 15). As an inorganic cofactor, iron can act alone or in iron-sulfur clusters as a prosthetic moiety for members of the oxidoreductase, nitrogenase, hydrogenase, dehydrogenase, and hydratase enzyme families (16-21). Therefore, organisms have evolved elaborate strategies to acquire, store, and regulate intracellular iron for heme-dependent and other iron-dependent enzymes.

Nutritional immunity limits host iron availability

Nutritional immunity, a concept articulated originally by Eugene Weinberg in the 1970s, describes the processes by which humans and other organisms sequester iron to limit acquisition by bacterial pathogens (22, 23). Nutritional immunity has since been expanded to include the host processes that manipulate local levels of manganese, zinc, and other transition metals in order to metal starve or intoxicate the invading pathogens (24-27). The limited access of pathogens to metals serves as an antimicrobial strategy and limits bacterial replication. For instance, free iron rarely exists in the mammalian host. The solubility of ferric iron in aerobic solution is exceedingly low, and high affinity iron-binding proteins, including transferrin, lactoferrin, albumin, and ferritin sequester iron extracellularly and intracellularly. Iron-binding proteins function to transport iron, protect host cells from iron-mediated oxidative

damage, and to keep iron from pathogens. However, bacterial pathogens have developed exquisite tactics to overcome iron limitation, and elaborate high affinity iron receptors and chelators. In this regard, an evolutionary arms race has developed at the host-pathogen interface involving host iron-binding proteins and the mechanisms bacteria encode to steal iron.

Heme is an important host iron source

Heme makes up the greatest reservoir of iron in the host and serves as an iron source for many bacterial pathogens. Humans and other metazoa synthesize heme through a variety of steps in the mitochondria and cytosol. This pathway, called the Shemin or four-carbon pathway, begins with the condensation of glycine and succinyl-CoA to form the committed precursor δ-aminolevulinic acid (ALA) (28-30). A series of enzymes produce protoporphyrin IX from ALA and iron is inserted, forming protoheme IX. For the sake of simplicity in this review, heme will refer to ferrous and ferric iron forms of protoheme IX. Heme is then bound by hemoproteins to serve a variety of intracellular and extracellular tasks. Catalase, peroxidase, and myeloperoxidase rely on heme to catalyze the hydrolysis of peroxide molecules. Energy generation by the electron transport chain relies on heme-dependent *c*- and *b*-type cytochromes of the ubiquinol-ferricytochrome-c oxidoreductase (Complex III) family (31, 32). Hemoproteins involved in tissue oxygen homeostasis include myoglobin and neuroglobin. Perhaps the most well-known hemoprotein is the oxygen transporter hemoglobin (Hb). Its abundance and location in erythrocytes make hemoglobin a rich heme source for pathogens. Hemoglobin contains about two-thirds of the body's iron, and a single erythrocyte contains more than 280 million molecules of Hb (24, 33). Bacterial pathogens have evolved high affinity Hb binding proteins for the acquisition of heme, and these proteins will be described below.

Owing in part to the reactive nature of heme-iron, free heme and hemoglobin are toxic to the human host and bacterial pathogens alike (34, 35). To prevent excess heme toxicity, eukaryotic heme synthesis is highly regulated and heme homeostasis and sequestration are well-orchestrated. When hemoglobin is released from erythrocytes or otherwise exists extracellularly, it is rapidly bound by haptoglobin (36). The abundance of cell-free Hb is thought to be very low in healthy adults, but a variety of genetic disorders, infections, and other disease states can increase the concentration of free Hb (37). Free hemoglobin and its modified forms, in the presence of reactive oxygen species, exhibit cytotoxic effects towards endothelial cells (38). However, the relevance of these *in vivo* studies is unclear, and a

comprehensive understanding of concentrations to achieve hemoglobin toxicity in healthy humans has not been achieved (34). On the other hand, in the absence of infection free heme that has been liberated from its hemoprotein likely only exists transiently in serum or in cells. In serum, heme is immediately bound by the highly abundant albumin (k_d ≈10 nM) then transferred to hemopexin (k_d <1 pM) (39). The heme is delivered to cells expressing the hemopexin receptor; these cells then degrade the heme using heme oxygenases. The rapid sequestration and degradation of free heme in the blood is vital to the survival of erythrocytes, as heme in the presence of reactive oxygen species exhibits cytotoxicity and lipid peroxidation at micromolar concentrations (40, 41). During infection of host heme- and hemoglobin-replete niches, bacterial pathogens likely experience heme toxicity and encode systems to protect from heme toxicity as well (42). Therefore, heme is at the center of a complex interplay between host and pathogen for survival.

Bacterial heme synthesis

Divergent heme synthesis pathways in Gram-negative and Gram-positive organisms

While both humans and bacteria share the early heme precursor δ-aminolevulinic acid (ALA), most bacteria (Alphaproteobacteria are the exception), archaea, and plants synthesize ALA from charged glutamyl-tRNA^{Glu} via the 'C5 pathway' (Figure 1) (30, 43, 44). Glutamyl-tRNA reductase produces the highly reactive intermediate glutamate-1-semialdehyde and glutamate-1-semialdehyde-2,1-aminomutase converts to ALA (45, 46). The three steps, from ALA to uroporphyrinogen, are well conserved and thought to be the evolutionary core of heme biosynthesis. ALA dehydratase (also called porphobilinogen synthase) is responsible for the condensation of two ALA to porphobilinogen (PBG) (47). The linear tetrapyrrole hydroxymethylbilane (HMB) is produced by a head to tail condensation and deamination of four PBG molecules, catalyzed by HMB synthase (alternatively called PBG deaminase) (48, 49). Under physiological conditions, HMB will spontaneously cyclize to form the uroporphyrinogen I isomer, a biosynthetic dead-end. Therefore, most bacteria utilize uroporphyrinogen III synthase to catalyze the cyclization of HMB through a *spiro*-intermediate to form uroporphyrinogen III (50).

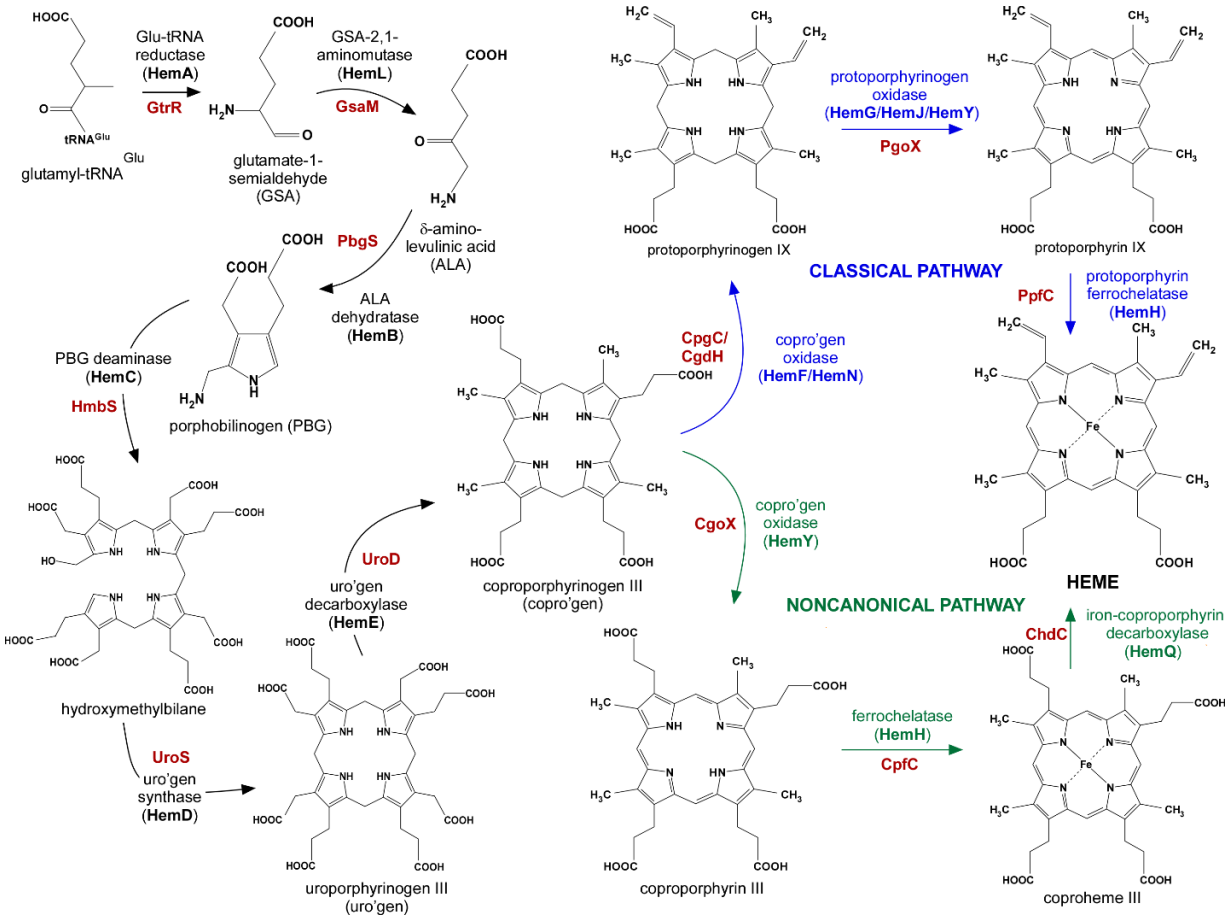

Figure 1 Bacterial heme biosynthesis. The heme synthesis pathway of most bacteria begins with charged glutamyl-tRNA^{Glu} to form the universal precursor ALA, and coproporphyrinogen III is formed through a series of conserved enzymatic steps. The classical pathway (blue), forms heme through the protoporphyrinogen IX intermediate; most organisms including Gram-negative bacteria and eukaryotes use this pathway. The noncanonical pathway (green) performed by most Gram-positive bacteria, produces heme through the coproporphyrin III intermediate. Shown for each step is the enzyme name followed by the previously used protein annotation in bold, and the new enzyme annotation set forth by Dailey and colleagues (51) in red.

Uroporphyrinogen III can be utilized for the synthesis of several tetrapyrrole-based cofactors. Uroporphyrinogen III decarboxylase decarboxylates the four acetate side chains to methyl groups, producing coproporphyrinogen III, the next step in heme synthesis (52). Additionally, uroporphyrinogen III can be shunted from heme synthesis and converted to precorrin-2 to synthesize vitamin B12, coenzyme F430, and siroheme (53). The Ahb enzymes of some archaea and sulfur-reducing bacteria can convert siroheme (produced from uroporphyrinogen) to heme (54, 55). The contribution of the Ahb alternative heme pathway has not been demonstrated in pathogenic bacteria.

In Gram-negative organisms, as well as eukaryotes, coproporphyrinogen III is converted to protoporphyrinogen IX by coproporphyrinogen III oxidase. This step is the first of the terminal three steps in the classical heme synthesis pathway (in blue in Figure 1) and is catalyzed by oxygen-dependent and oxygen-independent enzymes (56, 57). Protoporphyrinogen IX is subsequently oxidized to form protoporphyrin IX, by a six-electron oxidation catalyzed by one of three protoporphyrinogen oxidase enzymes. So called HemG, in Gammaproteobacteria and some Alphaproteobacteria and Deltaproteobacteria, uses the respiratory chain as its electron acceptor and is not dependent on oxygen (58). The enzyme annotated as HemJ is poorly characterized but represents the most common protoporphyrinogen oxidase among Alphaproteobacteria and Deltaproteobacteria (59). The third protoporphyrinogen oxidase was formerly called HemY, an FAD- and oxygen-dependent protoporphyrinogen oxidase found in some Proteobacteria as well as eukaryotes (60). The final step of the classical pathway is the insertion of ferrous iron by protoporphyrin ferrochelatase to form protoheme IX, called heme (61). From ALA to heme, the steps of the classical synthesis pathway are shared by eukaryotes and Gram-negative bacteria.

The terminal steps of the classical pathway were considered universally conserved for all heme-synthesizing organisms. However, just in the last few years, the terminal steps of heme synthesis in the Gram-positive phyla Firmicutes and Actinobacteria have been described with genomic and biochemical analysis and termed the non-canonical or coproporphyrin-dependent pathway (43, 62). Very few HemF or HemN coproporphyrinogen oxidases can be identified in Gram-positive genomes; instead it has been realized that the annotated HemY/CgoX in these organisms functions as a coproporphyrinogen oxidase to form coproporphyrin III (43, 63). The Gram-positive HemH/CpfC, a coproporphyrin ferrochelatase, inserts ferrous iron to form coproheme (62). Finally, coproheme is decarboxylated by HemQ/ChdC, an enzyme unique to members of the Firmicutes and Actinobacteria to form protoheme IX (64-67). It is now clear that Gram-positive organisms utilize a unique series of terminal steps to synthesize heme (in green in Figure 1).

Regulation of heme synthesis

Despite the vital role of heme to bacterial physiology, the regulation of heme biosynthesis has not been well studied outside of a few model organisms. In bacteria, regulation has been recognized to occur largely at two steps, abundance of the initial enzyme GtrR and transcription of the coproporphyrinogen oxidase enzymes. Regulation of GtrR is typically heme-dependent, indicating that bacteria reduce synthesis of heme and all

intermediates in heme-replete conditions. This process has been extensively studied in *Escherichia coli* and *Salmonella enterica* serovar. Typhimurium. The addition of heme to cell extracts of *E. coli* reduces total GtrR activity, without inhibiting the activity of the purified enzyme (68, 69). This was explained by the observation that excess heme results in the proteolytic degradation of GtrR in *Salmonella*, suggesting that GtrR might bind excess heme (70). The Clp and Lon proteases are responsible for this reduction in GtrR levels (71). Further, mutations in GtrR have been described that render GtrR resistant to heme- and protease-mediated degradation, indicating that GtrR binds excess heme, and holo-GtrR but not apo-GtrR is a substrate for proteolytic degradation (72, 73). In this manner, cellular levels of heme can regulate the first step of heme synthesis and limit the unnecessary synthesis of heme intermediates as well as the consumption of iron. Recent metabolic engineering efforts to enhance ALA production in *E. coli* suggest that protoporphyrin IX post-translationally inhibits PbgS, an additional example of feedback inhibition (74). It is likely that for many organisms, heme and terminal heme intermediates can have post-translational regulatory effects on heme synthesis enzymes. Like *Salmonella* and *E. coli,* the Gram-positive bacterium *Bacillus subtilis* regulates levels of GtrR. While a mechanistic explanation has not been described, the membrane protein HemX post-transcriptionally regulates GtrR abundance in *B. subtilis* (47, 75). Homologs of *B. subtilis* HemX exist in multiple Gram-positive pathogens; however, the function of HemX and GtrR regulation has yet to be detailed.

In addition to the regulation of GtrR enzyme levels, the transcription of *gtrR* is also a point of control for heme biosynthesis. Two promoters exist upstream of *gtrR* in the Gram-negative pathogen *Pseudomonas aeruginosa*, and these promoters contain binding sites for the regulators Anr (oxygen sensing), Dnr (redox regulator), IHF (integration host factor), and NarL (nitrate regulator) (76, 77). Therefore, *gtrR* expression is induced in the presence of oxygen or when oxygen is lacking but an alternative electron acceptor such as nitrate is present for utilization of heme-dependent respiration. In *B. subtilis*, the *uroD-cpfC-cgoX* operon is induced anaerobically and the *gtrR-hemX-hmbS-pbgS-gsaM* operon is induced by peroxide through de-repression of PerR (47, 78). As in *B. subtilis*, PerR has been implicated as a regulator of the *uroD-cpfC-cgoX* operon in *Staphylococcus aureus*; yet recent work has demonstrated that major differences exist between *B. subtilis* and *S. aureus* PerR orthologs and therefore it is difficult to conclude that PerR plays a role in *S. aureus* heme synthesis (79, 80). *Corynebacterium diphtheria*, a member of the Actinobacteria phylum, encodes two heme-responsive two-component systems (TCS). The response regulator HrrA directly binds the promoters of *gtrR*, *uroD*, and *cpfC* to repress their transcription in heme-replete conditions

(81). Similarly, ChrA can repress transcription of *gtrR* in heme replete conditions (82, 83). These data suggest that in *C. diphtheriae*, heme utilization is preferred over synthesis when exogenous heme is available. Together, these examples point to the transcriptional and post-translational control of GtrR as a central step in heme synthesis regulation.

The expression of coproporphyrinogen oxidase genes is the second major point of heme synthesis regulation. In several species, *hemF* and *hemN* are regulated by different oxygen- or anaerobic-responsive regulators to ensure proper expression of oxygen-dependent or oxygen-independent coproporphyrinogen oxidases. OxyR, a global regulator in *E. coli*, is responsible for the induction of oxygen-dependent *hemF* expression in hydrogen peroxide stress. It has been suggested that the Fe-S cluster in oxygen-independent HemN is vulnerable to peroxide damage, so HemF is produced to take the place of HemN (84). In *B. subtilis*, the transcription of coproporphyrinogen III oxidases *hemN* and *hemZ* (a second coproporphyrinogen oxidase, not to be confused with oxygen-dependent HemY) are induced anaerobically by the regulatory cascade of ResDE, Fnr, and YwiD to replace the oxygen-dependent HemY (85-88). Similarly, *Pseudomonas hemF* and *hemN* are expressed anaerobically under the control of Anr and Dnr, while Anr induces the expression of only *hemN* aerobically (89). It has been suggested, but not validated, that the expression of oxygen-dependent *hemF* in oxygen limited conditions by Anr and Dnr serves to consume residual oxygen during the transition to anaerobiosis, which would protect other anaerobically induced oxygen-sensitive proteins (89). Thus, oxygen is a key regulator of expression of coproporphyrinogen oxidase genes.

Contribution of heme synthesis to pathogenesis

With a few notable exceptions including *Bartonella hensaela*, *Enterococcus faecalis*, *Haemophilus influenzae*, and *Streptococcus* spp., most human pathogens encode complete heme biosynthetic pathways (90-93). However, the contribution of heme synthesis to the pathogenesis of bacterial pathogens is largely understudied. For *S. aureus*, whose reliance on heme acquisition during infection has been well established, it is now clear that heme biosynthesis is vital to cause disease in murine models of infection (94-96). Inactivation of *gtrR*, which renders *S. aureus* heme deficient, causes the small-colony variant (SCV) phenotype (97). During systemic infection, this mutant is highly defective at colonizing the murine heart and liver relative to wildtype *S. aureus* (97). A mutant lacking *pbgS*, also a heme deficient SCV, demonstrates reduced colonization and bone destruction in a murine model of osteomyelitis (98, 99). These data demonstrate that for *S. aureus*, heme acquisition is

insufficient to support organ colonization and therefore heme biosynthesis is critical to pathogenesis. Importantly, the SCV phenotype is encountered clinically. Despite their reduced virulence, SCVs are generally more resistant to antibiotics and oxidative stress, more equipped to evade the immune system by living intracellularly, and are likely the etiological agent of persistent staphylococcal infections (99-103).

Less evidence for the role of heme synthesis during infection is available for other pathogens. For the intracellular pathogen *Brucella abortus*, *hemH* is required for virulence in a murine model of brucellosis (104). Therefore, like *S. aureus*, host heme utilization is insufficient and synthesis is required for full virulence. In addition to *B. abortus* and *S. aureus*, the advent of whole genome *in vivo* analysis of mutants using techniques such as transposon-sequencing and signature tagged mutagenesis has highlighted the role of heme synthesis. In these infections, genes with marked mutations that are recovered at a lower frequency from the infected tissue relative to growth *in vitro* are considered important to infection. These types of experiments have demonstrated a role for different heme synthesis genes during infection. Transposon mutants disrupted in *hemY* were found to be defective for *P. aeruginosa* colonization of the murine gastrointestinal tract (105). *hemN* was found to be important for *Yersinia pestis* infection of deep tissue (106). Transposon mutants lacking *uroD* in *Acinetobacter baumannii* were less effective at colonizing the murine lung (107). Finally, *cgoX* was found to be important for *Listeria monocytogenes* oral infection (108). Based on these transposon library infections, and data described in above paragraph, heme synthesis is vital to the fitness of a variety of pathogens.

Current challenges and opportunities in bacterial heme synthesis

The divergence between the terminal steps of Gram-positive heme synthesis and the classical pathway utilized by Gram-negative organisms as well as humans presents the opportunity for targeted small molecule interventions to inhibit or activate Gram-positive heme synthesis. The terminal Gram-positive enzymes ChdC, which exists only in Actinobacteria and Firmicutes, as well as CgoX and CpfC, which recognize different substrates than the eukaryotic host enzymes, present three potential targets. Small molecules have been described that modulate heme synthesis *in vivo* while *in vitro* inhibitors of *S. aureus* CgoX have recently been reported, suggesting that Gram-positive heme synthesis is an attractive drug target (62, 109-111).

Outside of a few model pathogens, very little is understood regarding the regulation of heme synthesis, particularly during pathogenesis. Regulation is a central question in

understanding the role of heme synthesis in infection. Considering that in some niches host heme is available and can reach toxic levels, pathogens with the capacity to both steal and synthesize heme must regulate both pathways. For *S. aureus*, in which heme synthesis and acquisition are vital during infection, the strategies for regulation of heme synthesis is unknown. This is despite the observation over half a century ago that the rate of staphylococcal heme synthesis is modulated by exogenous heme (112). For other pathogens the contribution of heme synthesis to disease is still unclear, but whole genome *in vivo* fitness experiments like transposon-sequencing suggest many bacterial pathogens rely on heme biosynthesis to cause disease, and this field of research provides ample opportunity for further exploration.

Heme acquisition in Gram-positive bacteria

Bacterial pathogens utilize a variety of heme acquisition strategies during infection, ranging from surface receptors to secreted proteins that bind either heme or hemoproteins. Heme acquired from the host is used fully intact or degraded to liberate heme-iron and both processes are important during bacterial pathogenesis. Gram-positive pathogens, including *S. aureus, Bacillus anthracis*, and *C. diphtheriae* rely on heme acquisition during infection. The heme uptake pathways of these three pathogens will be presented as models for the Gram-positive processes, along with the regulation of the pathway and evidence for the role of heme uptake during pathogenesis.

The Staphylococcus aureus *Isd paradigm*

The *I*ron-regulated *s*urface *d*eterminant system (Isd), first described in *S. aureus*, is the paradigm for Gram-positive heme acquisition (113). During infection, *S. aureus* utilizes the leukocidins HlgAB and LukED to lyse erythrocytes and liberate hemoglobin into the bloodstream (114). This results in accessible free heme, heme bound by hemopexin (Hx), free hemoglobin (Hb), and hemoglobin bound by haptoglobin (Hp) to form the haptoglobin–hemoglobin (Hp-Hb) complex. The Isd system enables utilization of free heme, or heme bound to Hb and Hp-Hb complexes. Isd proteins bind heme and hemoglobin at the cell wall surface with conserved *nea*r *t*ransporter (NEAT) domains. The NEAT domains are 120-125 amino acid domains that constitute a conserved eight-stranded β-sandwich fold (115, 116). Heme is bound in a hydrophobic pocket with critical coordination by tyrosine residues in a YXXXY motif. These NEAT-containing surface proteins (IsdB, IsdH, IsdA in *S. aureus*) shuttle heme to NEAT-containing IsdC. IsdC transfers heme to the membrane-associated transporter

IsdDEF for transit across the membrane. To access host heme and hemoproteins, IsdB, IsdH, and IsdA are covalently attached to the peptidoglycan by the canonical Sortase A cysteine transpeptidase [106]. IsdB contains two NEAT domains, NEAT1 (N1) binds Hb and Hb-Hp, but not Hp and N2 binds heme; as such IsdB is believed to be the primary Hb binding protein (95, 117-119). IsdH contains three NEAT domains, N1 and N2 bind both Hb and Hp, and N3 binds heme (120, 121). IsdA, which is partially surface exposed, contains a single heme binding NEAT domain(113). The current model (Figure 2), supported by strong structural evidence, suggests that IsdB-N1 binds hemoglobin, and IsdB-N2 extracts heme (122). Similarly, IsdHN1 and N2 bind Hb and Hp, and IsdH-N3 extracts the heme. The heme is then transferred either directly to IsdC or shuttled via IsdA to IsdC.

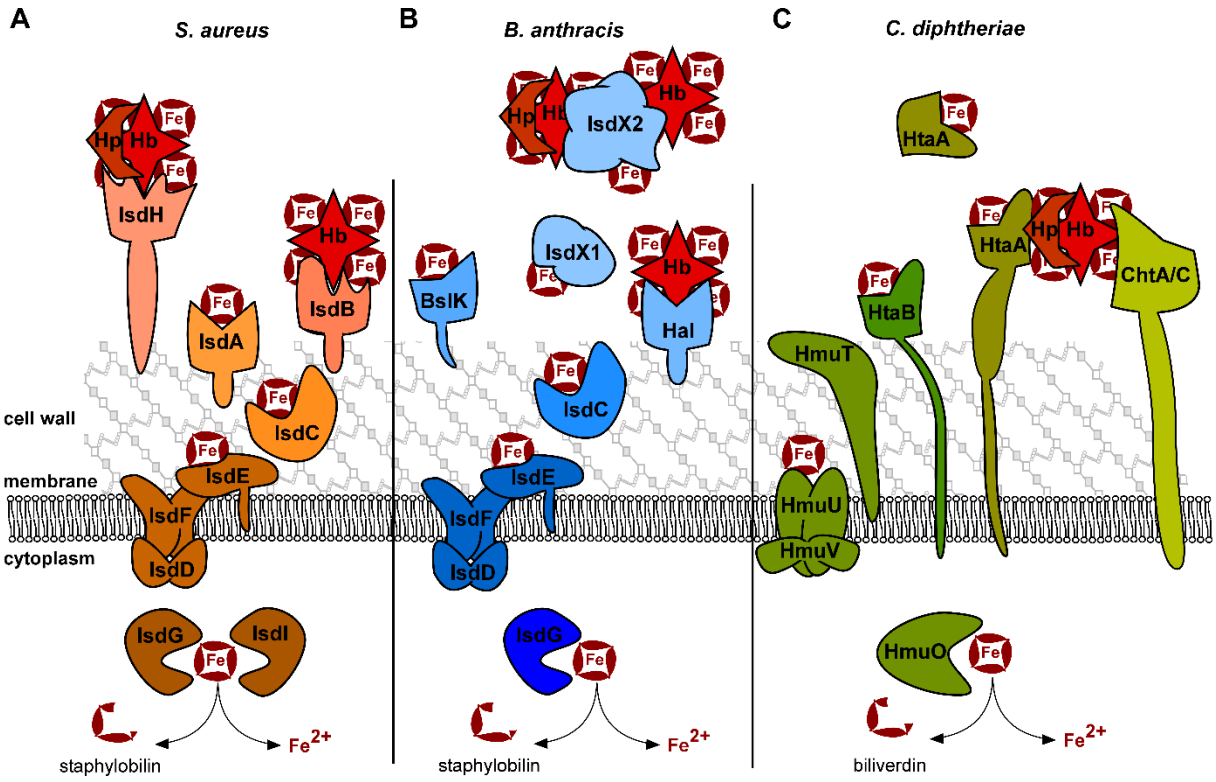

Figure 2 Gram-positive heme uptake systems. The *i*ron-regulated *s*urface *d*eterminant (Isd) systems for heme acquisition in *S. aureus* and *B. anthracis*, as well as the non-Isd systems of *C. diphtheriae* are diagrammed. Host hemoglobin (Hb), haptoglobin (Hp) bound Hb, and free heme (Fe-containing ring) can serve as heme sources during infection. **(A)** In *S. aureus* IsdH is the primary Hp-Hb receptor and IsdB is the principle Hb receptor. Both are sortase-linked on the surface of the cell wall, bind host hemoproteins with NEAT domains, and extract heme using additional NEAT domains. IsdA can bind free heme or accept heme from IsdB and IsdH. Heme is transferred to IsdC, which is embedded in the cell wall and transits heme to the membrane complex IsdDEF. IsdDEF transports heme to the cytoplasm for utilization intact or for degradation by the heme oxygenases IsdG/I. **(B)** Similarly, *B. anthracis* uses Isd proteins to acquire heme. IsdX1 and IsdX2 are secreted hemophores that bind Hb, Hp-Hb, or free heme as depicted. IsdX2, which has five NEAT domains, may also serve as a heme storage protein. Additionally, the sortase anchored Hal serves as a Hb receptor on the cell surface and uses its NEAT and leucine-rich repeat domains to acquire heme. BslK is cell-wall associated and binds heme via its NEAT domain. IsdC transports heme to the IsdDEF membrane importer for utilization or degradation by IsdG. **(C)** *C. diphtheriae* utilizes a unique set of heme uptake proteins for heme utilization. HtaA is a cell wall spanning lipoprotein that can acquire heme from Hp-Hb in conjunction with ChtA or ChtC. HtaB can bind free heme or accept heme transfer from HtaA and transfers heme to the HmuTUV membrane transporter. A portion of HtaA may also serve as a secreted hemophore. *C. diphtherae* HmuO heme oxygenase can liberate iron from imported heme.

S. aureus encodes an iron-regulated Sortase B (SrtB) for which IsdC is the only substrate, and SrtB attaches IsdC to peptidoglycan in such a way that IsdC is not surface exposed but rather buried in the cell wall, which is 15-30 nm thick (123, 124). This organization allows heme transferred from surface Isd proteins to pass through the cell wall to the membrane by IsdC's single heme binding NEAT domain. IsdC alone transfers heme to the IsdE of the IsdDEF transporter (125). At the membrane, IsdDEF transits heme across the membrane and into the cytosol.

Upon import, heme is incorporated into staphylococcal proteins or degraded. Exogenous heme accumulates in the membrane and is also capable of complementing the growth of heme-deficient mutants (96) . Alternatively, the heme oxygenases IsdG and IsdI degrade heme to release iron (126, 127). IsdG and IsdI are structurally similar and are the first described members of the Isd heme oxygenase family, which catabolizes heme to staphylobilin instead of biliverdin (128-130). IsdG and IsdI are required for growth using heme as a sole iron source, and are expressed during infection (127, 131).

The widely conserved ferric uptake regulator (Fur) is the principle regulator of the expression of heme acquisition systems in *S. aureus.* In iron-deplete conditions, Fur no longer represses its regulon, allowing the transcription of the *isdB*, *isdA*, *isdCDEFsrtBisdG,* and *isdI* loci (113). During infection of iron-deplete niches, the heme acquisition system and associated iron-liberating heme oxygenases are expressed. Further regulation of the heme oxygenases exist; IsdG abundance increases in the presence of heme and IsdG half-life is increased when heme-bound (131). Also, the Clp proteases have a role in Hb acquisition by modulating IsdB levels (132).

Isd-mediated heme acquisition is vital to the virulence of *S. aureus*. Heme is the preferred iron-source during systemic infection, in part because a heme-responsive transcriptional regulator activates iron siderophore synthesis only when heme-iron is unavailable (96, 133). The role of the Isd system has been extensively demonstrated in murine infection models. Mutants lacking components of the Isd system are highly defective in pathogenesis, highlighting the importance of heme acquisition to staphylococcal disease (94-96, 118, 131, 134, 135).

Isd-dependent heme uptake by Bacillus anthracis

B. anthracis encodes a heme uptake system that shares the core of the *S. aureus* Isd, but with additional unique proteins. *B. anthracis* encodes two secreted hemophores termed IsdX1 and IsdX2 (136). These are the first described Gram-positive hemophores and bind

heme, hemoglobin, and methemoglobin (136-140). IsdX1 contains one NEAT domain while IsdX2 contains five NEAT domains; both are secreted past the cell wall as they lack sortase signals or membrane spanning domains (136). *B. anthracis* also encodes other NEAT contain proteins; Hal contains a single NEAT domain and leucine-rich repeats, which extract heme from hemoglobin (141). Unlike IsdX1/2, Hal is sortase anchored to the cell wall (142). A second, recently described NEAT protein is BslK, which is non-covalently attached to the cell wall and transfers heme to IsdC (143). The current proposed model (Figure 2) is that IsdX1 is secreted, binds heme, and transfers heme to wall-anchored IsdC. IsdX2 can bind free heme, accept heme from IsdX1, and transfer heme to IsdC. The multiple NEAT domains of IsdX2 have been proposed to be important for these multiple functions, and it has been suggested that IsdX2 can serve as a heme storage protein. IsdDEF transports heme across the membrane for utilization by IsdG, an orthologue of the *S. aureus* heme oxygenase (144). The diversity of heme and Hb binding proteins relative to *S. aureus* may be the result of the greater variety of environmental niches that germinant and sporulent *B. anthracis* inhabits.

The role of *B. anthracis* heme acquisition during infection is not clear. A guinea pig infection model demonstrated that Δ*isdCX1X2* was as virulent as wildtype, yet these proteins are expressed during infection (145). Also, a mutant of *B. anthracis* lacking Hal demonstrated reduced virulence in a model of inhalational anthrax (146). It is likely that the IsdX1/X2 hemophores, BslK, and Hal are partially redundant, and a mutant lacking all four proteins would be highly defective in causing anthrax.

In addition to *S. aureus* and *B. anthracis*, many other pathogens have evolved NEAT-containing heme acquisition systems, including *Staphylococcus lugdunensis, Listeria monocytogenes,* and *Streptococcus pyogenes* (147-154). The conservation of NEAT-mediated heme uptake highlights the contribution of host heme to bacterial infection.

Corynebacterium diphtheriae *heme uptake*

C. diphtheriae utilizes non-NEAT mediated heme uptake systems for heme-iron acquisition, termed HmuTUV, HtaABC, and ChtABC/CirA. The Hmu (*h*emin-*u*ptake) system was the first heme acquisition system described in Gram-positive organisms. The associated heme oxygenase, HmuO, was discovered and described first, and then HmuTUV was discovered for the ability of a plasmid encoding *hmuTUV* to complement a *Corynebacterium ulcerans* strain that cannot grow on hemoglobin as a sole iron source (155, 156). Sequence analysis suggests that HmuTUV acts as an ABC transporter that shuttles heme across the cell membrane (157). It was later discovered that an additional gene is encoded within the

hmuTUV operon, termed *htaA* (*h*eme-*t*ransport *a*ssociated) (158). Adjacent to this locus are the genes *htaB* and *htaC*. Unlike the sortase anchoring of other Gram-positive uptake systems, HtaA and HtaB contain N-terminal secretion signals as well as C-terminal intermembrane domains. This results in surface exposure of HtaA and HtaB, which both bind heme. Interestingly, a portion of HtaA is secreted and not anchored to the cell envelope. HtaA isolated from cell culture is unable to complement the growth of an *htaA* mutant, suggesting that surface bound HtaA may serve as a heme receptor and secreted HtaA may serve as a hemophore (158, 159). However, heme transfer between HtaA molecules, and further description of the function of HtaA on the surface has not been reported. In addition to heme, HtaA can acquire heme from Hb and transfer heme to HtaB, suggesting a heme shuttle from HtaA to HtaB to HmuT; HmuT is a surface-anchored lipoprotein which then transfers heme to the cognate ABC transporter HmuUV (159). While the Isd NEAT domains rely on tyrosine alone as the axial ligand for heme binding, HmuT relies on an N-terminal histidine and a C-terminal tyrosine to coordinate heme (160).

Inactivation of the Hmu/Hta systems does not completely eliminate growth with heme as a sole iron source, suggesting the involvement of an additional heme uptake system (158). This led to the characterization of the ChtAB and CirAChrC operons, which are regulated by iron levels via DtxR. DtxR is the Diphtheria Toxin regulator which activates the expression of Diphtheria Toxin as well as HmuTUV and HtaABC (161, 162). ChtAB and ChtC appear to be the result of gene duplication of HtaAB, as all three groups of proteins have sequence similarity, N-terminal secretion signals, C-terminal transmembrane domains, and contain the same heme-binding domain (163). Like HtaAB, ChtAB and CirAChtC are surface exposed and ChtAB and ChtC bind heme and hemoglobin. It appears that these heme binding proteins serve redundant functions, and as such a mutant lacking both HtaB and ChtB is deficient at utilizing Hb as an iron source (163). Recently, it has been shown that ChtA and ChtC are both capable of binding Hp-Hb for heme extraction, and acquisition of heme from Hp-Hb requires HtaA (164). The current model (Figure 2) for Hp-Hb heme acquisition involves binding of Hp-Hb by a combination of HtaA and ChtA or ChtC, heme extraction either actively or passively, and transfer to HtaB, HmuT, and HmuUV (164).

Heme acquisition in Gram-negative bacteria

The outer membrane of the cellular envelope of Gram-negative organisms presents an additional barrier to heme acquisition. Therefore, Gram-negative heme uptake systems consist of outer membrane receptors that either bind heme and hemoproteins directly, or bind

heme-bound secreted hemophores. Heme then transits the periplasm and is brought into the cell via ABC transporters at the inner membrane. The versatile opportunistic pathogen *Pseudomonas aeruginosa* encodes direct heme uptake and hemophore systems at the outer membrane, *Haemophilus influenzae* uses a hemophore uptake system, and *Neisseria meningitidis* uses a unique bipartite receptor for heme acquisition from host hemoproteins. These pathogens are presented as models for Gram-negative heme uptake systems.

Pseudomonas aeruginosa

P. aeruginosa encodes direct and indirect systems for heme uptake. The Phu (P*seudomonas h*eme *u*ptake) consists of a TonB-dependent PhuR which binds heme and transports it to the periplasm. PhuR activity is representative of Gram-negative TonB-dependent outer membrane receptors. These β-barrel proteins bind substrates (often iron containing molecules) with high affinity, and rely on proton motive force and TonB for transport across the outer membrane (165). TonB is an inner membrane protein with a substantial periplasmic portion for direct interaction with periplasmic domains of the outer membrane proteins. Upon PhuR translocation of heme into the periplasm, the soluble periplasmic protein PhuT binds heme and brings it to PhuUV, an ABC transporter at the inner membrane.

In addition, HasA/HasR (*h*eme *a*ssimilation *s*ystem) are utilized for heme uptake. HasA is a secreted hemophore which binds heme and transfers it to a second TonB-dependent transporter, HasR. Like other Gram-negative heme-binding motifs, HasA coordinates heme using histidine and tyrosine residues with picomolar affinity. Data from the orthologous HasA hemophore of *Serratia marcescens* suggests HasA binds hemoglobin and extracts heme, then HasA transfers heme to HasR (166, 167). The present model (Figure 3) for these two heme uptake systems suggests that Phu is the principle heme acquisition system but full heme utilization requires HasA/HasR. HasA/HasR may be more relevant as a heme sensing system; in low heme conditions the inner membrane HasS binds the sigma factor inhibitor HasI. When heme is available, HasS instead binds HasR, and HasI is free to recruit RNA polymerase to activate the transcription of *hasAR*, *hasSI*, *phuSTUV*, and *phuR* (168).

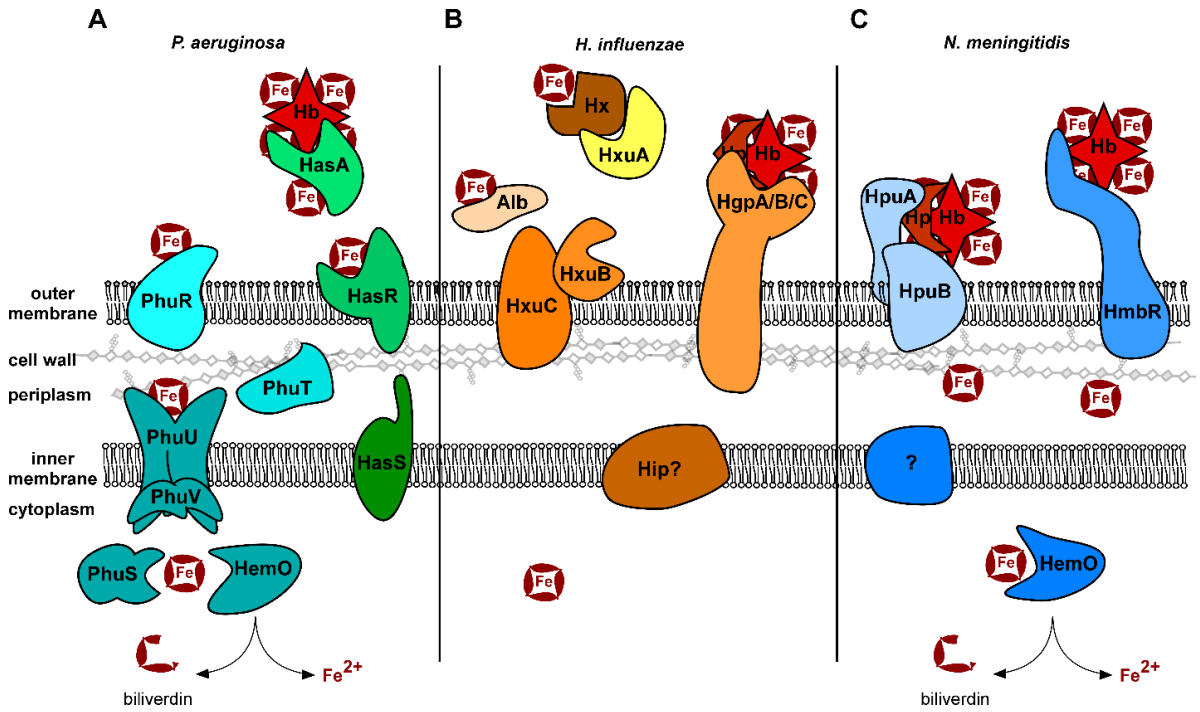

Figure 3 Gram-negative heme acquisition. The heme uptake systems as described in the text are depicted. **(A)** *P. aeruginosa* PhuR binds heme at the outer membrane and imports heme into the periplasm in a TonB-dependent manner. Heme is transferred to PhuT, which subsequently transfers heme to the PhuUV inner membrane transporter for transit into the cytoplasm. There, PhuS binds and stores heme or transfers heme to the heme oxygenase HemO for iron utilization. *P. aeruginosa* also secretes the hemophore HasA which binds hemoglobin (Hb) or free heme, and transfers heme to the TonB-dependent outer membrane receptor HasR. The fate of HasR imported heme is not fully understood, but may be trafficked to PhuTUV for import. HasS serves as an inner membrane sensor and regulates expression of the *has* and *phu* systems through the sigma factor HasI (not shown). **(B)** *H. influenzae* can utilize a variety of host heme sources. Secreted HxuA specifically binds hemopexin (Hx), and heme from Hx is transferred into the periplasm when HxuA interacts with HxuBC at the outer membrane. Independent of HxuA, HxuC can also import heme from serum albumin (Alb). HgpA, HgpB, and HgpC are highly similar outer membrane receptors for heme acquisition from Hb complexed with haptoglobin (Hp), free Hb, and Hp bound to myoglobin (not shown). The inner membrane heme transporter has not been clearly defined, but the Hip system has been implicated for heme transit into the cytoplasm. Interestingly, all imported heme may be utilized intact, as no heme oxygenase has been identified yet. **(C)** The *N. meningitidis* outer membrane, TonB dependent complex of HpuAB can acquire heme from Hb and Hp-Hb and bring heme into the periplasm. Additionally, the HmbR outer membrane receptor specifically extracts heme from Hb for transport. The identity of the inner membrane heme transporter is unclear at this time, but heme somehow enters the cytoplasm where it can be utilized or degraded by the HemO heme oxygenase.

The *P. aeruginosa* heme uptake system PhuSTUV/PhuR is regulated by Fur in addition to the HasI sigma factor detailed above. Recently, small regulatory RNAs have been described that impact *phuS* mRNA levels, suggesting another layer of heme-responsive regulation (169, 170).

In contrast to many other organisms, *Pseudomonas* encodes a soluble cytoplasmic heme binding protein that is not a heme oxygenase. This protein, PhuS, transfers heme to the heme-oxygenase HemO for iron liberation. PhuS, unlike many hemoproteins, binds ferric-iron heme and subsequently transfers it to HemO under iron-deplete conditions (171). The dissociation constant of the heme-PhuS-HemO complex is in the nanomolar range, suggesting PhuS transfers heme to HemO specifically and not to the second *Pseudomonas* heme oxygenase, BphO (171). While the PhuS heme transfer has not been described completely, PhuS has been shown to bind heme as a monomer utilizing one of two histidine residues (His209 and His212), and a third binding site exists when PhuS is in dimeric form (172). Further *in vitro* characterization and structural analysis has led to a model whereby heme coordination occurs primarily at the His212 ligand and induces a conformational change required for interaction with HemO (173, 174). Additionally, *in vitro* heme oxygenase activity has been attributed to PhuS, however the *in vivo* relevance of this function is unclear as no biliverdin-β (the product of HemO heme catabolism) is detected in a mutant lacking *hemO* (175, 176).

A recent clinical evaluation of genetic changes to *P. aeruginosa* during infection of cystic fibrosis lungs revealed the importance of heme acquisition during infection (177). Long-term infection led to the selection of mutations in the promoters of the *phuSTUWV* and *phuR* loci, resulting in greater Phu expression. These changes to *phu* transcription confer a growth advantage enabling the utilization of heme from Hb as the sole iron source and suggest that heme is an important iron source during chronic *Pseudomonas* infection. The infections also selected for mutants that demonstrate enhanced expression of the *feo* ferrous-iron acquisition genes, indicating that ferrous iron is also a source of bioavailable iron. These clinical data confirm experimental findings suggesting that *P. aeruginosa* heme acquisition contributes to chronic infection.

Haemophilus influenzae

H. influenzae is a notable exception to the other pathogens outlined here, as it is incapable of synthesizing heme and therefore requires heme uptake for aerobic respiration (178). It is capable of acquiring heme from diverse host sources (Figure 3), including

hemopexin, free heme, albumin-bound heme, myoglobin and hemoglobin; the variety of heme sources is in accordance with its absolute reliance on exogenous heme (179). *H. influenzae* has evolved a variety of heme uptake systems important for growth *in vitro* using various host heme sources. While some systems are well described, less is known about others, and a global understanding of the utilization of these heme uptake systems during infection is lacking.

The HxuCBA system, described primarily in *H. influenzae* type B, is capable of heme acquisition from free heme and heme-hemopexin (Hx). HxuA is a secreted hemophore that is released from the outer membrane by its transporter HxuB (180-182). HxuA exhibits no heme-binding motif but rather demonstrates high affinity binding specifically to Hx with little distinction between apo- and holo-Hx (183). HxuC is a TonB-dependent transporter that binds heme after release from the Hx-heme-HxuA complex and imports it into the periplasm (184). Additionally, HxuC is capable of acquiring heme from serum albumin (Alb) independent of HxuA (185). HpbA is another heme acquisition protein identified in nontypeable and type B *H. influenzae*. A lipoprotein, HbpA is important for growth using Hb, Hp-Hb, and human serum albumin as heme sources (186, 187). The inner membrane heme transporter has not been definitively identified, but the Hip proteins have been implicated.

Additionally, *H. influenza* encodes three receptors, HgpA, HgpB, and HgpC, that can acquire heme from Hp-Hb and haptoglobin bound myoglobin, albeit it at greater concentrations than thought to be physiologically relevant (188, 189). While the contribution of the Hgps seem redundant, HgpB has been demonstrated to be most important for utilization of Hp-Hb and Hp-myoglobin.

There are many outstanding questions regarding *H. influenzae* heme uptake. Many proteins have been attributed to be involved in heme uptake, but their function requires further investigation (190-194). The regulation of the heme uptake system expression is not well described, except that *hxuCBA* and the *hgp* genes are expressed under *in vitro* iron/heme deplete conditions during experimental infection of the chinchilla ear (195). Lastly, a heme oxygenase of *Haemophilus* has not been described, suggesting that acquired heme is utilized intact and that other iron acquisition pathways, from transferrin and lactoferrin sources, are sufficient for cellular iron needs. However, it is also possible that a heme oxygenase exists and has not yet been identified.

Genetic evidence from clinical isolates suggests that heme uptake is vital to pathogenic strains of *H. influenzae.* Isolates from otitis media infection in children relative to commensal throat isolates exhibit greater rates of *hxuA*, *hxuB*, *hxuC*, and *hgpB* gene

prevalence, indicating that heme uptake may be a virulence determinant (196, 197). Several animal models have been used to demonstrate the role of heme uptake during *H. influenzae* infection. In a model of *H. influenzae* bacteremia, infant rats infected with a mutant lacking HbpA completely clear the infection after one week while rats infected with wildtype remain infected (187). Likewise, a mutant lacking both HxuC and HgpABC uptake proteins is unable to cause bacteremia in the same rat model (198). Additionally, the Hgp proteins are required to cause otitis media in a chinchilla model (199). It is clear that for *H. influenzae* pathogenesis, heme uptake is a critical virulence determinant.

Neisseria meningitidis

N. meningitidis encodes a bipartite heme uptake system consisting of HpuAB and HmbR (Figure 3). HpuAB is expressed from an iron-repressed operon and consists of the HpuA lipoprotein and HpuB, the TonB-dependent receptor capable of binding Hb, apo-Hp, and Hp-Hb (200, 201). Upon heme transport into the cytoplasm, the HemO heme oxygenase degrades heme to biliverdin and liberates iron. As such, HemO is required for survival using heme, Hb, or Hp-Hb as a sole iron source (202, 203). Heme is extracted from these hemoproteins and is imported intact, as hemoglobin can complement the deficiencies of a heme synthesis mutant in an HpuAB-dependent manner (204). The inner membrane transporter has not yet been identified, but a zinc transporter has been implicated (205).

Initial studies of the individual function of HpuA and HpuB failed to describe the role of HpuA in heme acquisition. HpuB is sufficient to bind Hb, but a high affinity HpuB-Hb complex requires the presence of HpuA, even though HpuA-Hb binding was not detected by a flow cytometry assay (206, 207). Additionally, HpuA is required for growth with Hb as a sole iron source and heme import (208). However, a recent structural characterization has described a direct, albeit weak, interaction between HpuA and Hb, and a co-crystal structure of Hb and an HpuA homolog from *Kingella denitrificans* has been solved (209). While these data are not conclusive, they suggest that HpuA and HpuA homologs interact with Hb, and this interaction is required for HpuAB-mediate heme uptake.

HmbR (*hem*oglo*b*in *r*eceptor) is an additional *N. meningitidis* heme uptake protein that binds host Hb with species specificity, exhibiting a greater utilization of human Hb. but is unable to bind the Hp-Hb complex and therefore likely binds free Hb only (210). Like HpuAB, it is subject to phase variation (211). HmbR, based on spectroscopy and mutational analysis, also coordinates heme with a Tyr residue, which further confirms that diverse heme binding domains have evolved to utilize tyrosine as the axial ligand (212). The mechanism of heme

extraction by HmbR, the associated inner membrane heme transporter that partners with HmbR extraction, and structural descriptions of ligand binding are still undescribed for HmbR heme uptake.

In *N. meningitidis*, expression of *hemO* and *hmbR* is regulated by Fur as well as the MisRS TCS (213, 214). MisRS activates the expression of *hemO* and *hmbR* independent of Hb and iron concentration, which suggests an additional layer of regulation for Hb acquisition. However, the activating signal of MisRS has not yet been described.

The genetic diversity of *N. meningitidis* clinical isolates has highlighted the importance of heme uptake to meningococcal virulence. While not all *N. meningitidis* strains express both the HmbR and HpuAB systems, most express at least one. Most pathogenic isolates express at least HmbR, but HpuAB expression is equally associated with disease and carriage isolates, which indicates HmbR is an indicator of pathogenesis (215, 216). *N. meningitidis* serotype B isolates associated with disease also exhibit “on” phase variation of HmbR, correlating virulence with the expression of HmbR (217). Additionally, HmbR is required for virulence in an infant rat model of meningitis (210). These data implicate heme uptake, particularly HmbR, as an important component of *Neisseria* infection.

Current challenges and opportunities in bacterial heme acquisition

Study of heme uptake strategies has offered great insight into bacterial pathogenesis and nutrient acquisition. There is still great opportunity for discovery. For most bacterial heme-binding motifs, the transfer from host hemoprotein has not been demonstrated as either passive dissociation or active extraction. The redundancy of heme uptake systems in pathogens like *B. anthracis*, *P. aeruginosa,* and *H. influenzae* is well-appreciated, but the role of each system during infection of various niches has yet to be fully elucidated. The relative contribution of host heme to iron acquisition by bacterial pathogens during infection is understudied. It is unclear if pathogens rely on heme for iron in unique spatiotemporal niches and rely on ferrous iron and siderophore acquisition systems in other niches. Opportunity abounds to understand the role of heme-iron utilization across time and tissues during infection. Finally, while global abundance of heme and hemoglobin in the host has been measured, the local availability of heme and hemoproteins during infection has not been described and presents an opportunity to understand the microenvironment of an infectious niche as well as the host response to infection.

In terms of clinical application, heme uptake systems may be attractive therapeutic targets. *S. aureus* Isd proteins have been the target of vaccine development with mixed

success and monoclonal antibodies against IsdB have been studied for therapeutic use (218-222). Considering the importance of heme acquisition to infection, using surface exposed heme uptake proteins as targets for vaccine and antibodies should continue to be investigated. Additionally, the *Mycobacterium tuberculosis* heme uptake system, which comprises three unique proteins and is sufficient to rescue the growth of a heme auxotroph, has been proposed as a new mycobacteria-specific antimicrobial target to be explored (223-225).

The interactions between host hemoproteins and bacterial hemoprotein binding proteins offer an excellent opportunity to study host-pathogen co-evolution. It has been recently demonstrated that the human and primate iron binding protein transferrin has undergone positive selection at the interface of binding by bacterial transferrin receptors, suggesting that the co-evolution of humans and pathogens has produced an evolutionary arms race in the context of nutritional immunity (226, 227). In the same vein, the Hb-binding IsdB of *S. aureus* exhibits species specificity and more efficiently utilizes human hemoglobin relative to mouse hemoglobin (94). In keeping with this, transgenic mice expressing human hemoglobin are more susceptible to *S. aureus* disease (94). The contribution of bacterial heme acquisition to human evolution presents ample opportunity to further investigate co-evolution and nutritional immunity.

Heme toxicity and tolerance

Bacterial pathogens dedicate extensive cellular machinery to the synthesis and acquisition of heme. Paradoxically, excess heme is toxic and thus during infection, invading pathogens must contend with heme toxicity as a component of pathogenesis. While heme toxicity is well-studied in eukaryotes, less is known in bacteria (34, 228, 229). A brief description of heme toxicity in bacteria and strategies utilized to combat toxicity follow.

Multi-faceted mechanism of heme toxicity

The reactive nature of heme that makes it such a versatile cofactor also results in toxicity at excess concentrations. While the toxicity of heme towards bacteria has been observed for over 60 years, a complete understanding of the mechanisms of heme toxicity is lacking (35, 230). Free heme is rapidly bactericidal toward various Gram-positive and Gram-negative pathogens in low- to mid-micromolar concentrations (42, 231-234). However, investigation of heme toxicity in a variety of bacterial species has led to a model of heme inducing iron- and non-iron related damage to the cell.

The accumulation of heme results in excess iron by one of two mechanisms, both of which are likely at play under aerobic conditions. First, a portion of iron is freed by the heme oxygenases. Secondly, iron itself may be liberated from the porphyrin ring upon reaction with reactive oxygen species (ROS). Irrespective of the source, iron can cycle between ferrous and ferric states via Fenton chemistry and the Haber-Weiss reaction (reaction 1), yielding a regenerating supply of ROS.

(1) $Fe^{2+} + H_2O_2 \rightarrow Fe^{3+} + HO\bullet + OH^-$

(2) $Fe^{3+} + H_2O_2 \rightarrow Fe^{2+} + HOO\bullet + H^+$

Iron-mediated production of ROS can damage DNA, lipids, and proteins (235, 236). Further evidence for the contribution of oxidative stress to heme toxicity comes from *S. aureus*. In conditions of excess heme toxicity, membrane proteins are highly oxidized and superoxide is formed by redox cycling of heme-iron through membrane menaquinone (237). Superoxide production is a separate source of oxidative damage from ferrous iron mediated ROS and is a major component of heme damage in *S. aureus* (237). In addition to experimentally validating that heme-mediated ROS is a key to heme toxicity, this work also localized heme toxicity primarily to the membrane. The lipophilic nature of heme suggests it partitions to the membrane of bacteria, and this has been demonstrated in *S. aureus,* likely resulting in damage to membrane proteins and lipids (96).

Further evidence suggests iron-mediated ROS production and subsequent membrane damage is an insufficient description of heme toxicity. First, heme is toxic in anaerobic conditions and secondly, non-iron protoporphyrins are toxic to bacteria and activate the cellular response to heme toxicity (238-240). Also, porphyrins cause significant damage to bacterial DNA (241). Finally, resistance to heme toxicity is in part mediated in *N. meningitidis* by Ght (gene of hydrophobic agent tolerance), suggesting that damage by heme is similar to other hydrophobic molecules and may disrupt the Gram-negative outer membrane (233, 242). The toxicity of heme is likely the result of a combination of membrane disruption, membrane protein and lipid oxidation, and DNA damage. However, a total understanding of heme-mediated damage is far from complete.

Strategies to overcome heme toxicity

While the direct result of excess heme is unclear, it is evident that bacteria must contend with heme damage and have evolved a variety of strategies to overcome heme toxicity (Figure 4). These systems consist primarily of efflux and sequestration. Additionally,

the heme oxygenase outlined as part of heme acquisition strategies may contribute to the reduction of heme toxicity by cleaving the porphyrin ring and liberating iron for use.

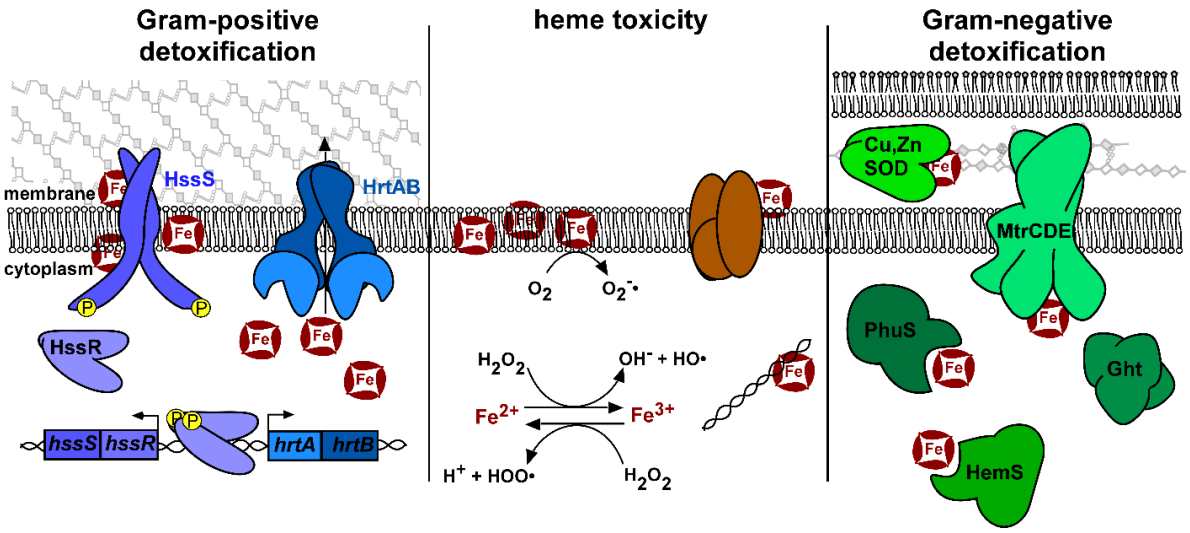

Figure 4 Strategies to avoid heme toxicity. Heme toxicity (center) is a combination of heme damage to membrane lipids, membrane proteins, DNA, and oxidative damage. Oxidative damage is mediated by the production of superoxide dismutase (O_2^-·), hydroxyl radical (HO·), and hydroperoxyl radical (HOO·). To reduce heme damage, many Gram-positive organisms (the *S. aureus* system is diagrammed here) encode the HrtAB efflux pump. The HssRS two component system responds to excess heme and activates the transcription of the *hrtAB* system, thus preventing the accumulation of toxic levels of heme. Alternatively, Gram-negative organisms rely on intracellular heme sequestration proteins (PhuS of *P. aeruginosa*, HemS of *Yersinia*), the periplasmic heme-binding, copper and zinc dependent superoxide dismutase (Cu,Zn SOD, of *H. ducreyi*), and systems that respond to hydrophobic molecules, including heme (MtrCDE efflux and Ght of *Neisseria*).

Heme efflux strategies have been primarily characterized in Gram-positive organisms, potentially because efflux across a single membrane barrier is simpler to achieve than in Gram-negative pathogens. Three systems have been described, HrtAB, PefAB/CD, and MtrCDE. The *S. aureus h*eme-*r*egulated *t*ransporter HrtAB is required for survival in toxic concentrations of heme. *hrtAB* expression is activated by the HssRS *h*eme *s*ensing TCS (232, 243, 244). While the ligand of the HssS histidine kinase has remained elusive, excess exogenous or endogenous heme leads to activation, either directly or indirectly (110). HrtA is an ATPase that drives efflux by HrtB permease of its ligand, likely heme. Orthologues of HrtAB have been described in *B. anthracis* and *Lactococcus lactis,* and are required for resistance to heme toxicity in these organisms (245). When the Hrt efflux pump is inactivated in both *S. aureus* and *L. lactis*, levels of intracellular heme increase, suggesting that heme is the

substrate of HrtAB export (238, 246). In *B. anthracis*, an HssRS orthologue controls the expression of HrtAB and cross-talks with a second TCS that responds to cellular envelope stresses, further implicating membrane damage as a component of heme stress (247). HrtAB is actively expressed during murine anthrax, suggesting organisms that replicate in the bloodstream must tolerate heme toxicity (42).

Additional efflux systems exist, suggesting that this strategy is well conserved. *Streptococcus agalactiae* encodes an orthologue of HrtAB, as well as a dual efflux system PefAB and PefRCD (231). In heme stress, *hrtAB* and *pefAB*/*RCD* are expressed at high levels, and the Pef systems are required for resistance to heme toxicity (231). The Gram-negative *N. gonorrhoeae* encodes an efflux pump, MtrCDE, for hydrophobic molecules that is required for resistance to heme stress (248).

Heme sequestration and storage is a second theme in strategies to resist heme toxicity. The conserved HemS family has been described in *Yersinia enterocolitica*, *Y. pestis, Shigella dysenteriae* (termed ShuS), *P. aeruginosa* (called PhuS, detailed above), and *E. coli* (ChuS, which also has heme oxygenase activity) (157, 171, 234, 249-254). While a variety of heme storage, transfer, and degradation properties have been assigned to these proteins, their involvement in resisting heme toxicity is clear. Additionally, non-HemS family proteins have been found to bind heme and play a role in heme homeostasis, including the small outer membrane Protein E of *H. influenzae* and the Cu,Zn superoxide dismutase of *Haemophilus ducreyi* (253, 254).

Current challenges and opportunities in bacterial heme toxicity

While numerous systems are involved in detoxifying heme, there are many outstanding questions. The efflux systems have been described genetically, but a complete understanding of the ligands exported is still murky. For Gram-positive pathogens, the efflux systems may provide an additional therapeutic target for infection. Inhibition of efflux may offer a treatment option for bloodstream infections by *S. aureus* and *B. anthracis*; presumably the effects of heme toxicity would be deadly to the bacterium if the HrtAB pump were pharmacologically inactivated. This strategy could also pair well with small molecule activation of heme synthesis, which has been developed (111). In terms of heme sequestration proteins, it has been difficult to fully interpret the contribution of heme sequestration because additional properties like oxygenase (PhuS and ChuS) and DNA binding (ShuS) been observed. Finally, the role of heme oxygenases in resisting heme stress has not been well studied, but heme degradation likely reduces heme toxicity in a variety of organisms.

Outstanding questions in *S. aureus* heme homeostasis

S. aureus relies on heme dependent enzymes including the terminal cytochrome oxidases of cellular respiration and the antioxidant proteins bacterial nitric oxide synthase and catalase. To fulfill the requirement for heme, *S. aureus* synthesizes heme via glutamyl-tRNA. During infection, when host heme becomes available, the IsdB system can acquire heme, while HssRS may respond to excess heme (Figure 5).

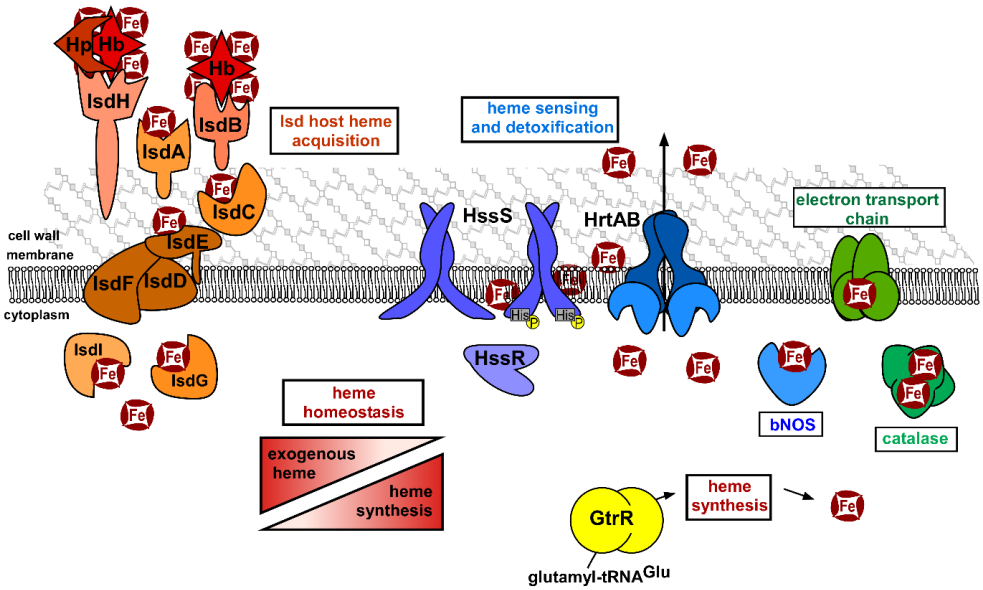

Figure 5 A model of heme acquisition, synthesis, utilization and detoxification in *S. aureus*.

Despite this experimentally supported model, a series of outstanding questions regarding *S. aureus* heme homeostasis remain.

1. **Unidentified hemoproteins**-the heme binding proteins of the Isd system (255), terminal oxidases (QoxABCD, CydAB (256)) bacterial nitric oxide synthase (bNOS), catalase (KatA), coproheme decarboxylase (ChdC (67, 257)), flavohemoprotein (Hmp;(258), and SbnI (133) have been studied *in vitro* or *in vivo*, yet no exhaustive investigation of *S. aureus* heme binding proteins has been completed. The non-covalent coordination by heme makes unbiased identification approaches difficult. However, as investigation continues into *S. aureus* heme homeostasis, more hemoproteins will be identified, adding to the quantity of heme-dependent physiology and more elaboration of the heme systems in Figure 5. In this thesis, GtrR is tentatively added to the list of *S. aureus* heme binding proteins.

2. **Biochemistry of terminal synthetic enzymes**- the field of study regarding coproporphyrin-dependent heme synthesis is new, and one of the most outstanding questions is how the terminal heme biosynthesis enzymes UroD, CgoX, CpfC, and ChdC coordinate their functions to ensure heme synthesis without toxic intermediate buildup, to ensure sufficient iron is available for insertion by CpfC, and the fate of the heme once formed by ChdC.
3. **Endogenous activation of HssRS**-previous work in our laboratory has found that HssRS can be activated by pharmacological activation of heme synthesis (109-111). Therefore, the true function of HssS may be to sense levels of endogenously synthesized heme rather than host-derived heme. The potential that HssS is a sensor for heme biosynthesis is explored further in this thesis.
4. **Toxicity of heme**-the basis for the toxicity of heme, as discussed above, is largely unknown for *S. aureus*. Considering that the regulon of HssS has been validated to contain only four genes, the transcriptional and proteomic response to heme toxicity has not offered much data to understand how heme kills *S. aureus*.
5. **Host heme utilized intact**-when host heme is bound and imported by the Isd system, the heme oxygenases IsdG and IsdI degrade heme to liberate iron. The fraction, if any, of host heme that can be incorporated intact into hemoproteins has not been measured. A heme synthesis mutant was able to infect kidneys to the same extent as WT *S. aureus*, but unable to replicate in the heart or liver, in a murine model of systemic infection. It is therefore unclear whether the kidney provides more available host heme to complement the heme deficiency, or if the kidney microenvironment is such that heme-independent fermentation is sufficient for replication in this niche.
6. **Function of heme degradation products**-the heme oxygenases degrade heme to staphylobilin and formaldehyde, yet no known function of these degradation products has been identified. Based on the analogous signaling roles that the heme degradation products in eukaryotes (carbon monoxide, biliverdin, and bilirubin) play, it is likely that staphylobilin and formaldehyde are important signaling molecules that affect *S. aureus* physiology.
7. **Regulation of heme synthesis** is the major question addressed in this thesis. Despite the duality of heme's necessity and toxicity, little is known regarding regulatory pathways guiding heme synthesis. Additionally, evidence of cross-talk between heme synthesis, uptake, utilization, and toxicity is lacking, despite the integrated functions of these heme systems. It is expected that the presence of exogenous heme would

impact heme synthesis, and that changes in the need for heme-dependent proteins would increase heme synthesis, while taking into account endogenous and exogenous heme availability to avoid toxicity.

CHAPTER II

A SMALL-MOLECULE INHIBITOR OF IRON-SULFUR CLUSTER ASSEMBLY UNCOVERS A LINK BETWEEN VIRULENCE REGULATION AND METABOLISM IN *STAPHYLOCOCCUS AUREUS*

A version of the following section (Chapter II, A Small-Molecule Inhibitor of Iron-Sulfur Cluster Assembly Uncovers a Link between Virulence Regulation and Metabolism in Staphylococcus aureus) was previously published in *Cell Chemical Biology* ;23(11):1351-1361 (November 2016)
Doi: 10.1016/j.chembiol.2016.09.012

Introduction

The Gram-positive pathogen *Staphylococcus aureus* is a leading cause of a wide range of devastating infections, including skin and soft tissue infections, osteomyelitis, infective endocarditis, and bacteremia (3). To infect, *S. aureus* employs a multitude of toxins, exoenzymes, and immune modulators, and its virulence regulators have long been appreciated as vital to pathogenesis. SaeRS is a key global regulator of toxin and exoenzyme production (259). SaeS is a two-component system (TCS) histidine kinase that responds to molecular components of neutrophils and activates the response regulator SaeR, which up-regulates transcription of the Sae regulon (260, 261). SaeRS is encoded in the *saePQRS* operon along with SaePQ, a membrane complex that aids the return of SaeRS to basal levels of activity (262). Complementary to its arsenal of virulence factors, *S. aureus* has also evolved antibiotic resistance. Methicillin resistant *S. aureus* accounts for the majority of clinical isolates (3). The dearth of antibiotics in the pharmaceutical development pipeline has led to renewed efforts to discover small molecules that probe the physiology of pathogens for the development of novel antimicrobials. In this regard, central metabolic pathways have become an attractive target in bacterial pathogens (263).

S. aureus is a facultative anaerobe, relying on both respiration and fermentation to cause disease (97, 264). In aerobic environments, respiration utilizes oxygen as the terminal electron acceptor and provides higher rates of ATP generation. However, *S. aureus* experiences many conditions in the host which makes fermentation vital. Fermentation is

utilized in hypoxic or anaerobic niches devoid of alternative terminal electron acceptors, including the bone and tissue abscess (97, 265). Host-produced nitric oxide directly inhibits the respiratory chain and the TCA cycle is inhibited in iron-deplete niches because of the iron dependency of many TCA cycle enzymes (264, 266). Additionally, respiration-deficient menaquinone or heme auxotrophs, called small colony variants (SCVs), are common isolates and etiological agents of persistent infections, an enormous clinical problem (101). Respiration-deficient SCVs rely on fermentation for growth and are intrinsically resistant to antibiotics that rely on membrane potential to enter the cell. Therefore, targeting of processes essential for fermentation is an exciting therapeutic option for the elimination of these cell populations.

Iron is crucial to the infectious lifecycle of *S. aureus* and a large portion of internalized iron is incorporated into proteins as Fe-S cluster cofactors. Fe-S cluster cofactors are required for a variety of cellular processes and the synthesis of Fe-S clusters is essential for *S. aureus* viability (267). Fe-S cluster-dependent enzymes play key roles in central carbon metabolism (268), branched chain amino acid synthesis (269), antibiotic resistance (270), and signal transduction (271). *S. aureus* factors required for Fe-S cluster assembly and maturation of apo-protein targets include SufS, SufBCD, SufU, SufT, SufA, and Nfu. SufS provides sulfur from cysteine to SufU or SufBCD, which synthesize [Fe_2-S_2] or [Fe_4-S_4] clusters (272). These Fe-S clusters are inserted into apo-proteins with or without the aid of the Fe-S cluster carriers Nfu or SufA, facilitating the maturation of holo-proteins (267, 273). SufT is an auxiliary factor involved in the maturation of apo-proteins that has an increased role during conditions that impose a high demand for Fe-S clusters (274). The genes encoding for Nfu and SufT display synergism for multiple phenotypes. Analyses of a Δ*nfu* Δ*sufT* strain have revealed the pleiotropic effects of defective Fe-S assembly upon central metabolism, iron homeostasis, oxidative stress, vancomycin resistance, biofilm formation and virulence (267, 274)

Previously, we identified small molecule VU0038882 (‘882) that activates endogenous heme biosynthesis in *S. aureus* while toxic to *S. aureus* grown anaerobically (275). ‘882 exhibits an IC_{50} of ~162 μM to aerobic *S. aureus* and an IC_{50} of ~5 μM to anaerobic *S. aureus* (275). Further experimentation revealed that ‘882 is toxic to *S. aureus* relying solely on fermentation for energy generation, as ‘882 is bacteriostatic to mutants that are respiration-deficient, regardless of oxygen availability. Through extensive structure-activity relationship (SAR) studies, we showed that the toxicity of ‘882 can be uncoupled from the capacity to activate heme synthesis, suggesting that ‘882 affects two distinct targets in *S. aureus* (276).

In this work, we sought to identify the mechanism of ‘882 toxicity in order to probe the physiology of *S. aureus* and uncover novel therapeutic targets. Genetic and proteomic approaches uncovered the SaeRS TCS as essential for ‘882 toxicity and the Suf Fe-S cluster biogenesis machinery as a likely target of ‘882. Here, we identify a unique link between virulence regulation and metabolic fitness in *S. aureus*. Additionally, this work employs a breadth of approaches to understand the effects of a small molecule and emphasizes the importance of Fe-S cluster metabolism in staphylococcal physiology. This study establishes ‘882 as a first-in-class manipulator of Fe-S cluster assembly, which may guide the development of new antimicrobials that target this essential pathway.

Materials and methods

Bacterial growth conditions

Strains, plasmids, and primers used are described in Tables 1-3. *S. aureus* strains Newman (wildtype is referred to throughout as NM), USA300 LAC, and JE2 and their mutants were grown on tryptic soy agar (TSA) or broth (TSB) and at 37°C unless noted otherwise. When appropriate, chloramphenicol or erythromycin was added to a final concentration of 10 µg/mL. ‘882 was dissolved in DMSO and added to media at concentrations noted throughout; an equivalent volume of DMSO was added as vehicle control to non-treated cultures. For routine anaerobic growth, a Coy (Grass Lake, MI) anaerobic chamber was used.

Table 1 Bacterial strains used in Chapter II

Species	Strain	Genotype	Description	Source
S. aureus	Newman	Wildtype	Methicillin sensitive strain	(277)
S. aureus	USA300 LAC	Wildtype	Methicillin resistant strain	(278)
S. aureus	USA300 LAC JE2	Wildtype	Methicillin resistant strain, erythromycin sensitive	(279)
S. aureus	RN4220	Wildtype	Restriction deficient cloning intermediate strain	(280)
S. aureus	Newman	Δ*saeRS*	Isogenic deletion of *saeRS*	(281)
S. aureus	Newman	$saeS^{P18L}$	Allelic replacement with repaired *saeS*	(281)
S. aureus	Newman	Δ*saeQRS*::$spec^{R}$	Allelic replacement of *saeQRS* with spectinomycin^{R}	(282)
S. aureus	Newman	*rimJ* (*NWMN_1957*)	Transduced from transposon insertion in JE2, *SAUSA300_2003*::*ermB*; NE1321	NARSA/BEI (279)
S. aureus	Newman	*fakA* (*NWMN_1136*)	Transduced from transposon insertion in JE2, *SAUSA300_1119*::*ermB*; NE221	NARSA/BEI; (279)
S. aureus	Newman	*fakB1* (*NWMN_0718*)	Transduced from transposon insertion in JE2, *SAUSA300_0733*::*ermB*; NE1540	NARSA/BEI; (279)
S. aureus	Newman	Δ*clpX*	In-frame deletion	(132)
S. aureus	USA300 LAC	Δ*sufA* (*SAUSA300_0843*)	In-frame deletion	(283)

S. aureus	USA300 LAC	Δ*sufA::tetM*	Tetracycline resistant allelic replacement	(283)
S. aureus	USA300 LAC	Δ*nfu* (*SAUSA300_0839*)	In-frame deletion	(283)
S. aureus	USA300 LAC	*nfu::tetM*	Tetracycline resistant allelic replacement	(283)
S. aureus	USA300 LAC	Δ*sufT* (*SAUSA300_0875*)	In-frame deletion	(274)
S. aureus	USA300 LAC	*nfu::ermB* Δ*sufT*	*nfu*::*ermB* transposon allele transduced into Δ*sufT*	(274)
S. aureus	USA300 LAC	*acnA*::*ermB*	Transposon mutation; NE861	(283)
S. aureus	Newman	*acnA*::*ermB*	Transposon allele transduced into strain Newman; NE861	This work
S. aureus	USA300 LAC	attP::pLL39_acnA_FLAG, *acnA*::*ermB*	Chromosomal integration of FLAG-tagged aconitase	(283)
E. coli	DH5α		Cloning Strain	
E. coli	PX5		Cloning Strain	Protein Express

Table 2 Plasmids used in Chapter II		
Plasmid	**Description**	**Source**
pOS1P$_{lgt}$	*S. aureus* shuttle vector with *lgt* (constitutive) promoter	(284)
pOS1P$_{lgt}$*saeQRS* (NM)	*saeQRS* cloned from Newman	Victor Torres
pOS1P$_{lgt}$*saeQRS* (LAC)	*saeQRS* cloned from LAC	Victor Torres
pCM11	Cloning vector for transcriptional reporters	(285)
pCM11_*sufC*	Reporter construct for *sufC*	(274)
pET24a	Protein production	EMD Millipore
pET24a_*acnA*	SAUSA300_1246	(283)
pEPSA5		(286)
pEPSA5_Flag_*acnA*	AcnA assays and immunoblots	(283)

Table 3 Primers used in Chapter II	
Primer name	**Sequence**
L202	GACCCCTATTTATTTAAATCAG
L197	AGCCCTCATTAATGGGAGCTTC
L186	GAGGTTTGTTTAGCTTAAGC
L190	GGGGCTCGAGATGACCCACTTACTGATCGTGG
L191	GGGGCTCGAGATGGTGTTATCAATTAGAAGTC
D474	GATGCTCAAGCACCAAAAGC
D475	ACTTTATGCTTCCGGCTCG
D476	GAAGAGATGTAAGAGTAGGG

Generation of spontaneously resistant mutants

Stationary phase cultures of aerobically grown NM in TSB alone were back-diluted 1:10,000 into TSB and 10 µl was spread onto TSA containing 20 or 40 µM ‘882 and moved into an anaerobic jar (Difco). After 24 h, colonies that appeared were restreaked onto TSA without ‘882, allowed to grow for 24 h, restreaked again on TSA alone, and after 24 h restreaked on TSA containing ‘882 to confirm resistance. For spontaneous resistance in NM pOS1P$_{lgt}$*saeQRS*, mutants were generated in the same manner except media contained chloramphenicol in addition to ‘882.

For resistant mutants, genomic DNA was purified using Wizard Genomic Kit (Promega) and the *sae* locus from the genome was amplified with primers L202 and L197 and Sanger sequenced (GenHunter) using primers L202, L186, L190, and L191. The plasmid from each resistant strain was purified using Plasmid Mini-prep kit (Thermo) and Sanger sequenced (GenHunter) using primers D474, D475, and D476 to check for mutations in the *sae* locus before whole genome sequencing.

Whole genome sequencing

Genomic DNA was isolated from mutant strains using the Wizard Genomic Kit (Promega) and sequenced along with the parental strain (NM or NM pOS1P$_{lgt}$*saeQRS*) by Perkin Elmer on the MiSeq Platform and analyzed for mutations using the Integrated Genomics Viewer available from the Broad Institute. Mutations were confirmed by Sanger sequencing.

Growth curves

Growth was monitored spectrophotometrically in 96-well plates containing 200 µL volume after stationary phase cultures were back-diluted into fresh medium. Percent (%) growth relative to vehicle is calculated from OD_{600} for each strain in ‘882 compared to DMSO.

For anaerobic growth curve, stationary phase statically grown anaerobic cultures in 5 mL of TSB of *S. aureus* strains were back-diluted to a calculated OD_{600} of 0.0001 (relative to media alone) in round-bottomed 96-well plates containing 200 µL of TSB (stored in anaerobic chamber at least 24 h prior to use) and covered with Breathe-Easy gas permeable seal (Sigma). Growth was monitored by optical density over time in a BioTek Synergy H1 or BioTek 808E Spectrophotometer. For growth with ‘882, 40 µM ‘882 or DMSO was added to the medium in the 96 well immediately before back-dilution. For pantothenate addition, TSB contained 20 µM ‘882 with or without 200 µM calcium pantothenate. For growth in defined medium, culture optical density was monitored at 630 nm. The staphylococcal-defined medium has been described previously (283) and contains all the canonical amino acids except leucine and isoleucine and glucose as a source of carbon (18AA glucose medium). Strains cultured overnight in TSB were harvested by centrifugation at 14,000 rpm for 1 min. The resulting cell pellet was washed twice to prevent the carryover of rich medium components. The optical density of the washed cultures was determined and strains were inoculated into minimal medium to an OD_{600} of 0.025. '882 or vehicle were added at point of inoculation. For microaerobic growth, the plate was depleted of dioxygen by passage through

an airlock into a Coy anaerobic chamber. The plate was sealed inside the chamber and subsequently removed to an aerobic environment and incubated statically. The data obtained were normalized with respect to the initial reading to negate for changes in absorbance between compound and vehicle. For growth curves comparing anaerobic growth of NM, ΔsaeRS, and saeSP18L, strains were grown to stationary phase in 5 mL of TSB in a Coy anaerobic chamber. OD_{600} was used to normalize strains, and each culture was diluted with anaerobic TSB to equivalent OD_{600}. One µl was added to 199 µl of TSB and OD_{600} was monitored over time. To compare these strain in a semi-defined carbon-limited medium (CLM; modified from (287)), strains were grown to stationary phase in 5 mL of TSB. OD_{600} was used to normalize strains, and then equal OD units were centrifuged and the cells were washed thrice in PBS, and then resuspended in equal volume of PBS. One µl of the cell suspension was added to 199 µl of CLM medium and OD_{600} was monitored over time. CLM consisted of 0.64 g/L NaCl, 0.15 g/L KCl, 0.01 g/L MgSO4-7H2O, 7 g/L K2HPO4, 2 g/L KH2PO4, 1 g/L (NH4)2SO4, 1 mg/L thiamine, 1.2 mg/L niacin, 0.25 mg/L calcium pantothenate, 5 µg/ml biotin, and 0.5% cas-amino acids. Glucose was added to 0.02% and glycerol to 0.04%. For anaerobic pantothenate rescue in CLM, washed cells from overnight cultures as above were back-diluted to a calculated OD_{600} of 0.0001 (relative to media alone). CLM contained 0.04% glycerol and 10 mM potassium nitrate.

Microarray

Strains NM and Δ*saeRS* were grown to stationary phase in 5 mL TSB anaerobically, and 100 µL was diluted into 10 mL of fresh, anaerobic TSB. After 5 h of growth (mid-log), ‘882 was added to a final concentration of 25 µM. After 10 min, the cultures were added to equal volume of ice-cold acetone:ethanol and stored at -80°C. To purify RNA, cells were collected by centrifugation at 10,000x g for 10 min at 4°C and then resuspended in 500 µL TE (10mM Tris, 1mM EDTA, pH 7.6). The cells were lysed in Bio101 FastPROTEIN BLUE lysing matrix tube using Bio101/Savant #FP120 FastPrep cell disruptor for 20 s at setting 5.0, cooled on ice, disrupted again 40 s at setting 4.5, and cooled on ice. The aqueous phase was separated by centrifugation at 10,000 x g for 15 min at 4°C. and transferred to a fresh tube. The RNA was isolated using Qiagen RNeasy kit according to directions.

RNA was reverse transcribed, cDNA fragmented, 3′ biotinylated, and hybridized to commercially available *S. aureus* GeneChips following the manufacturer's recommendations for antisense prokaryotic arrays (Affymetrix, Santa Clara, CA). GeneChips were washed, stained, and scanned as previously described (Beenken et al., 2004). The microarray data

has been uploaded to the National Center for Biotechnology Information Gene Expression Omnibus under accession number GSE85379.

Transductions

The USA300 LAC derivative JE2 strain containing the erythromycin-resistant NARSA (Network on Antimicrobial Resistance in *S. aureus*; available from BEI Resources) allele of interest was grown to stationary-phase in 5 mL of a 1:1 mix of TSB and lysogeny broth (LB), then subcultured 1:100 into 5 mL of 1:1 mix of TSB and LB containing 5 mM $CaCl_2$ and grown for 3 h. ϕ85 phage lysate was added (0.1-1 µl of high titer stock) and incubated at room temperature for 30 min. The culture was added to 6 mL of molten top agar and spread on TSA. After 16 h, the donor phage was collected as follows: the top agar was collected into 10 mL of sterile phage buffer (1.21 g Tris base, 1.20 g $MgSO_4$-7 H_2O, 0.10 g gelatin per liter; adjust to pH 7.4 with 6 M HCl), mixed, 250 µl chloroform was added, and mixed. The donor phage lysate from the supernatant is sterile filtered. The recipient strain is grown to stationary-phase in 20 mL TSB + 5 mM $CaCl_2$. The cells are collected by centrifugation and resuspended in 5 mL of 1:1 TSB:LB + 5 mM $CaCl_2$. 10^6-10^7 plaque forming units of the donor phage lysate are added to 500 µl of recipient strain and incubated together for 15 min at 37°C. The cells are then washed thrice in ice-cold 40 mM sodium citrate, resuspended in 40 mM sodium citrate, and spread on TSA + 40 mM sodium citrate + 10 µg/mL erythromycin. Colonies are patched on TSA containing erythromycin to confirm resistance, and the location of the transposon was confirmed by inverse PCR as described previously (279).

Hemolysis

5 µL of stationary-phase cultures of NM and resistant mutants grown in 5 mL TSB aerobically was spotted on blood agar plates (TSA+5% sheep's blood; BD) and allowed to incubate overnight at 37°C aerobically.

SaeQ immunoblot

5 mL of stationary-phase cultures were grown in TSB and were collected by centrifugation. Cell walls were removed by lysostaphin (8 µg/mL final) treatment in TSM (100 mM Tris, pH7; 500 mM sucrose; 10 mM $MgCl_2$) and protoplasts were collected by centrifugation. Protoplasts were lysed by sonication and total protein was quantified by BCA (Thermo). Sixty µg of protein per lane was loaded to a 15% acrylamide gel and subject to SDS-PAGE. Gel was transferred to Odyssey nitrocellulose membrane (Li-Cor) and probed

with a 1:2000 dilution of anti-SaeQ antibodies (Taeok Bae, Indiana University School of Medicine-Northwest) for 1 h in 5% milk in TBST. Secondary antibodies were a 1:5,000 dilution of goat anti-rabbit Alexa Fluor 660 (Thermo) and visualized with Odyssey Imaging System (Li-Cor)

Exoprotein profile

NM and resistant mutants were grown to stationary phase in 5 mL of TSB. Cells were removed by centrifugation and the spent medium was concentrated in a 3 kDa molecular weight cut-off spin column (Millipore Amicon) by centrifugation for 60 min at 3,200 x g. The concentrated medium was mixed with loading buffer and subjected to SDS-PAGE in 15% acrylamide gels. The gels were stained for total protein (BioRad Protein Assay) and imaged.

‘882 and ‘882-biotin synthesis

‘882 was synthesized as previously described (110). Synthesis of biotinylated ‘882 probe was performed as follows:

General Procedures

All non-aqueous reactions were performed in flame-dried flasks under an atmosphere of argon. Stainless steel syringes were used to transfer air- and moisture-sensitive liquids. Reaction temperatures were controlled using a thermocouple thermometer and analog hotplate stirrer. Reactions were conducted at room temperature (rt, approximately 23° C) unless otherwise noted. Flash column chromatography was conducted using silica gel 230-400 mesh. Analytical thin-layer chromatography (TLC) was performed on E. Merck silica gel 60 F254 plates and visualized using UV and iodine stain.

Materials

All solvents and chemicals were purchased from Sigma-Aldrich unless otherwise noted. Dry dichloromethane was collected from an MBraun MB-SPS solvent system. N,N-dimethylformamide (DMF), tetrahydrofuran (THF), and acetonitrile (MeCN) were used as received in a bottle with a Sure/Seal. Triethylamine was distilled from calcium hydride and stored over KOH. Deuterated solvents were purchased from Cambridge Isotope Laboratories. Methyl-4-bromo-3-methoxybenzoate was purchased from Combi-Blocks. Trimethylsilylacetylene and 1-(Chloro-1-pyrrolidinylmethylene) pyrrolidinium hexafluorophosphate were purchased from Oakwood Chemicals.

Instrumentation

^{1}H NMR spectra were recorded on Bruker 400 or 600 MHz spectrometers and are reported relative to deuterated solvent signals. Data for ^{1}H NMR spectra are reported as follows: chemical shift (δ ppm), multiplicity (s = singlet, d = doublet, t = triplet, q = quartet, p = pentet, m = multiplet, br = broad, app = apparent), coupling constants (Hz), and integration. ^{13}C NMR spectra were recorded on Bruker 100 or 150 MHz spectrometers and are reported relative to deuterated solvent signals. Low-resolution mass spectrometry (LRMS) was conducted and recorded on an Agilent Technologies 6130 Quadrupole instrument.

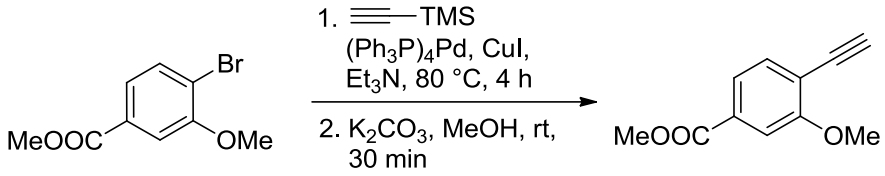

S1

Methyl 4-ethynyl-3-methoxybenzoate (S1)

To a stirred solution of 2.08 g (8.49 mmol, 1.0 eq) methyl-4-bromo-3-methoxybenzoate in 25 mL of triethylamine was added 455 mg (0.394 mmol, 0.046 eq) palladium tetrakistriphenylphosphine, 160 mg (0.842 mmol, 0.099 eq) copper(I) iodide, and 2.50 mL (17.6 mmol, 2.1 eq) trimethylsilylacetylene. The reaction was refluxed for 2 h when it was judged complete by LC-MS. The reaction was diluted with ethyl acetate (50 mL), filtered through celite, washed with saturated ammonium chloride (3x) and brine (2x), dried ($MgSO_4$), and concentrated. The crude residue was dissolved in 25 mL of methanol and 1.80 g of potassium carbonate was added. The reaction was stirred for 15 min when judged complete by LC-MS. The reaction was concentrated and partitioned between 50 mL of ethyl acetate and 20 mL of brine. The organic layer was filtered through silica gel, concentrated, and the residue purified by flash chromatography to provide 1.24 g (77 %) of S1 as a brown solid over 2 steps. ^{1}H-NMR (400 MHz, $CDCl_3$) δ 7.56 (dd, J=7.88 Hz, J=1.44 Hz, 1H), 7.51 (d, J=1.28 Hz, 1H), 7.47 (d, J=7.88 Hz, 1H), 3.92 (s, 3H), 3.89 (s, 3H), 3.43 (s, 1H); ^{13}C-NMR (100 MHz) δ 166.4, 160.5, 134.0, 131.6, 121.7, 116.0, 111.3, 83.9, 79.4, 56.1, 52.4; LRMS calculated for $C_{11}H_{10}O_3$ $[M+H]^+$ *m/z*: 191.1, measured 191.1.

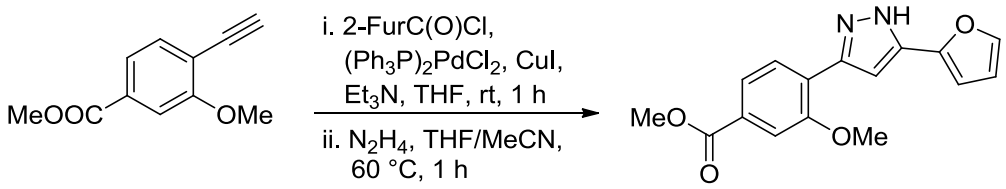

S2

Methyl 4-(5-(furan-2-yl)-1H-pyrazol-3-yl)-3-methoxybenzoate (S2)

To a stirred solution of 2.97 g (15.6 mmol, 1.0 eq) S1 in 50 mL of THF was added 2.18 mL (15.6 mmol, 1.0 eq) of triethylamine, 118 mg (0.167 mmol, 0.011 eq) of bis(triphenylphosine)palladium chloride, 111 mg (0.584 mmol, 0.037 eq) of copper(I) iodide, and 2.30 mL (23.3 mmol, 1.5 eq) 2-furoyl chloride. The reaction was stirred at room temperature for 1 h until it was judged complete by TLC. The reaction was diluted with 25 mL of acetonitrile, 1.50 mL (23.4 mmol, 1.5 eq) of hydrazine hydrate was added, and the mixture was heated to 60° C for 2 h until judged complete by TLC. The reaction was filtered through celite, concentrated, and purified by flash chromatography to give 3.98 g (86 %) of S2 as a yellow solid. ^{1}H-NMR (600 MHz, $CDCl_3$) δ 7.76 (d, J=8.10 Hz, 1H), 7.71 (dd, J=8.04 Hz, J=1.44 Hz, 1H), 7.67 (d, J=1.26 Hz, 1H), 7.46 (d, J=1.14 Hz, 1H), 6.93 (s, 1H), 6.72 (d, J=3.28 Hz, 1H), J=3.30 Hz, J=1.74 Hz, 1H), 4.0δ2 (s, 3H), 3.94 (s, 3H); ^{13}C-NMR (150 MHz) δ 166.5, 155.8, 148.7, 142.0, 141.2, 130.8, 127.8, 122.9, 121.9, 112.7, 111.5, 106.0, 101.0, 56.2, 52.3; LRMS calculated for $C_{16}H_{14}N_2O_4$ $[M+H]^+$ m/z: 299.1, measured 299.1.

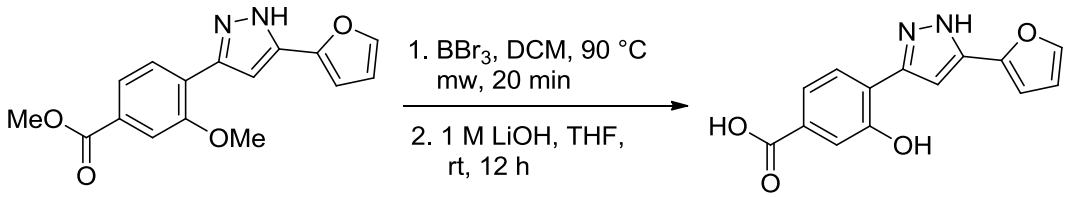

S3

4-(5-(furan-2-yl)-1H-pyrazol-3-yl)-3-hydroxybenzoic acid (S3)

To a stirred solution of 258 mg (0.864 mmol, 1.0 eq) of S3 dissolved in 1 mL dichloromethane in a microwave vial was added 3.45 mL (3.45 mmol, 4.0 eq) of a 1 M solution of boron tribromide in dichloromethane. The vial was sealed and maintained at 90° C for 20 min. The reaction was quenched in15 mL of saturated sodium bicarbonate, extracted with 30 mL of ethyl acetate (2x). The aqueous layer was acidified with 1 N HCl and extracted with 30 mL of ethyl acetate (2x) and set aside. The organic layer from the bicarbonate wash was concentrated and the residue dissolved in 2 mL THF. To the stirred THF solution was added 2.0 mL of 2 M lithium hydroxide and the resulting mixture was maintained at 50° C for 3 h until the reaction was judged complete by TLC. The mixture was acidified with 1 N HCl, extracted with ethyl acetate, and the organic layer combined with the organic layer from the acid wash from the previous step. The organics were concentrated and the residue purified by flash chromatography to provide 143 mg (61 %) of S3 as a light brown solid. ^{1}H-NMR (600 MfHz, acetone-d6) δ 7.90 (br, 1H), 7.73 (br, 1H), 7.61 (br, 2H), 7.25 – 7.22 (m, 1H), 6.98 – 6.94 (m, 1H), 6.64 (br, 1H); ^{13}C-NMR (150 MHz) δ 167.3, 156.7, 145.5, 144.2, 132.0, 127.7, 121.5,

121.4, 118.7, 112.7, 108.7, 100.0: LRMS calculated for $C_{14}H_{10}N_2O_4$ $[M+H]^+$ m/z: 271.1, measured 271.1.

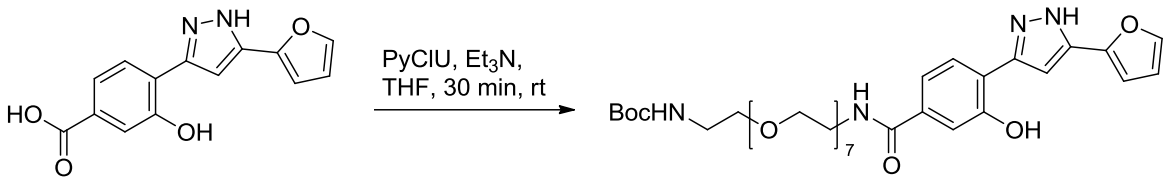

S4

tert-butyl (1-(4-(5-(furan-2-yl)-1H-pyrazol-3-yl)-3-hydroxyphenyl)-1-oxo-5,8,11,14,17,20,23-heptaoxa-2-azapentacosan-25-yl)carbamate (S4)

To a stirred solution of 15.0 mg (0.555 mmol, 1.0 eq) of S3 in 1 mL THF was added 51.9 mg (0.111 mmol, 2.0 eq) of O-(2-Aminoethyl)-O′-[2-(Boc-amino)ethyl]hexaethylene glycol, 15.5 µL (0.111 mmol, 2.0 eq) of triethylamine, and 36.9 mg (0.111 mmol, 2.0 eq) of 1-(Chloro-1-pyrrolidinylmethylene)pyrrolidinium hexafluorophosphate. The reaction was stirred at room temperature for 1 h when it was judged complete by LC-MS. The solvent was removed, the residue was dissolved in DMSO and purified by preparative scale reverse phase HPLC (MeCN:H_2O mobile phase) to provide 14.9 mg (37 %) of S4. ^{1}H-NMR (400 MHz, $CDCl_3$) δ 10.77 (br, 1H), 7.65 (d, J=8.00 Hz, 1H), 7.50 (d, J=1.24 Hz, 1H), 7.46 – 7.40 (m, 2H), 6.98 (br, 1H), 6.76 (d, J=3.32 Hz, 1H), 6.52 (dd, J=3.24 Hz, J=1.76 Hz, 1H), 5.08 (br, 1H), 3.71 – 3.48 (m, 30H), 3.33 – 3.26 (m, 2H), 1.43 (s, 9H).

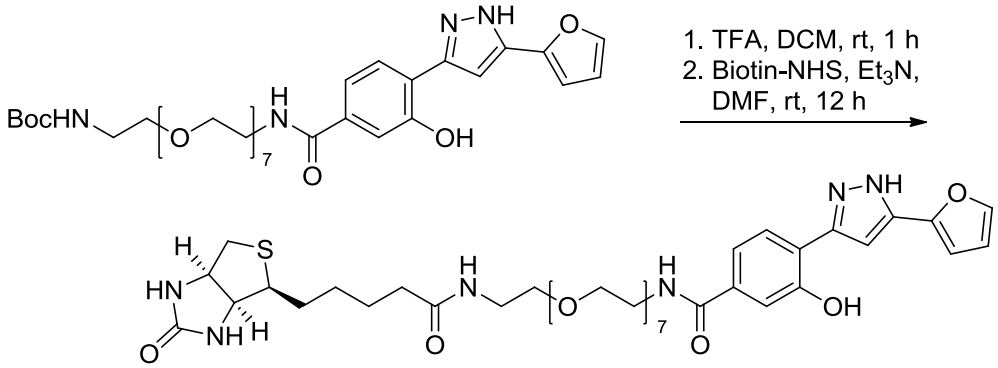

4-(5-(furan-2-yl)-1H-pyrazol-3-yl)-3-hydroxy-N-(25-oxo-29-((3aS,4S,6aR)-2-oxohexahydro-1H-thieno[3,4-d]imidazol-4-yl)-3,6,9,12,15,18,21-heptaoxa-24-azanonacosyl)benzamide ('882-biotin)

A total of 200 µL TFA was added to a solution of 14.9 mg (20.6 µmol, 1.0 eq) of S4 in 1 mL dichloromethane. The reaction was stirred at room temperature for 1 h when it was judged complete by TLC. The volatiles were removed *in vacuo* and the residue dissolved in 1 mL of DMF. To this stirred solution was added 8.6 µL (61.8 µmol, 3.0 eq) of triethylamine and

8.4 mg (24.4 μmol, 1.2 eq) of biotin-NHS ester. The reaction was stirred at room temperature for 1 h when it was judged complete by LCMS. The reaction was concentrated and the residue purified by preparative scale HPLC to provide 9.5 mg (48 %) of ‘882 biotin probe as TFA salt. ^{1}H-NMR (600 MHz, MeOD) δ 7.80 (d, J=8.04 Hz, 1H), 7.63 (d, J=1.20 Hz, 1H), 7.44 – 7.38 (m, 2H), 7.10 (br. 1H), 6.85 (d, J=3.30 Hz, 1H), 6.58 (dd, J=3.24 Hz, J=1.74 Hz, 1H), 4.49 – 4.45 (m, 1H), 4.29 – 4.26 (m, 1H), 3.71 – 3.55 (m, 30H), 3.51 (t, J=5.43 Hz, 2H), 3.34 (t, J=5.43 Hz, 2H), 3.19 – 3.14 (m, 1H), 2.90 (dd, J=12.75 Hz, J=5.01 Hz, 1H), 2.70 (d, J=12.72 Hz, 1H), 2.20 (t, J=7.35 Hz, 2H), 1.75 – 1.54 (m, 4H), 1.44 – 1.38 (m, 2H); LRMS calculated for $C_{40}H_{58}N_6O_{12}S$ $[M+H]^+$ *m/z*: 847.4, measured 847.2.

‘882-biotin pull-down sample preparation

The cellular lysate of mid-exponential cultures was collected from NM grown in TSB; the cells were collected by centrifugation and resuspended in PBS containing 30 μL of 2 mg/mL lysostaphin and 100 μM PMSF protease inhibitor. Cells were incubated at 37° C for 20 min to remove the cell wall and then sonicated. 500 μL of lysed cells were added to 50 μL of DMSO or ‘882-biotin (10 μg/μL concentration) and incubated for 30 min at room temperature. 500 μL of the lysate and probe solution was added to 500 μL of washed streptavidin-agarose resin (Thermo) and incubated at room temperature for 1 h. The resin was centrifuged and washed in PBS five times, and then bound proteins were eluted after the addition of SDS buffer and boiling for 10 min. 20 μL of each elution was run in 15% acrylamide SDS-PAGE and bands were visualized by PlusOne silver stain (GE) according to the manufacturer’s directions, and destained before proteomic analysis.

‘882 MudPIT sample preparation

5 mL of cultures of NM were started from single colonies in TSB containing 20 μM ‘882 or DMSO and grown aerobically for 15 h. The cells were collected by centrifugation. Cell walls were removed by lysostaphin (8 μg/mL final) treatment in TSM and protoplasts were collected by centrifugation. The protoplasts were resuspended in 450 μL PBS + 100 μM phenylmethanesulfonyl fluoride (PMSF; Thermo), and lysed by sonication. The suspension was clarified by ultracentrifugation for 30 min at 4°C at 100,000 x g. The protein was quantified by BCA (Thermo) and subjected briefly to SDS-PAGE before proteomic analysis.

LC-MS/MS analysis and protein identification

Proteins subject to SDS-PAGE after ‘882-biotin pull-down and ‘882 MudPIT experiments were excised and subjected to in-gel trypsin digestion and peptide extraction as previously described (288). The resulting peptides were analyzed using a Thermo Finnigan LTQ ion trap instrument equipped with a Thermo MicroAS autosampler and a Thermo Surveyor high-performance liquid chromatography (HPLC) pump, a nanospray source, and an Xcalibur 2.0 SR2 instrument control. Peptides were separated using a packed capillary tip (100 mm by 11 cm; Polymicro Technologies) with Jupiter C18 resin (5 mm; 300 Å; Phenomenex) and an in-line trapping column (100 µm by 6 cm) packed with the same C18 resin (using a frit generated with liquid silicate Kasil) similar to the column described previously (Tabb et al., 2007). The flow from the HPLC pump was split prior to the injection valve to obtain flow rates of 700 nL min−1 to 1,000 µL min−1 at the column tip. Mobile phase A consisted of 0.1% formic acid, and mobile phase B consisted of 0.1% formic acid in acetonitrile. A 95-min gradient was used with a 15-min washing period (100% mobile phase A for the first 10 min, followed by a gradient to 98% mobile phase A at 15 min) to allow loading and flushing of any residual salts. Following the washing period, the gradient was changed to 25% mobile phase B at 50 min and then to 90% mobile phase B by 65 min, which was used for 9 min before the conditions were returned to the initial conditions. Tandem spectra were acquired using a data-dependent scanning mode in which one full mass spectrometry (MS) scan (m/z 400 to 2,000) was followed by nine MS/MS scans. Tandem spectra were compared with data for the Newman strain of the *S. aureus* subset in the UniRef100 database using the SEQUEST algorithm. The database was concatenated with the reverse sequences of all proteins in the database to allow determination of false-positive rates. The Sequest outputs were filtered through the ID Picker suite, which allows the user to set a false discovery rate threshold (e.g., 0.05 or 5%) based on reverse sequence hits in the database, and proteins were required to be identified by two or more unique peptides. Reassembly of a protein from identified peptide sequences was done with the aid of a parsimony method (289).

Fe-S cluster reconstitution

All steps were performed under strictly anaerobic conditions inside a Coy chamber (<1 ppm oxygen). Recombinant purified AcnA was incubated with reconstitution buffer (50 mM Tris, 150 mM NaCl, 5 mM DTT, pH 7.5) anaerobically for 1 h. Cluster reconstitution was initiated by the addition of a 5-fold excess of ferrous ammonium sulfate and lithium sulfide as previously described (283, 290). The reaction mixture was allowed to proceed for 1 h before

excess Fe, S, and DTT were removed by desalting using a PD-10 column (GE Healthcare) that had been pre-equilibrated with reconstitution buffer. Reconstituted protein was concentrated using YM-3 Centriplus Centrifugal Concentrators (Millipore), prior to use in activity assays.

Recombinant protein purification

Escherichia coli strains BL21(AI*) containing a protein production vector were grown at 37 °C in a 3 L Fernbach flasks containing 1 L of 2X standard lysogeny broth (LB) medium. Cultures that had been grown to an OD_{600} of 0.6 were cooled to 25 °C and arabinose (1 mM) and IPTG (0.1 mM) were added. Cultures were grown for an additional 12 h before cells were harvested by centrifugation. Cell paste was flash frozen with liquid nitrogen and stored at -80 °C. Subsequently, AcnA was purified as described earlier (283). Protein concentrations were determined using a copper/bicinchonic acid based colorimetric assay modified for a 96-well plate (291). Bovine serum albumin (2 mg mL^{-1}) was used as a standard.

Cell-free extract and purified AcnA enzyme assays

Strains cultured overnight in TSB were diluted into fresh TSB to a final OD_{600} of 0.1. The culture medium was amended with 1% xylose to induce gene expression for the *acnA* gene (for strains carrying p*acnA*). Cells were subsequently cultured for 8 h (~OD of 8) and at a culture vessel headspace to culture medium volume ratio (hereafter HV ratio) of either 10, 2.5 or 0. The HV ratios were altered as per experimental requirements and details are mentioned in each figure legend.

For AcnA assays using anaerobically cultured *S. aureus*, strains were cultured in 2 mL microcentrifuge tubes containing 2 mL of culture medium at a HV ratio of zero, as described earlier (283). The culture medium was as described above. Anaerobic conditions were verified by the addition of 0.001% resazurin to control tubes and the medium color was monitored over time, as described earlier (292). Anaerobiosis was achieved by 3 h post inoculation. To examine the requirement of *de novo* protein synthesis, cells were treated by the addition of anaerobic 100 µg/mL rifampicin inside a Coy chamber, prior to treatment with '882 or vehicle.

To assess AcnA activity, cell pellets were harvested by centrifugation, placed inside a Coy anaerobic chamber, and were re-suspended in 100 µL anaerobic lysis buffer (50 mM Tris, 150 mM NaCl, pH 7.4). Cells were lysed by the addition of 4 µg lysostaphin and 8 µg DNase and incubated at 37 °C until confluent lysis was observed. The cellular lysates were

clarified using a 10 min high-speed spin. Lysates were removed from the anaerobic chamber and between 15-25 µL of lysate was added to 985-975 µL (total volume of 1 mL) of lysis buffer containing 20 mM DL-isocitrate. Aconitase activity was determined by monitoring the conversion of isocitrate to cis-aconitate spectrophotometrically using a Beckman Coulter DU530 UV-Vis absorption spectrophotometer (cis-aconitate ε240 nm = 3.6 $mM^{-1}cm^{-1}$) (293). Enzymatic activity was standardized with respect to the total protein concentration and subsequently as indicated in the figure legend.

Transcriptional reporter fusion assay

Strains cultured overnight in TSB-Erm medium were diluted into fresh TSB-Erm medium to a final OD_{600} of 0.1 and cultured, with shaking, at a HV ratio of 6. At periodic intervals culture density and fluorescence were assessed as described previously (Mashruwala et al., 2015). Fluorescence data were normalized to the culture OD_{600}.

FLAG_AcnA immunoblot analyses

Immunoblots were conducted as described earlier (283). 40 µg of total protein was separated using a 12% SDS-PAGE gel. Proteins were then transferred to a PVDF membrane and incubated with mouse monoclonal anti-FLAG primary antibody (Sigma-Aldrich) (1:4000 dilution) and subsequently HRP conjugated secondary antibody (Bio-Rad) (1:12000 dilution). The blots were developed using chemiluminescent detection (ECL kit, Pierce). The blots were scanned as high quality TIFF images.

Results

Constitutive Sae TCS signaling is required for ‘882 toxicity

To identify the cellular target of ‘882 toxicity in anaerobic *S. aureus*, we selected for spontaneously resistant mutants of *S. aureus* strain Newman (NM) growing fermentatively (anaerobically in the absence of alternative terminal electron acceptors) on medium containing 20 or 40 µM ‘882. Seven independently isolated mutants grew under these conditions, at a rate of ~$7x10^{-7}$ and were stably ‘882 resistant after multiple passages on medium alone. To evaluate the growth of these mutants relative to NM, strains were back-diluted from stationary phase cultures in medium alone into medium containing 40 µM ‘882 and the optical density was measured after 18 h of anaerobic growth (Figure 7A). These conditions allowed a demarcation between ‘882 sensitivity and resistance based on the growth of NM (Figure 6). To identify the mutations that allowed growth in the presence of ‘882,

we sequenced the genomes of the 7 isolates, and each was found to have a mutation in the *saePQRS* locus and no other nonsynonymous mutations were found in the genome (Figure 7B). Each mutation is predicted to disrupt the function of the Sae system by altering the protein-coding sequence or disrupting both promoters (P1, P3), thereby changing expression. Indeed, the ‘882 resistant isolates demonstrate phenotypes consistent with inactivation of the Sae system, as evidenced by reduced hemolysis, diminished exoprotein secretion, and undetectable SaeQ expression (Figure 8). These data suggest that Sae activity is required for sensitivity to ‘882, and mutations that reduce Sae signaling are sufficient to abrogate ‘882 toxicity.

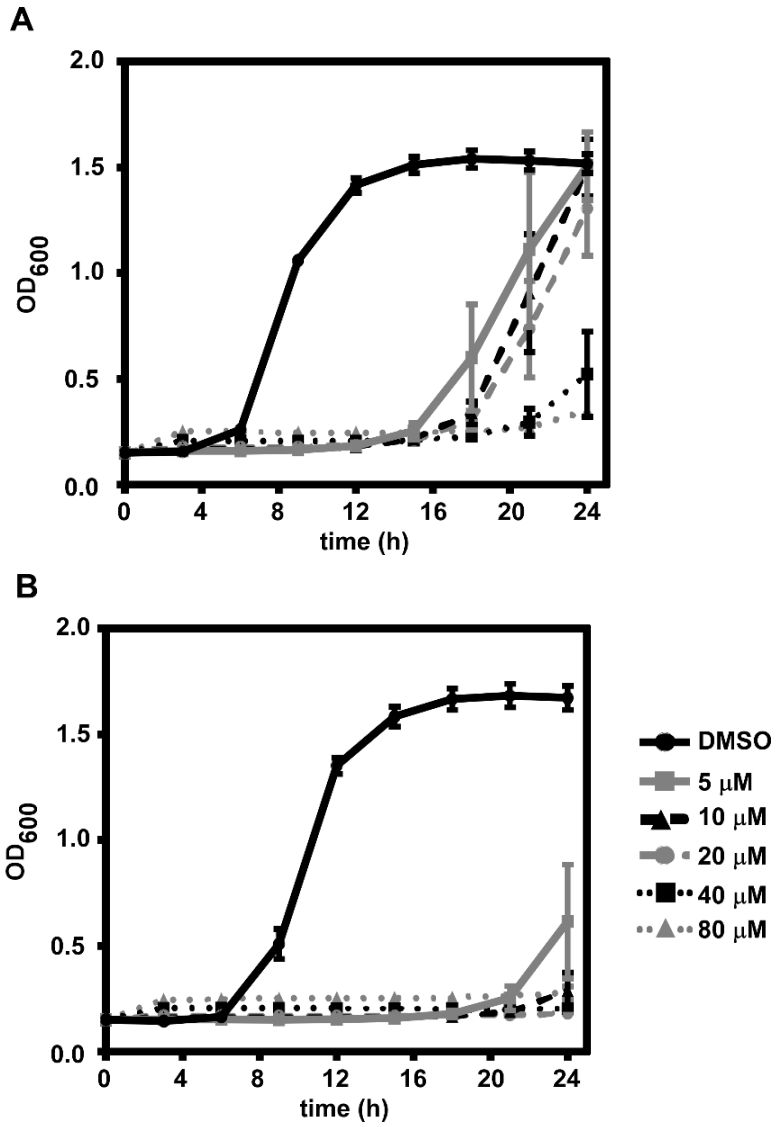

Figure 6 Toxicity of '882 to anaerobic *S. aureus*. Growth of NM grown anaerobically in the concentration of '882 shown at right, backdiluted to approximately **(A)** OD_{600} 0.001 and **(B)** OD_{600} 0.0001 from overnight cultures at time=0 h. Error bars indicate SEM, from means combined from three independent experiments with n>3 for each.

Importantly, SaeS of *S. aureus* NM is unique due to an amino acid substitution of leucine to proline at residue 18, located in the first transmembrane helix of SaeS (294). The Leu18 residue is encoded by nearly every other sequenced *S. aureus* genome. The L18P mutation renders NM SaeS constitutively active and resistant to SaeQ regulation, resulting in high levels of exoprotein transcription, translation, and secretion. Therefore, I hypothesized that constitutive Sae activity may be required for sensitivity to '882. Consistent with this, strains of *S. aureus* that do not express constitutively active SaeS: Δ*saeRS* (NM) and $saeS^{L18P}$ allele

repaired to *saeS*^{P18L} (NM), as well as the clinical isolate USA300 LAC (LAC), are more resistant to ‘882 than NM (Figure 7C). The NM *sae* locus (carrying *saeS*^{L18P}) expressed *in trans* in a LAC Δ*saeQRS* strain increased sensitivity to ‘882 while the LAC *sae* locus (carrying *saeS*^{L18}) expressed *in trans* did not make NM Δ*saeRS* sensitive to ‘882, confirming that constitutive Sae activity is sufficient for sensitivity to ‘882 (Figure 7D). These data demonstrate that increased Sae activity is required for ‘882 toxicity and decreased Sae signaling is sufficient for resistance to ‘882.

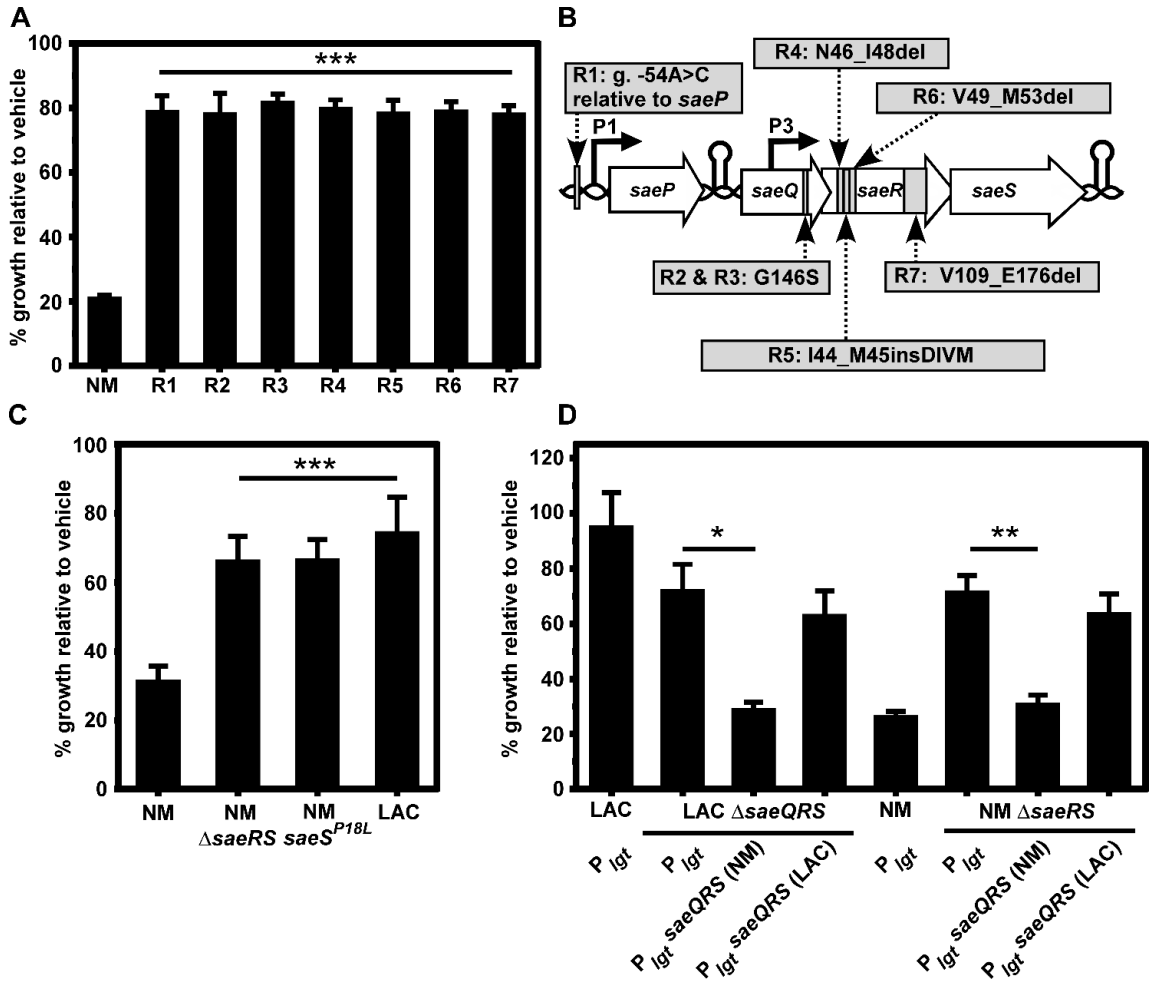

Figure 7 *S. aureus* constitutive Sae function is required for '882 toxicity [L.A.M. in part]. Spontaneously resistant mutants of strain Newman (NM) were isolated in the presence of 20 or 40 μM '882 in anaerobic conditions. **(A)** After four passages on plain medium, the spontaneous mutants still grew robustly by fermentation in medium containing 40 μM '882 relative to NM, indicating stable resistance to '882. **(B)** Whole genome sequencing of the isolates in (A) revealed mutations in the *saePQRS* locus. R1 has a nucleotide substitution at position -54 of the genome sequence (g.) relative to the start of *saeP*. Mutations resulting in changes to amino acid sequence are shown, where del signifies a deletion of noted amino acids and ins signifies insertion. **(C)** Strains that do not encode a constitutive SaeS: Δ*saeRS*, $saeS^{P18L}$, and the USA300 LAC (LAC) clinical isolate are resistant to '882. **(D)** *trans*-expression of constitutively active Sae (NM) under control of the *lgt* promoter in plasmid pOS1 is sufficient to induce '882 enhanced susceptibility in LAC, and the non-constitutively active *saeQRS* (LAC) locus provides '882 resistance to NM. For A, C, and D, error bars represent SEM from data combined from at least three independent experiments with n>2 for each. * indicates $p<0.05$, ** indicates $p<0.01$, and *** indicates $p<0.001$, calculated by one-way ANOVA with Sidak correction for multiple comparisons.

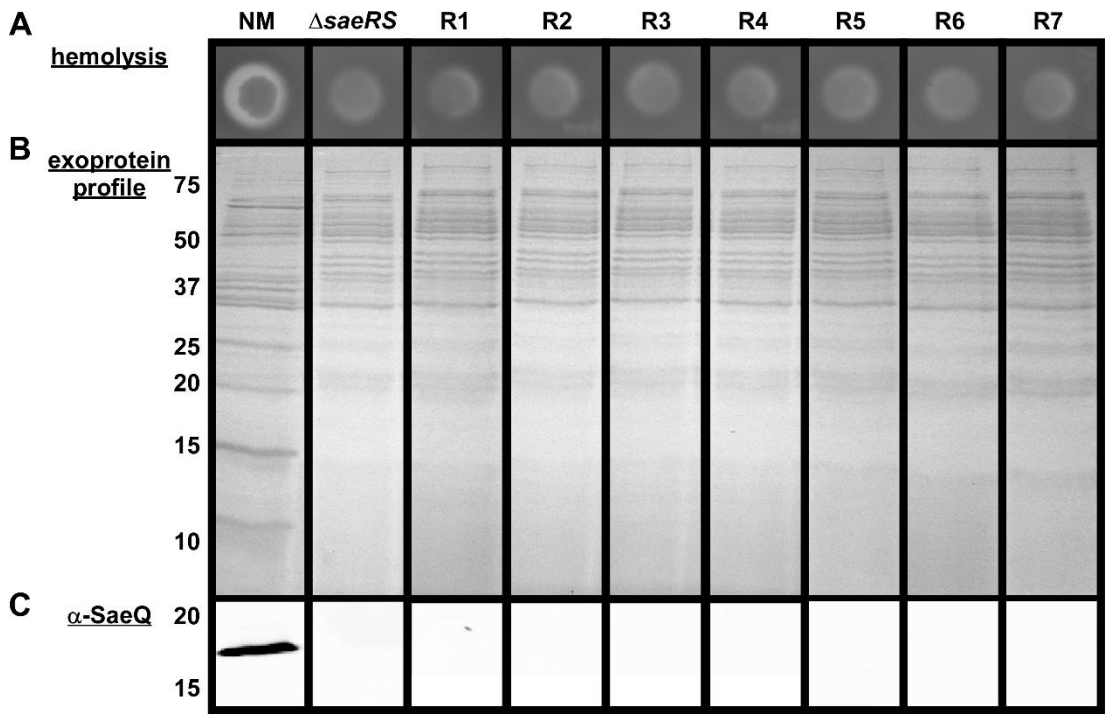

Figure 8 Spontaneously resistant mutants phenocopy Δ*saeRS* [L.A.M.]. Mutants in Figure 7A-B had similar **(A)** hemolytic, **(B)** exoprotein, and **(C)** SaeQ expression profiles as Δ*saeRS*. **(A)** hemolysin activity was assayed by spotting a suspension of each strain on blood agar plates and examining the zone of hemolysis. **(B)** Coomassie stained SDS-PAGE of culture supernatant from each strain. **(C)** Immunoblot for SaeQ expression in each strain. Protein size (kDa) is shown on left in B and C.

Inactivation of genes implicated in Sae signaling provides increased resistance to ‘882

To identify additional factors required for ‘882 toxicity, we again selected for spontaneously resistant mutants that grew by fermentation on medium containing ‘882. However, due to the strong selection for mutations in *sae*, we chose to create NM with a plasmid encoding an additional copy of the native *sae* locus (p*sae*) to prevent the identification of additional Sae mutants, and increase the likelihood of identifying genes other than *sae* that could provide ‘882 resistance. We isolated eight spontaneously resistant mutants in strain NM carrying p*sae* at a rate of ~1.3×10^{-5}, sequenced their genomes, and found mutations in three separate genes. Six of the isolates have changes in the protein-coding sequence of the fatty acid kinase FakA, a seventh isolate encodes a change in an additional fatty acid kinase FakB1, and the eighth has a stop codon incorporated in the coding sequence of the chaperone ClpX (Figure 9A). No other nonsynonymous mutations were identified in these isolates. To determine whether mutations in these genes were sufficient to increase ‘882 resistance in a NM background, I tested the growth of NM and strains inactivated for these genes in the

presence of ‘882 (Figure 9B). These strains all displayed increased resistance to ‘882 relative to NM, which indicates that FakA, FakB1, and ClpX are required for ‘882 toxicity. Interestingly, previous findings established that the Fak system impacts Sae function in strain USA300 (295). Also, SaeR was identified as a substrate of the ClpXP complex in NM, suggesting SaeR might be affected post-translationally (296). Therefore, I hypothesized that these resistant mutants were identified because they alter Sae activity, and are not themselves the target of ‘882.

Constitutive Sae is deleterious to growth in energy-limiting conditions

The strong selective pressure against Sae indicated that constitutive Sae activity may prevent anaerobic *S. aureus* from overcoming the toxic effects of ‘882. Under growth conditions devoid of a terminal electron acceptor, *S. aureus* relies on fermentation, which is less efficient at energy generation than respiration. Based on the large SaeR regulon, including the expression and secretion of many exoproteins, I hypothesized that the constitutive Sae activity in NM would be deleterious during fermentative growth. First, SaeQ abundance in aerobic and anaerobic conditions was measured as a proxy for transcription from promoter 1 of two different transcripts: *saePQRS* (transcript T1) and *saeQRS* (transcript T2) (297). Indeed, LAC did not express SaeQ during fermentation, indicating that transcription from Sae promoter 1 is inactive regardless of the presence or absence of ‘882 (Figure 9C-D). This suggested that the increased Sae activity during fermentation may impact growth in NM. As predicted, Δ*saeRS* and $saeS^{P18L}$ grew better than NM undergoing fermentation in rich medium (Figure 9E). Additionally, Δ*saeRS* and $saeS^{P18L}$ displayed enhanced growth in carbon-limited medium utilizing glucose or glycerol as the primary carbon source aerobically (Figure 9F,G respectively). These data confirm that constitutive SaeS activity is deleterious to growth during energy limiting conditions and are consistent with the hypothesis that the constitutively active SaeS contributes to the toxic effects of ‘882.

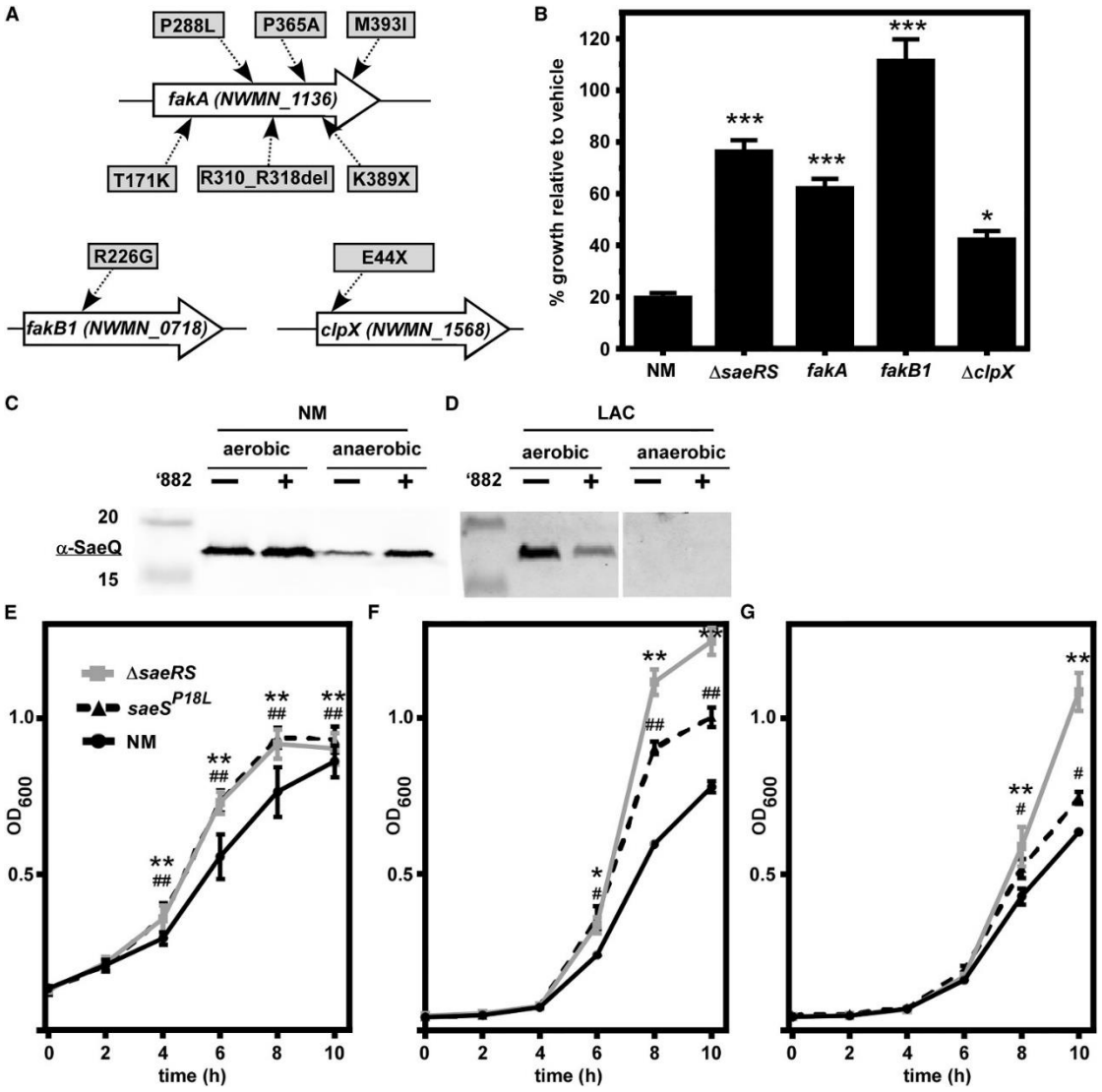

Figure 9 Genes required for toxicity are implicated in Sae signaling, which is a metabolic drain to NM [L.A.M.: panels A,C]. (A) Genomes of 8 spontaneously '882 resistant mutants in the NM pOS1P$_{lgt}$*saeQRS* strain were sequenced. Non-synonymous mutations were found in *fakA*, *fakB1*, and *clpX*. Changes to the protein sequence are shown in uppercase, as well as a deletion. **(B)** Strains inactivated for *saeRS*, *fakA*, *fakB1*, and *clpX* grow better than NM anaerobically in the presence of 40 μM '882. **(C)** Immunoblot with α-SaeQ at ~17 kDa from strains NM and **(D)** LAC during aerobic respiration and anaerobic fermentation in the presence or absence of 40 μM (aerobic) or 4 μM (anaerobic) '882 or DMSO. Growth of NM, Δ*saeS*, and *saeS*^{P18L} without '882 **(E)** anaerobically in TSB, and aerobically in carbon limited medium containing **(F)** glucose or **(G)** glycerol as the sole carbon source. Error bars represent SEM from data combined from at least three independent experiments with n>3 for each. For E-G, * and # indicate $p<0.05$, ** and ## indicate $p<0.001$, calculated by two-way ANOVA with Sidak correction for multiple comparisons, comparing *Δ*saeRS* or #*saeS*^{P18L} to NM at each time point.

‘882 disrupts coenzyme A pathways in *S. aureus*

I next hypothesized that Sae may additionally contribute to ‘882 toxicity by transcriptionally activating or repressing expression of the gene encoding the target of ‘882. To test this hypothesis, transcriptional differences between NM and Δ*saeRS* in the presence of ‘882 were identified using microarray (Appendix A Table 1). In addition to changes in expected virulence factor and exoprotein genes, the transcription of many genes involved in protein synthesis, energy production, and amino acid metabolism were altered. To test whether any of these genes encode the target of ‘882, strains lacking each of the non-essential or non-virulence factor genes were tested for resistance to ‘882. The inactivation of only two genes, *rimJ* and *NWMN_2021,* provided increased resistance to ‘882 (Figure 10). RimJ is a ribosomal protein N-acetyltransferase that is predicted to use acetyl-CoA as its substrate (298). I hypothesized that the presence of RimJ increases ‘882 toxicity due to increased cellular consumption of acetyl-CoA. To further test this hypothesis, I inactivated four other putative acetyl-CoA consuming enzymes. These proteins were significantly increased in abundance in NM grown in the presence of ‘882 relative to DMSO as identified by proteomics (Appendix A Table 2). Genetic inactivation of two of these four genes also provided resistance to ‘882, suggesting that acetyl-CoA consumption by non-essential proteins contributes to the anaerobic toxicity of ‘882 (Figure 11A). Together, these data indicate that ‘882 disrupts acetyl-CoA or CoA homeostasis. As the effect of CoA limitation by ‘882 would affect the growth of NM undergoing fermentation as well as anaerobic respiration, I tested whether increasing CoA abundance would rescue ‘882 toxicity. Indeed, the addition of the CoA precursor pantothenate rescued growth of NM anaerobically in rich medium containing ‘882 (Figure 11B) as well as in carbon-limited medium containing the non-fermentable carbon source glycerol and terminal electron acceptor nitrate (Figure 11C). In sum, these data suggest that ‘882 alters CoA homeostasis which can be rescued by reducing acetyl-CoA consumption through genetic manipulation or increasing CoA precursor availability.

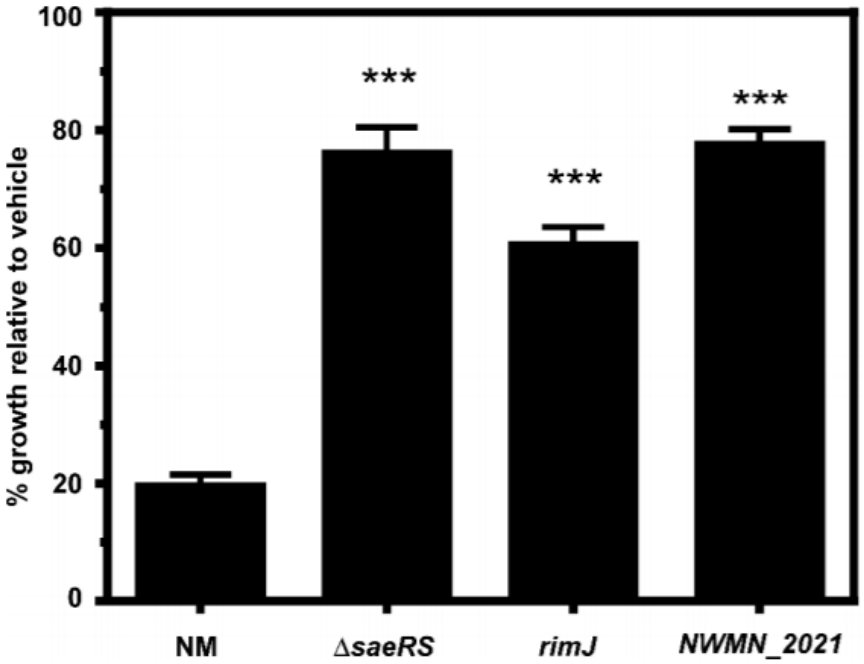

Figure 10 Two Sae-regulated genes are required for '882 toxicity. Strains lacking either rimJ or NWMN_2021, genes that were identified by microarray to be differentially transcribed after treatment with '882 between strains NM and ΔsaeRS, are resistant to 40 μM '882 relative to NM. Error bars represent SEM from data combined from at least three independent experiments with n>3 for each. % growth relative to vehicle is calculated from OD_{600} for each strain in '882 compared to DMSO (vehicle) after 18 h. * indicates $p<0.05$, ** indicates $p<0.01$, and *** indicates $p<0.001$, calculated by one-way ANOVA with Sidak correction for multiple comparisons.

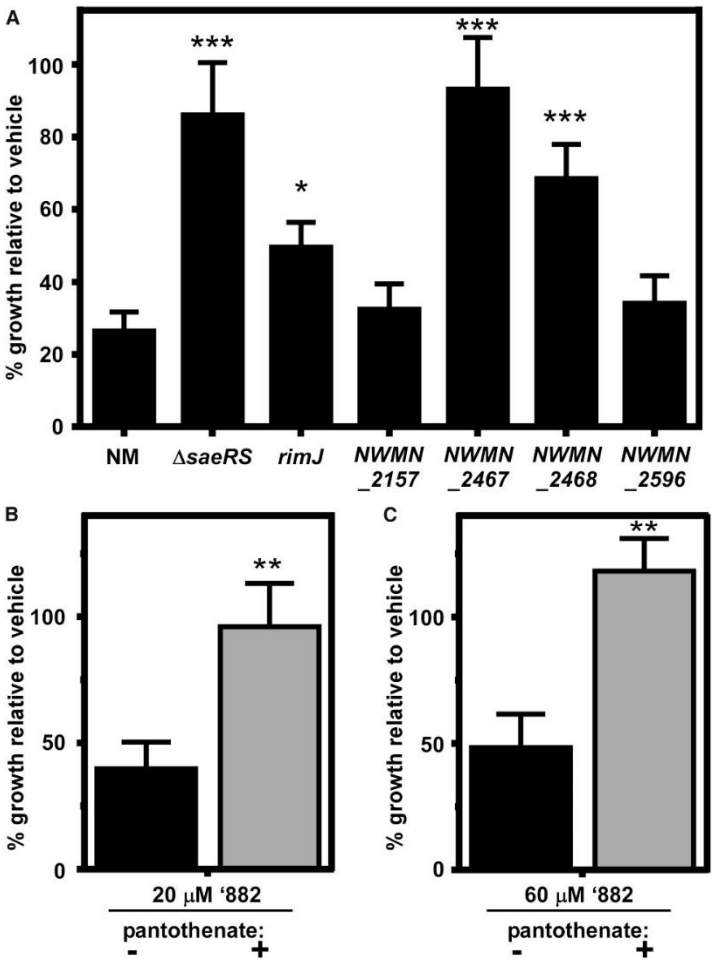

Figure 11 '882 alters coenzyme A pathways. (A) Inactivation of certain acetyltransferases provides resistance to '882. **(B-C)** Anaerobic growth of NM can be rescued by addition of the CoA precursor pantothenate in **(B)** rich medium containing '882 or **(C)** semi-defined medium containing glycerol as the primary carbon source, '882, and nitrate as the terminal electron acceptor. For A, * indicates $p<0.05$, ** indicates $p<0.01$, and *** indicates $p<0.001$, calculated by one-way ANOVA with Sidak correction for multiple comparisons. For B-C, ** indicates $p<0.01$, calculated by Student's t-test comparing the absence or presence of pantothenate.

'882 interacts with the Fe-S cluster biogenesis machinery

While these genetic approaches illuminated the role of Sae in '882 toxicity and fermentative growth, as well as the effects of '882 on CoA homeostasis, they did not identify a target of '882 toxicity. Therefore, in an attempt to identify a cellular target of '882, we performed a pull-down with cellular lysate and biotin-conjugated '882. One protein band visualized by SDS-PAGE exhibited differential abundance between the '882-biotin sample and the control. This band was excised and subjected to MudPIT LC-MS/MS for peptide identification (Figure 12A). Peptides from three proteins were enriched by the '882 pull-down, representing putative targets including SufC, NWMN_0632, and PdxS (Figure 12B). We

repeated the pull-down experiment and performed proteomics on the entire lanes of the control and ’882-biotin pull-down in an attempt to identify protein complexes bound by ‘882. We found that proteins of the Suf complex (SufB, SufC, and SufD) displayed greater enrichment in the ‘882 pull-down, while NWMN_0632 and PdxS were not enriched (Figure 12C-D).

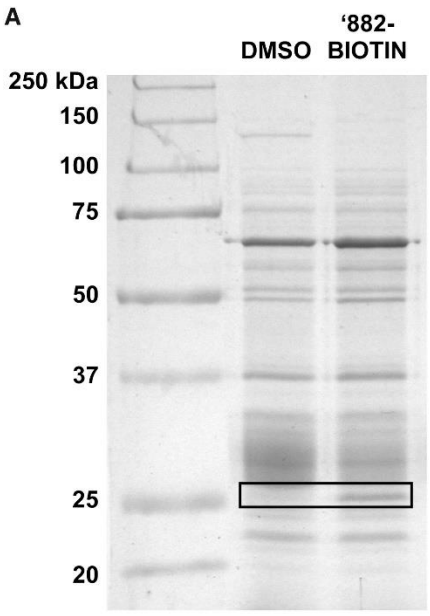

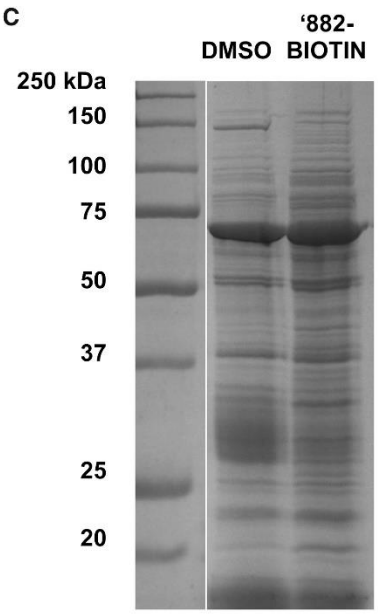

B

PROTEIN	DMSO COUNTS	‘882-BIOTIN COUNTS
SufC	30	44
NWMN_0632	13	24
PdxS	0	5

D

PROTEIN	DMSO COUNTS	‘882-BIOTIN COUNTS
SufC	44	106
SufB	8	34
SufD	3	16
SufS	1	9

Figure 12 ‘882 associates with Fe-S cluster biogenesis machinery. [L.A.M.] (A) SDS-PAGE of NM proteins collected by streptavidin after pull-down with DMSO or biotinylated ‘882. The boxed section of the gel was excised and subjected to proteomics. **(B)** Spectral counts of peptides from the boxed area in (A) most enriched in ‘882-biotin include SufC; the molecular weight of SufC is ~28 kDa. **(C)** SDS-PAGE of NM proteins collected by streptavidin after pull-down with DMSO or biotinylated ‘882. **(D)** Spectral counts of Suf protein peptides detected by proteomics after whole lane digest of (C) and mass spectrometry.

To further investigate the interaction between ‘882 and SufC, we measured direct binding using biolayer interferometry (BLI). Purified biotinylated SufC bound ‘882 with a K_D of ~ 4 µM (Table 4). We then repeated the BLI using purified SufC and biotinylated ‘882 and measured binding with a K_D of ~2 µM (Table 4). Additionally, purified NWMN_0632 did not bind ‘882, demonstrating that the SufC-‘882 interaction is specific and the enrichment of

NWMN_0632 peptides in the initial ‘882 pull-down was likely not the result of direct binding (Table 4). These data are consistent with a direct interaction between ‘882 and SufC.

Biotinylated ligand	Analyte	K_D (μM)	K_{on} ($M^{-1}s^{-1}$) [error]	K_{off} (s^{-1}) [error]
SufC	‘882	4.4	$3.27x10^4$ [$5.72x10^3$]	$1.45x10^{-1}$ [$1.02x10^{-2}$]
‘882	SufC	2.1	$9.46x10^3$ [$4.16x10^2$]	$1.96x10^{-2}$ [$2.66x10^{-4}$]
NWMN_0632	‘882	N.D.	--	--

Table 4 Direct binding between SufC and ‘882. [L.A.M.] Interactions with low micromolar K_D between purified SufC and ‘882, regardless of which served as the ligand, was observed by biolayer interferometry. Binding was not detected (N.D.) between ‘882 and NWMN_0632.

Assembly of FeS clusters upon aconitase is disrupted by ‘882

SufC is essential in *S. aureus* and forms a complex with SufB and SufD to assemble Fe-S clusters using sulfur from SufS and SufU (299). Monitoring *in vitro* Fe-S cluster assembly by the Suf machinery is technically challenging, and can produce non-physiologically relevant Fe-S clusters (299). As an alternative readout, the effect of ‘882 supplementation upon the activity of the Fe-S cluster-dependent enzyme aconitase (AcnA) were interrogated. These experiments revealed that ‘882 treatment results in decreased activity of AcnA *in vivo* in strains NM and LAC (Figure 13A). Because the transcription of *sufC* is decreased during fermentative growth (267), we hypothesized that the relative ratio of ‘882 to SufC would increase under these conditions and result in greater inhibition of AcnA activity by ‘882, relative to aerobic growth. Indeed, as the oxygenation during growth was reduced, the inhibitory effect of ‘882 increased (Figure 13B). Likewise, the effect of ‘882 on AcnA function was greater during anaerobiosis and a concentration of 25 μM ‘882 was sufficient to reduce AcnA activity to 50% (Figure 13C).

Six explanations could underpin the inhibitory effects of ‘882 on AcnA activity: 1) decreased transcription of the *suf* operon, 2) decreased abundance of the Suf machinery or auxiliary factors required for apo-protein maturation, 3) decreased transcription of *acnA*, 4) decreased abundance of AcnA, 5) direct inhibition of holo-AcnA activity by ‘882, or 6) inhibition of assembly of the Fe-S cluster on AcnA. We found that the transcriptional activity of *sufC* (first gene in the *suf* operon) was not decreased upon supplementing media with ‘882 (Figure 14A and Appendix A Table 1) and the abundances of Suf machinery proteins were increased upon treatment with ‘882 (Appendix A Table 2). The abundances of auxiliary factors involved

in Fe-S protein maturation such as SufT were also increased upon ‘882 supplementation (Appendix A Table 2). Next, AcnA activity was monitored in an *acnA*::TN strain containing a plasmid with an *acnA*_FLAG allele under the transcriptional control of a xylose inducible promoter (p*acnA*). Introduction of p*acnA* allowed for the control of *acnA* transcription and the determination of AcnA_FLAG abundance (267). ‘882 supplementation resulted in decreased AcnA activity in the *acnA*::TN strain carrying p*acnA*, but did not alter abundance of AcnA_FLAG (Figure 14B). Further, the inhibitory effect of ‘882 on AcnA function was not observed if ‘882 was added to purified AcnA containing an *in vitro* reconstituted Fe-S cluster (Figure 13D). Inhibition of protein synthesis prior to supplementation of the medium with ‘882 did not result in inhibition of AcnA activity *in vivo* (Figure 14C). The data presented in Figures 13 and 14 lend support to a model wherein ‘882 diminishes AcnA function by disrupting the assembly of the FeS cofactor upon AcnA.

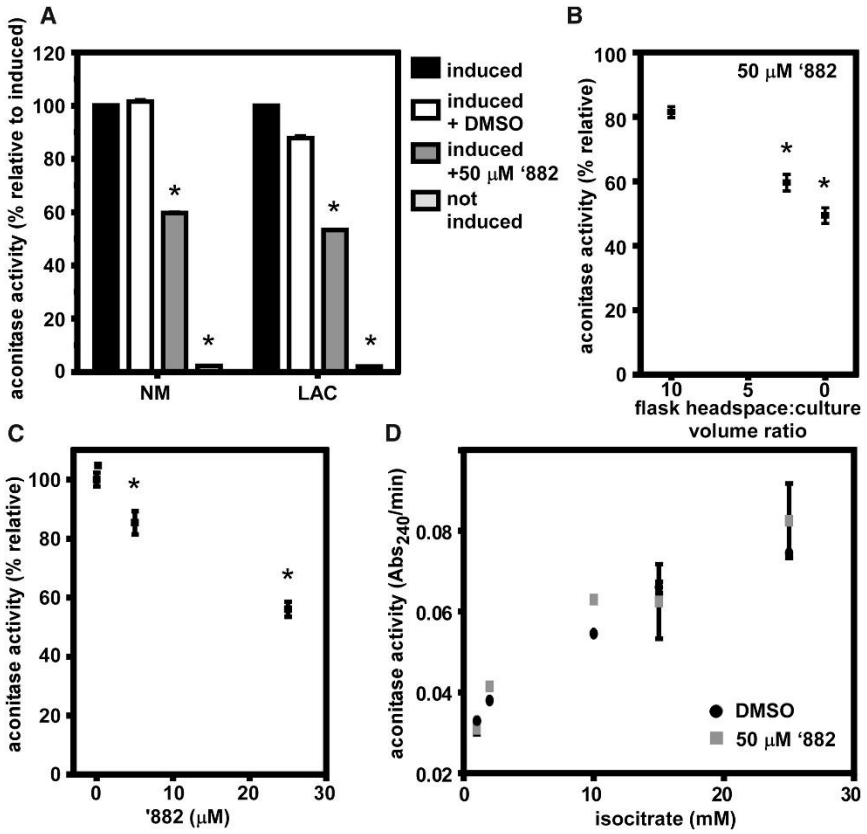

Figure 13 '882 impairs aconitase function. [A.A.M. and J.M.B.] (A) Aconitase activity is reduced in NM and LAC cultured in the presence of '882 after xylose induction of *acnA* transcription. * indicates p<0.001 by Student's *t*-test with Holm-Sidak correction for multiple comparisons, compared to induced + DMSO. **(B)** Aconitase activity in LAC is inhibited by 50 μM '882 to a greater extent as oxygen availability is reduced by decreasing the volume of gas above growth medium. * indicates p<0.05 relative to headspace:culture volume of 10, calculated by one-way ANOVA with Sidak correction for multiple comparisons (**C**) The inhibition of aconitase by '882 is greater under anaerobic conditions in LAC, where ~50% inhibition is achieved by 25 μM '882, compared to 50 μM '882 in (B). * indicates p<0.05 relative to no '882 calculated by one-way ANOVA with Sidak correction for multiple comparisons. (**D**) '882 does not inhibit the activity of purified aconitase protein that has been chemically reconstituted with Fe-S cofactor *in vitro* prior to exposure to '882. For A-D, error bars represent SD combined from two independent experiments. For panels A-D, the *acnA*::Tn strain carried p*acnA*, which encodes for *acnA* under the transcriptional control of a xylose inducible promoter.

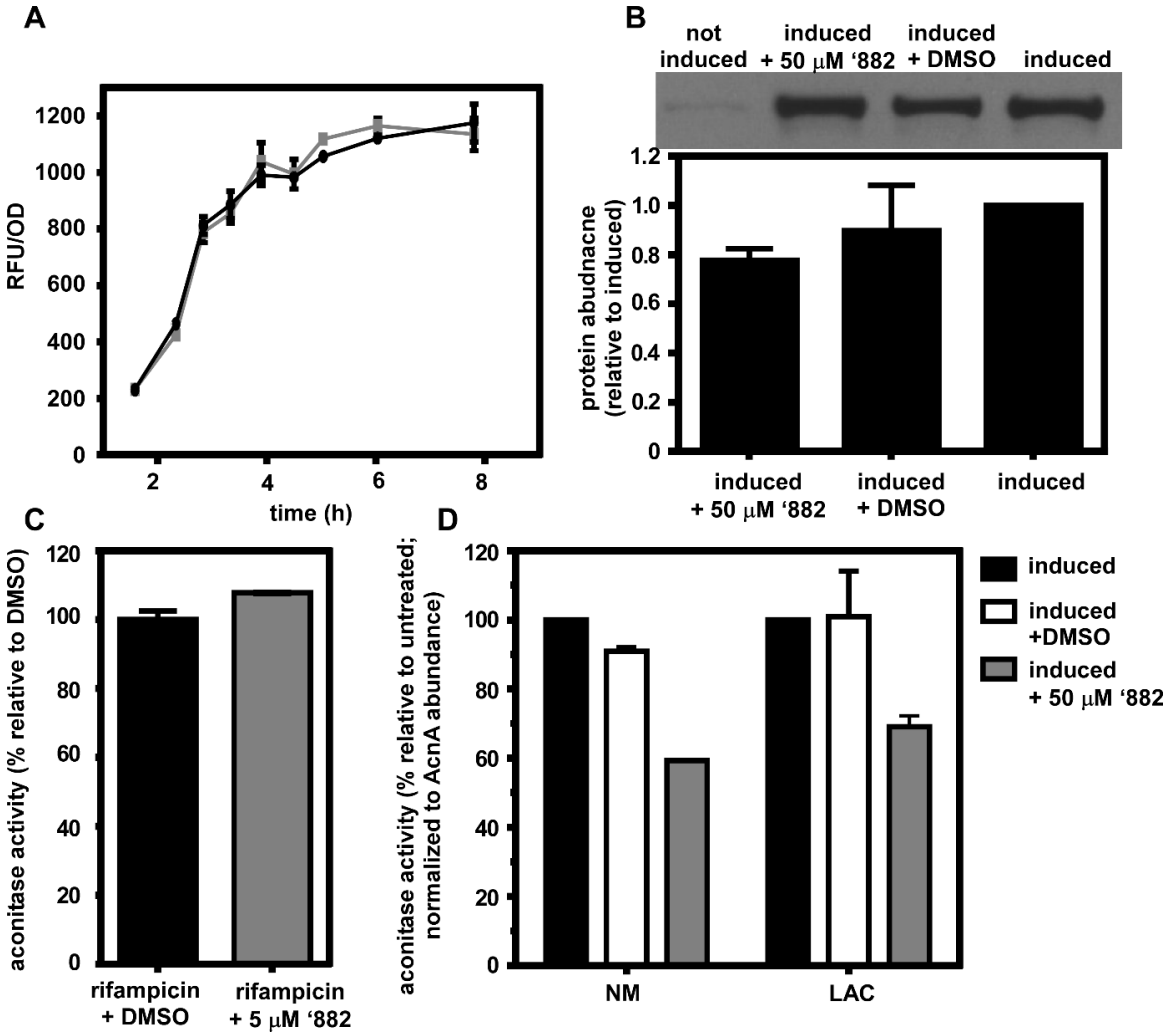

Figure 14 '882 disruption of aconitase function is post-translational. [A.A.M. and J.M.B.] **(A)** expression of *sufC* as measured by P_{sufC}.*gfp* is unchanged in '882 or DMSO treatment, shown in relative fluorescence units (RFU) normalized to optical density over time. **(B)** The relative protein abundance of aconitase is unchanged by '882 or DMSO treatment. Shown is an immunoblot of FLAG-tagged AcnA using α-FLAG antibodies, and the relative density of the band is quantified. **(C)** The inhibition of aconitase by '882 requires *de novo* protein synthesis, as '882 does not inhibit aconitase activity when it is added to the culture medium after pre-treatment of the culture with a protein synthesis inhibitor. **(D)** AcnA activity is decreased upon treatment with '882 in both the NM as well as the LAC strains and this phenotype is independent of relative AcnA protein abundance. For A-D, error bars represent SD.

Strains defective in the maturation of Fe-S proteins are sensitive to ‘882 intoxication

We hypothesized that if ‘882 inhibits Fe-S cluster assembly *in vivo,* then strains deficient in the maturation of Fe-S proteins would display increased sensitivity to ‘882 with respect to AcnA activity, as well as growth. Consistent with our prediction, LAC strains deficient in Fe-S cluster assembly (Δ*sufT* and Δ*sufA*) exhibit reduced AcnA activity, which was further decreased by co-culture with ‘882 (Figure 15A). Growth upon defined media lacking the amino acids isoleucine and leucine (18AA medium) is reliant upon the Fe-S cluster dependent enzymes LeuCD and IlvD. Growth of a Δ*nfu* Δ*sufT* double mutant in 18AA medium was diminished by ‘882 (Figure 15B). These data support a model whereby ‘882 inhibits the function of Fe-S cluster dependent processes by targeting the Suf machinery.

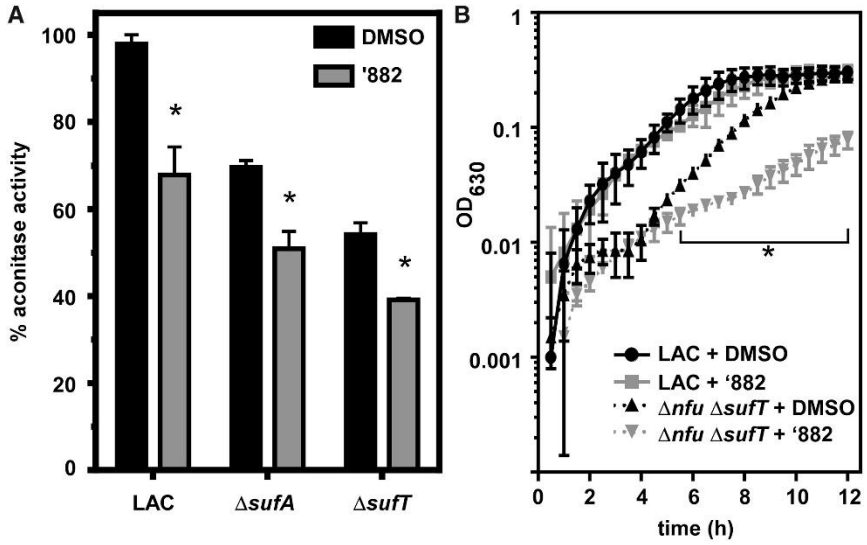

Figure 15 Strains defective in Fe-S cluster assembly are sensitive to ‘882. [A.A.M. and J.M.B.] (A) Aconitase activity is reduced in mutants lacking Fe-S cluster assembly factors when cultured in the presence of 50 μM ‘882. * indicates $p<0.05$ by Student’s *t*-test for each strain comparing DMSO to ‘882. **(B)** A LAC strain defective in Fe-S protein maturation is sensitive to 10 μM ‘882 under microaerobic conditions in defined media lacking Ile and Leu. * indicates $p<0.05$ by Student’s *t*-test for each time point comparing Δ*nfu* Δ*sufT* + ’882 to Δ*nfu* Δ*sufT* + DMSO. For A and B, error bars indicate SD combined from two independent experiments.

Discussion

In this study, we sought to characterize the factors responsible for ‘882 toxicity. Our attempts using genetic selection offered insight into the interplay between the SaeRS virulence regulation system and energy generation (Figure 8). The toxicity of ‘882 was first

observed in *S. aureus* strain NM, which has a constitutively active SaeS as the result of a mutation resulting in a proline at amino acid 18 (294). The genetic strategies employed here point to a strong selection against SaeS signaling during anaerobic growth. In addition to showing that inactivation of Sae is sufficient to make NM resistant to ‘882, our findings (Figure 9A-B) that genetic inactivation of *fakA*, *fakB1*, and *clpX* also provide increased resistance to ‘882 are consistent with previous work connecting fatty acid kinases (Fak) and the ClpXP protease complex with Sae signaling (295, 296). FakA (previously called VfrB) and FakB1, along with FakB2, constitute a fatty acid incorporation system required for hemolysis, biofilm formation, and the transcription of SaeR target genes (295, 300, 301). The direct mechanism of Fak regulation of these virulence determinants is unclear. ClpX is an ATPase that serves as a chaperone as well as forms a complex with the peptidase ClpP (302). While the complete interaction between ClpX and Sae signaling has not been elucidated, ClpX likely affects Sae signaling by altering SaeR abundance in NM, as SaeR has been identified as a substrate of ClpXP (296). The effects on Sae of ClpX and the Fak system highlight the diverse cellular processes that intersect with Sae virulence regulation.

The inhibition of fermentative growth by ‘882 may be observed because the constitutive SaeS activity in NM reduces growth even in the absence of ‘882. The finding that LAC and presumably other strains with non-constitutive SaeS alter Sae signaling in anaerobic conditions is consistent with the hypothesis that pathogens have evolved control of metabolically expensive virulence factor production to ensure synthesis occurs only when required (Figure 9C-G). This is similar to the description of the metabolic cost associated with expression of the *Salmonella* Type III Secretion System 1 (303). Cells that express this virulence factor *in vitro* demonstrate reduced fitness relative to non-expressing cells. It seems that the canonical SaeS of *S. aureus* has evolved to limit the metabolically expensive synthesis of its regulon during energetically unfavorable conditions.

Our finding that ‘882 alters CoA homeostasis (Figure 10) substantiates the effects of Suf disruption on *S. aureus* undergoing fermentation. Genetic inactivation of *rimJ* and other non-essential acetyl-CoA consuming enzymes provided increased resistance to ‘882, and based on this I hypothesized that ‘882 may reduce available CoA levels during anaerobic growth. The ‘882 inhibition of Fe-S cluster assembly are consistent with our model that ‘882 disrupts the CoA pool. First, the Fe-S cluster-dependent enzyme dihydroxy-acid dehydratase (IlvD) is required for pantothenate and CoA synthesis. In addition, under anaerobiosis, pyruvate formate lyase (PflB) is the probable source of acetyl-CoA as the transcription of *pflA* and *pflB* increase anaerobically while transcription of the pyruvate dehydrogenase complex

decreases (304). PflB is activated by PflA, which is an Fe-S cluster-dependent radical S-adenosyl methionine dependent activase (305). This information is consistent with the model that ‘882 disrupts CoA pathways during fermentation by potentially impeding the function of Fe-S cluster-dependent IlvD and PflA enzymes in CoA synthesis and consumption.

The SufBCD proteins were pulled down with biotinylated ‘882 and ‘882 interacted with purified SufC with high affinity (Figure 12, Table 4), which support our model that ‘882 inhibits Fe-S cluster assembly. The effects of ‘882 on Fe-S cluster assembly are widespread. A strain deficient in Fe-S cluster assembly (Δ*nfu* Δ*sufT*) was more sensitive to ‘882 intoxication when cultured in a medium wherein the growth is reliant upon the Fe-S cluster dependent enzymes IlvD and LeuCD (Figure 6) (269, 306). Under these conditions, ‘882 inhibits the growth of LAC, suggesting that even in the absence of constitutive Sae activity, the pleiotropic effects of ‘882 can be observed, which would be expected if ‘882 inhibits Fe-S cluster assembly. The inhibitory effects of ‘882 are most pronounced under anaerobic growth, and evidence suggests this is the result of (1) reduced energy generation and the metabolic burden of constitutive Sae, (2) reduced expression of Fe-S cluster assembly factors, which decreases the effective concentration of ‘882 required to inhibit Fe-S cluster assembly, and (3) the dependency of CoA homeostasis on Fe-S cluster requiring enzymes.

The investigations into the effect of ‘882 on aconitase (AcnA) support the model that ‘882 disrupts the Suf machinery (Figure 13). It was recently demonstrated that AcnA function is reduced in strains with inhibited Fe-S cluster assembly (267), and here we show that ‘882 decreases AcnA activity. The magnitude of inhibition of AcnA activity by ‘882 is amplified as culture dioxygen levels are reduced. These data agree well with the decreased expression of *sufC* during anaerobic conditions (267). Lending further support to the idea that ‘882 inhibits the assembly of the Fe-S cluster upon apo-AcnA but does not directly inhibit AcnA, ‘882 does not alter the activity of purified AcnA containing a chemically reconstituted Fe-S cluster. Consistent with the *in vitro* data, we find that *in vivo* the inhibitory effect of ‘882 upon AcnA requires *de novo* protein synthesis (307). These findings support the conclusion that ‘882 decreases AcnA activity through the inhibition of Suf-mediated Fe-S cluster biogenesis.

Proteomics analysis found that cells toxified by ‘882 increase the abundance of the core Suf machinery proteins. The transcription of *sufC* is increased under growth conditions that impose an increased demand for Fe-S cluster biogenesis (267, 274). SufT is a Fe-S maturation factor selectively utilized under growth conditions that impose an increased demand for Fe-S cluster biogenesis and the transcription of *sufT* increases under such conditions (267, 274). The abundance of SufT increases in cells toxified by ‘882, further

emphasizing that intoxication by ‘882 results in an increased need for the Fe-S cluster assembly machinery. Thus, taken with the other findings presented in this study, one explanation is that cells toxified by ‘882 increase abundance of the Suf proteins to aid in mediating resistance towards this molecule and bypassing toxicity.

In summary, this work has identified ‘882 as an inhibitor of Fe-S cluster assembly and our data suggest that inhibition of Fe-S cluster dependent enzymes is, in part, responsible for the toxicity of ‘882. Fe-S cluster assembly is one of the two distinct cellular targets of ‘882 that also include activation of heme biosynthesis. Our medicinal chemistry efforts have demonstrated the structural components of ‘882 required for each of these activities (276). Our previous findings demonstrated the utility of ‘882 as an inhibitor of *S. aureus* undergoing fermentation; treatment of mice with a derivative of ‘882 reduced the burden of *S. aureus* in the liver during systemic infection (275). Here, we demonstrate a candidate staphylococcal target for this therapeutic effect. The Suf proteins are not conserved in humans, which rely on an *E. coli*-like Isc system, making Suf an attractive pathogen-specific drug target (308, 309). This work underscores the opportunity to develop small molecule inhibitors of the Suf machinery as potential novel therapeutics.

CHAPTER III

GENETIC DISSECTION OF *S. AUREUS* HEME BIOSYNTHESIS

Introduction

The biosynthetic route to heme in *S. aureus* remains an under-explored physiological process. As discussed in Chapter I, recent work has illuminated novel intermediates in the terminal steps of heme synthesis, ascribed new functions to the enzymes responsible for these intermediates, and identifed the enzyme responsible for the final step in *S. aureus* heme synthesis. However, in this Chapter I investigate a series of outstanding questions in staphylococcal heme synthesis. While many groups are working diligently to investigate the unexplored enzymology of the coproporphyrin-dependent heme synthesis route, particularly focused on ChdC and CgoX, in this study I turn to genetics to answer the following question: which steps in *S. aureus* heme synthesis produce heme auxotrophy?

The general consensus for heme biosynthesis (and most co-factor and secondary metabolite synthesis) contends that each step is required for production of heme. However, some outstanding data and observations suggest this might not be entirely true for *S. aureus*. First, there are conflicting data regarding the conversion of glutamate-1-semialdehyde to δ-aminolevulinic acid (ALA). *In vitro* experiments demonstrated that the conversion can occur in the absence of enzyme (45), yet a *gsaM* (annotated as *hemL*) mutant in *Salmonella* is a heme auxotroph that can be complemented with ALA, suggesting the enzyme is required *in vivo* (310). Additionally, *S. aureus* and other members of the Firmicutes phylum encode a second annottated *gsaM* at a separate chrmomosal locus. Therefore, I sought to determine the contributation of each GsaM to heme synthesis.

A second outstanding question is the identity of an anaerobic CgoX. CgoX performs the oxidation of coproporphyrinogen III to coproporphyrin, and *in vitro* this reaction uses molecular oxygen. This suggests the existence of an anaerobic enzyme capable of the same reaction with a different proton acceptor. Existence of oxygen-dependent and -independent enyzmes for this step would be in line with the protoporphyrin-dependent heme synthesis pathway (43) as discussed in Chapter I. Three potential options exist to resolve this question- the annotated HemN described as an oxygen-independent coproporphyinogen III oxidase fills this gap, the DUF1444 enzyme (NWMN_1636) is the enyzme in question, or CgoX functions

anaerobically and aerobically. This Chapter investigates these possibilities and finds that CgoX is required for aerobic and anerobic heme synthesis.

Materials and methods

Bacterial strains (Table 5), plasmids (Table 6), and primers (Table 7) are listed in the specified table. *S. aureus* strains were grown routinely on tryptic soy agar (TSA) or broth (TSB) supplemented with 10 µg/mL chloramphenicol or 10 µg/mL erythromycin when necessary. When used, heme (hemin chloride) was used at concentrations noted. Heme was prepared fresh at 10 mM in 0.1 M NaOH; for experiments in which heme was used, an equal volume of 0.1 M NaOH was used for all conditions. *E. coli* strains were grown on lysogeny broth (LB) or LB agar (LBA), supplemented with 50 µg/mL carbenicillin or kanamycin when necessary. For growth in liquid medium, an Innova44 incubator shaking at 180 rpm was used. For standard cultures of 4-5 mL, 15 mL round bottomed polypropylene tubes with aeration lids were used, at a 45° angle in the incubator. For cloning and mutagenesis in plasmids, all constructs were confirmed by sequencing (GeneWiz). Unless noted otherwise, all chemicals are from Sigma. All molecular biology reagents were New England Biolabs and used according to manufacturer's instructions, unless otherwise noted. Phusion 2X Hi-fidelity master mix was used for all PCR reactions for cloning. As necessary, plasmids were transformed by electroporation from *E. coli* into the *S. aureus* cloning intermediate strain RN4220 before isolation and subsequent electroporation into final *S. aureus* strains.

Inactivation of *S. aureus* heme biosynthesis enzymes

Deletion of genes were performed by allelic exchange as described in (311) with some modifications. The pKOR1 plasmids containing ~1kb homologous regions flanking upstream and downstream of the gene to be deleted were prepared using NEB Hi-Fi assembly according to manufacturer's suggestions. The pKOR1 backbone was amplified by PCR using JC291/292 which produces a linear product not including the *attB* recombination sites. The ~1kb flanking regions were amplified from *S. aureus* Newman genomic DNA. Deletions were confirmed by PCR using isolated genomic DNA and complemented by providing the gene in *trans.*

For *gsaM2*, flanking regions were amplified using JC29/30 (upstream flanking) and JC31/32 (downstream flanking). The deletion was confirmed with PCR using primers JC49/46. For *uroS*, flanking regions were amplified using JC415/416 (upstream flanking) and JC417/418 (downstream flanking). The deletion was confirmed with PCR using primers

JC184/189. For *uroD,* flanking regions were amplified using JC419/420 (upstream flanking) and JC421/422 (downstream flanking). For *uroD-cpfC*, flanking regions were amplified using JC500/501 (upstream flanking) and JC502/503 (downstream flanking). For *uroD-cgoX*, flanking regions were amplified using JC500/504 (upstream flanking) and JC507/508 (downstream flanking), and JC505/506 amplify *cpfC*; for this plasmid, the upstream and downstream flanking regions are on either side of *cpfC* so that deletion of *uroD* and *cgoX* is in-frame and retains cpfC. For *uroD-cpfC-cgoX*, flanking regions were amplified using JC419/423 (upstream flanking) and JC424/425 (downstream flanking). For *cgoX*, flanking regions were amplified using JC631/632 (upstream flanking) and JC633/508 (downstream flanking). Mutagenesis of this locus was confirmed with PCR using primers JC427/428.

For inactivation of *gsaM*, the transposon insertion mutant was transduced to *S. aureus* Newman WT and Δ*gsaM2* as described previously (312) using bacteriophage φ-85. Inactivation of *isdC* was performed by transducing the *isdC*::*erm* allele into Newman Δ*gtrR* as described previously (312) using bacteriophage φ-85 and confirmed with PCR using primers AF75 and AF1-4.

Complementation of *S. aureus* heme synthesis phenotypes

To complement heme synthesis phenotypes, the gene(s) were cloned from *S. aureus* Newman genomic DNA with homology to pOS1 P_{lgt} digested with NdeI and BamHI (NEB), and ligated using NEB Hi-fi assembly mix. Complementation plasmids were confirmed by restriction digest after isolated from DH5α following transformation, transformed to *S. aureus* RN4220 by electroporation, and transduced as described previously (312) using bacteriophage φ-85. Primers used were JC P447/448 for *uroS*, JC449/450 for *uroD*, JC449/451 for *uroD-cpfC-cgoX*, JC449/4509 for *uroD-cpfC*, and JC449/510 for *uroD* with homology to *cgoX*, and JC511/512 with homology to *uroD* for *uroD-cgoX*. After generation of merodiploids, 2 µM heme was included in every step to complement heme deficiency.

Growth in carbon-limited medium

For growth in a semi-defined carbon-limited medium (CLM; modified from (287)), strains were grown to stationary phase in 5 mL of TSB. The cultures were diluted 1:100 into CLM medium with or without 0.02% glucose and OD_{600} was monitored over time. CLM consisted of 0.64 g/L NaCl, 0.15 g/L KCl, 0.01 g/L MgSO4-7H2O, 7 g/L K2HPO4, 2 g/L KH2PO4, 1 g/L (NH4)2SO4, 1 mg/L thiamine, 1.2 mg/L niacin, 0.25 mg/L calcium pantothenate, 5 µg/ml biotin, and 0.5% cas-amino acids.

Inactivation of *E. coli gsaM*

gsaM of *E. coli* MG1655 was inactivated using lambda red recombination as described elsewhere (313). Primers JC85/86 were used to amplify the kanamycin resistance casette from pKD4, in which the 5' 40 bp of JC85 aligns to the 5' of *gsaM*, and the 5' 40 bp of JC 86 aligns 3' of *gsaM*. 50 µg/ml aminolevulinic acid was included in each step following transformation of the PCR product. Insertional inactivation was confirmed with colony PCR using JC P87/88. To demonstrate ALA auxotrophy, MG1655 and *gsaM*::*kan* were streaked to LBA or LBA supplemented with 50 µg/ml ALA.

Anaerobic growth

For anaerobic experiments, a Coy (Grass Lake, MI) anaerobic chamber was used, filled with a mix of 90% nitrogen, 5% carbon dioxide, and 5% hydrogen gases, and hydrogen levels are monitored to ensure a minimum of 2% hydrogen concentration. Palladium catalysts (Coy) were used to remove any residual oxygen by reaction with hydrogen. A Coy static incubator was maintained at 37° C. Solutions and plastic-ware were allowed to equilibrate for >24 h inside the glove-box before use. For anaerobic samples, strains were streaked to TSA and grown aerobically for 24 h at 37° C. Single colonies of WT, and a few colonies for each other strains were used to overnight cultures in 2 ml TSB in aeration tubes and grown anaerobically without shaking at 37° in four biological replicates. After 14 h, the cultures were diluted 1:100 into 200 µl of TSB or RPMI + 1% cas-amino acids, both supplemented with water (vehicle) or 40 mM nitrate (from sodium nitrate; Fisher). Growth was monitored in a BioTek plate reader with shaking at 37°.

Table 5 Bacterial strains used in Chapter III			
Species	**Genotype**	**Description**	**Reference**
S. aureus strain Newman	WT	Wildtype laboratory stock	(277)
S. aureus strain Newman	Δ*gtrR*	In frame deletion of *NWMN_1566*	(97)
S. aureus strain Newman	*gsaM*	Transposon insertion in *NWMN_1561*	This study; (279)
S. aureus strain Newman	Δ*gsam2*	In frame deletion of *NWMN_1756*	This study
S. aureus strain Newman	*gsaM* Δ*gsaM2*	*gsaM* transposon allele transduced into Δ*gsaM2*	This study
S. aureus strain Newman	*pbgS*	In frame allelic exchange with *ermC* gene, transduced into Newman; *NWMN_1562*	(97)
S. aureus strain Newman	Δ*uroS*	In frame deletion of *NWMN_1563*	This study
S. aureus strain Newman	Δ*uroD*	In frame deletion of *NWMN_1725*	This study
S. aureus strain Newman	Δ*uroD* Δ*cpfC*	In frame deletion of *NWMN_1724* and *NWMN_1725*	This study
S. aureus strain Newman	Δ*uroD* Δ*cgoX*	In frame deletion of *NWMN_1723* and *NWMN_1725*	This study
S. aureus strain Newman	Δ*uroD* Δ*cgoX* Δ*cgoX*	In frame deletion of *NWMN_1723, NWMN_1725, and NWMN_1725*	This study
S. aureus strain Newman	Δ*cgoX*	In frame deletion of *NWMN_1723*	This study
S. aureus strain Newman	Δ*chdC*	In frame deletion of *NWMN_0550*	(64)
S. aureus strain Newman	Δ*isdC*::*erm*	Allelic exchange inactivation of *isdC* (*NWMN_1042*)	(113)
S. aureus strain Newman	Δ*isdC*::erm Δ*gtrR*	Δ*isdC*::*erm* transduced to Δ*gtrR*	This study
E. coli MG1655	WT		
E. coli MG1655	*gsaM*::*kan*	Insertional inactivation of gsaM (*b0154*)	This study

Table 6 Plasmids used in Chapter III		
Plasmid	**Description**	**Reference**
pKOR1	Allelic exchange vector for *S. aureus*	(311)
pKOR1-*uroS*	Vector to delete *uroS*	This study
pKOR1-*uroD*	Vector to delete *uroD*	This study
pKOR1-*uroD-cpfC*	Vector to delete *uroD* and *cpfC*	This study
pKOR1-*uroD-cgoX*	Vector to delete *uroD* and *cgoX*	This study
pKOR1-*uroD-cpfC-cgoX*	Vector to delete *uroD, cpfC,* and *cgoX*	This study
pKOR1-*cgoX*	Vector to delete *cgoX*	This study
pOS1 P_{lgt}		(314)
pOS1 P_{lgt}*uroS*	*uroS* complementation vector	This study
pOS1 P_{lgt}*uroD*	*uroD* complementation vector	This study
pOS1 P_{lgt}*uroD-cpfC*	*uroD-cpfC* complementation vector	This study
pOS1 P_{lgt}*uroD-cgoX*	*uroD-cgoX* complementation vector	This study
pOS1 P_{lgt}*uroD-cpfC-cgoX*	*uroD-cpfC-cgoX* complementation vector	This study

Table 7 Primers used in Chapter III	
Primer name	**Sequence**
JC291	GGGCCCGAGCTTAAGACT
JC292	GATATCCCCTATAGTGAGTCGTATTAC
JC29	TAAGCTCGGGCCCCGCAGTTCTAGTAGC
JC30	CTTCCTTAAAAGTTATTATATCAACCTCTTTTAA
JC31	TTAAAAGAGGTTGATATAATAACTTTTAAGGAAG
JC32	GTAATACGACTTACTTCATAAGCTTGTCTAG
JC49	ATTGTCGCAACACTTATATTTGGA
JC46	GTCATAATTTAAAACAACGTGTCG
JC415	TATAGGGGATATCAGAAAATAATCTAGAGCAATCCG
JC416	AAATTTCATTTATTTAAACGTCACTCCATTATTTAATG
JC417	GACGTTTAAATAAATGAAATTTGATAGACATAGAAG
JC418	GGCCAGTCTTAAGCTCGGGCCCAAGTAAATTCCTCCTACAGTTTATG
JC184	GATATGGACCCAGACGATACAATTG
JC189	CAGAACCAGCTTTGATTAATAACGAATCAC
JC419	TATAGGGGATATCTGACATTTATTATAAAACATATGACG
JC420	TAAAACTATGATATGCACCATAAAGGCCTC
JC421	TATGGTGCATATCATAGTTTTACATTGAAGCAC
JC422	GGCCAGTCTTAAGCTCGGGCCCAACGTTTCACGCTTCTTTC
JC500	CACTATAGGGGATATCTGACATTTATTATAAAACATATGACG
JC501	TCTTTCGTCATTAATTATGCACCATAAAGGCCTC
JC502	ATGGTGCATAATTAATGACGAAAGAAGCGTGAAAC
JC503	CCAGTCTTAAGCTCGGGCCCACTTACAACTCTGCGATTACTTC
JC504	TGTAAAACTATGATTAATTATGCACCATAAAGGCCTC
JC507	GTCTATATTTTAAGTTAATTGTTGGATGGTGTTG
JC508	GACGGCCAGTCTTAAGCTCGGGCCCAACGCCTATACCTTCTGAAAAAG
JC505	TTTATGGTGCATAATTAATCATAGTTTTACATTGAAGCAC
JC506	TCCAACAATTAACTTAAAATATAGACTTGATTTCATCAAC
JC423	ATCCAACAATTAACTATGCACCATAAAGGCCTC
JC424	TATGGTGCATAGTTAATTGTTGGATGGTGTTG
JC425	GGCCAGTCTTAAGCTCGGGCCCAACGCCTATACCTTCTGAAAAAG
JC631	CGACTCACTATAGGGGATATCTTATTAGCACCATGGAATG
JC632	CATCCAACAATTAACAACGTTTCACGCTTCTTTC
JC633	GAAGCGTGAAACGTTGTTAATTGTTGGATGGTGTTG
JC427	GCAATGGTATCAATCGGGACTTAAAAC
JC428	GAATGGTTCAGGACAGAGTCGAA
AF75	CAT AGC TGATGAACGTTGTTCTG
AF1-4	GGGGACCACTTTGTACAAGAAAGCTGGGTGCAAATAACATATATTGCTTTTTAT
JC447	GGGGCATATGAAGCCAGTTGTAGTTATG
JC448	GGGCGGATCCGCCTTAGCCCCTACTTTCTAAAATC
JC449	AAATACAATTGAGGTGAACATATGATGGTGCATAATAAAAACAATAC
JC450	AAACACTACCCCCTTGTTTGGATCCTTATCTTTGTGTATATGTGTGTACG
JC451	AAACACTACCCCCTTGTTTGGATCCTTACAACTCTGCGATTACTTC
JC509	AAACACTACCCCCTTGTTTGGATCCTTAAAATATAGACTTGATTTCATCAAC
JC510	TCTTTCGTCATTATCTTTGTGTATATGTGTGTACG
JC511	ACAAAGATAATGACGAAAGAAGCGTGAAAC
JC512	AAACACTACCCCCTTGTTTGGATCCTTAACTTACAACTCTGCGATTACTTC
JC85	ATGAGTAAGTCTGAAAATCTTTACAGCGCAGCGCGCGAGCGTGTAGGCTGGAGCTGCTTC
JC86	TCACAACTTCGCAAACACCCGACGTGCAGCATCGATGGTGCATATGAATATCCTCCTTAG
JC87	GCGGCTCGAGATGAGTAAGTCTGAAAATCTTTACAGCGCAGCGCGC
JC88	GGCCGCGGCAGATCCTCTTCTGAGATGAGTTTTTGTTCCAACTTCGCAAACACCCGA

Results

S. aureus synthesizes heme *de novo* using nine enzymes encoded from three (and potentially four) genomic loci (Figure 16A). Glutamyl-tRNA is committed to heme biosynthesis by GtrR (Figure 16B) and proceeds to heme. To first assess the essentiality and redundancy of each biosynthetic enzyme to *S. aureus* heme synthesis, I created a series of mutants and compared their growth to previously characterized heme synthesis mutants. (Figure 16C). Inactivation of *gtrR* (97), *pbgS* (97), *uroS*, *uroD*, *cgoX*, and *chdC* (64) results in heme auxotrophy and these mutants adopt the small colony variant phenotype associated with inactive cellular respiration. Inactivation of *hmbS* has not been attempted to date. Inactivation of *cpfC* was extensively attempted without success, which is likely due to the inherent toxicity of coproporphyrin III, which would build up in a strain lacking *cpfC* but with intact upstream heme biosynthesis. However, *cpfC* has been deleted by another group in *S. aureus*, albeit without demonstrating complementation (62). To confirm that *cpfC* can be inactivated if upstream enzymes are inactivated to eliminate coproporphyrin III build up, *uroD* and *cpfC* were deleted together. This mutant strain is viable and is a small colony variant, and is complemented by both genes *in trans* (Figure 17). The Δ*uroD* Δ*cpfC* mutant has similar growth to the Δ*uroD* Δ*cgoX* and Δ*uroD* Δ*cpfC* Δ*cgoX* mutant strains.

Of note, inactivation of either *gsaM*, *gsaM2*, or both does not create heme deficiciency (Figure 16). While Δ*gsaM2* appears wildtype in colony morphology, a mutant lacking *gsaM* or *gsaM* and *gsaM2* has slightly smaller and hyperpigmented colonies.

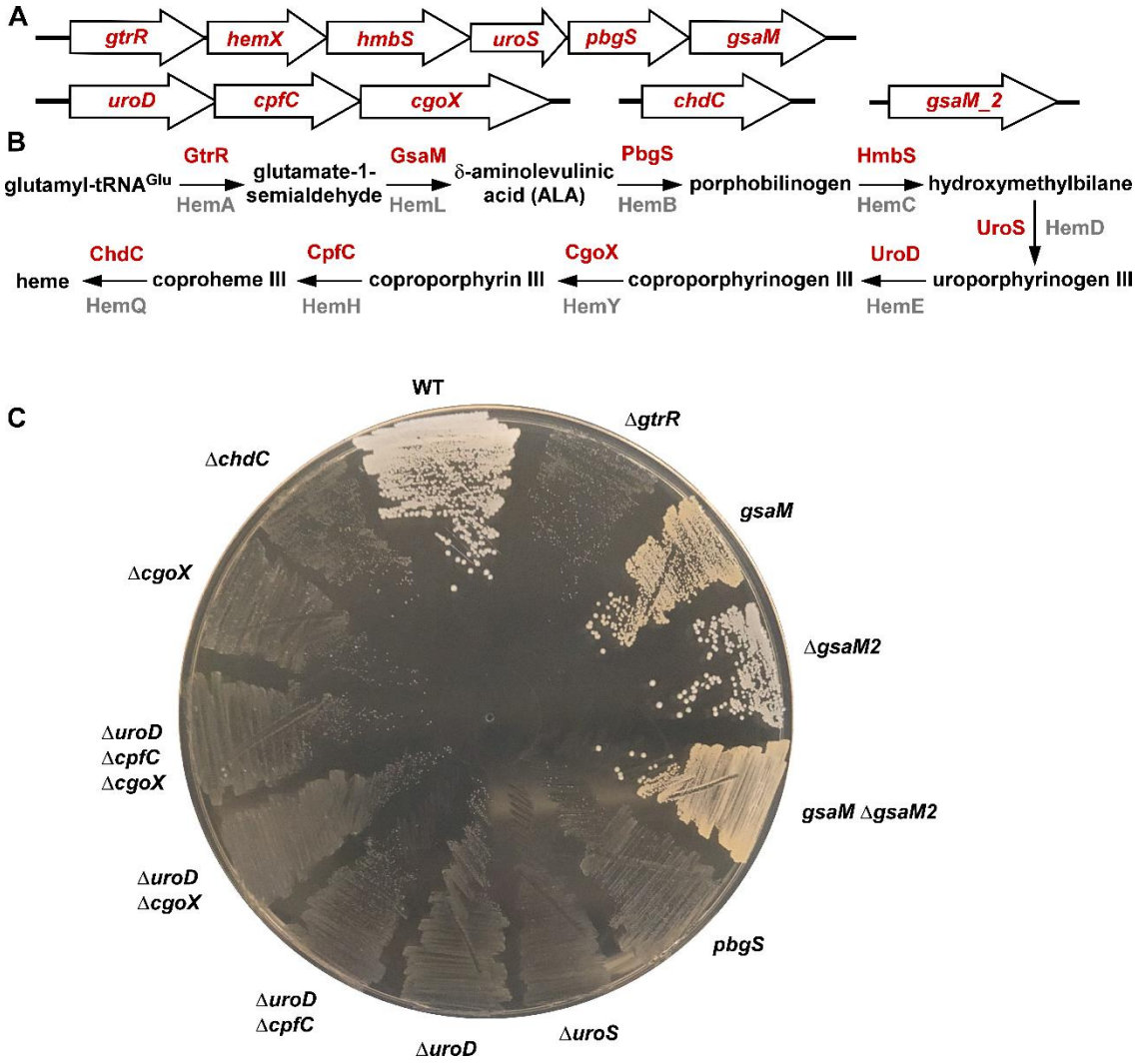

Figure 16 Genetic inactivation of most heme biosynthesis genes blocks heme synthesis. (A) The genes encoding heme biosynthesis enzymes are located at four chromosomal loci. **(B)** An overview of the *S. aureus* heme biosynthetic pathway. In red are the updated enzyme names set forth by Dailey and colleagues (51), which correspond to the previously used gene locus names in gray. **(C)** Genetic inactivation of most of the steps of the heme biosynthesis pathway blocks heme synthesis. TSA plate was imaged 24 h after streaking strains from freezer stock.

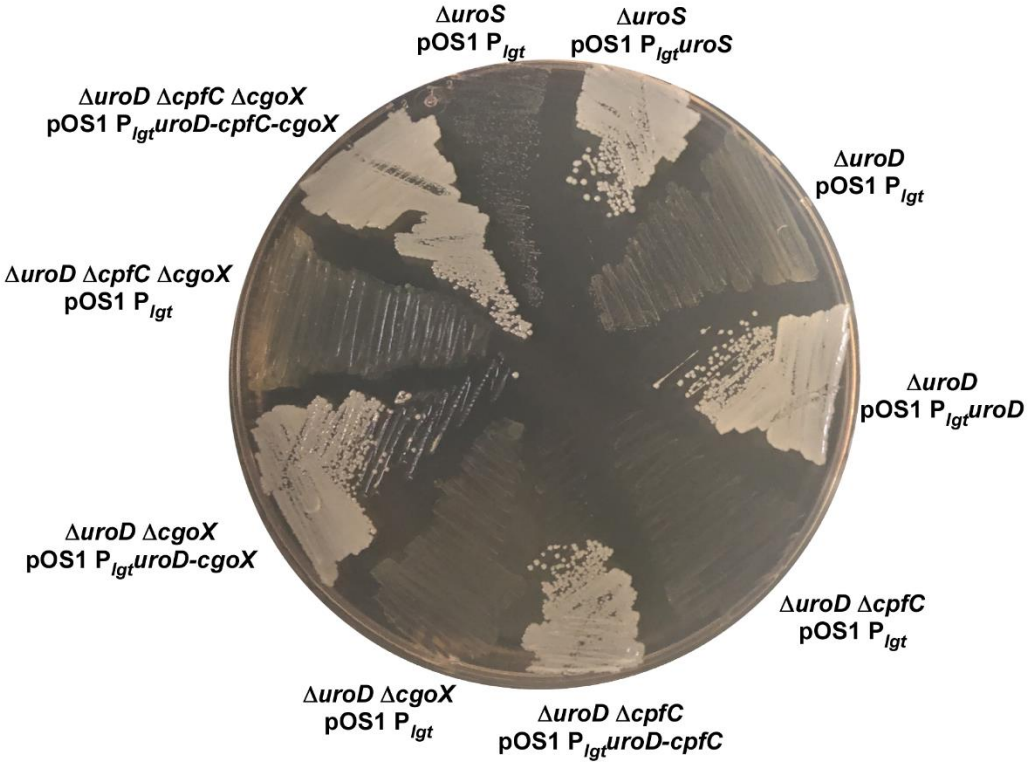

Figure 17 Complementation of terminal heme synthesis mutants. Previously uncharacterized mutants with in-frame deletions of terminal heme synthesis genes are shown, encoding the vector pOS1 P_{lgt} with or without the complementing gene(s). Shown is growth after 24 h on TSA containing chloramphenicol.

In performing these studies, I routinely complemented the small colony variants with exogenous heme. While the Isd system (Chapter I) is the only known active heme uptake system in *S. aureus*, it is expressed only under iron limitation and co-expressed with heme oxygenases. Therefore, I hypothesized that complementation of heme auxotroph SCVs is likely through passive diffusion of the lipophilic heme molecule. Consistent with this hypothesis, inactivation of the Isd system by deleting *isdC* does not affect the ability of low concentrations of exogenous heme to complement the Δ*gtrR* small colony variant (Figure 18).

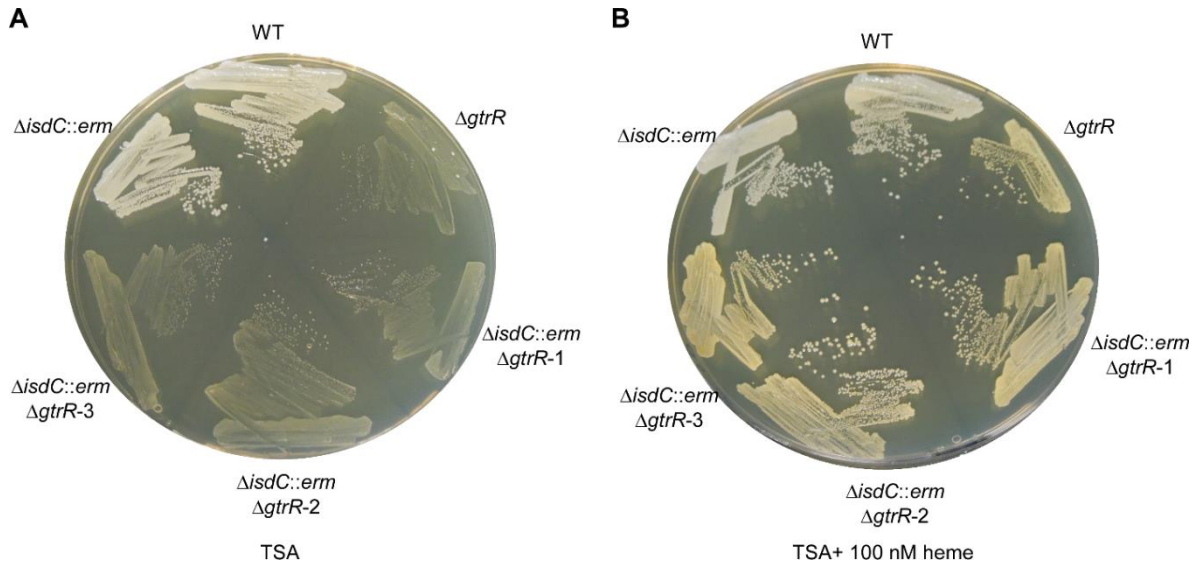

Figure 18 Heme synthesis mutants do not require Isd heme uptake for complementation with exogenous heme. *S. aureus* WT and strains lacking either *isdC*, *gtrR*, or both after 24 h of growth on **(A)** TSA **(B)** TSA supplemented with 100 nM heme.

Next, to investigate further the contribution of either *gsaM* genes to heme biosynthesis, I turned to aerobic growth to more sensitively measure growth of strains lacking one or both of the annotated *gsaM* genes. Growth in a semi-defined carbon limited medium, with glucose supplemented as the primary carbon source, shows that inactivation of either *gsaM* does not affect growth (Figure 19A). These conditions require heme synthesis, as the Δ*gtrR* mutant grows very poorly. However, in conditions without glucose and heme-independent glycolysis, a modest growth defect is observed in strains lacking *gsaM* but not *gsaM2* (Figure 19B). These data suggest that *gsaM* is only partially required for heme synthesis, and *gsaM2* may not be at all.

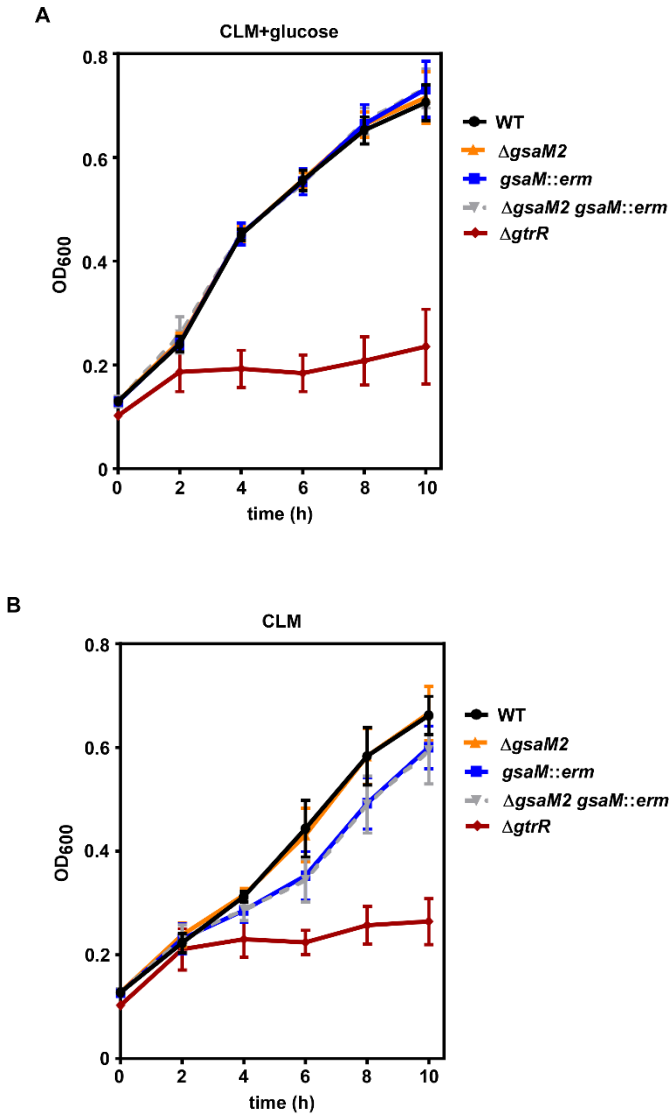

Figure 19 GsaM contributes modestly to respiration dependent growth. *S. aureus* strains as shown were grown aerobically in carbon-limited medium **(A)** with glucose or **(B)** without glucose supplementation. Growth was monitored over time by measuring OD_{600}.

To corroborate findings in *Salmonella* and create a resource to investigate *S. aureus* GsaM function, we insertionally inactivated *gsaM* in *E. coli* MG1655. This mutant is a heme auxotroph (not shown) that can be complemented with exogenous ALA (Figure 20). This mutant can be used to measure the contribution of *S. aureus gsaM* and *gsaM2* to the conversion of ALA when ectopically expressed in *E. coli gsaM*::*kan.*

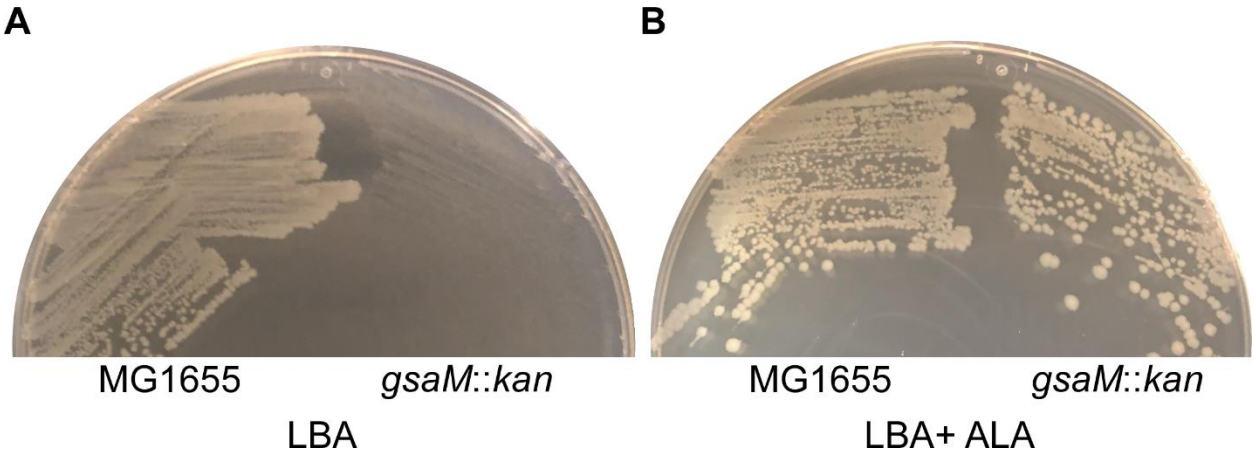

Figure 20 *E. coli* GsaM is required for heme biosynthesis. [M.R. in part] *E. coli* MG1655 WT or a strain with *gsaM* inactivated grown on **(A)** LBA or **(B)** LBA containing 50 µg/ml ALA. Shown is growth after 24 h.

Thus far, I have demonstrated that most genes are required for heme biosynthesis, in the presence of oxygen. I next turned to CgoX to investigate the presence or absence of a second oxygen-independent coproporphyrinogen oxidase. The obvious gene is *hemN*, NWMN_1486, annotated as oxygen-independent coproporphyrinogen oxidase. However, recent work in *E. coli* and *Lactococcus lactis* (315, 316) has found that often this annotation is incorrect for reasons that are true for *S. aureus* (Figure 21). NWMN_1486, when aligned to a bona fide coproporphyrinogen oxidase from *E. coli*, is missing the N-terminal 47 amino acids that are critical for substrate recognition, and the fourth cysteine of the radical SAM motif has been mutagenized to a phenylalanine in *S. aureus*. As such, NWMN_1486 is likely not an anaerobic coproporphyrinogen oxidase.

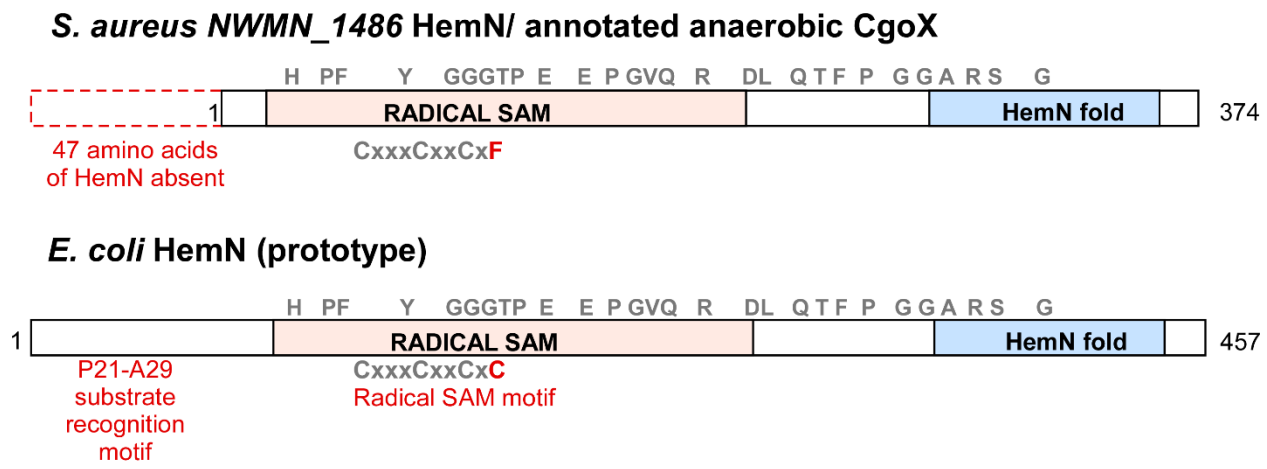

Figure 21 *S. aureus* NWMN_1486 lacks key features of an anaerobic coproporphyrinogen oxidase. A model of the primary sequence of the annotated HemN/anaerobic coproporphyrinogen oxidase of *S. aureus* (top) and *E. coli* (bottom). Gray indicates amino acids conserved between proteins, red indicates divergent amino acids that are critical to function of *E. coli* HemN.

Therefore, I considered the other remaining possibilities-that an enzyme of the DUF1444 domain-containing family performs as an oxygen-independent coproporphyrinogen oxidase as previously suggested (51), or that CgoX functions anaerobically and aerobically. To test the latter hypothesis, I compared growth under anaerobic conditions in medium that requires heme synthesis for full growth rate and yield. In both TSB (which contains glucose) and RPMI supplemented with cas-amino acids and the non-fermentable carbon source glycerol, the alternative terminal electron acceptor nitrate enhances growth by allowing anaerobic respiration, which relies on heme. However, inactivation of either *cgoX* or the *uroD-cpfC-cgoX* operon prevents heme-dependent respiration in anaerobic media (Figure 22). These data suggest that *cgoX* is required for anaerobic heme synthesis.

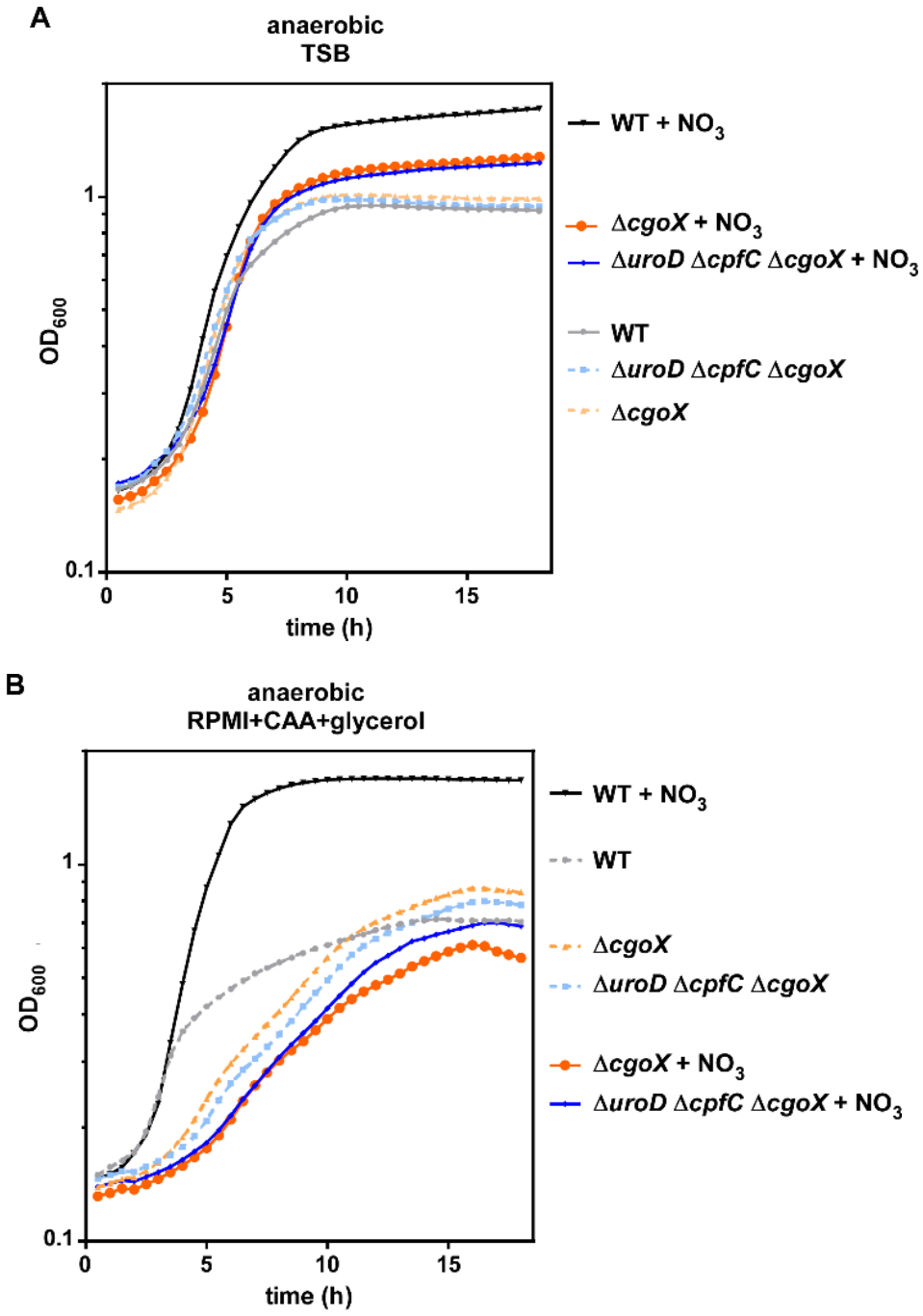

Figure 22 CgoX is required for anaerobic heme-dependent growth. Growth of *S. aureus* WT, Δ*cgoX*, and Δ*uroD* Δ*cpfC* Δ*cgoX* was monitored over time in an anaerobic chamber in **(A)** TSB or **(B)** RPMI supplemented with cas-amino acids and glycerol in the presence or absence of the alternative terminal electron acceptor nitrate. Shown are the means of a single experiment in biological quadruplicate for each medium.

Discussion

In this chapter, I find that while most of *S. aureus* heme synthesis enzymes function as expected from annotation and the literature of other species, there are a few exceptions. First, the enzymatic conversion of glutamate-1-semialdehyde to ALA by GsaM remains a question. The genes annotated as *gsaM* and *gsaM2* are not required for heme production, but GsaM may contribute modestly (Figures 16, 19). This is consistent with the rapid non-enzymatic conversion of glutamate-1-semialdehyde to ALA, but inconsistent with *in vivo* evidence in *E. coli* (Figure 20). Experimentally, there is no evidence that GsaM2 is a glutamate-1-semialdehyde-2,1-aminomutase. However, expression of GsaM and GsaM2 in *E. coli gsaM*::*kan* could test if these proteins can perform glutamate-1-semialdehyde-2,1-aminomutase function. Further work is needed to determine if another gene encodes a glutamate-1-semialdehyde-2,1-aminomutase that is responsible for heme synthesis in the absence of *gsaM*.

Most notably, in this chapter I present evidence that the annotated CgoX is required for heme synthesis anaerobically and anaerobically (Figures 21 and 22). This is consistent with an incorrect annotation of HemN (NWMN_1486) as an anaerobic coproporphyrinogen oxidase, and underscores the need for further biochemicil analyses of CgoX in the presence and absence of oxygen. Taken together, work in this chapter has helped define genetically the requirements for *S. aureus* heme synthesis and provides preliminary evidence to suggest that more is to be learned in both early and late steps of heme production by this organism.

CHAPTER IV

STAPHYLOCOCCUS AUREUS HEMX MODULATES GLUTAMYL-TRNA REDUCTASE ABUNDANCE TO REGULATE HEME BIOSYNTHESIS

A version of the following section (Chapter IV, *Staphylococcus aureus* HemX modulates glutamyl-tRNA reductase abundance to regulate heme biosynthesis was previously published in *mBio* 9(1). pii: e02287-17 (February 2018)
doi: 10.1128/mBio.02287-17.

Introduction

The tetrapyrrole cofactor heme is critical to the physiology of organisms from humans to bacteria. Heme is composed of a porphyrin ring complexed to iron at its center, making it an excellent redox-active moiety for a variety of enzymes. Across kingdoms, heme is used to shuttle electrons in the respiratory chain and is also required for the function of many critical proteins including nitric oxide synthase, catalase, and hemoglobin. To satisfy the cellular need for heme, most heme-dependent organisms synthesize heme *de novo* from simple and abundant precursors.

The versatility of heme as a cofactor is based on its reactivity, which also results in its toxicity at high concentrations through a largely unknown mechanism. Excess heme can cause damage to cellular macromolecules, accumulate in the membrane and likely cause damage (96, 237) and the redox cycling of heme-iron may produce reactive oxygen species via Fenton chemistry (317). Bacteria encode a variety of mechanisms to resist heme toxicity (317), but the most important of these strategies may be the prevention of self-imposed toxicity by regulating endogenous heme synthesis. A variety of transcriptional and post-transcriptional strategies have evolved to regulate heme synthesis centered around providing sufficient heme to occupy hemoproteins while preventing excess heme synthesis to limit unnecessary consumption of substrates and preclude toxicity.

In this study, I sought to uncover regulatory pathways controlling heme synthesis in the human pathogen, *Staphylococcus aureus*. *S. aureus* is a Gram-positive bacterium that causes a variety of devastating diseases including skin and soft tissue infections, osteomyelitis, endocarditis, and bacteremia (318). *S. aureus*, as a facultative anaerobe, generates energy through aerobic respiration, anaerobic respiration, or fermentation. The final step in aerobic respiration is reduction of oxygen to water, which *S. aureus* performs with

either of the heme-dependent QoxABCD or CydAB terminal oxidases (97, 256). Although a great deal is known about heme synthesis, heme utilization, and heme toxicity in *S. aureus*, no heme synthesis regulatory pathway has been identified in this organism. *S. aureus* encodes the newly appreciated coproporphyrin-dependent heme synthesis pathway to populate its hemoproteins (43, 62). These include the terminal oxidases, catalase, and bacterial nitric oxide synthase, all of which contribute to growth, protection from host defenses, and pathogenesis (97, 319-321). In conditions of excess exogenous heme, the heme stress response in *S. aureus* is activated by the heme sensing two-component system HssRS which regulates the transcription of a putative efflux pump HrtAB. This system is critical for growth and survival in toxic concentrations of heme and modulates pathogenesis in a murine model of disease (244). Sensing or regulatory pathways that connect heme synthesis with heme availability, hemoprotein abundance, or HssRS activation have not been identified.

S. aureus synthesizes δ–aminolevulinic acid (ALA), the first dedicated and universal precursor for protoheme synthesis, via the conversion of glutamyl-tRNA to glutamate-1-semialdehyde by glutamyl-tRNA reductase (GtrR) and subsequent production of ALA by glutamate-1-semialdehyde 2,1- aminomutase (322-324). Uroporphyrinogen is the precursor to heme, siroheme, and other tetrapyrroles, and the stepwise transformation of ALA to uroporphyrinogen comprises the core of the synthesis pathway. The pathway from uroporphyrinogen to heme was historically considered to be universally conserved for all organisms. However, the field's understanding of bacterial heme synthesis has undergone a revolution as recent studies uncovered diversity in bacterial strategies to convert uroporphyrinogen to heme (reviewed in ((51)). Gram-positive bacteria proceed through a coproporphyrin-dependent branch (43, 62, 63) which is unique from the classic protoporphyrin-dependent branch in humans and many Gram-negative model organisms.

In this work, I identify GtrR abundance as a critical regulator of *S. aureus* heme synthesis. GtrR is post-transcriptionally maintained at low abundance in heme-proficient cells by the membrane protein HemX, but levels increase when *S. aureus* is deprived of heme. Without HemX regulation, GtrR abundance increases which results in the concomitant increase in flux through the heme synthesis pathway and accumulation of heme. This excess heme synthesis activates HssRS and disrupts iron homeostasis. Together, this report reveals that *S. aureus* regulates heme synthesis by modulating GtrR abundance via intracellular heme levels and the widely conserved HemX.

Materials and methods

Bacterial strains and reagents

Bacterial strains (Table 8), plasmids (Table 9), and primers (Table 10) are listed in the specified table. *S. aureus* strains were grown routinely on tryptic soy agar (TSA) or broth (TSB) supplemented with 10 µg/mL chloramphenicol or 10 µg/mL erythromycin when necessary. When used, heme (hemin chloride) was used at concentrations noted. Heme was prepared fresh at 10 mM in 0.1 M NaOH; for experiments in which heme was used, an equal volume of 0.1 M NaOH was used for all conditions. *E. coli* strains were grown on lysogeny broth (LB) or LB agar (LBA), supplemented with 50 µg/mL carbenicillin when necessary. For growth in liquid medium, an Innova44 incubator shaking at 180 rpm was used. For standard cultures of 4-5 mL, 15 mL round bottomed polypropylene tubes with aeration lids were used, at a 45° angle in the incubator. For cloning and mutagenesis in plasmids, all constructs were confirmed by sequencing (GeneWiz). Unless noted otherwise, all chemicals are from Sigma. All molecular biology reagents were New England Biolabs and used according to manufacturer's instructions, unless otherwise noted. Phusion 2X Hi-fidelity master mix was used for all PCR reactions for cloning. As necessary, plasmids were transformed by electroporation from *E. coli* into the *S. aureus* cloning intermediate strain RN4220 before isolation and subsequent electroporation into final *S. aureus* strains.

Table 8 Bacterial strains used in Chapter IV				
Species	**Strain**	**Genotype**	**Description**	**Source**
S. aureus	Newman	WT	Wildtype, methicillin sensitive clinical isolate	(277)
S. aureus	Newman	*pbgS*	*pbgS* (*NWMN_1562*) gene interrupted with erythromycin resistance gene *ermB* by homologous recombination, transduced into Newman	(97)
S. aureus	Newman	Δ*chdC*	In-frame unmarked deletion of *chdC* (*NWMN_0550*) generated by allelic exchange	(64)
S. aureus	Newman	Δ*hemX* Δ*chdC*	In-frame unmarked deletion of *chdC* (*NWMN_0550*) generated by allelic exchange in Δ*hemX*	This work
S. aureus	Newman	Δ*menB*	In-frame unmarked deletion of *menB* generated by allelic exchange	(237)
S. aureus	Newman	Δ*qoxB cydB*	In-frame unmarked deletion of *qoxB* and *cydB*::*Tn*	(97)
S. aureus	JE2	*katA*	*katA*::*Tn (NE1366*)	BEI; (279)
S. aureus	Newman	*katA*	*katA*::*Tn (NE1366*), transduced into Newman	This work
S. aureus	Newman	Δ*hemX*	In-frame unmarked deletion of *hemX* (*NWMN_1565*)	This work
S. aureus	RN9011		RN4220 carrying pRN7023 integrase plasmid	(325)
S. aureus	RN9011	::P_{lgt}	pJC1111 P_{lgt} integrated into chromosome at *attC* locus	This work
	RN9011	::P_{lgt}*hemX*	pJC1111 P_{lgt}*hemX* integrated into chromosome at *attC* locus	This work
S. aureus		Δ*hemX*::P_{lgt}	pJC1111 P_{lgt} integrated into chromosome at *attC* locus	This work
S. aureus		Δ*hemX* ::P_{lgt}*hemX*	pJC1111 P_{lgt}*hemX* integrated into chromosome at *attC* locus	This work
S. aureus	Newman	::P_{lgt}	pJC1111 P_{lgt} integrated into chromosome at *attC* locus	This work
S. aureus	Newman	*sodA sodM*	Antibiotic cassette insertion mutants	(326)
S. aureus	Newman	Δ*hemX sodA sodM*	In-frame unmarked deletion of *hemX* (*NWMN_1565*) in *sodA sodM* strain	This work
S. aureus	Newman	Δ*hemX pbgS*	In-frame unmarked deletion of *hemX* (*NWMN_1565*) in *pbgS* strain	This work
S. aureus	Newman	Δ*hssRS*	In-frame unmarked deletion of *hssRS* generated by allelic exchange	(42)
S. aureus	Newman	Δ*hrtB*	In-frame unmarked deletion of *hrtB* generated by allelic exchange	(327)
S. aureus	Newman	*hrtB*	*hrtB*::*Tn*(PhiNE01762)	(244)
S. aureus	Newman	Δ*hemX hrtB*	*hrtB*::*Tn*(PhiNE01762) allele transduced to Δ*hemX*	This work
S. aureus	JE2	*cysG*	*cysG::Tn (NE1931; SAUSA300_2553::Tn)*	BEI;(279)
S. aureus	Newman	*cysG*	*cysG::Tn (NE1931)* transduced into Newman	This work
S. aureus	Newman	Δ*hemX cysG*	*cysG::Tn (NE1931)* transduced into Newman Δ*hemX*	This work
S. aureus	JE2	*nirD*	*nirD::Tn (NE1279)*	BEI; (328)
S. aureus	Newman	*nirD*	*nirD::Tn (NE1279)* transduced into Newman	This work
S. aureus	Newman	Δ*hemX nirD*	*nirD::Tn (NE1279)* transduced into Newman Δ*hemX*	This work
S. aureus	Newman	Δ*gtrR-hemX*	In-frame unmarked deletion of *gtrR* and *hemX (NWMN_1566-1565)* generated by single allelic exchange	This work
S. aureus	RN4220		Restriction deficient cloning intermediate strain	(280)
S. aureus	Newman	*hrtAB*::*kan*	Allelic exchange of *hrtAB* with kan^R (*ahpA-3*)	This work
S. aureus	Newman	Δ*hemX hrtAB*::*kan*	Allelic exchange of *hrtAB* with kan^R (*ahpA-3*) in Δ*hemX*	This work
S. aureus	Newman	Δ*hssRS hrtAB*::*kan*	Allelic exchange of *hrtAB* with kan^R (*ahpA-3*) in Δ*hssRS*	This work
E. coli	BL21 DE3		Protein expression strain	NEB
E. coli	EC55	Δ*phoA*	*phoA* mutant	Horswill lab (329)

Table 9 Plasmids used in Chapter IV		
Plasmid	**Description**	**Source**
pKOR1	Temperature sensitive allelic exchange vector	(311)
pKOR1-*hemX*	Allelic exchange vector for deletion of *hemX*	This work
pKOR1-*hrtAB*::*kan*	Allelic exchange vector for exchange of *hrtAB* with kan^R (*ahpA-3*)	This work
pXen1 (*luxABCDE*)	Promoterless plasmid encoding *Photorhabdus luminescens* luciferase operon (*luxABCDE*), carbenicillin (*E. coli*) and chloramphenicol (*S. aureus*) selection	Xenogen; (110)
pXen1 P_{hrt}*luxABCDE*	*hrtAB* promoter cloned in pXen1	(110)
pOS1 P_{hrt}*xylE*	*hrtAB* promoter driving *xylE* expression; carbenicillin (*E. coli*) and chloramphenicol (*S. aureus*) selection	(244)
pOS1 P_{isdA}*gfp*	*isdA* promoter driving *gfp* expression	This work
pOS1 P_{lgt}	*lgt* (constitutive) promoter	(314)
pOS1 P_{lgt}*hemX*	*hemX* cloned in pOS1 P_{lgt}	This work
pJC1111	carbenicillin (*E. coli*) and cadmium chloride (*S. aureus*) selection	Torres lab; (325)
pJC1111 P_{lgt}	Integration vector with constitutive promoter	This work
pJC1111 P_{lgt}*hemX*	*hemX* cloned in pJC1111 P_{lgt}	This work
pOS1 P_{lgt}*gtrR*	*gtrR* cloned in pOS1 P_{lgt}	This work
pOS1 P_{lgt}*gtrR-hemX*	*gtrR-hemX* cloned in pOS1 P_{lgt}	This work
pET15b.*gtrR*	*gtrR* cloned in pET15b for His-tagged affinity purification	This work
pOS1 P_{lgt}*hemX_Y17A*	Y17A point mutation in HemX	This work
pOS1 P_{lgt}*hemX_H135A*	H135A point mutation in HemX	This work
pOS1 P_{lgt}*hemX_G203A*	G203A point mutation in HemX	This work
pBAD33	*E. coli* expression vector; IPTG inducible promoter	Hadjifrangiskou lab; (330)
pBAD33.*hemX_phoA*	C-terminal fusion of phoA to *hemX*	This work
pBAD33.*hemX:N244_phoA*	*phoA* inserted between N244 and S245 of *hemX*	This work
pBAD33.*hemX_phoA Y17A*	Y17A point mutation in HemX	This work
pBAD33.*hemX_phoA H135A*	H135A point mutation in HemX	This work
pBAD33.*hemX_phoA G203A*	G203A point mutation in HemX	This work
pBAD33.*hemX_phoA Y231A*	Y231A point mutation in HemX	This work

Table 10 Primers used in Chapter IV	
Primer name	**Sequence**
JC291	GGGCCCGAGCTTAAGACT
JC292	GATATCCCCTATAGTGAGTCGTATTAC
JC105	TCACTATAGGGGATATCGCGTTTCAAATGCATTTTATTG
JC106	TTATTTCTCATTATTCAAAACTAAAGATACGTCG
JC108	GTTTTGAATAATGAGAAATAATCTAGAGCAATCC
JC109	CTTAAGCTCGGGCCCTTTATAAAAGAATTTCACAGCATTTTTAG
JC103	TCACTATAGGGGATATCTTGATGTGTTATAAAAGTGAAAAGC
JC104	TTATTTCTCATTGAAACGCCCCCATATATAC
JC107	GCGTTTCAATGAGAAATAATCTAGAGCAATCC
JC157	GGGGGGCATATGCAAGAAAACCTGTTTATTCGATTCAATG
JC155	GGGCGGATCCGGCTCAATTCACAAAATGTGTTGC
CG38	ACGATCCGGGGAATTCCATATGTTATTTGTAGAGCTCATCCATGCCATG
CG39	CTTGTTTGGATCCTCGAGGGATCCATGCCCGGGAGCAAAGGA
CG50	GCCGAAGAATTCCAAAACATAATCCTCCTTTTTATG
CG51	GCCAAGCATATGGTTGTTTTCCTCCTAAGGATACAA
JC101	GCGGCATATGGCCATGCATTTTATTGCAATTAGTAT
JC102	GCGGGGATCCGCCTTATTCAAAACTAAAGATACGTC
JC83	GTGATTTTAGTCATACGCGCTTC
JC84	GAACCCTGATATTTCAATTGCTG
JC53	TTTGTTCCGAAATTGTTGCA
JC54	GAAAGATCCTATTAAACAGGCCAAA

JC55	AACCAATCATTGAACCTGCTC
JC56	CATTTGATACGGCTTTAAGTCGT
JC81	CAGTCTTACCTGCTCGATTCC
JC82	GTGGAATATTCGTTGCCATACC
HS1	TGTTGGGTGTTGTTCCAGTG
HS2	GCTTAACCCTGGCAATTTACG
HS3	CGAGAAATGGCAAAAGAAGG
HS4	TTCTTTCGTGTGTGCCGTAG
JC158	GCCGTCGACGCCACTAATGATTTATTATGTAGTGGTTC
JC229	GGGGGAAACACTACCCCCTTG
JC184	GATATGGACCCAGACGATACAATTG
JC185	GCACCACGACGTAATGAACTAG
JC228	TAAGAAGAGATGTAAGAGTAGGG
JC229	GGGGGAAACACTACCCCCTTG
JC283	ATTATTAATAGCATTAATCAGTATCATTTGCTATTTTTATGATTTTG
JC284	ATAATTTCATTGAATCGAATAAAC
JC285	ACTGTTAGTCGCAATCGGTCTAGCTGTGTTAAG
JC286	AACTCGTCTACAACAGCAATTTTC
JC287	TATTATTTTAGCAACACAGTGGGGTG
JC288	CTAAATATGAGAATTATCCACC
JC289	TACAGTATTAGCAGGAAGTTATATTTTACTTAGAATCAAC
JC290	ATAATTGAAGAGAGTATTACCTTC
JC240	GCTAGCGAATTCGAGCTCGGTACCCGGGATTAAGGAGGAATAAATAATGCAAGAAAACCTG TTTATTC
JC241	CAGGAACTGCAACTGCATTCACAAAATGTGTTGCAAAAAATAAATTAATC
JC242	ACATTTTGTGAATGCAGTTGCAGTTCCTGTTCTGGAAAACCGG
JC243	AAGCTTGCATGCCTGCAGGTCGACTCTAGATTATTTCAGCCCCAGAGC
JC244	CAGGAACTGCAACTGCATTCAACCATTTGTTGATTC
JC245	CAAATGGTTGAATGCAGTTGCAGTTCCTGTTCTGGAAAACCGGG
JC246	CTTGAAACTGCAACTGCTTTCAGCCCCAGAGCGGC
JC247	TCTGGGGCTGAAAGCAGTTGCAGTTTCAAGATATTTAATATACTATAACATTATTTTATT
JC248	AAGCTTGCATGCCTGCAGGTCGACTCTAGATCAATTCACAAAATGTGTTG

Deletion of genes by allelic exchange

Deletion of genes were performed by allelic exchange as described in (311) with some modifications. The pKOR1 plasmids containing ~1kb homologous regions flanking upstream and downstream of the gene to be deleted were prepared using NEB Hi-Fi assembly according to manufacturer's suggestions. The pKOR1 backbone was amplified by PCR using JC291/292 which produces a linear product not including the *attB* recombination sites. The ~1kb flanking regions were amplified from *S. aureus* Newman genomic DNA. Deletions were confirmed by PCR using isolated genomic DNA and complemented by providing the gene in *cis* or *trans.* For *hemX*, flanking regions were amplified using JC105/106 (upstream flanking) and JC108/109 (downstream flanking). The allelic exchange protocol to create an in-frame unmarked deletion of *hemX* was performed in *S. aureus* WT, *pbgS*, *sodA sodM*, and Δ*chdC*. Deletion of *hemX* was confirmed by PCR using JC184/185. For deletion of *gtrR-hemX,* which are co-transcribed from adjacent positions in the chromosome, allelic exchange was performed as described above. The ~1kb flanking regions were amplified from *S. aureus* Newman genomic DNA using JC103/104 (upstream flanking) and JC107/109 (downstream

flanking). The allelic exchange protocol to create an in-frame unmarked deletion of *gtrR-hemX* was performed in *S. aureus* WT. Deletion was confirmed by PCR using JC184/185.

pOS1 P_{isdA}-*gfp* cloning

The sequence for codon optimized *gfp* was amplified from pGFP-F (328) using primers CG38/39 and subsequently assembled using Gibson Assembly into pOS1 that was digested with NdeI and BamHI. P_{isdA} was amplified from *S. aureus* Newman genomic DNA using primers CG50/51 and was ligated into pOS1 *gfp* after digestion with EcoRI and NdeI to produce pOS1 P_{isdA}*gfp*.

pOS1 P_{lgt}*gtrR* and P_{lgt}*gtrR-hemX* cloning

gtrR was amplified from *S. aureus* Newman genomic DNA using primers JC101/102, while *gtrR-hemX* was amplified using JC101/155 and ligated into pOS1 P_{lgt} after digestion of PCR products and vector with NdeI and BamHI to produce pOS1 P_{lgt}*gtrR* and pOS1 P_{lgt}*gtrR-hemX*

***hemX* chromosomal integration**

Chromosomal complementation was performed by cloning P_{lgt} or P_{lgt}*hemX* into pJC1111. P_{lgt} was PCR amplified from pOS1 P_{lgt} using JC158/229, and subsequently cloned into the multiple cloning site of pJC1111 after restriction digest with SalI and BamHI. *hemX* was cloned into pOS1 P_{lgt} by amplifying *hemX* flanked by NdeI and BamHI sites from *S. aureus* Newman genomic DNA using primers JC157/155, and ligated (T4 ligase) into multiple cloning site of pOS1 P_{lgt} after restriction digest with NdeI and BamHI. P_{lgt}*hemX* was amplified from pOS1 P_{lgt}*hemX* using JC158/155 and subsequently cloned into the SalI and BamHI sites of pJC1111 after restriction digest with SalI and BamHI. pJC1111 P_{lgt} and pJC1111 P_{lgt}*hemX* were integrated into the chromosome of strain RN9011 as described (325), then transduced into *S. aureus* Newman WT or Δ*hemX* as noted. Transductions of pJC1111 loci were performed with φ-85 as described in (312), with some modifications: after incubation of donor phage with recipient strains and washing with sodium citrate, cells were allowed to recover for 4 h in TSB with 40 mM sodium citrate at 37°C with shaking and plated to TSA containing 0.15 mM cadmium chloride.

Transduction of transposon library alleles

katA::*Tn* (NE1366), *cysG::Tn (NE1931), nirD::Tn (NE1279), and hrtB*::*Tn* (PhiNE01762) transposon alleles were transduced to *S. aureus* Newman and Δ*hemX* as listed in Table 8 as described previously (312) using bacteriophage φ-85; alleles were confirmed by an inverse PCR method and Sanger sequencing (279).

***hemX* site-directed mutagenesis**

pOS1 P_{lgt}*hemX* was subjected to site-directed mutagenesis according to NEB Q5 Site-directed mutagenesis kit. Following mutagenesis, the plasmid was transformed to DH5α, subjected to sequencing (GeneWiz) using primers JC228/229, transformed to RN4220 by electroporation, and transformed into Δ*hemX* by electroporation. Primers JC283/284 were used for Y17A, primers JC285/286 for H135A, JC287/288 for G203A, and JC289/290 for Y231A. pOS1 P_{lgt}hemX_Y231A was successfully created but no colonies were ever recovered following transformation into RN4220 despite multiple attempts.

HemX-alkaline phosphatase fusions

HemX-PhoA fusions were generated by NEB Hi-Fi assembly. Full length *hemX* without stop codon was amplified from *S. aureus* Newman genomic DNA using JC240/241; JC240 incorporates a Shine-Dalgarno sequence. *phoA* was amplified from *E. coli* MG1655 genomic DNA with JC242/243, which do not amplify the signal sequence or first five amino acids of mature PhoA, but do include sequence for an AVAV linker at the N-terminus. The PCR products of JC240/241 and JC242/243 were assembled with pBAD33 digested with SmaI and XbaI according to manufacturer's instructions. Site directed mutagenesis was performed in pBAD33 *hemX_phoA* using NEB Q5 Site Directed Mutagenesis kit with primers JC283/284 (for Y17A), JC285/286 (for H135A), JC287/288 (for G203A), and JC289/290 (for Y231A). To create pBAD33 *hemX:N244_phoA*, the nucleotide sequence for HemX residues 1-244 was amplified from *S. aureus* Newman genomic DNA using JC240/244; JC240 incorporates a Shine-Dalgarno sequence. HemX sequence encoding residues 245-271 was amplified from *S. aureus* Newman genomic DNA using JC247/248. *phoA* was amplified from *E. coli* MG1655 genomic DNA with JC245/246, which do not amplify the signal sequence or first five amino acids of mature PhoA, but do include sequence for an AVAV linker at the N- and C-termini. *hemX(1-244)-phoA-hemX(245-271)* were assembled in pBAD33 using NEB HiFi assembly according to manufacturer's instructions. Following assembly, plasmids were transformed into

DH5α, reisolated, and subjected to sequencing by GeneWiz. Plasmids were subsequently transformed to *E. coli*

***hrtAB::kan* selection strain**

hrtAB were replaced with a kanamycin resistance cassette by allelic exchange using pKOR1 as described above. The upstream flanking region was amplified from Newman genomic DNA using primers JC634/635, the downstream flanking region was amplified from Newman genomic DNA using primers JC638/639. The kanamycin resistance gene (below) was amplified using primers JC636/637, and the three fragments were ligated with NEB HiFi assembly. The kanamycin resistance gene *ahpA-3* was synthesized by IDT with a *S. aureus* codon optimized sequence based on pKAN (328) preceded by a 5' terminator, the P_{hrt} sequence, 5' PstI, XbaI, and SalI sites, and 3' BamHI and KpnI sites. The fragment sequence was cloned into pJC1111 (not further utilized) and then only the *ahpA-3* protein coding sequence was amplified using primers JC636/637 such that the gene is under control of the native chromosomal P_{hrt}. The sequence of codon optimized *ahpA-3*:

ATGGCGAAGATGCGTATATCACCTGAGTTGAAAAAGTTAATCGAAAAATATAGATGCGT
GAAGGACACTGAAGGTATGTCACCGGCTAAGGTATACAAATTAGTAGGCGAGAATGAG
AACTTATATTTAAAAATGACGGATTCAAGATACAAGGGCACTACTTACGATGTAGAAAGA
GAGAAAGATATGATGTTATGGTTGGAGGGTAAGTTACCAGTCCCGAAGGTGTTGCATTT
CGAACGTCACGATGGATGGTCTAACTTGTTGATGTCAGAAGCTGACGGCGTCTTATGTT
CAGAGGAATACGAAGACGAACAAAGTCCTGAGAAAATAATTGAGTTATATGCGGAATGT
ATCAGATTGTTCCATTCTATAGACATTTCAGATTGCCCATATACGAACTCATTGGACAGT
CGTTTGGCAGAATTGGATTACTTGTTGAATAATGACTTGGCGGATGTGGACTGTGAGAA
TTGGGAGGAGGACACACCATTCAAAGATCCGCGAGAGTTGTACGATTTTTTAAAGACAG
AGAAACCTGAAGAAGAGTTGGTTTTTTCACATGGAGATTTAGGAGATAGTAACATATTTG
TGAAGGACGGCAAGGTGTCTGGATTCATCGATTTAGGCCGATCTGGTAGAGCTGATAA
ATGGTACGATATTGCATTTTGCGTGCGTAGTATACGTGAGGATATTGGTGAAGAGCAAT
ACGTCGAGTTATTCTTCGACTTATTAGGCATAAAGCCAGACTGGGAGAAGATTAAATAC
TACATCTTATTGGACGAATTGTTCTAA

The allelic exchange of pKOR1-*hrtAB*::*kan* was performed in *S. aureus* Newman WT, Δ*hemX*, and Δ*hssRS*.

Catalase activity

To assess catalase activity, strains were grown for 16 h in TSB then 50 µL of each culture was spotted to a TSA plate and streaked for isolation. After 24 h of growth at 37°C, 50 µL of 30% H_2O_2 was added to each strain and immediately imaged.

LC-MRM-MS/MS

Strains were streaked to TSA and grown for 24 h at 37° C. Cultures were started from single colonies in 5 ml of RPMI+1% cas-amino acids and grown at 37° C for 15 h. Overnight cultures were subcultured 1:100 into RPMI+1% cas-amino acids and grown until mid-exponential phase. For small colony variants without chemical complementation, overnight cultures were sub-cultured 1:25. For conditions in which heme was added, 2 µM was used; for menaquinone, 12.5 µM of menaquinone/vitamin K_2 was used.

For anaerobic experiments, a Coy (Grass Lake, MI) anaerobic chamber was used, filled with a mix of 90% nitrogen, 5% carbon dioxide, and 5% hydrogen gases, and hydrogen levels are monitored to ensure a minimum of 2% hydrogen concentration. Palladium catalysts (Coy) were used to remove any residual oxygen by reaction with hydrogen. A Coy static incubator was maintained at 37° C. Solutions and plastic-ware were allowed to equilibrate for >24 h inside the glove-box before use. For anaerobic samples, strains were streaked to TSA and grown aerobically for 24 h at 37° C. Cultures were started from single colonies in 5 ml of anaerobic TSB and grown at 37° C for 15 h. Overnight cultures were subcultured 1:100 into anaerobic TSB containing 40 mM sodium nitrate and grown until mid-exponential phase. Protein was collected, tryptically digested, and subjected to LC-MRM-MS/MS as described below.

Cells were collected by centrifugation, washed in PBS, and resuspended in 500 µl of TSM (100 mM Tris, pH 7; 500 mM sucrose; 10 mM $MgCl_2$) containing 4 µg of lysostaphin. Cells were incubated for 60 min at 37° C. Protoplasts were collected by centrifugation and resuspended in 150 µl of PBS containing 100 µM PMSF. Protoplasts were lysed by sonication and the soluble lysate was collected after centrifugation to remove unlysed protoplasts. Protein content was quantified using the Pierce BCA Assay (Thermo) and lysate was added to 4X NuPAGE LDS sample buffer with reducing agent (Thermo) and 100 µg of total protein for each replicate was subject to brief SDS-PAGE in NuPAGE gel (Thermo) according to manufacturer's instructions.

The gel regions were excised and subjected to in-gel trypsin digestion and peptide extraction as previously described (331). Proteins were quantified with multiple reaction monitoring (332). Representative peptides for each protein were selected based on theoretical trypsin digest. Skyline software (University of Washington, MacCoss lab (333) was used to set up scheduled, targeted MRM methods and three to five MS/MS transitions were monitored per peptide.

The 20 µL digest was transferred to an autosampler vial and 4 µL sample per run was injected via autosampler (NanoAcuity HPLC system, Waters) onto a vented column setup utilizing a 40 mm by 0.1 mm (Jupiter 5 micron, 300A) kasil fritted trap followed by a 250 mm by 0.1 mm (Jupiter 3 micron, 300A), self-packed analytical column coupled directly to a TSQ-Vantage (Thermo Scientific) via a nanoelectrospray source. After trapping and equilibration, peptides were resolved using a 90-minute aqueous to organic gradient (solvent A = 0.1% FA in water and B = 0.1% FA in ACN) operating at 400 nL/min. A series of unscheduled runs determined retention times and the most useful transitions to monitor and then a scheduled instrument method encompassing a 8-minute window around the measured retention time along with calculated collision energies was created using Skyline. Q1 peak width resolution was set to 0.7, collision gas pressure was 1 mTorr, and utilized an EZ method cycle time of 3 seconds. The resulting RAW instrument files were imported into Skyline for peak-picking and quantitation. Transition or fragment ion peak areas were summed to represent the intensity of endogenous peptides, and normalized to *S. aureus* Newman GyrA as noted.

Purification of recombinant GtrR and heme binding assay

The gene encoding GtrR was cloned from Newman genomic DNA using primers JC 101/102 and ligated (NEB T4 DNA ligase)into pET15b (REF) after the vector and insert were digested with NdeI and BamHI-HF (NEB) and transformed into DH5α. The plasmid was re-isolated and subjected to sequencing using GeneWiz and subsequently transformed into BL21 DE3 pRIL using 50 µg/ml carbenicillin and 34 µg/ml chloramphenicol for selection.

For protein expression and purification, BL21 DE3 pRIL pET15b.*gtrR* was grown overnight in LB containing 50 µg/ml carbenicillin and 34 µg/ml chloramphenicol for 14 h at 37° with shaking, then subcultured 1:100 into 1.5L Terrific broth (Sigma) in a 2.8 L Fernbach flask supplemented with 50 µg/ml carbenicillin and 34 µg/ml chloramphenicol. Growth at 37° with shaking at 200 rpm was monitored and when the culture OD_{600} reached 0.5, the incubator was changed to 30° and expression was induced with 0.5 mM IPTG. After overnight growth, cells were collected by centrifugation for 10 minutes at 5,000xg and resuspended in 30 ml of 50 mM Tris (pH 8) containing 300 mM NaCl, 1 mM EDTA, 10 mM imidazole, 10% glycerol, and a protease inhibitor table (Roche). 40 µg/ml deoxyribonuclease I from bovine pancreas (Sigma) was added and the suspension was incubated on ice for 15 min, then 1 mg/ml lysozyme was added and suspension was incubated at room temperature for 20 min. The resulting suspension was lysed using an Emulsaflex. The solution was clarified by ultracentrifugation at 100,000xg for 45 min at 4°. GtrR was affinity purified using 7 ml of Ni-

NTA resin in a gravity column. The resin was washed with 50 ml of 50 mM Tris (pH 8) containing 300 mM NaCl, 1 mM EDTA, 10 mM imidazole, 10% glycerol. Cell lysate was applied to the column, washed with 75 ml of the same buffer, and GtrR was eluted from the column with 50 mM Tris (pH 8) containing 300 mM NaCl, 1 mM EDTA, 80 mM imidazole, 10% glycerol. This eluate was dialyzed at 4° in 50 mM Tris (pH 8) containing 200 mM NaCl, 1 mM EDTA, 10 mM imidazole, 10% glycerol for 1 h, then in 50 mM Tris (pH 8) containing 100 mM NaCl, 1 mM EDTA, 10 mM imidazole, 10% glycerol for 1 h, then overnight in 50 mM Tris (pH 8) containing 1 mM EDTA, 10 mM imidazole, 10% glycerol. Purified protein was quantified by BCA, assessed for purity by SDS-PAGE, and stored at -20°.

For heme binding, GtrR was diluted in 20 mM Tris (pH7.4) to 10 µM. Heme (hemin chloride) was prepared fresh in 0.1 M NaOH at 10 mM, then diluted in 20 mM Tris (pH7.4). Solutions of GtrR, heme, or combined were added to spectrophotometric cuvette and incubated for 5 min, then absorbance was measured in a Cary WinUV from 300 to 650 nm.

GtrR structure modeling

GtrR structure was modeled on Arabidopsis thaliana glutamyl tRNA reductase (334), PDB:4N7R using SWISS-MODEL (335).

XylE reporter assay

XylE abundance in cellular lysate was assessed spectrophotometrically by measuring formation of 2-hydroxymuconic acid from catechol after growth in TSB containing chloramphenicol vehicle, ALA (aminolevulinic acid HCl; stock prepared at 50 mg/ml in water), or heme, as described previously (244).

Heme toxicity and adaptation growth curves

Strains were streaked to TSA and grown for 24 h at 37°C. Single colonies were used to start 5 mL cultures of TSB and grown for 16 h at 37°C supplemented with or without heme or ALA as noted. One µL of each culture was added to 199 µL of medium containing vehicle or heme as noted in a 96 well round-bottomed plate, and growth was monitored over time at 37°C by measuring OD_{600} in a BioTek Synergy2 spectrophotometer and analyzed with BioTek Gen5 software.

Hydrogen peroxide killing assay

S. aureus strains were grown in biological triplicate overnight in aeration tubes in 5 ml TSB at 37° from single colonies. The cultures were subcultured 1:100 into 5 ml TSB in aeration tubes and allowed to grow for 3.5 h at 37°. Cells were collected, washed in 1 ml sterile PBS, and resuspended in 600 µl PBS. 40 µl of the cell suspension was added to 560 µl of PBS with or without H_2O_2 at a final concentration of 0.25%. The suspension was incubated at 37° with shaking in Eppendorf microcentrifuge tube. At each time point noted, 40 µl was removed, added to 40 µl of PBS containing 2000 U/ml catalase (filter sterilized; Sigma), serially diluted, and plated to TSA for enumeration.

Growth in paraquat

For growth in carbon-limited medium, overnight cultures in four biological replicates of each strain were grown in 5 ml TSB in aeration tube at 37. After 14 h, cultures of each strain were normalized for density by measuring OD_{600}, equal OD units were centrifuged, the cells were washed twice in PBS, and diluted 1:100 in carbon limited medium (CLM) containing glucose as described (287) containing 0 or 0.5 mM paraquat in a round bottomed 96 well plate and growth was monitored over time at 37°C by measuring OD_{600} in a BioTek Synergy2 spectrophotometer and analyzed with BioTek Gen5 software.

For growth in TSB, overnight cultures of each strain were grown in 3 ml TSB in aeration tube at 37° in biological triplicate. After 14 h, strains were subcultured 1:200 in TSB containing 0 or 10 mM paraquat in a round bottomed 96 well plate and growth was monitored over time at 37°C by measuring OD_{600} in a BioTek Synergy2 spectrophotometer and analyzed with BioTek Gen5 software.

Anaerobic growth curves

S. aureus Newman WT, Δ*hemX*, *cysG*, Δ*hemX cysG*, *nirD*, and Δ*hemX nirD* were streaked to TSA and grown aerobically for 24 h at 37° C. Cultures were started from single colonies in 3 ml of anaerobic TSB and grown at 37° C for 15 h. Overnight cultures were subcultured 1:200 in round-bottomed 96-well plates with 200 µL of anaerobic TSB containing 40 mM sodium nitrate or an equal volume of sterile water, and covered with Breathe-Easy gas permeable seal (Sigma). Growth was monitored by optical density over time in a BioTek Synergy H1.

Quantitative reverse-transcriptase polymerase chain reaction

Strains were streaked to TSA and grown at 24 h at 37° C. Cultures were started from single colonies in 5 ml of RPMI+1% cas-amino acids and grown at 37° C for 15 h. Overnight cultures were subcultured 1:100 (WT and Δ*hemX*) or 1:25 (*pbgS* Δ*hemX pbgS*) into RPMI+1% cas-amino acids and grown until mid-exponential phase. An equal volume of ice-cold acetone: ethanol was added and the mixture was stored in -80. RNA was isolated using TRI reagent, chloroform, and precipitated with isopropanol. Isolated RNA were treated with DNAse I (Thermo) according to manufacturer's instructions, and RNA was re-isolated using Qiagen RNeasy kit. cDNA was synthesized from 2 µg of RNA by incubating with M-MLV reverse transcriptase (Thermo), using transcript specific primers (JC83/84 for *gyrA*, JC53/54 for *gtrR*, and JC55/56 for *gsaM*). Quantitative PCR was performed using SYBR Green (Thermo) according to manufacturer's instructions, using primers JC81/82 for *gyrA*, HS1/2 for *gtrR*, and HS for *gsaM*. Transcript abundance was quantified using the $\Delta\Delta C_T$ method after normalization to *gyrA* abundance.

ALA quantification

ALA quantification was modified from (336). *S. aureus* WT and Δ*hemX* were streaked to TSA and grown for 18 h at 37°C. Single colonies were used to start 5 mL cultures in TSB and grown for 12 h at 37°C, then 1 mL was inoculated into 100 mL of TSB in a 250 mL Erlenmeyer flask and grown at 37°C for 14h. The cell wall was removed by incubation in TSM + 40 µg/mL lysostaphin and incubated at 37°C for 45 minutes. Protoplasts were collected by centrifugation and resuspended in 1 mL 10% TCA. Samples were incubated on ice and intermittently lysed by sonication. The soluble fraction was collected by centrifugation and neutralized to pH 7 with 6M NaOH, then added to a Dowex 1x-4 resin in column converted to acetate form before use. In this form, the column retains porphobilinogen but allows ALA to flow-through. Six hundred µL of flow-through was added to 200 µL of 8% acetylacetone in a 2 M sodium acetate buffer, incubated for 15 min at 90°C to form the pyrrolic condensation product, and cooled to room temperature. Five hundred µL of sample was added to 500 µL of modified Ehrlich's reagent, incubated for 10 min at room temperature, and the resulting absorbance was measured at 552 and 650 nm in a Cary 50 Bio UV-Vis spectrophotometer. The relative concentration of ALA was calculated based on an extinction coefficient of 7.2×10^{-4} M^{-1} cm^{-1}.

LC-qTOF-MS porphyrin quantification

S. aureus strains were streaked to TSA and grown for 18 h at 37°C. For WT, Δ*hemX*, *hrtB*, and Δ*hemX hrtB*, single colonies were used to start 5 mL cultures in TSB and grown for 10 h at 37°C. One hundred µL of this culture was inoculated into 50 mL of TSB in a 250 mL Erlenmeyer flask and grown at 37°C for 14 h. For Δ*chdC* and Δ*hemX* Δ*chdC*, multiple colonies colonies were used to start 5 mL cultures in TSB containing 2 µM heme and grown for 10 h at 37°C. Four hundred µL of this culture was inoculated into 200 mL of TSB in a 500 mL Erlenmeyer flask and grown at 37°C for 14 h. Total CFU were determined by serial dilution and plating to TSA for enumeration, and cells were collected by centrifugation and frozen at -80°C. Any negligible levels of heme measured in Δ*chdC* or Δ*hemX* Δ*chdC* is likely carry-over from the heme containing initial culture.

Porphyrin extraction. To the cell pellets, 1 mL of 1M HCl:DMSO (1:1, v/v) was added and samples vortexed, sonicated (2x2 min total, 1 sec on/1 sec off, ice, Ultrasonic Homogenizer, Biologistics Inc. Model 3000), and centrifuged (10,000 rpm, 5 min, 4°C). Supernatants were collected and kept in the dark. Pellets were resuspended in 1 mL of 1M HCl:DMSO (1:1, v/v), vortexed vigorously for 30 s twice, and centrifuged again as above. Supernatants were pooled and the resuspension/centrifugation cycle repeated. The pooled supernatants were filtered using a 0.22 µM PES syringe filter (GE Healthcare Life Sciences) and subsequently diluted to 25 mL with ddH_2O. The extracts were purified using a Sep-Pak® Vac 3cc tC_{18} cartridge (Waters 036815), eluted with 2 mL of acetonitrile + 0.1% TFA then 2 mL of methanol. Extracted porphyrins were concentrated under N_2(g) purge and resuspended in 50 µL of acetonitrile + 0.1% TFA. All samples were immediately dispensed into vials for analysis. Excess remaining samples were stored at -20°C in the dark.

Preparation of standards. 2 mM stock solutions of porphyrin standards (porphobilinogen, uroporphyrin III, coproporphyrin I and III, coproheme III, protoporphyrin IX, and heme *b*) were individually prepared in DMSO and then mixed to make a 100 µM (final concentration of each porphyrin). This stock was then diluted to 0.25-6 µM in acetonitrile + 0.1% TFA.

LC-qTOF-MS analysis. Twenty-five µL samples were diluted with 75 µL of ultrapure water immediately prior to measurement. The column (Agilent PLRP-S 100Å, 4.6x150x5 µm) was equilibrated to an 85:15 ratio of solvent A (ultrapure water with 0.1% formic acid) to solvent B (acetonitrile + 0.1% formic acid). LC separations were achieved by linear gradient elution, transitioning from 15% to 95% solvent B over 6 min followed by a 2 min hold at 95% B. The column was re-equilibrated to 15% solvent B for 2 min between injections of the same

sample (two technical replicates per sample). Two blank runs were implemented between samples (2 µL injection volume, 600 µL/min flow rate, 50°C) to ensure against column holdover of analytes. Electrospray ionization mass spectrometry analysis was carried out in positive mode with a capillary voltage of 2 Hz (Agilent 6538 UHD q-TOF).

Data were analyzed using MassHunter Qualitative Analysis Software and MZmine 2. Values for *m/z* were determined empirically for standards. From the total ion chromatogram (TIC) traces, extracted ion chromatograms (EICs) were derived for each individual standard on the basis of its mass per charge (*m/z*) in positive ion mode, which is equivalent to the exact mass of its positive ion (parent compound plus H^+). Peaks associated with each analyte were integrated and areas were plotted versus concentration (µM). Linear regression analysis (Kaleidagraph) was used to determine the correlation coefficient between integrated peak area and porphyrin concentration (slope of standard curve, m_{porph}).

All cell samples were analyzed for the full set of standards. Only analytes present above the limit of detection are reported; detection limits were at least 250 nM per injection; for a saturated culture with 10^9 CFU mL-1, this is equivalent to 250 x 10^{-9} pmoles CFU^{-1}. For the quantification of analytes from cells, values for the integrated peak intensities (measured in units of *ion counts*) were converted to units of concentration (µmol/L injected) via: counts x $(m_{porph})^{-1}$. The concentration of each analyte in the injected volumes [A] was subsequently converted to units of nmol analyte per CFU in sample as: [A] x (volume used to resuspend dried sample) x $(\text{CFUs in analyzed cell pellet})^{-1}$. Reported values are averages of technical replicates.

Pyridine hemochromagen quantification

Strains were streaked to TSA and grown for 18 h at 37°C. Single colonies were used to start 5 mL cultures of TSB and grown at 37°C for 10 h. Sixty µL of each culture was added to 6 mL of TSB and grown for 16 h at 37°C. Cells were collected by centrifugation and cell wall was removed by incubation in 20 mM potassium phosphate buffer pH 7.4 containing 20 µg of lysostaphin for 45 min at 37°C. Samples were lysed by sonication, and unbroken cells were collected by centrifugation. Four-hundred fifty µL of the soluble supernatant was added to 450 µL of 0.2 M NaOH containing 40% pyridine and 500 µM potassium ferricyanide. Absorbance was measured in a Cary 50 Bio UV-Vis spectrophotometer from 540-590 nm. Ten µL of 0.5 M sodium dithionite prepared in 0.5 M NaOH was added to samples, incubated for 5 minutes, and absorbance was measured again from 540-590 nm. Heme quantity is

calculated using $\Delta A = (557_{reduced}-557_{oxidized}) - (575_{reduced}-575_{oxidized})$ and an extinction coefficient of 32.4 mM^{-1} cm^{-1}.

Bioluminescent reporter assay

S. aureus WT and Δ*hemX* with pXen-1 or P_{hrt}*luxABCDE* were streaked to TSA-chloramphenicol prepared with 0 or 20 µM heme. After 18 h, the plates were imaged using a Xenogen IVIS 2000.

Heme killing assay

S. aureus WT, Δ*hemX*, and Δ*hrtB* were streaked to TSA and grown for 24 h at 37°C. Single colonies were used to start 5 mL cultures of TSB and grown at 37°C for 14 h. Two µL of each culture was added to 148 µL of TSB containing different concentrations of heme in a 96 well round-bottomed plate, and incubated at 37°C for 2 h. Samples were serially diluted in PBS and plated to TSA for CFU enumeration after 24 h of growth at 37°C.

The same procedure was completed for WT pOS1 P_{lgt}, Δ*hemX* pOS1 P_{lgt} Δ*hemX* pOS1 P_{lgt}*hemX*, and the mutagenized *hemX* constructs as above, except that 10 µg/ml of chloramphenicol was used throughout.

Systemic murine infections

Bacterial suspensions for infections were prepared as follows: overnight cultures for each strain were grown from single colonies in 4 ml TSB in an aeration tube at 37° for 14 h. This culture was diluted 1:100 into 5 ml TSB in a 15 ml conical tube and grown for 3.5 h at 37° in a roller drum. Bacteria were collected by centrifugation at approximately 5,000xg for 6 minutes at 4°, washed twice in ice-cold PBS, and resuspended to OD_{600} of 0.4. The suspension was serially diluted, plated to TSA, and enumerated after 24 h of growth at 37° to confirm a density of 1-2x10^7 CFU/100 µl.

Approximately 7-week old female Balb/c mice (Jackson) were anesthetized with 1.25% avertin in PBS by intraperitoneal injection and then injected with 100 µl of appropriate bacterial suspension retro-orbitally. Infections proceeded for 96 h with daily monitoring of weight and health status. Mice that reached moribund status before the endpoint were humanely euthanized with CO_2 asphyxiation. At 96 h post infection, mice were euthanized, organized were removed under sterile conditions, homogenized in sterile PBS, serially diluted and plated to TSA for enumeration following growth at 37° for 24 h.

Growth in minimal medium

Chemically defined media (CDM) supplemented with 5 mg/mL glucose was prepared as previously described (337) with the exception that iron was not added. Strains were streaked to TSA and grown for 24 h at 37°C. Single colonies were used to start 5 mL cultures in TSB and grown for 14 h at 37°C. Cells were collected by centrifugation and washed in PBS twice, then resuspended in 5 mL of PBS. One µL was added to 199 µL of CDM containing 1 µM ethylenediamine-N,N'-bis(2-hydroxyphenylacetic acid) (EDDHA; LGC Standards) or equal volume of 0.1 M NaOH (vehicle) in a 96 well round-bottomed plate. Growth was monitored for 24 h with shaking at 37°C in a BioTek EPOCH2 spectrophotometer and analyzed with BioTek Gen5 software.

pOS1 P_{isdA}*gfp* reporter assay

S. aureus WT pOS1 P_{isdA}*gfp* and Δ*hemX* pOS1 P_{isdA}*gfp* were streaked to TSA-chloramphenicol and grown for 14 h at 37°C. Single colonies were used to inoculate 5 mL cultures of TSB-chloramphenicol and grown at 37°C for 8.5 h. One µL of each culture was used to inoculate 199 µL of TSB-chloramphenicol containing 1 mM 2,2-dipyridyl or equal volume ethanol (vehicle). Growth was monitored over the course of 16 h by measuring OD_{600} nm as well as relative fluorescence at 485 nm (excitation) and 510 nm (emission) in a BioTek Cytation5 spectrophotometer and analyzed with BioTek Gen5 software.

Comparative genome analysis

With over 100,000 prokaryotic genomes currently available in public databases and many more in the pipelines (www.genomesonline.org), it is not practical or possible to perform meaningful comparative analysis on all of them simultaneously. Thus, a set of diverse representative prokaryotic genomes have been developed in the SEED database as follows. The algorithm for computing molecular operational taxonomic units (OTUs) based on DNA barcode data (338, 339) was used to group ~12,600 prokaryotic genomes available in the SEED database in October 2013 into about 1,000 taxon groups. One or two representative genomes (rarely three) for each OTU were selected based on the largest amount of published experimental data and the highest level of research interest within the scientific community. The resultant collection of 982 diverse eubacterial [928] and archaeal [54] genomes creates a manageable set that accurately represents the immense diversity of the over 12,000 prokaryotic organisms with sequenced genomes. Importantly, it is not skewed by an

overabundance of genomes for a handful of microbial genera (medically or industrially important), such as Enterobacteriaceae, streptococci, mycobacteria, etc.

The HemX protein family was exhaustively annotated for this set of 982 representative microbial genomes in the SEED database (340). Contextual associations for this family were predicted based on the patterns of co-occurrence and/or colocalization of its members with other protein families using the set of tools for comparative genome analysis available in SEED (341)) within the functional and genomic contexts provided by the subsystem "Heme Biosynthesis: protoporphyrin-, coproporphyrin- and siroheme-dependent pathways" (http://pubseed.theseed.org//SubsysEditor.cgi?page=ShowSubsystem&subsystem=Heme_Biosynthesis%3A_protoporphyrin-%2C_coproporphyrin-_and_siroheme-dependent_pathways). Phylogenetic distribution of HemX protein family was mapped onto the Tree of Life (342) and protoheme biosynthetic pathway analysis was adapted from (51).

HemX multiple sequence alignment and topology prediction

The HemX multiple sequence alignment was KEGG CLUSTALW ((343)); http://www.genome.jp; accessed 3/2017) using *Staphylococcus aureus* strain (str.) Newman, *Staphylococcus epidermidis* str. ATCC 12228, *Bacillus anthracis* str. Sterne, *Chlorobioum tepidum* str. TLS, *Aquifex aeolicus* str. VF5, *Desulfovfibrio vulgaris* str. DP4, and *Geobacter sulfurreducens* str. PCA. The transmembrane domains depicted were predicted by MEMSAT3 (http://bioinf.cs.ucl.ac.uk; accessed 3/2017) as described (55). All models were confirmed using TMHMM 2.0 ((344)); (http://www.cbs.dtu.dk; accessed 3/2017) and predictions matched across prediction servers with the exception of *Chlorobium tepidum*, which TMHMM2.0 predicts to have seven rather than eight transmembrane domains.

HemX-alkaline phosphatase assays

Single colonies were used to start 4 ml cultures of LB with chloramphenicol and grown for 16 h at 37° C. Each culture was streaked to LBA with chloramphenicol, 60 µg/ml 5-Bromo-4-chloro-3-indolyl phosphate (BCIP) and 0.1% L-(+)-arabinose. After 24 h of growth at 37° C, plates were imaged. This assay was repeated thrice, and a representative image is shown.

Statistical analysis

All data analysis and statistical tests were performed using GraphPad Prism 6 software. Replicate numbers and statistical tests for each experiment are listed in the figure legends.

Results

Heme deficiency increases GtrR abundance

To identify key steps in the regulation of heme synthesis (Figure 23A), we measured the abundance of each biosynthetic enzyme by liquid chromatography-multiple reaction monitoring-tandem mass spectrometry (LC-MRM-MS/MS). This technique allows for quantification with high resolution of even very-low-abundance cellular proteins (332). I hypothesized that comparing the *S. aureus* wild type (WT) to a strain incapable of synthesizing heme (*pbgS* mutant) (Figure 23A) would allow the identification of specific steps in heme synthesis that respond to cellular heme content, directly or indirectly. Abundance of GtrR is approximately 30-fold higher in the *pbgS* mutant relative to the WT, while the abundances of all other biosynthetic enzymes are nearly unchanged (Figure 23B). In WT cells, GtrR abundance is low relative to other heme synthesis enzymes (Figure 24). The *pbgS* mutant is a heme auxotroph and therefore adopts the respiration-deficient small-colony variant (SCV) phenotype. SCVs arise as the result of inactivation of respiration via inactivation of heme synthesis, the terminal oxidases, or the electron carrier menaquinone, and SCVs have a dramatically different physiology than respiration-proficient cells (101). Therefore, I sought to determine whether the increase in GtrR abundance in the *pbgS* mutant was the result of heme deficiency or a general defect in respiration. To confirm that the menaquinone auxotroph SCV Δ*menB* strain and the Δ*qoxB cydB* strain lacking both terminal cytochrome oxidases synthesize heme despite being unable to respire, each strain was streaked onto agar and assessed for catalase activity (Figure 23C). Activity of the heme-dependent catalase KatA leads to the production of oxygen bubbles when hydrogen peroxide is added. The Δ*menB* and Δ*qoxB cydB* mutants produce bubbles, demonstrating that these SCVs synthesize heme and are not heme auxotrophs. We measured GtrR abundance in a variety of SCV strains by LC-MRM-MS/MS. GtrR abundance increases relative to the WT only in *pbgS* and Δ*chdC* strains (Figure 23A and D), which are heme auxotroph SCVs (Figure 23C). When chemically complemented with heme, GtrR abundance returned to WT levels for both strains. GtrR levels do not increase in the Δ*menB* or Δ*qoxB cydB* strain. Together these data demonstrate that the abundance of GtrR is low in heme-proficient cells but increases specifically in response to heme deficiency.

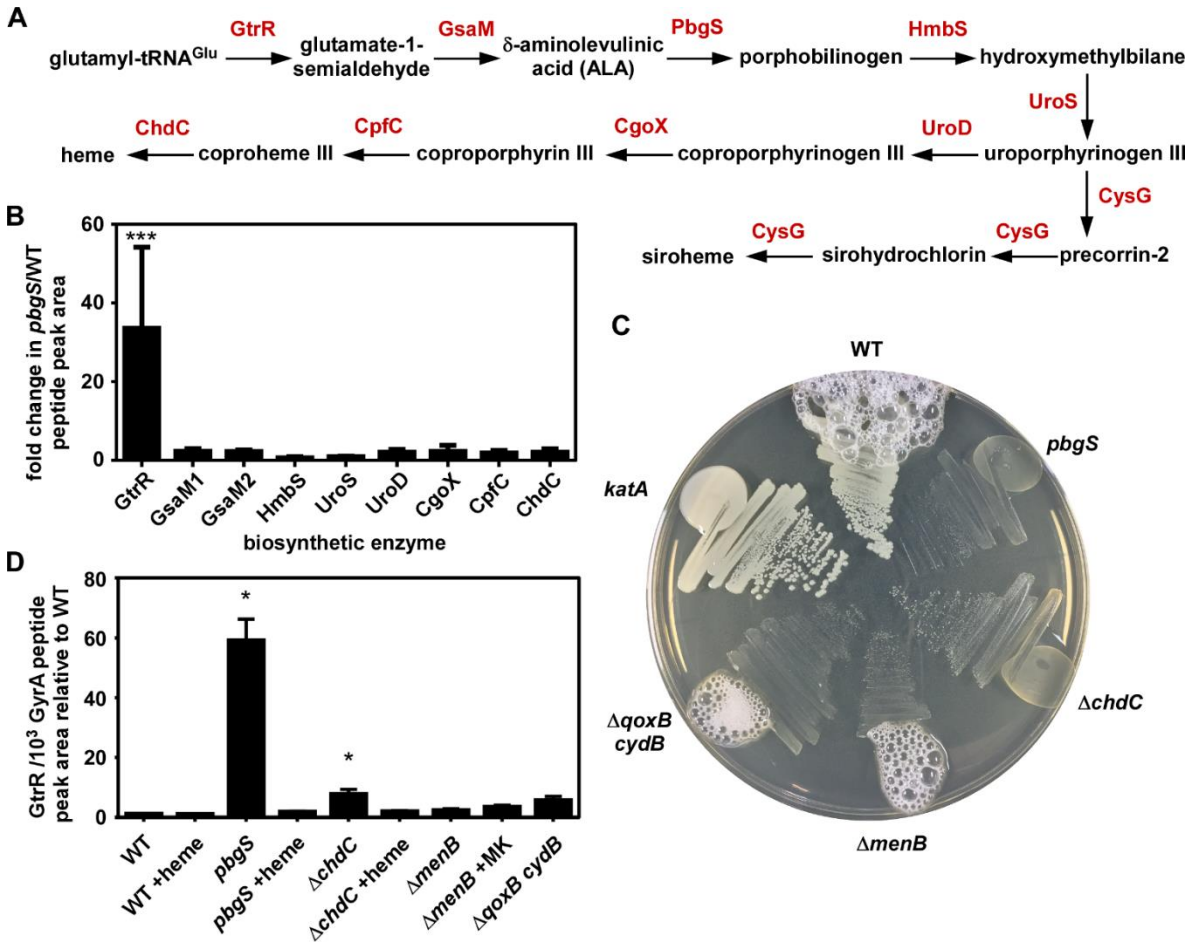

Figure 23 Heme deficiency increases GtrR abundance. (A) The heme and siroheme biosynthesis pathways in *S. aureus*. **(B)** The abundance of each biosynthetic enzyme was measured by LC-MRM-MS/MS and quantified by integrated chromatogram peak areas. Graphed is the ratio of each enzyme abundance in a strain lacking *pbgS* relative to WT *S. aureus*; the data are the average of a single experiment performed in biological triplicate with standard deviation shown. Statistical significance was determined using a one-way ANOVA with Dunnett's correction for multiple comparisons, using a reference value of 1.0; *** $P<0.001$. **(C)** *S. aureus* strains listed were streaked to rich agar medium plates and after growth, hydrogen peroxide was added at the perimeter of each streak. **(D)** The abundance of GtrR was measured by LC-MRM-MS/MS in *S. aureus* strains treated with vehicle, heme, or menaquinone (MK). The data are the average of a single experiment performed in biological triplicate with standard deviation shown. Statistical significance was determined using a one-way ANOVA with Dunnett's correction for multiple comparisons, comparing GtrR abundance for each condition relative to WT; * $P<0.05$

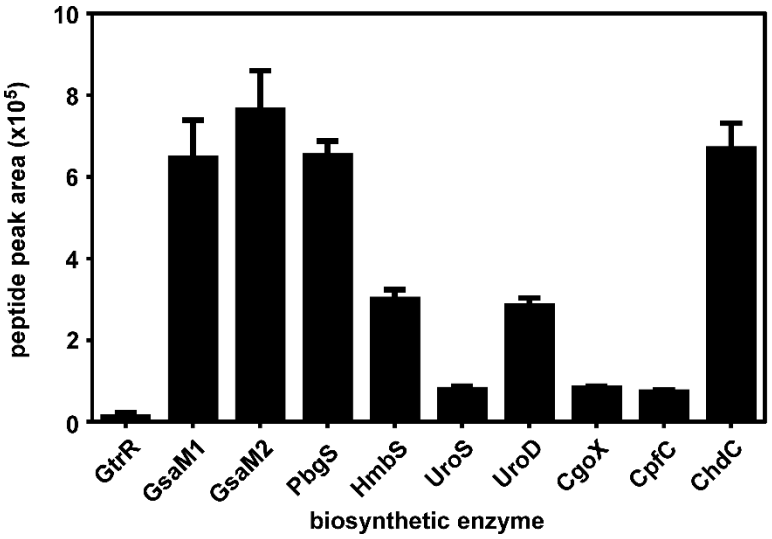

Figure 24 GtrR abundance is uniquely low among heme synthesis enzymes. Shown is the abundance of each heme synthesis enzyme as measured by LC-MRM-MS/MS in WT cells. The data are the average from a single experiment performed in biological triplicate with standard deviation shown.

Recombinant GtrR binds heme

Considering that GtrR levels change in abundance depending on the ability to synthesize heme, I hypothesized that GtrR my directly bind heme and thereby affect its own abundance. To assess heme-binding capabilities, GtrR was recombinantly expressed in *E. coli* and purified to homogeneity. Purified GtrR was incubated in the presence or absence of heme and absorbance was measured. Consistent with ability to bind heme, the presence of GtrR resulted in a Soret shift. The peak absorbance of heme alone was a broad peat at around 395 nm, but in the presence of GtrR, the peak became sharper and centered around 413 nm (Figure 25).

Because the prediction of non-covalent heme-coordinating motifs in hemoproteins are challenging to predict, we turned to structural homologs. Using SWISS-MODEL (335), we identified the glutamyl tRNA reductase of *Arabidopsis* as a GtrR homolog with solved crystal structure (Figure 26). We modeled GtrR and found it conformed well to the *Arabidopsis* protein, with the monomer forming one half of a predicted V-shaped dimer, as also observed in other glutamyl tRNA reductases (324). However, no heme ligand was observed in the solved crystal structure. Therefore, identification of the heme-binding residues of GtrR, and the impact of heme binding on GtrR regulation, remains to be investigated.

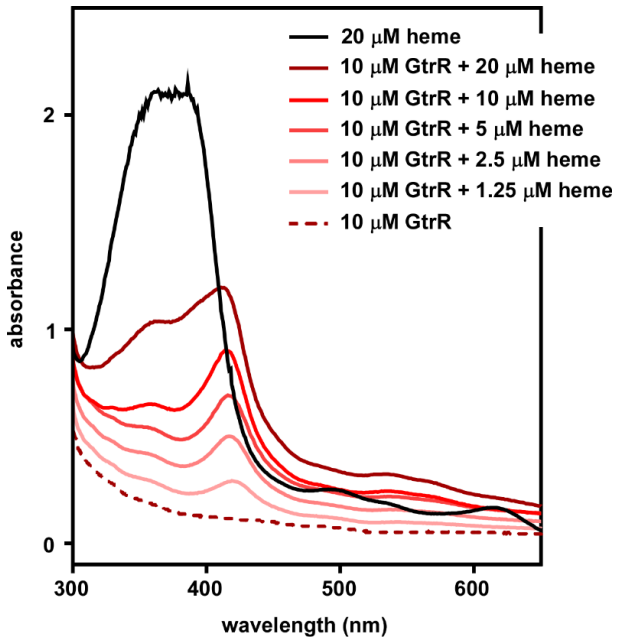

Figure 25 Recombinant GtrR binds heme. GtrR expressed recombinantly and purified from *E. coli* was assessed for ability to bind heme by measuring absorbance with and without increasing concentrations of heme added.

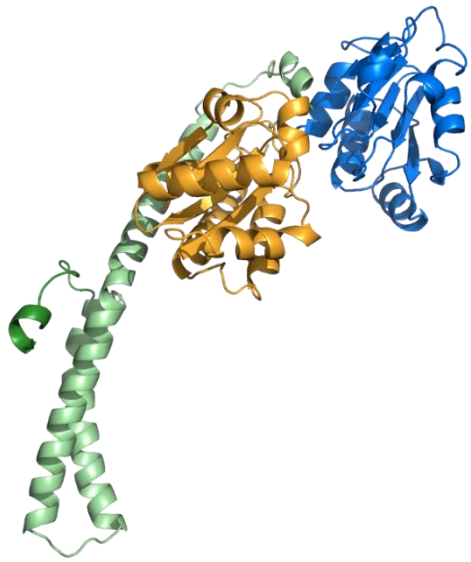

Figure 26 A model of GtrR monomer. [H.K.] The structure of GtrR was modelled on *Arabidopsis* glutamyl tRNA reductase (PDB:4N7R), with C-terminal dimerization domain (dark green, truncated in model), N terminal catalytic domain in orange, and NADPH binding domain in blue.

Excess ALA is sufficient to increase heme synthesis and activate HssRS

Upon observation that GtrR protein abundance was specifically modulated in response to heme deficiency, I hypothesized that changes to GtrR abundance would be sufficient to increase intracellular heme levels. As ALA is considered a rate-limited intermediate, and glutamate-1-semialdehyde is a short-lived intermediate that may spontaneously convert to ALA (Chapter III), I tested whether exogenous ALA could enhance endogenous heme biosynthesis. First, I measured activation of P_{hrt} by HssRS as a proxy for intracellular heme levels, based on the supposition that excess heme synthesis could activate HssS. Indeed, ALA supplementation induced P_{hrt} activation in an HssRS dependent manner (Figure 27A). Next, to test whether this level of P_{hrt} induction was physiologically relevant, I measured the ability of ALA to pre-adapt *S. aureus* to heme toxicity. *S. aureus* grown overnight in medium containing heme or ALA subsequently displays a reduced lag time when grown in toxic concentrations of heme (Figure 27B). This pre-adaptation is the result of HssRS-mediated induction of the HrtAB efflux pump.

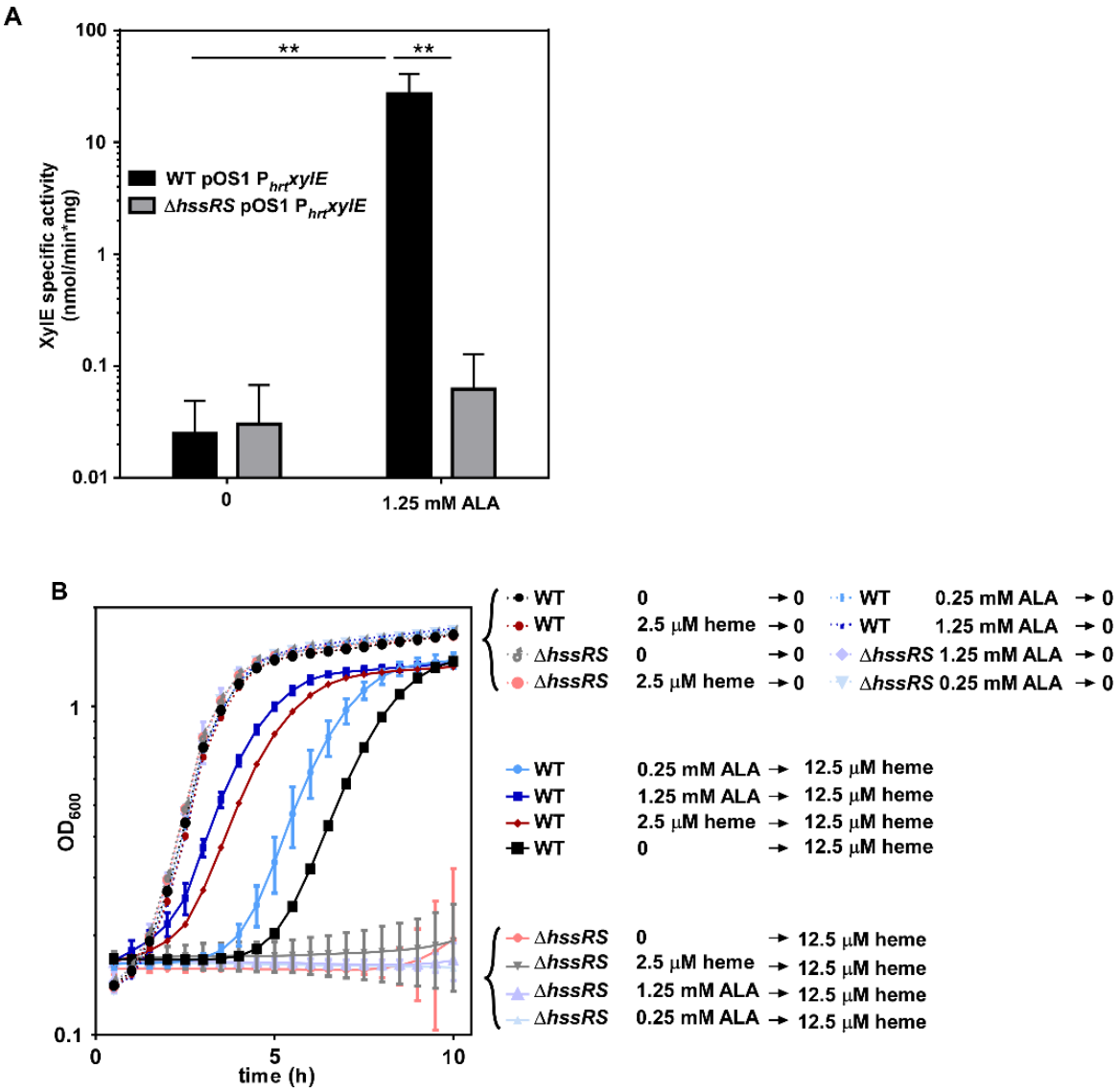

Figure 27 Excess ALA is sufficient to increase heme synthesis and activate HssRS. (A) XylE assay measuring P_{hrt} activation in the presence or absence of the heme precursor ALA. **(B)** Heme adaptation assay in which isogenic mutants are grown in 0 or 12.5 μM heme following pre-growth in TSB containing vehicle, 2.5 μM heme, or ALA. For both, graphed are the means of three independent experiments in biological triplicate. For A ** indicates $p<0.01$ by one-way ANOVA with Sidak correction for multiple comparisons.

HemX controls GtrR abundance in heme-proficient cells to regulate heme synthesis

Among both Gram-negative and Gram-positive bacteria, regulation of GtrR abundance is a common feature of heme synthesis regulation pathways (70, 75, 82). In the model organism *Bacillus subtilis*, which is also a member of the Firmicutes phylum, GtrR abundance is impacted by the membrane protein HemX through an unknown mechanism (75, 345). While *S. aureus* is in the same Bacillales order as *B. subtilis*, *S. aureus* heme homeostasis is distinct because of its access to host heme and its resistance to heme toxicity mediated by HssRS. Both *B. subtilis* and *S. aureus* encode an operon comprised of *gtrR-hemX-hmbS-uroS-pbgS-gsaM* (formerly *hemAXCBDL*) (47, 346). I therefore hypothesized that in *S. aureus*, HemX also impacts GtrR abundance in heme-proficient cells. I created an in-frame unmarked deletion of *hemX* and integrated either pJC1111 P_{lgt} or P_{lgt}*hemX* at a neutral site in the chromosome (24). GtrR abundance was measured by LC-MRM-MS/MS and is increased in Δ*hemX*::P_{lgt} relative to WT::P_{lgt} (Figure 28A). The phenotype can be complemented when *hemX* is provided in *cis*, showing that it is the result of deletion of *hemX* and not other effects of disrupting the operon. These data are consistent with the hypothesis that HemX regulates GtrR abundance in heme-proficient cells (75, 345).

I next sought to determine whether the increase in GtrR at the protein level in both *pbgS* and Δ*hemX* is the result of an increase in mRNA transcript abundance of *gtrR*. Therefore, *pbgS* and Δ*hemX* were grown to mid-exponential phase and RNA was isolated, converted to cDNA, and quantified with quantitative polymerase chain reaction (Figure 28C). The steady state mRNA abundance of *gtrR* transcript is unchanged in Δ*hemX* or *pbgS* relative to WT, suggesting that the increase in GtrR abundance in these strains is not the result of a transcriptional change. Additionally, the increase in GtrR levels in *pbgS* is not affected by the insertion of *ermB* to interrupt the *pbgS* gene, which is upstream of *gsaM* in the operon; there is no change in the transcript abundance of *gsaM* in *pbgS* relative to WT (Figure 29).

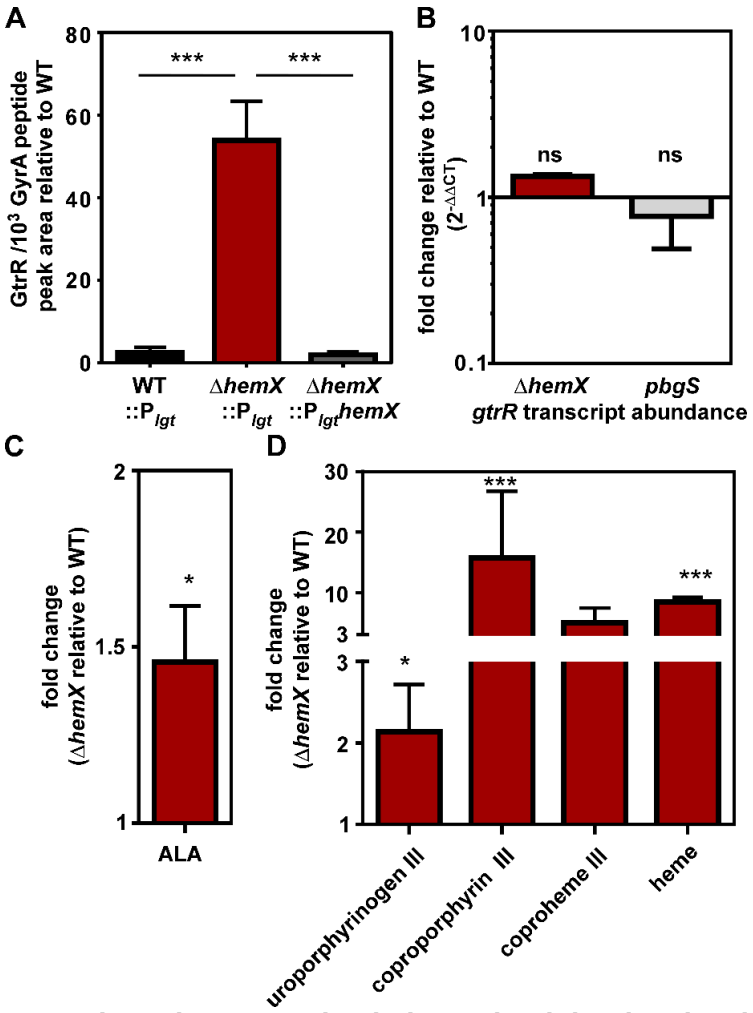

Figure 28 HemX regulates heme synthesis by maintaining low levels of GtrR in heme proficient cells [A.I.C: panel D]. (A) The abundance of GtrR was measured by LC-MRM-MS/MS in multiple *S. aureus* strains. The data are the average of a single experiment performed in biological triplicate with standard deviation shown. Statistical significance was determined using a one-way ANOVA with Dunnett's correction for multiple comparisons, comparing GtrR abundance for each strain relative to Δ*hemX*::P_{lgt}; *** P<0.001. **(B)** Steady state transcript abundance of *gtrR* mRNA isolated from mid-exponential growth of *S. aureus* strains was measured by q-RT-PCR and is graphed as fold change relative to WT. Data are combined from two independent experiments with biological triplicate and standard deviation shown. ns indicates no significance by one-way ANOVA with Dunnett's correction for multiple comparisons, comparing fold change of *pbgS* and Δ*hemX* to WT. **(C)** δ-aminolevulinic acid (ALA) abundance was measured in *S. aureus* strains by a spectrophotometric quantification. Graphed is fold change of ALA in Δ*hemX* relative to WT, with data combined from two independent experiments with three biological replicates with standard error of the means shown. **(D)** Uroporphyrinogen III (detected as uroporphyrin III), coproporphyrin III, coproheme III and heme were quantified by LC-qTOF-MS. Graphed is fold change of metabolite abundance in Δ*hemX* relative to WT, from a single experiment performed in biological triplicate with standard error of the means shown. For C and D, statistical significance was determined with Student's *t*-test comparing Δ*hemX* to WT before data transformation to fold change; * P<0.05, *** P<0.0001.

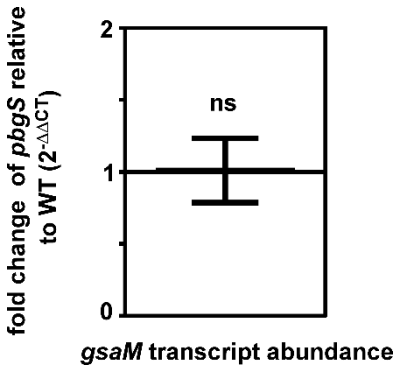

Figure 29 The *pbgS* allele is not polar on *gsaM* transcription. Steady-state transcript abundance of *gsaM* mRNA isolated from mid-exponential growth of *S. aureus* strains was measured by qRT-PCR and is graphed as fold change relative to the WT. Data are combined from two independent experiments in biological triplicate with standard deviation shown. "ns" indicates no significance by one-way ANOVA with Dunnett's correction for multiple comparisons, comparing fold change of the *pbgS* mutant to the WT.

I hypothesized that the increase in GtrR observed in Δ*hemX* would increase the amount of heme synthesized by increasing abundance of the heme precursors downstream of GtrR. As glutamate-1-semialdehyde is unstable and can convert to δ–aminolevulinic acid (ALA) in the absence of enzyme (45), I measured ALA abundance via a colorimetric method. ALA abundance increases approximately 50% in Δ*hemX* relative to WT (Figure 28C). We subsequently sought to determine the impact of increased ALA availability on downstream heme intermediates and heme abundance. Total cellular porphyrins were extracted from WT and Δ*hemX* and analyzed by quantitative exact-mass liquid chromatography-quadrupole time of flight mass spectrometry (LC-qTOF-MS); total extracted ion chromatograms for porphyrins that were observed above the limits of detection are shown in Figure 30, where a dramatic change in porphyrin levels is visible. Based on standard curves for individual porphyrins (including porphobilinogen, uroporphyrin I and III, coproporphyrin I and III, coproheme III, protoporphyrin IX, and heme *b*) and enumeration of colony forming units, absolute quantifications were obtained and referenced per cell for each porphyrin molecule; data are presented in Figure 28D in terms of fold-change relative to WT. As shown in Figure 28D; Δ*hemX* exhibits increased abundance of uroporphyrin III, coproporphyrin III, coproheme III, and heme *b* relative to WT. Notably, because samples were prepared aerobically, the metabolite uroporphyrinogen III was detected as uroporphyrin III, in which its methylene-bridge carbons have spontaneously oxidized in air; likewise, any coproporphyrinogen III that might have been present would be detected as the oxidation product, coproporphyrin III, which is also the product of the enzyme CgoX (Figure 23). Hydroxymethylbilane spontaneously

cyclizes to uroporphyrinogen I, which is decarboxylated by UroD to coproporphyrinogen I. The absence of uroporphyrin or coproporphyrin I isomers indicates that hydroxymethylbilane did not accrue in Δ*hemX.* I hypothesize that, in the presence of excess GtrR, the initial step of the pathway may no longer be rate limiting. This may allow other subsequent steps in the pathway to become partly rate-limiting, leading to the observed pattern of metabolite accumulation. Finally, the increase in heme abundance in Δ*hemX* observed by LC-qTOF-MS is complemented when *hemX* is provided in *cis* from a neutral site in the chromosome as measured by the pyridine hemochromagen method (Figure 32A). Together, these data demonstrate that inactivation of *hemX* results in increased GtrR abundance, which increases abundances of both early and late-pathway biosynthetic precursors and cellular heme. Therefore, dysregulation of GtrR alone is sufficient to disrupt heme homeostasis.

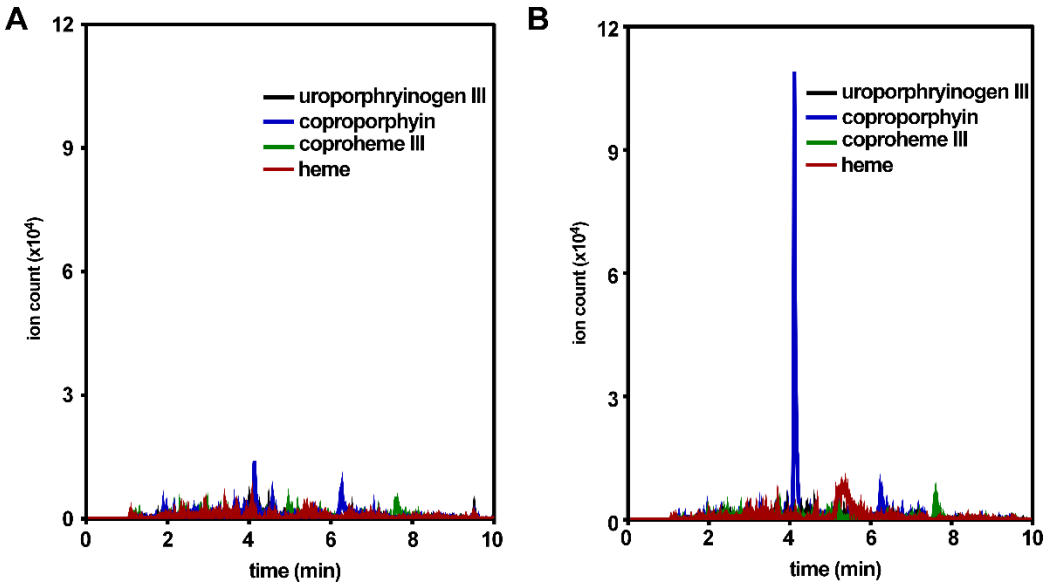

Figure 30 Representative extracted ion chromatograms of extracted porphyrins [A.I.C.]. Chromatograms of **(A)** the *S. aureus* WT and **(B)** the Δ*hemX* mutant; each is quantified and shown in Figure 29. Chromatograms for porphyrins above the limits of detection (250 nM) are shown.

Excess endogenous heme synthesis in Δ*hemX* activates the heme stress response

The unregulated GtrR abundance in Δ*hemX* results in greater cellular heme levels (Figure 29D), which I hypothesized would activate the heme sensor system HssRS in the absence of exogenous heme, leading to transcriptional induction of the *hrtAB* efflux pump. WT and Δ*hemX* were transformed with plasmids containing the luminescence producing operon *luxABCDE* cloned from *Photorhabdus luminescens* without a promoter (pXen-1) or controlled by the HssRS-regulated promoter P_{hrt}. P_{hrt} promoter activity, visualized by

luminescent imaging, shows that HssRS is activated in Δ*hemX* in the absence of exogenous heme whereas HssRS is not activated in WT (Figure 31A). The P_{hrt}*lux* activity in WT becomes apparent when 20 µM exogenous heme is added to the agar medium, and luminescence depends on the heme-responsive P_{hrt}. To more quantitatively measure P_{hrt} activity as a readout of HssRS activation by endogenous heme, I transformed WT, Δ*hemX*, and Δ*hssRS* with the pOS1 P_{hrt}*xylE* plasmid. These strains report P_{hrt} activity with the production of the XylE catechol oxidase enzyme, which can be quantified spectrophotometrically from cell lysate. Data in Figure 31B demonstrate that in the absence of exogenous heme, P_{hrt} is induced in Δ*hemX*. P_{hrt} activity does increase in WT and Δ*hemX* in a dose-dependent manner as exogenous heme is added, but P_{hrt} activity remains higher in Δ*hemX* than WT at all tested heme concentrations. Additionally, XylE activity in this system is dependent on the HssRS two-component system. Taken together, these data suggest that excess endogenous heme synthesized in Δ*hemX* is sufficient to activate the HssRS two-component system.

I next hypothesized that the intermediate levels of HssRS activation in Δ*hemX*, in the absence of exogenous heme (Figure 31A-B), would be sufficient to pre-adapt Δ*hemX* to heme toxicity. As the HssRS-HrtAB heme stress response provides resistance to heme toxicity, pre-treatment with subtoxic concentrations of heme adapts *S. aureus* to subsequent growth in toxic concentrations of heme by activating HssRS and increasing the abundance of HrtAB (10). WT grown in 10 µM heme without pre-adaptation has a severe growth defect evident by a six hour lag time (Figure 31C). When pre-adapted in 2 µM heme, WT demonstrates a reduced lag time and greater overall growth, albeit at a lower rate and yield than when grown without heme. In contrast, Δ*hemX* grown in 10 µM heme with or without pre-adaptation exhibits increased growth as compared to WT. The enhanced growth of Δ*hemX* in 10 µM heme is dependent on the HrtAB efflux system, as Δ*hemX hrtB* does not grow in 10 µM heme (Figure 31C). Additionally, pre-adaptation of Δ*hemX* in this assay can be complemented by providing *hemX* in the chromosome (Figure 32B). Similarly, Δ*gtrR-hemX* pOS1 P_{lgt}*gtrR* is resistant to heme toxicity, but becomes sensitive again when *hemX* is introduced on the plasmid (Figure 32C). This is further evidence that HemX control of GtrR is not transcriptional, as HemX exerts its effect independent of the native *gtrR* promoter and ribosome binding site in this assay. Further, Δ*hemX* is resistant to the bactericidal effects of acute heme toxicity, compared to a 4-log reduction in viable WT cells after 2 h in the presence of 20 µM heme (Figure 31D). In sum, these data demonstrate that increased cellular heme in Δ*hemX* is sufficient to activate HssRS and cause expression of HrtAB, which leads to resistance to heme toxicity.

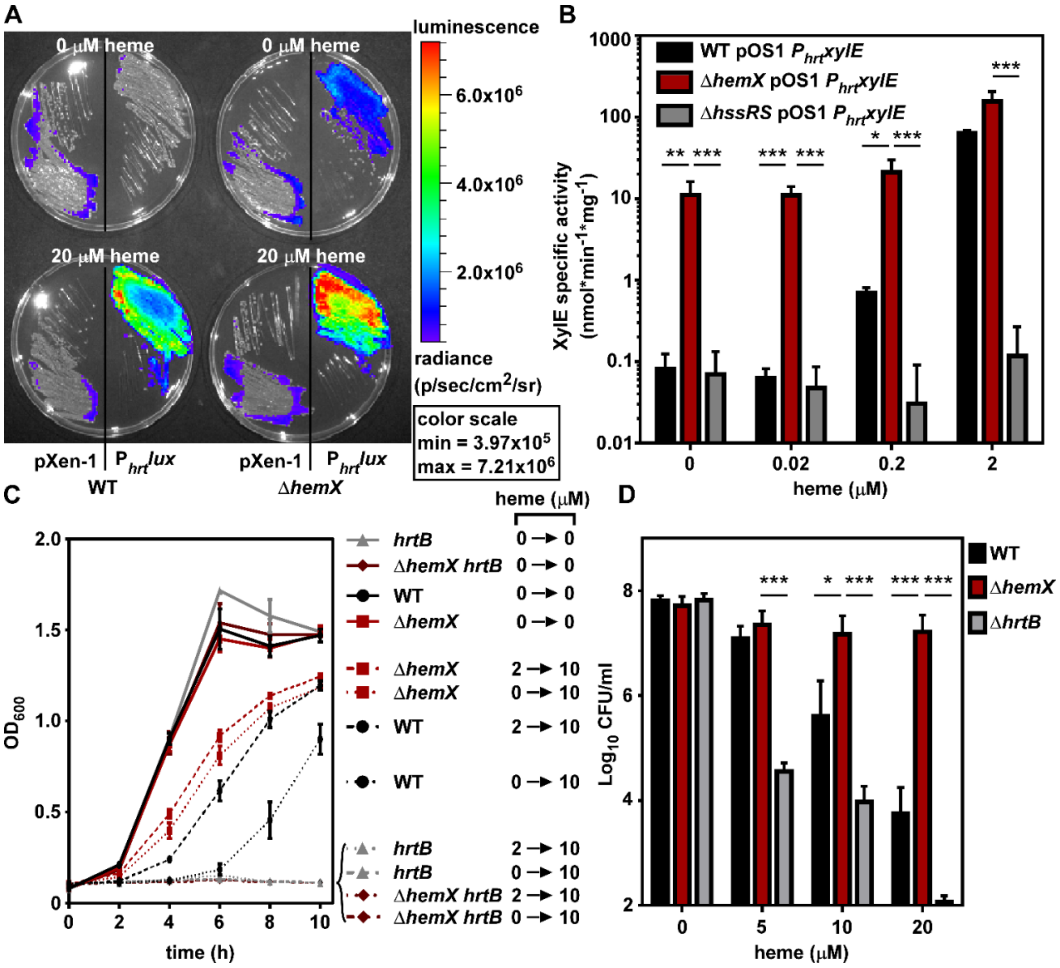

Figure 31 Excess heme synthesis in Δ*hemX* activates the heme stress response. (A) Bioluminescence was imaged on agar medium plates containing vehicle or heme to which strains were streaked. All four plates were imaged simultaneously, and luminescence was converted to a heat map with scale shown on right. **(B)** XylE catechol oxidase activity was measured in *S. aureus* strains after growth in vehicle or increasing concentrations of heme. The data are the average of three independent experiments each with biological triplicate with standard deviation shown. Statistical significance was determined using a two-way ANOVA with Tukey's correction for multiple comparisons, comparing log-transformed data for Δ*hemX* pOS1 P_{hrt}*xylE* at each heme concentration abundance to each other strain; * *P*<0.01,** *P*<0.001, *** *P*<0.0001. **(C)** Growth as measured by optical density (600 nm) was monitored over time for *S. aureus* strains in medium containing either vehicle or 10 μM heme. Prior to the measured growth, the strains were pre-grown to stationary phase in medium containing vehicle or 2 μM heme. The data are the average of the means of at least three independent experiments each with biological triplicate, with standard error of the means shown. **(D)** Viable bacteria from *S. aureus* strains were enumerated after incubation for 2 h in medium containing vehicle or increasing amounts of heme. The data are the average of the means of three independent experiments each with biological triplicate with standard error of the means shown. The y-axis is set to the limit of detection. Statistical significance was determined using a two-way ANOVA with Tukey's correction for multiple comparisons, comparing log-transformed data for WT and Δ*hrtB* to Δ*hemX* at each heme concentration abundance; * P<0.01, *** *P*<0.0001.

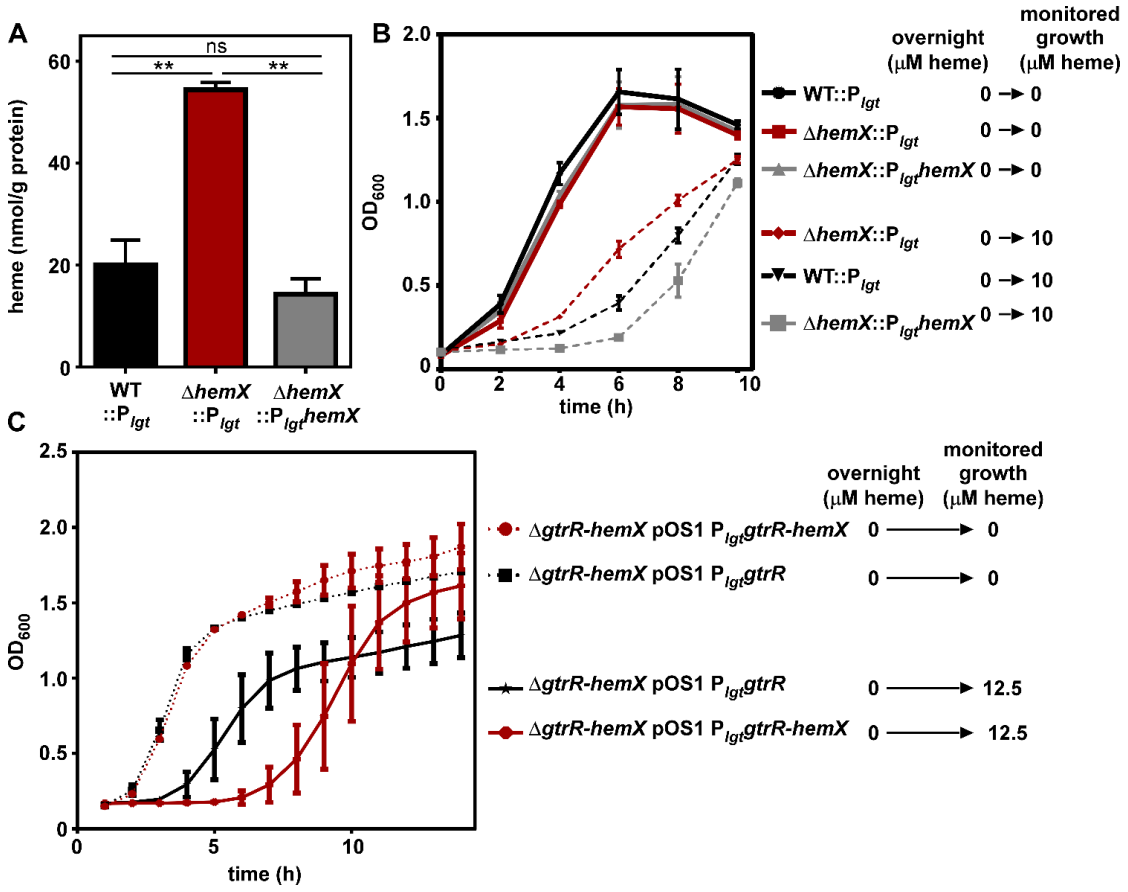

Figure 32 Excess heme and resistance to heme toxicity in the Δ*hemX* mutant can be complemented. (A) Heme abundance was quantified using a pyridine hemochromagen assay in *S. aureus* strains. Data are combined from three independent experiments with four biological replicates with standard error of the mean shown. Statistical significance was determined by a one-way ANOVA with Tukey's correction for multiple comparisons, comparing each strain against the others. **, $P < 0.005$. **(B)** Growth as measured by optical density (600 nm) was monitored over time for *S. aureus* strains in medium containing 0 or 10 µM heme. Strains were grown overnight to the stationary phase in medium alone before inoculation of the growth curve. The data are the average of the means from three independent experiments each in biological triplicate with standard error of the mean shown. **(C)** Growth as measured by optical density (600 nm) was monitored over time for *S. aureus* strains in medium containing chloramphenicol and 0 or 12.5 µM heme. Strains were grown overnight to stationary phase in medium alone before inoculation of the growth curve. The data are means from three biological replicates with standard error of the mean shown from a single experiment, representative of at least three independent experiments.

Inactivation of *hrtB* affects heme synthesis in Δ*hemX*

Considering the increase in heme levels observed in Δ*hemX*, I hypothesized that a mutant lacking HemX-mediated control of heme synthesis and the heme exporter HrtB would accumulate further intracellular heme. To test this hypothesis, porphyrins were measured in WT, Δ*hemX*, *hrtB*, and Δ*hemX hrtB* as described above. Surprisingly, Δ*hemX hrtB*

demonstrated reduced heme levels compared to Δ*hemX* alone, suggesting there is some cross-talk between heme synthesis and efflux. The conversion of coproporphyrin to coproheme appears to be inhibited in Δ*hemX hrtB*, as this strain accumulates less coproheme despite equal levels of coproporphyrin (Figure 33).

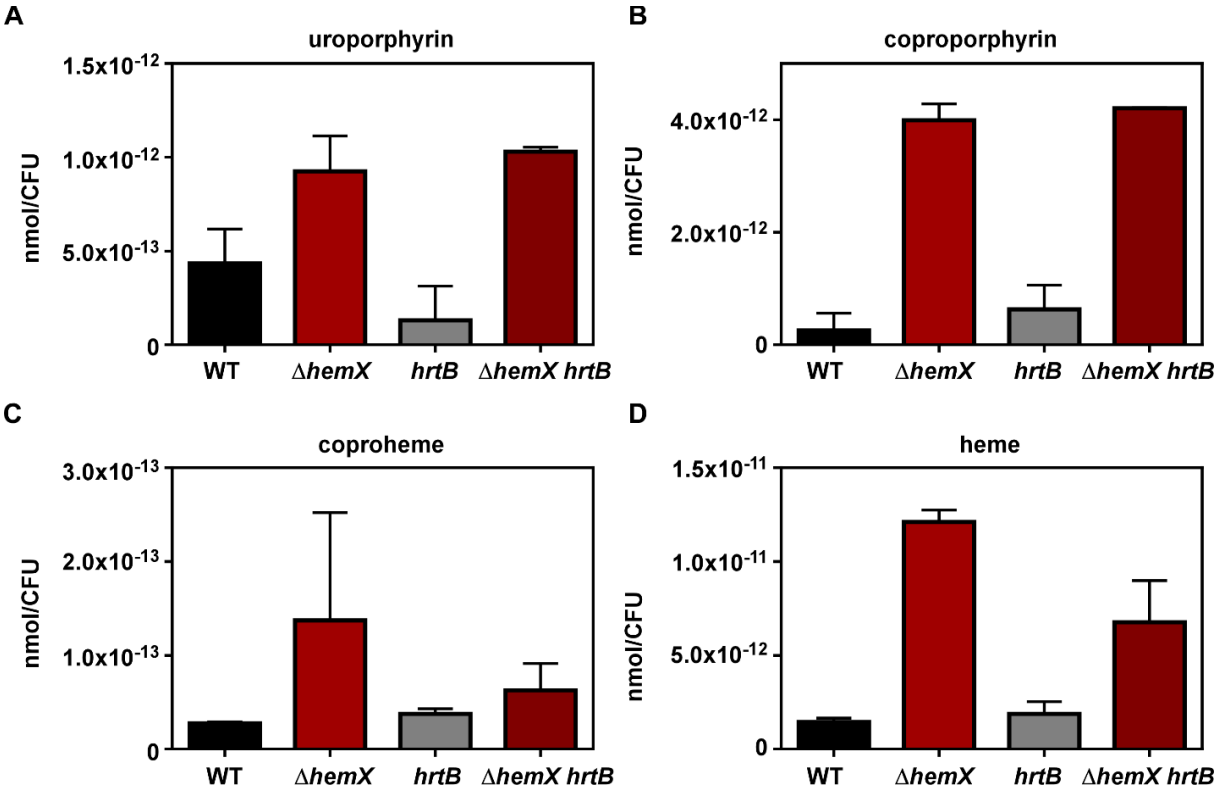

Figure 33 Inactivation of *hrtB* affects heme synthesis in Δ*hemX* [A.I.C.]. Uroporphyrinogen III (detected as uroporphyrin III), coproporphyrin III, coproheme III and heme were quantified by LC-qTOF-MS. Graphed are data from a single experiment performed in biological triplicate with standard error of the means shown.

Δ*hemX* is not more sensitive to oxidants despite higher amounts of intracellular heme

Inactivation of *hemX* results in increased intracellular heme, which imparts resistance to heme toxicity due to activation of HssS. However, I hypothesized that Δ*hemX* would be more susceptible to oxidants, based on our previous observations that excess heme induces superoxide formation and oxidative damage (237). I first tested this hypothesis by assessing survival of WT and Δ*hemX* in the presence of hydrogen peroxide (Figure 34A). Contrary to our hypothesis, there was no difference between WT and Δ*hemX*. Next, I tested growth in the presence of the superoxide donor paraquat and again observed no difference between WT and Δ*hemX* (Figure 34B). To test whether the presence of cytoplasmic superoxide dismutase enzymes was masking the sensitivity of Δ*hemX* to superoxide, I created a mutant lacking

hemX and both *sodA* and *sodM*, and assessed its growth in the presence of paraquat. Again, no difference was noted for superoxide sensitivity in the presence or absence of HemX (Figure 35).

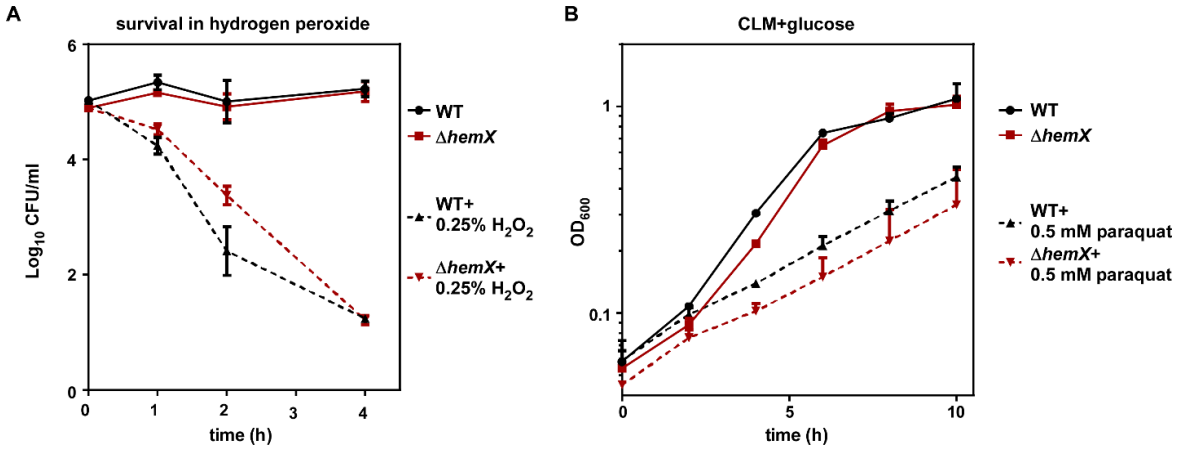

Figure 34 HemX is not more sensitive to oxidants despite higher amounts of intracellular heme. (A) Survival of WT and Δ*hemX* following incubation in 0.25% H_2O_2. **(B)** Growth in carbon-limited medium supplemented with glucose of WT and Δ*hemX* in the presence of vehicle or 0.5 mM paraquat. For both, graphed are the means with standard deviation of (A) two independent experiments in biological triplicate and (B) the means of a single experiment in biological quadruplicate.

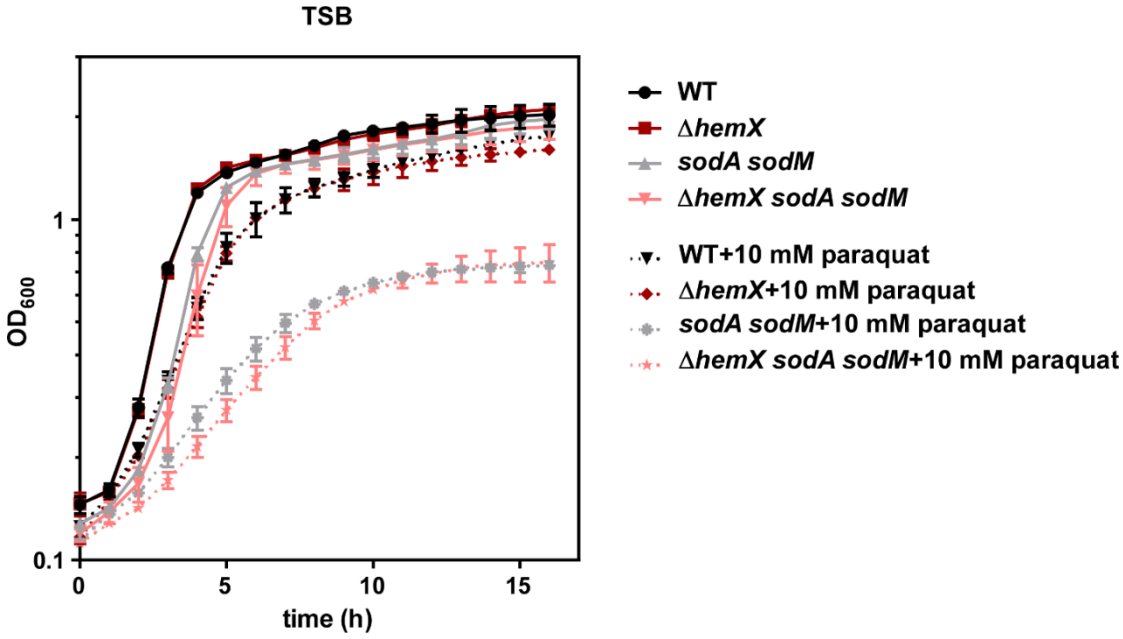

Figure 35 Inactivation of superoxide dismutases does not sensitize Δ*hemX* to paraquat. Growth in TSB of *S. aureus* strains in the presence of vehicle or 10 mM paraquat as measured by OD_{600}. Shown are the means from a single experiment (representative of two) in biological triplicate with standard deviation.

Excess heme synthesis disrupts iron homeostasis

Considering that every molecule of heme contains an atom of iron, I hypothesized that unregulated heme synthesis in Δ*hemX* would consume high levels of iron and alter iron homeostasis. To test this hypothesis, growth in minimal medium containing the iron chelator EDDHA was compared to growth in minimal medium alone. As shown in Figure 36A, Δ*hemX*::P_{lgt} demonstrates reduced total yield after growth for 24 h relative to WT::P_{lgt} and the complemented strain Δ*hemX*::P_{lgt}*hemX*. To corroborate this finding, I assessed promoter activity using a P_{isdA}*gfp* reporter plasmid. P_{isdA} is controlled by the ferric uptake regulator (Fur) and is de-repressed in iron-deplete conditions (113). Data in Figure 36B show that after growth in rich medium with an alternative iron chelator 2,2-dipyridyl, Δ*hemX* pOS1 P_{isdA}*gfp* has enhanced P_{isdA} activity relative to WT pOS1 P_{isdA}*gfp*. These data suggest excess heme synthesis depletes the cell of available iron.

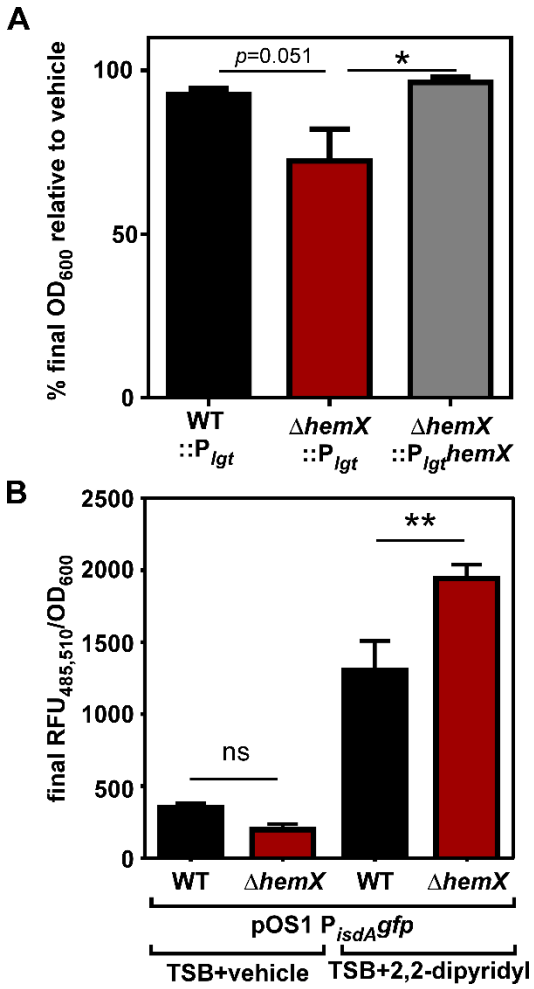

Figure 36 Unregulated heme synthesis alters iron homeostasis. (A) Growth was measured in minimal medium containing vehicle or 1 µM of the iron chelator EDDHA. Graphed is the final growth as measured by optical density at 600 nm for each *S. aureus* strain in medium containing EDDHA relative to vehicle. The data are the average of the means of five independent experiments each with at least biological triplicate, with standard error of the means shown. Statistical significance was determined using a one-way ANOVA with Dunnett's correction for multiple comparisons, comparing Δ*hemX*::P_{lgt} to each other strain; * $P<0.05$ **(B)** The activity of the iron-limitation responsive promoter P_{isdA} was measured by recording fluorescence intensity over time in rich medium containing vehicle or the iron chelator 2,2-dipyridyl. The data are the average of the means of three independent experiments each with biological triplicate, with standard error of the means shown. Statistical significance was determined using a one-way ANOVA with Sidak's correction for multiple comparisons, comparing data for WT and Δ*hemX* under each condition; ** $P<0.01$.

Inactivation of *hemX* does not alter pathogenesis in a murine model of *S. aureus* infection

I next hypothesized that the effect of unregulated heme synthesis on iron homeostasis in the Δ*hemX* mutant would result in reduced fitness during infection, as iron uptake and homeostasis is a critical determinant of *S. aureus* virulence. I infected mice retro-orbitally which allows for dissemination to the organs and subsequent replication. At four days post-infection, mice were humanely euthanized and the bacterial burdens across organs were enumerated. No difference was observed between WT and Δ*hemX* (Figure 37A). I therefore sought to test the hypothesis that the intrinsic heme resistance of the Δ*hemX* mutant is a fitness advantage that might compensate for the defect incurred by excess iron consumption. Therefore, I tested the virulence of WT, Δ*hemX*, *hrtB*, and Δ*hemX hrtB* in the same model, and found that inactivation of heme efflux in the Δ*hemX* background does not reduce *in vivo* fitness (Figure 37B).

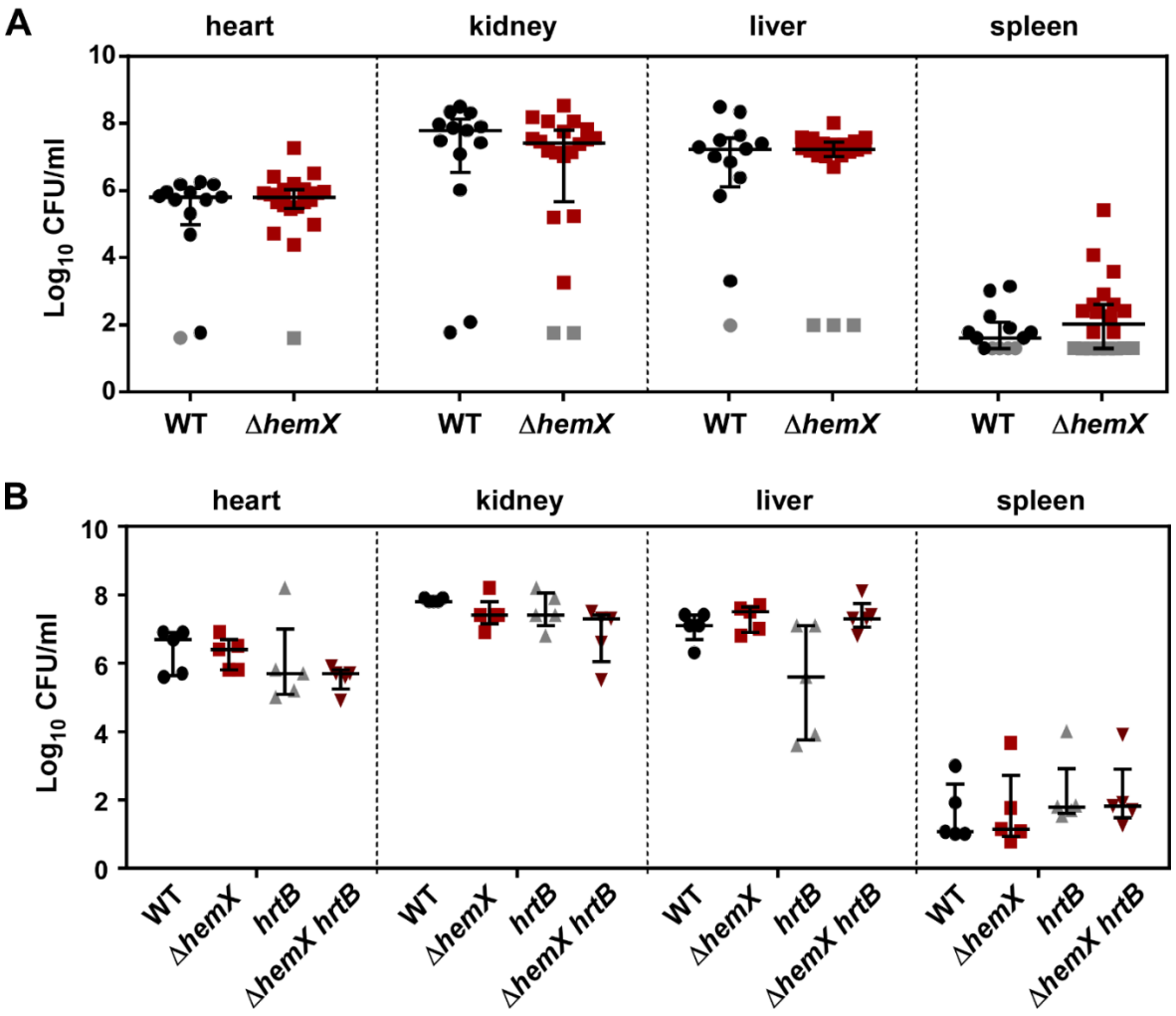

Figure 37 Inactivation of *hemX* does not alter pathogenesis in a murine model of *S. aureus* infection. (A and B) bacterial burdens in noted organs following 96 h of systemic infection of *S. aureus* Newman and isogenic mutants following retroorbital injection of approximately 2x10^7 CFU. **(A)** Data are combined from two independent experiments and **(B)** a single experiment where each dot indicates a single mouse. No significance by Kruskal-Wallce test with Dunn's correction for multiple comparisons, comparing burdens between genotypes for each organ. In (A), gray indicates the limit of detection.

Inactivation of *hemX* reduces GtrR abundance in heme-deficiency

Based on the observations that HemX and cellular heme both impact GtrR abundance, I hypothesized that measuring GtrR abundance in a strain lacking *hemX* and unable to synthesize heme would uncover the nature of the relationship between HemX, heme, and GtrR. Surprisingly, GtrR abundance in Δ*hemX pbgS* is unchanged from Δ*hemX* and lower than *pbgS* (Figure 38A), and this effect is not the result of a change in *gtrR* transcription in Δ*hemX pbgS* relative to *pbgS* (Figure 39) Similarly, Δ*hemX* Δ*chdC* has lower levels of GtrR than Δ*chdC* (Figure 38A). To corroborate these findings, we measured total cellular

porphyrins by LC-qTOF-MS as before; total extracted ion chromatograms are shown in Figure 41. Consistent with the abundance of GtrR, porphyrin intermediates are drastically increased in Δ*hemX* relative to WT (Figure 38B). Δ*chdC* demonstrates intermediate buildup through coproheme because of elevated GtrR levels but is unable to convert coproheme to heme (see Figure 23A). As expected based on the reduced GtrR abundance shown in Figure 38A, the porphyrin intermediates are at lower levels in Δ*hemX* Δ*chdC* relative to Δ*hemX* or Δ*chdC*. These data suggest that heme and HemX do not independently and directly repress GtrR levels, because if so, removal of both would likely have an additive effect on GtrR abundance. Instead, the relationship between HemX, heme synthesis and GtrR levels is still unclear. However, the data are consistent with a model whereby the increase in GtrR levels in heme deficient strains is dependent on the activity of HemX.

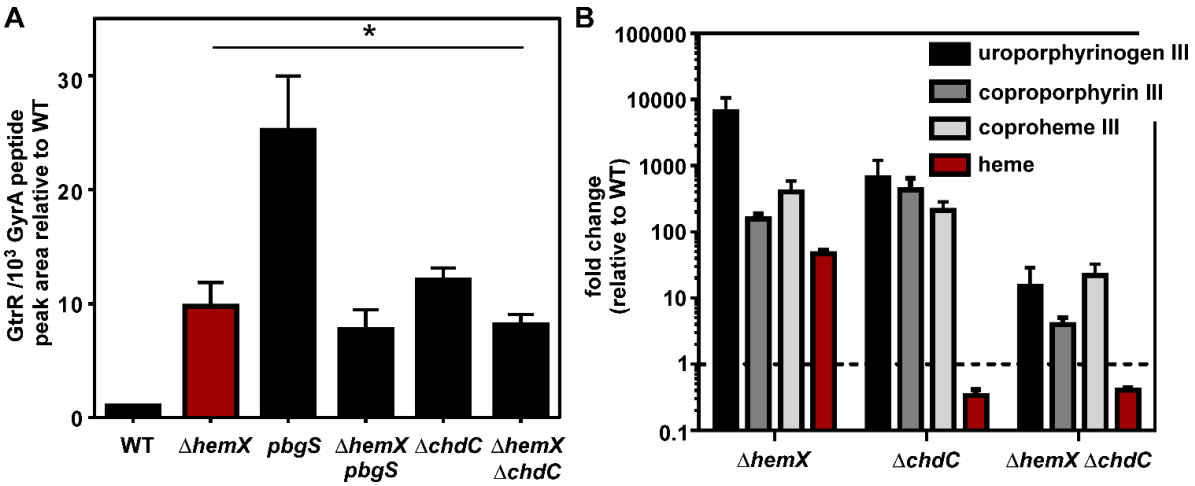

Figure 38 Inactivation of *hemX* reduces GtrR abundance in heme-deficient strains [A.I.C.: panel B]. (A) The abundance of GtrR was measured by LC-MRM-MS/MS in multiple *S. aureus* strains. The data are the average of a single experiment performed in biological triplicate with standard deviation shown. Statistical significance was determined using a one-way ANOVA with Dunnett's correction for multiple comparisons, comparing GtrR abundance for each strain relative to WT; * $P<0.05$. **(B)** Uroporphyrinogen III (detected as uroporphyrin III), coproporphyrin III, coproheme III and heme were quantified by LC-qTOF-MS. Graphed is fold change of metabolite abundance in each mutant relative to WT, from a single experiment performed in biological triplicate with standard error of the means shown.

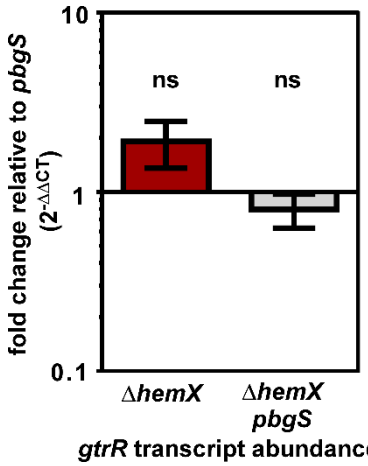

Figure 39 *gtrR* transcription is unchanged in the Δ*hemX* and Δ*hemX pbgS* strains compared to the *pbgS* strain. Steady-state transcript abundance of *gtrR* mRNA isolated from mid-exponential growth of *S. aureus* strains was measured by qRT-PCR and is graphed as fold change relative to the WT. Data are combined from two independent experiments in biological triplicate with standard deviation shown. "ns" indicates no significance by one-way ANOVA with Dunnett's correction for multiple comparisons, comparing fold change of the Δ*hemX* mutant and Δ*hemX pbgS* strains to the *pbgS* strain.

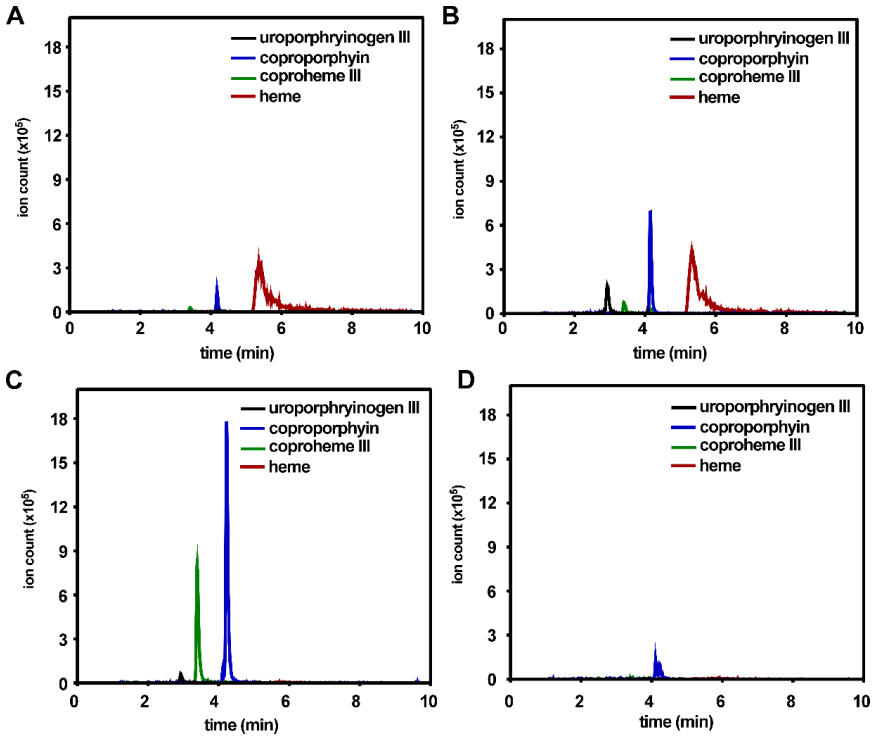

Figure 40 Chromatograms for Figure 39 [A.I.C.]. Representative extracted ion chromatograms of extracted porphyrins of **(A)** the *S. aureus* WT and **(B)** the Δ*hemX*, **(C)** Δ*chdC*, and **(D)** Δ*hemX* Δ*chdC* strains. Each is quantified and shown in Figure 39B. Chromatograms for porphyrins above the limits of detection (250 nM) are shown.

Siroheme synthesis impacts GtrR levels under conditions of nitrite reduction

The increase in GtrR levels identified in Δ*hemX* likely impacts siroheme synthesis, as the cofactor siroheme is synthesized in *S. aureus* from the shared uroporphyrinogen III intermediate (Figure 23A; (51)). I therefore hypothesized that siroheme levels might also affect GtrR abundance. In experiments presented thus far, in which *S. aureus* is grown aerobically, siroheme has likely not been synthesized. The siroheme synthesis and siroheme-dependent nitrite reductase genes are transcribed primarily in anaerobic conditions (347). To therefore test the role of siroheme, I first identified conditions in which siroheme synthesis via CysG, and siroheme-dependent nitrite reduction by the NirD nitrite reductase, were important for growth. As demonstrated in Figure 41, when grown anaerobically, the growth of WT is enhanced when the terminal electron acceptor nitrate is provided. Mutants lacking *cysG* or *nirD* cannot grow to WT levels when nitrate is provided, suggesting that WT cells synthesize siroheme and utilize it in NirD. It is thought that in these conditions, the anaerobic nitrate reductase will reduce nitrate to nitrite, followed by NirD-dependent reduction of nitrite. Deletion of *hemX* does not overtly impact nitrite reduction, as Δ*hemX* grows well in nitrate, Δ*hemX nirD* phenocopies *nirD,* and *ΔhemX cysG* phenocopies *cysG.* Therefore, GtrR abundance was measured by LC-MRM-MS/MS after growth in TSB containing nitrate (Figure 42). The strain lacking *cysG*, which can make heme but not siroheme, does not demonstrate elevated GtrR levels. However, Δ*hemX cysG* has reduced levels compared to Δ*hemX*, suggesting that siroheme synthesis could impact GtrR regulation.

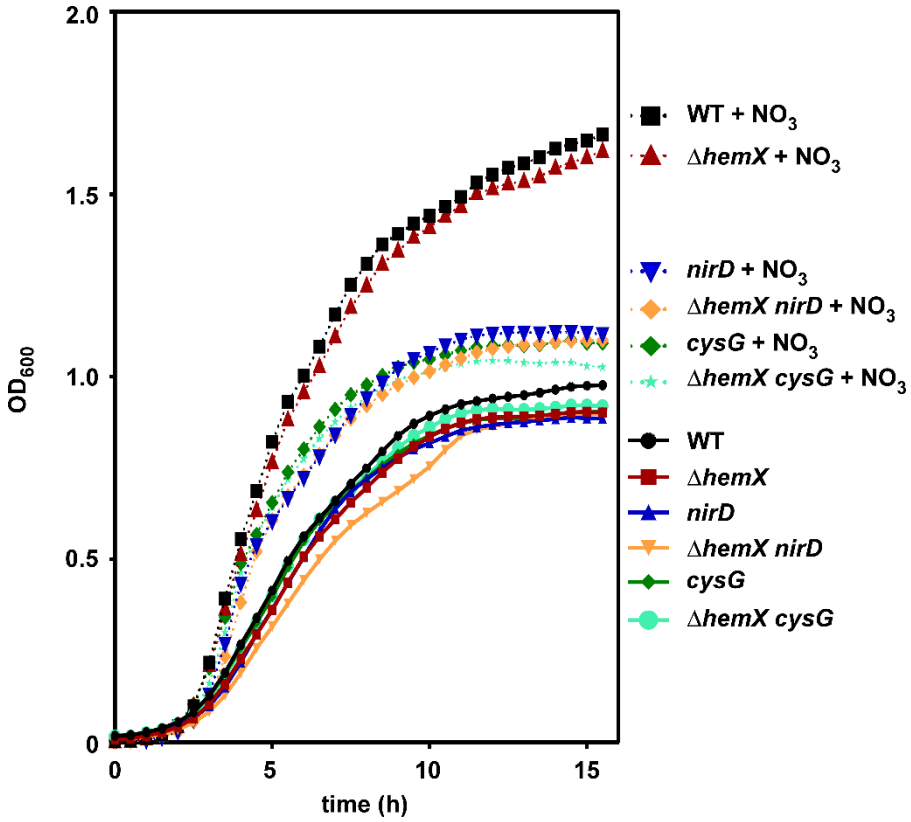

Figure 41 Nitrite reductase and the cofactor siroheme are required for full growth with nitrate as an alternative terminal electron acceptor. Shown is growth anaerobically as measured by optical density (600 nm) monitored over time for *S. aureus* strains in medium containing 0 or 40 mM NO_3. Strains were grown overnight to the stationary phase in medium alone before inoculation of the growth curve. The data are means from three independent experiments with at least three biological replicates.

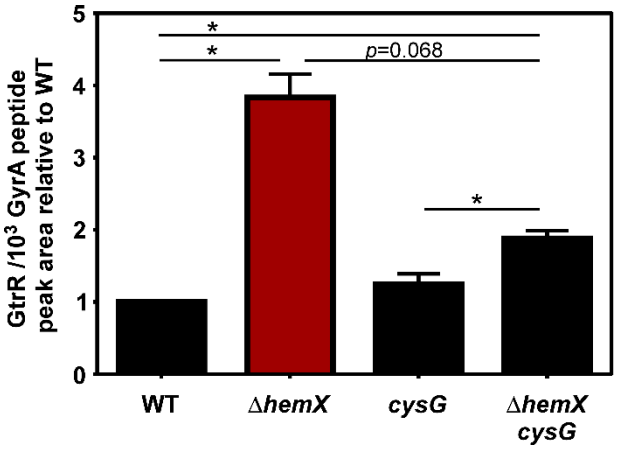

Figure 42 Siroheme synthesis impacts GtrR levels under conditions of nitrite utilization. GtrR was measured by LC-MRM-MS/MS in multiple *S. aureus* strains grown anaerobically with NO_3 provided as the terminal electron acceptor. The data are the average of a single experiment performed in biological triplicate with standard deviation shown. Statistical significance was determined using a one-way ANOVA with Dunnett's correction for multiple comparisons, comparing GtrR abundance for each strain relative to WT; *** P<0.001.

HemX co-occurs with capacity for heme biosynthesis and the corresponding genes often co-localize on the chromosome

We hypothesized that *B. subtilis* HemX and *S. aureus* HemX might represent only a subset of HemX homologs that exist across bacterial phyla and function to regulate heme synthesis. Diverse genomes from 978 organisms (924 bacterial and 54 archaeal) were analyzed for the presence of *hemX*. Of these, 113 encode HemX; representative members of this analysis are shown in Figure 43A. These newly identified homologs expand past the Bacillales order, of which representative HemX homologs were previously identified and shown to share function (75). HemX appears to represent an ancient protein family, as it is present in some of the evolutionarily oldest taxa, including Firmicutes, Aquificae, and Planctomycetes. The distribution of *hemX* strongly correlates with the capacity for *de novo* heme synthesis, as *hemX* never occurs in a genome without *gtrR,* and *hemX* never occurs without the capacity for *de novo* heme synthesis. This correlation holds across the microbial kingdom, where *hemX* never occurs in taxa lacking heme biosynthesis genes (within any representatives with sequenced genomes now available), e.g. *Thermotogae, Fusobacteria, Mollicutes.* Additionally, the distribution of *hemX* among the Firmicutes phylum supports this correlation; *hemX* is present largely in *Bacillales* but does not occur in *Lactobacillales* and only rarely in *Clostridia* (in 2 out 91 genomes analyzed), which is consistent with the frequent capacity for heme synthesis in *Bacillales* relative to *Lactobacillales* and *Clostridia*. Notably, the genomic co-occurrence of *hemX* and *gtrR* holds true in organisms that synthesize heme via any of the 3 heme biosynthetic pathways identified to date: coproporphyrin-dependent,

siroheme-dependent, or the classic protoporphyrin-dependent route (presented in Figure 43A).

Interestingly, HemX is more commonly found in organisms that encode the ability to synthesize both heme and siroheme (Figure 44A) than in organisms that synthesize heme and not siroheme. This suggests that HemX likely impacts siroheme synthesis as a consequence of affecting GtrR abundance by increasing abundance of uroporphyrinogen III, the final shared biosynthetic intermediate. The co-occurance of *hemX*, g*trR*, and *cysG* is also consistent with our findings in Figure 6 that siroheme synthesis impacts GtrR abundance.

Next we examined the genomic context of *hemX* homologs across 113 organisms encoding *hemX,* as genes associated with the same pathway or area of metabolism tend to colocalize in prokaryotic genomes (348). In 106 (94%) out of these 113 genomes the *hemX* and *gtrR* are adjacently encoded and likely co-transcribed, which is very strong indicator of their functional association. Seven representatives of these organisms are shown in Figure 43B, highlighting the common genomic context of *hemX*, *gtrR*, and other genes involved in uroporphyrinogen synthesis (*hmbS*, *uroS*, *pbgS*, *gsaM*) and siroheme synthesis (*cysG*).

HemX homologs share predicted membrane topology and residues

Comparative genome analysis identified several contextual characteristics of HemX homologs. I therefore investigated the sequences of representative HemX homologs. A multiple sequence alignment revealed relatively low overall identity among HemX sequences (Figure 43B); however, the alignment presented in Figure 44B shows that each HemX homolog shares the same predicted eight transmembrane domain topology with N- and C-termini predicted to be extra-cytoplasmic. Additionally, these divergent homologs share four conserved residues, all in predicted transmembrane domains. Taken together with comparative genome analysis, identification of HemX across bacteria uncovered a strong correlation between *gtrR*, *hemX*, and *de novo* heme synthesis, suggesting that HemX control of GtrR to modulate heme synthesis is a common regulatory strategy among bacteria.

A

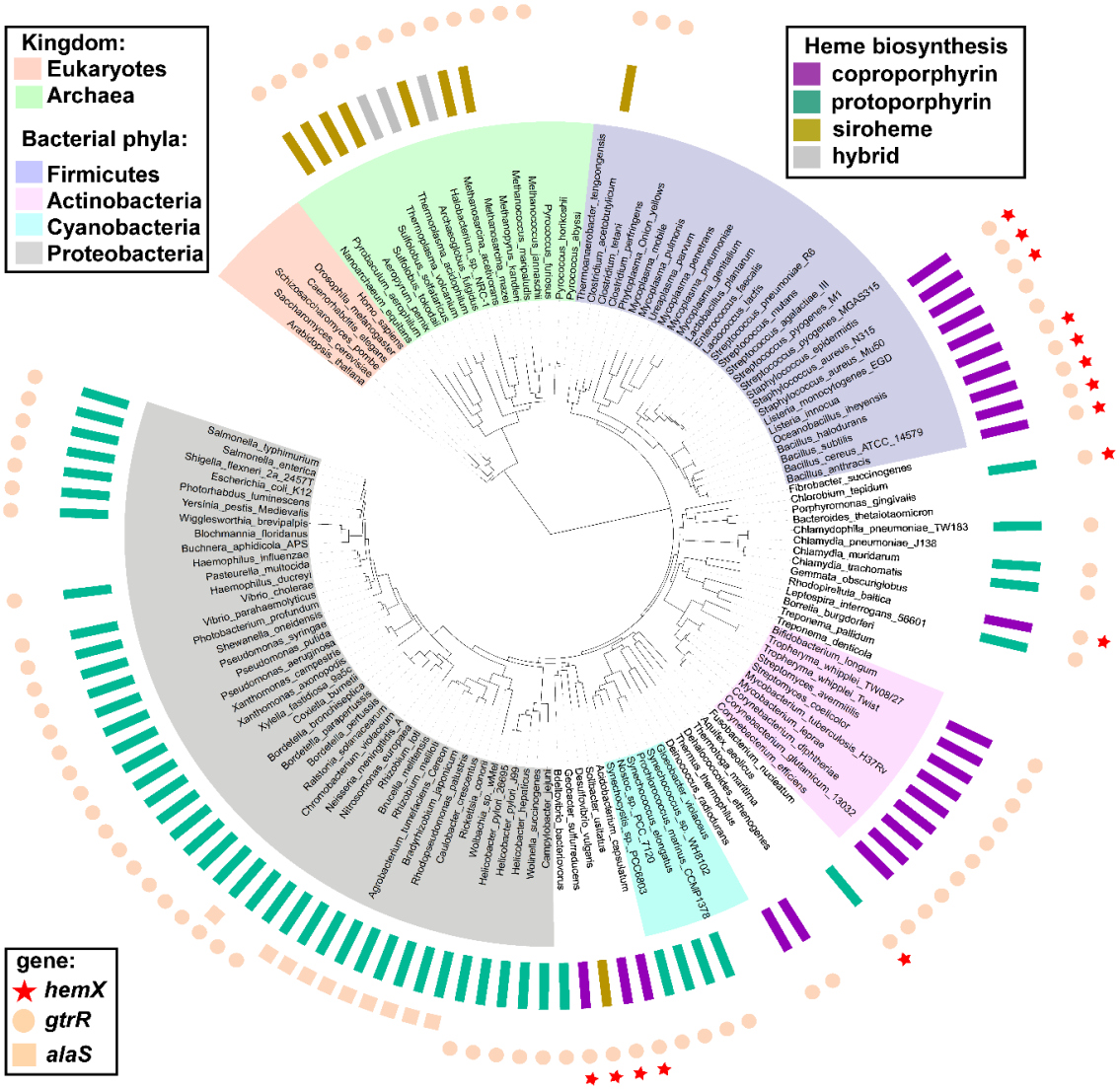
Kingdom:
Eukaryotes
Archaea
Bacterial phyla:
Firmicutes
Actinobacteria
Cyanobacteria
Proteobacteria
Heme biosynthesis
coproporphyrin
protoporphyrin
siroheme
hybrid
gene:
hemX
gtrR
alaS

B

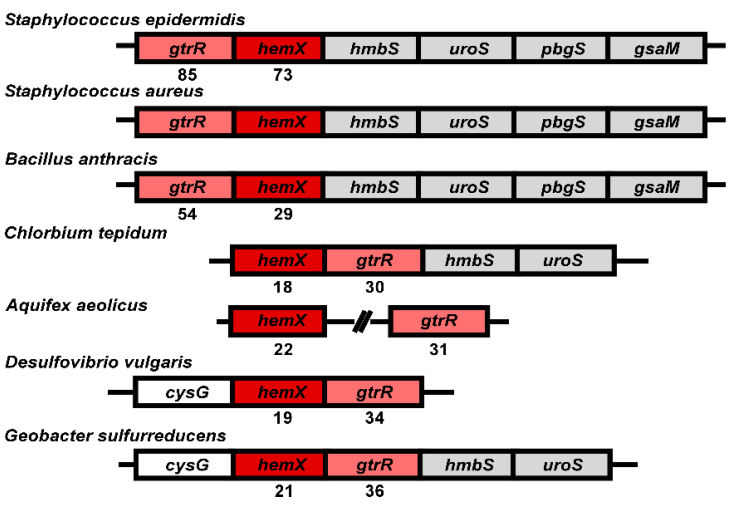
Staphylococcus epidermidis
gtrR hemX hmbS uroS pbgS gsaM
85 73
Staphylococcus aureus
gtrR hemX hmbS uroS pbgS gsaM
Bacillus anthracis
gtrR hemX hmbS uroS pbgS gsaM
54 29
Chlorbium tepidum
hemX gtrR hmbS uroS
18 30
Aquifex aeolicus
hemX gtrR
22 31
Desulfovibrio vulgaris
cysG hemX gtrR
19 34
Geobacter sulfurreducens
cysG hemX gtrR hmbS uroS
21 36

Figure 43. *hemX* is conserved across bacterial phyla, and invariably co-occurs (A) and co-localizes (B) with *gtrR* [S.Y.G.]. **(A)** The occurrence of *hemX* (star), *gtrR* (circle), and *alaS* (square) homologs (outermost rings) was mapped onto the Tree of Life (342). The pathway by which protoheme is synthesized in each of the analyzed organisms is presented in the middle ring as follows (adapted from (51)): classic protoporphyrin-dependent pathway (teal), coproporphyrin-dependent path (purple) or siroheme-dependent path (gold). Gray rectangles mark the organisms that contain unusual combinations of genes normally involved in different pathways for protoheme synthesis (hybrid paths, (51)). The absence of a rectangle in the middle ring indicates the absence of any known route for protoheme synthesis in an organism. Likewise, the absence of a circle (*gtrR*) or square (*alaS*) in the outermost ring shows the inability of an organism to produce tetrapyrroles of any kind. Note, that hemX does not occur in such organisms. **(B)** The immediate genomic neighborhood of the *hemX* gene in seven representative genomes, with CLUSTALW alignment scores for HemX and GtrR for each organism relative to *S. aureus*.

A

Presence of *hemX* and co-occurrence with heme and siroheme synthesis in SEED database analysis		
genome characteristic	**number of organisms**	**presence of *hemX***
heme and siroheme synthesis	592	107 (18%)
heme synthesis only	122	6 (5%)
incapable of heme synthesis	247	0 (0%)

B

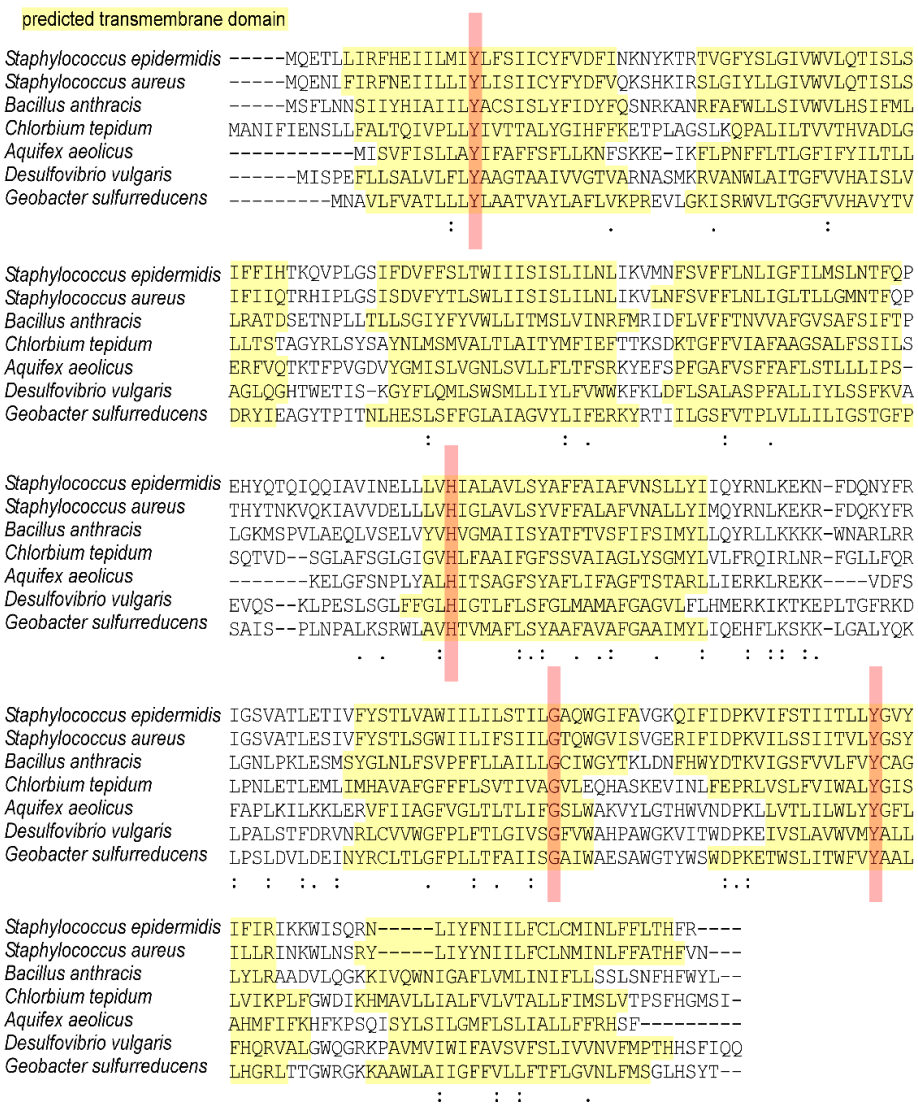

Figure 44 *hemX* co-occurs with heme synthesis and shares conserved secondary structure and residues [with S.Y.G.]. (A) The genomes shown in Figure 43 were analyzed for the capacity to synthesize heme or both heme and siroheme, as well as the presence of *hemX*. **(B)** Alignment of HemX for each of the seven representative organisms, with predicted transmembrane domains in yellow, conserved residues in red, and moderately conserved residues marked with ":" to show conservation among strongly similar amino acids or "." to show conservation among weakly similar amino acids.

Mutations to conserved HemX residues impact function

I hypothesized that each of the four conserved HemX residues would be important for function, considering their conservation among divergent HemX homologs. To test this hypothesis, each residue was mutagenized to an alanine in a plasmid-borne copy of *hemX*. The heme killing assay was then performed to assess whether mutagenized *hemX* would complement Δ*hemX* to the same extent as a wildtype copy of *hemX*. As shown in Figure 46A, H135 and G203 amino acids contribute to the function of HemX in this assay. Mutagenesis of Y17, on the other hand, did not impact HemX function (Figure 46A). Of note, while pOS1 P_{lgt}*hemX* Y231A could be readily created by site-directed mutagenesis and replicated in *E. coli,* it was unable to be transformed into *S. aureus* despite multiple efforts. This suggests that Y231A alters HemX in a way that makes it toxic to *S. aureus*.

I next created HemX-alkaline phosphatase fusions. The alkaline phosphatase enzyme (PhoA) is only active when translocated across the inner membrane. By creating in-frame translational fusions, I could experimentally validate the predicted topology of HemX and test the impact of mutagenesis on expression and membrane insertion of HemX in *E. coli*. As presented in Figure 46B, HemX-PhoA is blue on agar containing BCIP which demonstrates that when PhoA is a C-terminal fusion, it is enzymatically active and is in the periplasm. PhoA is inactive in the HemX:N244-PhoA fusion; N244 is in a predicted inner membrane loop between transmembrane domains 7 and 8 (highlighted in Figure 45). Together, these alkaline phosphatase fusions confirm the predicted HemX topology. Mutagenesis of the four conserved residues in HemX-PhoA fusions did not affect PhoA activity, suggesting that this mutagenesis did not impact ectopic expression of HemX or its membrane topology, and supporting the hypothesis that H125 and G203 impact HemX function through means unrelated to secondary structure.

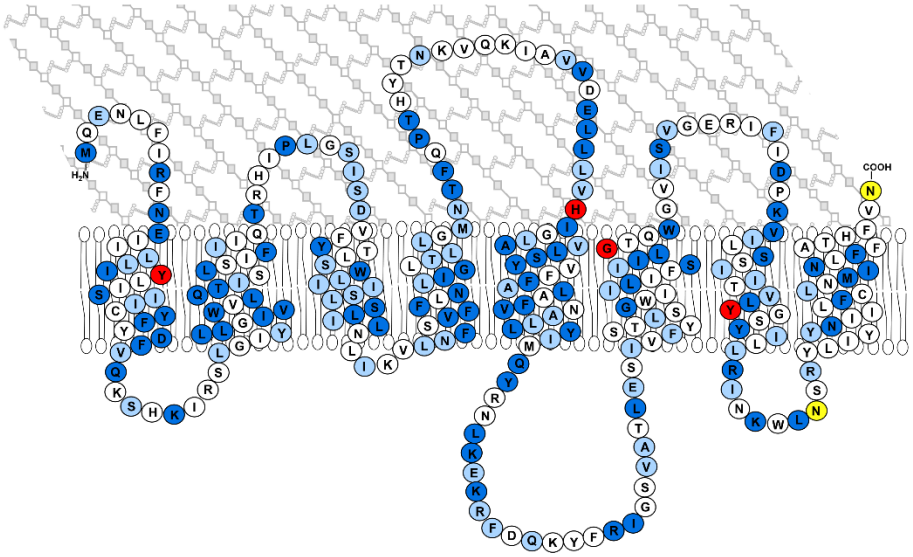

Figure 45 Predicted topology and conservation of HemX. A model of HemX topology based on multiple transmembrane domain prediction tools. Dark blue are residues conserved in *B. subtilis*, light blue are highly similar residues in *B. subtilis*, red are four conserved residues across species indicated in Figure 44, and yellow are residues following which alkaline phosphatase fusions were inserted (Figure 46).

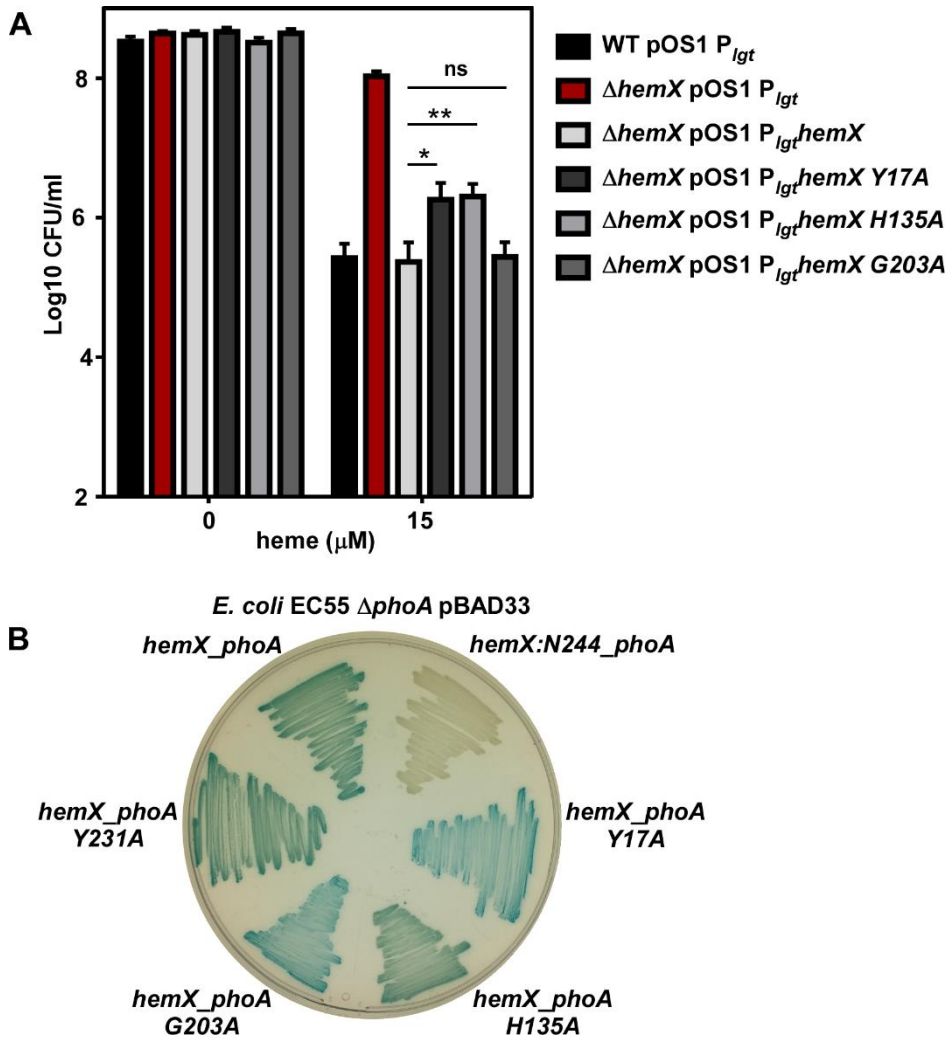

Figure 46 Conserved HemX residues impact function without disrupting membrane topology and expression. (A) Resistance to killing by heme was measured after incubation for 2.5 h and serial dilution of WT, Δ*hemX*, and Δ*hemX* complemented with wildtype of mutagenized *hemX*. pOS1 P_{lgt}*hemX Y231A* was unable to be transformed into *S. aureus*. **(B)** Alkaline phosphatase activity was monitored in *E. coli* lacking endogenous *phoA* gene on LB agar containing IPTG to induce expression of *hemX*:*N244_phoA* in frame insertion, C-terminal *phoA* fusion, and mutagenized C-terminal fusion, and BCIP to measure activity of alkaline phosphatase.

A heme-inducible selection strain

Finally, I sought to design a genetic selection that could be used to further investigate heme homeostasis. Taking advantage of the P_{hrt} activation by endogenous heme in the Δ*hemX* strain (Figure 31), I performed an allelic exchange of the native *hrtAB* genes with a kanamycin resistance cassette. Therefore, when HssRS activates the P_{hrt}, kanamycin resistance will be induced and can be used to select for mutants with enhanced P_{hrt} activity (See Chapter VI for further discussion).

Discussion

In this report, I identify GtrR abundance as a critical regulator of *S. aureus* heme biosynthesis. GtrR catalyzes the initial step in the heme biosynthetic pathway, is maintained at low levels in WT cells proficient for heme biosynthesis, but specifically increases in response to heme deficiency (Figure 23B). In this study, I used heme auxotrophs to stimulate production of GtrR (Figure 23B,D), but I would predict that in particular niches during infection an increase in heme synthesis is required and GtrR abundance increases to accommodate this need. Host-imposed nitrosative stress, oxidative stress, and hypoxia, for example, all cause *S. aureus* to increase expression of heme-dependent cytochrome oxidases, catalase, and nitric oxide synthase (349-351).

The drastic difference in GtrR enrichment between the heme auxotrophs *pbgS* and Δ*chdC* (Figures 23 and 38), with deficits in genes at the beginning and end of the heme biosynthetic pathway respectively, suggests that GtrR abundance during heme deficiency could be impacted by mechanisms other than heme availability. This is an interesting observation in light of the comparative genome analysis of *hemX*, which suggests that HemX could impact siroheme synthesis as well as heme synthesis. It is possible that GtrR abundance is impacted by differences in heme or siroheme abundance as well as abundance in earlier precursor levels, explaining the difference in GtrR levels in *pbgS* relative to Δ*chdC*.

In addition to the impact of heme-deficiency on GtrR, I also identify HemX as a key regulator of GtrR in heme-proficient cells (Figure 28A). Our broad genomic analysis has identified HemX homologs across bacterial phyla, suggesting that HemX control of heme synthesis via GtrR is a conserved strategy (Figure 43 and 44). This finding is consistent with the model set forth by Hederstedt and colleagues (75, 345); in both *B. subtilis* and now *S. aureus*, it appears that HemX regulates GtrR abundance post-transcriptionally (Figure 28B) through an as-yet-undefined mechanism. *B. subtilis* HemX is sufficient to affect GtrR abundance when both are expressed ectopically in *E. coli* (75); however, the contribution of heme or conserved *E. coli* proteins in this system is unclear, making it challenging to conclude if HemX directly interacts with GtrR. Together, our findings are consistent with a model whereby GtrR is regulated by heme abundance and HemX through a multi-protein mechanism. Our finding that GtrR abundance is reduced in *pbgS hemX* relative to *pbgS* and not increased supports this model; heme and HemX both do not directly repress GtrR levels (Figure 38). In *Salmonella*, which do not encode HemX, GtrR is regulated by N-terminal proteolysis by ClpAP and Lon proteases to keep levels low (71). Additionally, *Salmonella* GtrR binds excess heme through a cysteine-170 residue (72). Mutagenesis of the N-terminus

degradation sequence or heme binding cysteine disrupts regulation, and it has been proposed that heme-bound GtrR but not apo-GtrR is a substrate for the proteases (71, 73). The mechanism by which *Salmonella* GtrR is regulated by proteases via its N-terminus and heme binding is not fully understood, and these regulatory amino acids are not conserved in *S. aureus* GtrR. However, here I identify that *S. aureus* GtrR binds heme *in vitro*, suggesting heme binding by GtrR may contribute to its regulation as observed in Gram-negative bacteria (Figure 26). Likewise, further work is needed to dissect the unique regulatory effects of heme and HemX on GtrR levels, and the potential involvement of proteolysis in this process in *S. aureus*.

In the absence of HemX, *S. aureus* synthesizes excess heme. The increase in heme synthesis disrupts intracellular iron homeostasis (Figure 36), which could additionally disrupt the expression of the staphyloferrin B siderophore biosynthetic genes, which were recently identified to be under the control of a transcriptional activator that is inactive when bound to heme (133). This altered iron homeostasis would likely reduce the function of many important Fe-S cluster-containing enzymes critical to staphylococcal physiology. Additionally, excess heme synthesized in Δ*hemX* activates the heme stress response (Figure 31). While activation of the HssRS two-component system was first recognized as the result of exogenous heme, our findings add to a growing body of literature that supports a model whereby endogenous and exogenous heme both contribute to HssRS activation and heme toxicity. We have previously identified small molecule activators of heme synthesis that increase intracellular heme and activate HssRS (36-38), adding to our genetic evidence presented in this work that endogenous heme activates HssRS. Here, the increase in endogenous heme in Δ*hemX* is not toxic because of the HssRS-HrtAB detoxification response. Rather, endogenous heme activation of HssRS provides resistance to heme toxicity through preadaptation and expression of *hrtAB* (Figure 31). The impact of inactivating *hemX* on the fitness of pathogens that do not encode the HssRS-HrtAB system would offer insight into whether dysregulated heme synthesis is sufficient to induce heme toxicity from within.

While excess heme synthesis in Δ*hemX* results in a modest disruption of iron homeostasis (Figure 36), no virulence phenotype was detected in a murine model of systemic infection. Even in a strain lacking heme efflux, deletion of *hemX* has no defect. This underscores our lack of understanding of the mechanism of heme toxicity and the niches in which *S. aureus* experiences heme toxicity. No virulence defect has been measured in *S. aureus* mutants lacking various components of HssRS-HrtAB. In terms of the mechanism of heme toxicity, superoxide formation has been found to contribute, yet the Δ*hemX* mutant,

which has about ten-fold more intracellular heme, is not more sensitive to oxidants even in the absence of cytoplasmic superoxide dismutase enzymes. Further, HssRS has been bioinformatically predicted to induce expression of *sodA*. This would suggest heme toxicity could directly induce superoxide dismutase activity, but remains to be investigated (352).

This study found that regulating GtrR abundance is sufficient to regulate total heme synthesis (Figure 28), consistent with multiple reports that ALA formation is a critical rate-limiting step in heme synthesis (51). In line with these data, exogenous ALA is sufficient to drive excess heme synthesis, suggesting ALA formation is a rate-limiting step in *S. aureus* as well (Figure 27) Indeed, regulation of ALA synthesis via control of either GtrR or ALAS has emerged as a theme across kingdoms. In metazoans, two ALAS isoforms exist and are impacted by heme (reviewed in (353)). In the plant model organism *Arabidopsis thaliana*, ALA synthesis is regulated by degradation of GluTR via Clp proteolysis from the N-terminus as well as stabilization and activation of a regulatory binding protein (334, 354). In Gram-negative model organisms, as mentioned above, GtrR abundance is regulated by heme and proteolysis (71). Our findings extend this paradigm further into the Firmicutes phylum of bacteria.

The specific mechanism by which HemX impacts GtrR abundance remains undefined. HemX is annotated as a member of the cytochrome *c* assembly protein family (Pfam:PF01578) suggesting that it may be involved in heme binding and trafficking at the membrane. However, *S. aureus* does not encode *c*-type cytochromes. The capacity of HemX to bind heme has not been experimentally validated, but excess heme does accumulate in the membrane (96) suggestive of a potential role for membrane-localized heme reservoirs or chaperones. Additionally, three of the four highly conserved amino acids in HemX, some of which contribute to the function of HemX, are classical heme-coordinated amino acids and localized to transmembrane domains, implicating them as potential heme binding residues (Figure 45). The limited regions of HemX predicted to be cytoplasmic suggest that protein-protein interactions likely occur between other membrane proteins, but no HemX-interacting partners have been identified to date. Additionally, GtrR residues that impact regulation by either heme or HemX are unknown, but would offer information as to the regulatory steps between heme, HemX, and GtrR, which appear to be complex. Although heme-dependent inhibition of *S. aureus* was first proposed in 1962 (112), the impact of HemX and heme on GtrR abundance continue to warrant further investigation.

CHAPTER V

MOLECULAR BASIS FOR THE EVOLUTION OF SPECIES-SPECIFIC HEMOGLOBIN CAPTURE BY *STAPHYLOCOCCUS AUREUS*

A version of the following section was previously published in *mBio* 9(6). pii: e01524-18 (November 2018)
Doi: 10.1128/mBio.01524-18

Introduction

Animals possess a variety of molecular factors that effectively sequester essential metals from invasive microbes, contributing to an innate immune function termed nutritional immunity (6, 22). Iron, as a critical cofactor for many host and bacterial enzymes, has provided the paradigm for our current understanding of nutritional immunity. Since the discovery of iron limitation by egg white ovotransferrin in the 1940s (355), mechanisms underlying nutritional immunity and bacterial iron scavenging have been the subject of intense study (24). Many vertebrate-associated bacteria encode high affinity uptake systems targeting heme, an abundant iron-containing porphyrin cofactor (317).

The most abundant source of heme-iron in the mammalian host is hemoglobin, which mediates oxygen transport within circulating erythrocytes. The predominant adult hemoglobin consists of a tetramer containing two α-globin and two β-globin protein subunits, each of which binds a single heme molecule for coordination of oxygen. The Gram-positive bacterium *Staphylococcus aureus* is well-adapted to the human host and is a leading cause of skin and soft tissue infections, endocarditis, osteomyelitis, and bacteremia (318). In order to acquire iron during infection, *S. aureus* has evolved a high-affinity hemoglobin binding and heme extraction system, termed the *i*ron regulated *s*urface *d*eterminant (Isd) system (113). Following the lysis of proximal erythrocytes via secreted bacterial toxins, released hemoglobin is captured by receptors at the *S. aureus* cell surface (114, 118). The Isd system of *S. aureus* in part consists of cell-wall anchored IsdB and IsdH, which bind hemoglobin and haptoglobin-hemoglobin, respectively (118, 120).

We and others have shown that IsdB is the primary hemoglobin receptor for *S. aureus* and critical for pathogenesis in murine infection models (94, 95, 118, 134). Additionally, IsdB

is highly expressed in human blood (356) and a promising vaccine target (218), underscoring its importance in human disease. IsdB extracts heme from hemoglobin, and heme is subsequently passed across the cell wall and into the cytoplasm for degradation by the heme oxygenases IsdG and IsdI, liberating iron (122, 125, 127, 129, 357). Underscoring the importance of IsdB for pathogenesis, heme is the preferred iron source of *S. aureus* during murine infection (96). The cell-wall anchored IsdABCH proteins share between one and three NEAT (*nea*r *t*ransporter) domains for coordination of hemoglobin or heme. IsdB NEAT1 binds hemoglobin while NEAT2 binds heme, tethered by an intervening linker (119). Consistent with adaptation of *S. aureus* to colonize and infect humans, we previously found that *S. aureus* IsdB binds human hemoglobin more effectively than mouse hemoglobin, the common laboratory animal used to model *S. aureus* infection (94). These results suggest that hemoglobin variation among mammals could dictate effective heme acquisition by *S. aureus* and other Gram-positive bacteria.

Previous work has demonstrated that pathogens can promote rapid adaptation of host immunity genes through repeated bouts of positive selection (358-360). While adaptation during such evolutionary conflicts can take many forms, theoretical and empirical studies indicate that an elevated rate of nonsynonymous to synonymous substitutions in protein-coding genes is often indicative of recurrent positive selection (361, 362). To date, most empirical studies of host-pathogen 'arms races' have focused on viruses (363-366). Recently it was shown that the transferrin family of iron-binding proteins has undergone extremely rapid evolution in primates at protein surfaces bound by iron-acquisition receptors from Gram-negative bacteria (226, 367). These findings are consistent with the existence of a long-standing evolutionary conflict for nutrient iron, whereby mutations in iron binding proteins that prevent bacterial scavenging protect the host from infection and are favored by natural selection. While these studies have expanded our understanding for how pathogens shape the evolution of host genomes, they also raise the question of whether other components of nutritional immunity might be subject to similar evolutionary dynamics.

In addition to its role as the principal bloodstream oxygen transporter, hemoglobin has provided an important biological model for diverse areas of the life sciences. Elegant studies have illustrated how hemoglobin variation underlies multiple instances of adaptation to high altitudes in diverse vertebrate taxa (368-371). Hemoglobin alleles have also likely been subject to balancing selection in human populations, where mutations that produce sickle-cell disease also confer resistance to severe malaria (372) and have reached high frequencies in regions where malaria is endemic. Despite its long history of study, the consequences of

hemoglobin evolution for vertebrate nutritional immunity remain unclear. In the present study, we set out to investigate the evolution of hemoglobin family proteins in primates and determine whether primate hemoglobin evolution impacts the ability to sequester heme-iron from bacterial pathogens.

Materials and methods

Bacterial strains

Bacterial strains and plasmids used in this study are listed in Table 11. For *E. coli* strains, LB agar and broth (Fisher, Hampton, NH) were routinely used and grown at 37°C. For selection of pHUG21, 12.5 µg/ml of carbenicillin (Fisher) was used; for selection of pHb0.0, 5 µg/ml of tetracycline hydrochloride (Alfa Aesar, Havermill, MA) was used, and for selection of pOS1 P_{lgt}, 50 µg/ml of carbenicillin was used. *Staphylococcus* strains were grown at 37°C using tryptic soy agar and broth (Fisher), except when noted throughout. For selection of pOS1 P_{lgt} 10 µg/ml chloramphenicol (Fisher) was used. Strains were streaked to agar from stocks stored at -80°C two days prior to each experiment.

Table 11 Bacterial strains and plasmids used in Chapter V	
Bacterial Strain	**Source**
Escherichia coli DH5α	Laboratory stock, Thermo Fisher
Escherichia coli BL21(DE3) pHUG21	Douglas Henderson (University of Texas of the Permian Basin); (373)
Staphylococcus aureus RN4220	(280)
S. aureus Newman	Laboratory stock; (277)
S. aureus Newman Δ*isdB*::*erm*	(113)
S. argenteus MSHR1132	DSMZ
S. schweitzeri FSA084	DSMZ
Plasmid	Source
pHb0.0-human	John Olson (Rice University); (373)
pHb0.0-white-cheeked gibbon	This work
pHb0.0-baboon	This work
pHb0.0-talapoin	This work
pHb0.0-marmoset	This work
pHb0.0-$alpha_{human}beta_{baboon}$	This work
pHb0.0-$alpha_{baboon}beta_{human}$	This work
pHb0.0-human αT8K	This work
pHb0.0-human αA5D;T8K;N9H	This work
pHb0.0-human αN78Q	This work
pHb0.0-human αN78H	This work
pHb0.0-human βS9N	This work
pHb0.0-human βS9T	This work
pHb0.0-human βS9K	This work
pHb0.0-human βS9A	This work
pHb0.0-human βA76N	This work
pHb0.0-human βA76T	This work
pOS1 P_{lgt}	(314)
pOS1 P_{lgt}*isdB*$_{aureus}$	This work
pOS1 P_{lgt}*isdB*$_{schweitzeri}$	This work

pOS1 P_{lgt}*isdB*$_{argenteus}$	This work
pOS1 P_{lgt}*isdB*$_{aureus}$ Q162R	This work
pOS1 P_{lgt}*isdB*$_{aureus}$ S170T	This work
pOS1 P_{lgt}*isdB*$_{aureus}$ Q162R;S170T	This work

Hemoglobin cloning and genetic manipulation

We compiled a subset of α- and β-globin sequences from GenBank, as well as cloned α-globin orthologs from cDNA derived from primate cell lines and β-globin orthologs from primate genomic DNA. Hemoglobin gene sequences have been deposited in GenBank (accession numbers MH382883- MH382906). Hemoglobin gene sequences obtained from GenBank: olive baboon, bonobo, white-headed capuchin, chimpanzee, Angolan colobus, northern white-cheeked gibbon, green monkey, human, drill, crab-eating macaque, common marmoset, Sumatran orangutan, rhesus macaque, black snub-nosed monkey, golden snub-nosed monkey, and squirrel monkey. Primate cell lines were purchased from the Coriell Institute for Medical Research (Camden, NJ). The α-globin orthologs cloned from cDNA (with Coriell ID numbers): African green monkey (PR01193), black-and-white colobus (PR00240), white-handed gibbon (PR01131), Western lowland gorilla (AG05251), Francois' leaf monkey (PR01099), black crested mangabey (PR01215), white-faced marmoset (PR00789), Nancy Ma's night monkey (PR00627), patas monkey (AG06116), proboscis monkey, Allen's swamp monkey (PR01231), talapoin (PR00716), and Wolf's guenon (PR00486). The β-globin orthologs cloned from genomic DNA: crested macaque (PR01215), Bolivian red howler monkey (PR00708), pigtailed macaque, black-crested mangabey (PR01215), Nancy Ma's night monkey(PR00627), patas monkey (AG06116), white-faced saki (PR00239), island siamang (PR00722), Allen's swamp monkey (PR01231), talapoin (PR00716), Spix's saddle-back tamarin (AG05313), dusky titi (PR00742), Wolf's guenon (PR00486), and common woolly monkey (PR00525).

Primate hemoglobin cDNA was cloned into pHb0.0 using Gibson assembly (New England Biolabs [NEB], Ipswich, MA). In general, each α- and β-globin gene cDNA was amplified from template (above) using Phusion 2X Master Mix (Thermo, Waltham, MA) with primers that also had homology to pHb0.0. All primers are listed in Table 12. Because of cDNA sequence homology, some primers were used for multiple species. pHb0.0-human was digested with PacI (NEB) and HindIII-HF (NEB) and the double-digested vector was isolated by gel purification (Qiagen, Germantown, MD). PCR products were assembled with digested pHb0.0, transformed to DH5α, re-isolated by mini-prep (Thermo) and were confirmed by sequencing (GeneWiz, South Plainfield, NJ) with pHb0.0_for/pHb0.0_rev. Globin cDNA was amplified for assembly as follows: white-cheeked gibbon α-globin-primers AF327/328, white-

cheeked gibbon β-globin-primers AF329/330, baboon α-globin-primers AF331/332, baboon β-globin-primers AF329/330, talapoin α-globin-primers AF327/328, talapoin β-globin-primers AF329/330, marmoset α-globin-primers AF333/334, and marmoset β-globin-primers AF329/335.

Table 12 Primers used in Chapter V.

Primer name	Sequence	Description
AF327	TTCACTAAGGAGGTTAATTAATGGTGCTGTCTCCTGCC	Forward primer for white-cheek gibbon and talapoin α-globin
AF328	TCTAGATCATTAACGGTATTTGGAGGTCAGC	Reverse primer for white-cheeked gibbon and talapoin α-globin
AF329	TACCGTTAATGATCTAGATAAGGAGGTAAATATATG	Forward primer for white-cheeked gibbon, baboon, talapoin, and marmoset β-globin
AF330	GAGCCTTTCGTTTTATTTAAGCTTCATTAGTGGTACTTGTGG	Reverse primer for white-cheeked gibbon, baboon, and talapoin β-globin
AF331	TTCACTAAGGAGGTTAATTAATGGTGCTGTCTCCTGAC	Forward primer for baboon α-globin
AF332	TCTAGATCATTAACGGTATTTGGAGGTCAG	Reverse primer for baboon α-globin
AF333	TTCACTAAGGAGGTTAATTAATGGTGCTGTCTCCCGCC	Forward primer for marmoset α-globin
AF334	TCTAGATCATTAACGGTATTTGGAGGTCAGCAC	Reverse primer for marmoset α-globin
AF335	GAGCCTTTCGTTTTATTTAAGCTTCATTAGTGGTACTTGTGAG	Reverse primer for marmoset β-globin
AF289	CTGTCTCCGGCCGATAAAAAGAACGTTAAAGCTGCTTGG	Forward primer to create T8K in human α-globin
AF290	CCAAGCAGCTTTAACGTTCTTTTTATCGGCCGGAGACAG	Reverse primer to create T8K in human α-globin
JC112	TCTCCGGCCGATAAAAAGCACGTTAAAGCTGCTTGGGGT	Forward primer to create N9H in human α-globin using pHb0.0-human αT8K as template
JC113	ACCCCAAGCAGCTTTAACGTGCTTTTTATCGGCCGGAGA	Reverse primer to create N9H in human α-globin pHb0.0-human αT8K as template
JC114	TAATTAATGCTGTCTCCGGACGATAAAAAGCACGTTAAA	Forward primer to create A5D in human α-globin using pHb0.0-human αT8K;N9H as template
JC115	TTTAACGTGCTTTTTATCGTCCGGAGACAGCATTAATTA	Reverse primer to create A5D in human α-globin using pHb0.0-human αT8K;N9H as template
AF291	CACGTTGATGATATGCCGCAGGCGTTGTCTGCTCTGTC	Forward primer to create N78Q in human α-globin
AF292	GACAGAGCAGACAACGCCTGCGGCATATCATCAACGTG	Reverse primer to create N78Q in human α-globin
AF293	CACGTTGATGATATGCCGCACGCGTTGTCTGCTCTGTC	Forward primer to create N78H in human α-globin
AF294	GACAGAGCAGACAACGCGTGCGGCATATCATCAACGTG	Reverse primer to create N78H in human α-globin
AF303	CTGACTCCGGAAGAAAAAAACGCGGTTACTGCTCTG	Forward primer to create S9N in human β-globin
AF304	CAGAGCAGTAACCGCGTTTTTTTCTTCCGGAGTCAG	Reverse primer to create S9N in human β-globin
AF307	CTGACTCCGGAAGAAAAAACCGCGGTTACTGCTCTG	Forward primer to create S9T in human β-globin

AF308	CAGAGCAGTAACCGCGGTTTTTTCTTCCGGAGTCAG	Reverse primer to create S9T in human β-globin
AF305	CTGACTCCGGAAGAAAAAAAGGCGGTTACTGCTCTG	Forward primer to create S9K in human β-globin
AF306	CAGAGCAGTAACCGCCTTTTTTTCTTCCGGAGTCAG	Reverse primer to create S9K in human β-globin
AF309	CTGACTCCGGAAGAAAAAGCCGCGGTTACTGCTCTG	Forward primer to create S9A in human β-globin
AF310	CAGAGCAGTAACCGCGGCTTTTTCTTCCGGAGTCAG	Reverse primer to create S9A in human β-globin
AF313	GCTTTCTCTGACGGTCTGAATCACCTGGACAACCTG	Forward primer to create A76N in human β-globin
AF314	CAGGTTGTCCAGGTGATTCAGACCGTCAGAGAAAGC	Reverse primer to create A76N in human β-globin
AF311	GCTTTCTCTGACGGTCTGACTCACCTGGACAACCTG	Forward primer to create A76T in human β-globin
AF312	CAGGTTGTCCAGGTGAGTCAGACCGTCAGAGAAAGC	Reverse primer to create A76T in human β-globin
pHb0.0_for	CGACTGGAAAGCGGGCAG	Forward sequencing primer for pHb0.0
pHb0.0_rev	GCATTGTTAGATTTCATACACG	Reverse sequencing primer for pHb0.0
JC343	AAATACAATTGAGGTGAACATATGATGAACAAACAGCAAAAAG	Forward primer to clone *S. aureus isdB* into pOS1 P_{lgt} by Hi-fi assembly
JC344	AAACACTACCCCCTTGTTTGGATCCTTAGTTTTTACGTTTTCTAGGTAATAC	Reverse primer to clone *S. aureus isdB* into pOS1 P_{lgt} by Hi-fi assembly
JC218	AAATACAATTGAGGTGAACATATGATGAACAAACAGCAAAAAG	Forward primer to clone *S. schweitzeri isdB* into pOS1 P_{lgt} by Hi-fi assembly
JC219	AAACACTACCCCCTTGTTTGGATCCTTAGTTTTTACGTTTTCTAGGTAATAC	Reverse primer to clone *S. schweitzeri isdB* into pOS1 P_{lgt} by Hi-fi assembly
JC216	AAATACAATTGAGGTGAACATATGATGAACAAACAGCAAAAAG	Forward primer to clone *S. argenteus isdB* into pOS1 P_{lgt} by Hi-fi assembly
JC217	AAACACTACCCCCTTGTTTGGATCCTTAGTTTTTACGTTTTCGAGG	Reverse primer to clone *S. argenteus isdB* into pOS1 P_{lgt} by Hi-fi assembly
JC317	TTATGCAAGTACTGTTAAACCTG	Forward primer, creates S170T in pOS1 P_{lgt}*isdB* $_{aureus}$
JC318	TGATAAAACTGTTGAGTTCC	Reverse primer, creates S170T in pOS1 P_{lgt}*isdB* $_{aureus}$
JC315	AGATGGAACTAGACAGTTTTATCATTATG	Forward primer, creates Q162R in pOS1 P_{lgt}*isdB* $_{aureus}$
JC316	TTCTTTTTCATTTCAAAATCAATTG	Reverse primer, creates Q162R in pOS1 P_{lgt}*isdB* $_{aureus}$
JC319	TTATGCAAGTACTGTTAAACCTGCTAGAGTTATTTTC	Forward primer, simultaneously creates Q162R;S170T in pOS1 P_{lgt}*isdB* $_{aureus}$
JC320	TGATAAAACTGTCTAGTTCCATCTTTCTTTTTCATTTC	Reverse primer, simultaneously creates Q162R; S170T in pOS1 P_{lgt}*isdB* $_{aureus}$
JC228	TAAGAAGAGATGTAAGAGTAGGG	pOS1 P_{lgt} forward sequencing primer
JC229	GGGGGAAACACTACCCCCTTG	pOS1 P_{lgt} reverse sequencing primer

Chimeric hemoglobins were prepared by subcloning the α-globins. To enable digestion with XbaI (NEB) (which is sensitive to *dam* methylation) pHb0.0-human and pHb0.0-baboon were transformed and re-isolated from *E. coli* K1077 (*dam*$^{-}$ *dcm*$^{-}$). The α-globin from each plasmid was excised by digestion with XbaI (NEB) and PacI (NEB) and the α-globin and double-digested pHb0.0 containing β-globin were separately isolated by gel purification (Qiagen). Human α-globin was ligated into pHb0.0 containing baboon β-globin and baboon α-

globin was ligated (T4 ligase; NEB) into pHb0.0 containing human β-globin. Chimeras were confirmed by sequencing (GeneWiz) with pHb0.0_for/pHb0.0_rev.

pHb0.0-human was mutagenized using QuikChange Site-Directed Mutagenesis Kit (Agilent, Santa Clara, CA) to create changes in the α-gene: T8K (primers AF289/290), T8K;N9H (primers JC112/113; using pHb0.0-human αT8K as template), A5D;T8K;N9H (primers JC114/115; using pHb0.0-human αT8K;N9H as template), N78Q (primers AF291/292) and N78H (primers AF293/294). Changes in the human β-gene were as follows: S9N (primers AF303/304), S9T (primers AF307/308), S9A (primers AF309/310), S9K (primers AF305/306), A76N (primers AF313/314), and A76T (primers AF311/312).

Phylogenetic analyses

Hemoglobin DNA sequence alignments were performed using MUSCLE. Input phylogenies were based upon supported species relationships (374) as well as maximum-likelihood gene phylogenies generated using PhyML with SPR topology search and 1000 bootstraps for branch support (375). Tests for positive selection were performed using codeml from the PAML software package with the F3X4 codon frequency model. Likelihood ratio tests (LRTs) were performed by comparing pairs of site-specific models (NS sites): M1 (neutral) with M2 (selection), M7 (neutral, beta distribution of dN/dS<1) with M8 (selection, beta distribution, dN/dS>1 allowed). Additional tests which also account for synonymous rate variation and recombination, including FUBAR, FEL, and MEME, were performed using the HyPhy software package via the Datamonkey server (376, 377). Sites under positive selection were mapped onto three-dimensional molecular structures using Chimera (378) (http://www.cgl.ucsf.edu/chimera/).

The staphylococcal DNA gyrase gene tree was generated using PhyML with 1000 bootstraps as above. *M. caseolyticus* DNA gyrase was included as an outgroup. The similarity of IsdB in *S. argenteus* and *S. schweitzeri* relative to *S. aureus* is shown at right (Figure 57).

Recombinant purification of hemoglobin

Hemoglobin expression strains [BL21(DE3) pHUG21 pHb0.0] were streaked to LB agar containing 12.5 μg/ml carbenicillin and 5 μg/ml tetracycline hydrochloride. pHb0.0 encodes both α- and β-globin genes, and proper folding and tetramerization require sufficient intracellular heme. Therefore, pHUG21, which encodes a heme uptake system is co-expressed, and hemin is supplemented in the medium (373). Single colonies were inoculated into 5 ml of LB broth supplemented with 12.5 μg/ml carbenicillin and 5 μg/ml tetracycline

hydrochloride and grown for 14 h at 37°C with shaking. This culture was used to inoculated 1:500 into 1.5 L of LB with 12.5 µg/ml carbenicillin, 5 µg/ml tetracycline hydrochloride, 100 µM hemin (prepared fresh at 10 mM in 0.1 M NaOH; Sigma St. Louis, MO), and 50 µg/ml of the iron chelator ethylenediamine-di(o-hydroxyphenylacetic acid (EDDHA [LGC Standards, Teddington, UK; solid added directly to medium) in a 2.8 L Fernbach flask. Cultures were grown at 37°C until OD_{600} reached 0.6-0.8. The expression of hemoglobin was induced with 40 µg/ml IPTG (RPI, Mount Prospect, IL). After 16 h post-induction at 37°, cells were collected by centrifugation. The cell pellet was resuspended in 20 ml PBS containing 10 mM imidazole (Fisher), 5 mM $MgCl_2$ (Sigma), 1 Roche Protease inhibitor tablet (Fisher), approximately 1 mg/ml of lysozyme (Thermo) and 100 µg/ml deoxyribonuclease from bovine pancreas (Sigma). The cell pellet resuspended with rocking for 20 min at room temperature following incubation on ice. Cells were lysed using an Emulsaflex (Avestin, Ottawa, CA) then cell lysate was clarified by ultracentrifugation (60 min at 17,000 g). Cell lysate was applied to a 3 mL of Ni-NTA resin (Qiagen) in a gravity column, to which hemoglobin binds, washed with 50 ml PBS with10 mM imidazole. Hemoglobin was eluted with 6 ml PBS with 500 mM imidazole, with the first 1 ml of eluate discarded. The hemoglobin-containing eluate was dialyzed twice sequentially in PBS at 4°C. Purified hemoglobin was filter sterilized with a 0.45 micron filter and stored in aliquots in liquid nitrogen. Hemoglobin concentration was measured with Drabkin's reagent (Sigma) using human hemoglobin as a standard, ranging from 2-6 mg/ml. Relative purity was assessed using SDS-PAGE before use in experiments, as shown in Figure 47.

Whole cell hemoglobin binding assay

S. aureus strains were streaked on tryptic soy agar (containing 10 µg/ml chloramphenicol for strains carrying plasmids) and grown at 37°C for 24 h. Single colonies were used to inoculate 3 ml of RPMI containing 1%cas-amino acids and 0.5 mM 2,2'-dipyridyl (Acros/Fisher) to induce expression of chromosomal *isdB*) or 10 µg/ml chloramphenicol (for strains carrying plasmids with constitutive *isdB* expression). After 14-16 h of growth at 37°C with shaking, 2 OD_{600} units (except for experiments shown in part in Figure 53D and Figure 54C, were 1 OD_{600} unit was used) were collected by centrifugation in a 1.5 ml Eppendorf tube. The cell pellet was resuspended with 1 ml PBS or PBS containing recombinant hemoglobin. 10 µg/ml (chromosomal IsdB) or 2.5 µg/ml (plasmid-borne IsdB) of hemoglobin was used. The cells were incubated with hemoglobin or PBS for 30 min at 37°C with shaking, then cells were collected by centrifugation at 4°C at 8,000x g. Cells were washed thrice by pipetting with 1 ml

ice-cold PBS, centrifuging at 4°C at 8,000x g. After the final wash, the cells were resuspended in 30 µl 0.5 M Tris pH 8.0 (Fisher) containing 4% SDS (Fisher) and heated at 90°C for 5 min to remove surface bound proteins. Cells were collected by centrifugation at 8,000x g, and eluate was added to 6X loading buffer and heated at 90°C for 5 min. Samples were subjected to 12 or 17.5% SDS-PAGE and silver stained (GE, Boston, MA). Gels were imaged using an Alpha Innotech Alpha Imager or BioRad ChemiDoc MP imaging system. Quantification was performed by densitometry analysis with Image J (NIH) according to software instructions, and quantifying the area under the peak that corresponds to the hemoglobin band, excluding background density. Because of variation in stain intensity and quantity of non-specific bands across gels, all comparisons were made within the same gel, and relative density was calculated for each biological replicate within the same gel; the comparison was either to human hemoglobin or wildtype IsdB, depending on assay. Additionally, PBS only samples and *S. aureus* Δ*isdB*::*erm* were used to verify that hemoglobin binding in this assay is IsdB dependent (Figures 50, 55, and 57) as previously observed, and that recombinant human hemoglobin is bound equally as well as hemoglobin purified from human blood (Figure 49) (94, 95).

Growth with hemoglobin as sole iron source

For hemoglobin variants (Figure 50 and Figure 52) *S. aureus* Newman WT was streaked to tryptic soy agar and allowed to grow for 24 h at 37°C. A few colonies were used to inoculate 5 ml of RPMI (Corning, Corning, NY) supplemented with 1% cas-amino acids (Fisher) and 0.5 mM of EDDHA (prepared fresh in ethanol). After growth to stationary phase at 37°C with shaking, approximately 16 h, 4 µl of culture was inoculated into 196 µl of medium in a 96 well plate and OD_{600} at 37°C with shaking was monitored over time using a BioTek plate reader. Medium was RPMI containing 1% cas-amino acids that had been stripped of cations with Chelex 100 (Sigma) according to manufacturer's instructions, filter sterilized, and supplemented with 25 µM $ZnCl_2$, 25 µM $MnCl_2$, 100 µM $CaCl_2$, and 1 mM $MgCl_2$ (all from Fisher) to restore non-iron cations, 1.5 mM EDDHA to chelate any remaining free iron, and 2.5 µg/ml of recombinant purified hemoglobin as the sole iron source.

For IsdB variants (Figure 59), *S. aureus* strains were streaked to tryptic soy agar containing 10 µg/ml chloramphenicol and allowed to grow for 24 h at 37°C. A single colony was resuspended in 120 µl RPMI containing 1 µM EDDHA (prepared fresh in 0.1 M NaOH) and 5 µg/ml chloramphenicol and 100 µl was added to 2 ml of RPMI containing 1 µM EDDHA and 5 µg/ml chloramphenicol and grown at 37° with shaking in aeration tubes for 8 h. The

OD_{600} was measured of each culture and normalized to 1, and 5 µl was used to inoculate 2 ml of RPMI containing 1 µM EDDHA, 5 µg/ml chloramphenicol, and 50 nM hemoglobin or no hemoglobin (for Δ*isdB* pOS1 P_{lgt}*isdB*). Growth was monitored every 12 h by removed 50 µl of culture and adding to 150 µl PBS and measuring OD_{600} with pathlength correction in a BioTek plate reader. supplemented with 1% cas-amino acids (Fisher) and 0.5 mM of EDDHA (prepared fresh in ethanol). Growth using hemoglobin as a sole iron source in both assays is IsdB dependent (94, 95, 119).

Cloning of *isdB*

The full length coding sequences of IsdB were amplified from genomic DNA using Phusion 2X High-Fidelity Master Mix (Thermo); cells were treated with 20 µg of lysostaphin (AMBI Products, Lawrence, NY) and DNA was isolated with Wizard genomic DNA extraction kit (Promega, Madison, WI). *S. aureus isdB* (*NWMN_1040*) was amplified using primers JC343/344, *S. schweitzeri isdB* (*ERS140239_01018*) using primers JC218/219, and *S. argenteus isdB* (*SAMSHR1132_09750*) using primers JC216/217. Each primer pair included homology to pOS1 P_{lgt} digested with NdeI and BamHI-HF (NEB), and PCR products were ligated to pOS1 P_{lgt} with Hi-Fi assembly (NEB), transformed into *E. coli* DH5α and re-isolated by miniprep (Thermo). All plasmids were sequence confirmed by sequencing (GeneWiz). Plasmids were transformed into RN4220 by electroporation, re-isolated, and transformed into *S. aureus* Newman Δ*isdB*::*erm* by electroporation.

***S. aureus* IsdB site-directed mutagenesis**

pOS1 P_{lgt}*isdB*$_{aureus}$ was subjected to site-directed mutagenesis by PCR with Q5 Site Directed Mutagenesis (NEB). Primer pairs with desired mutation were used to create Q162R (primers JC315/316), S170T (primers 317/318) and Q162R;S170T (primers JC319/320). PCR products were transformed to DH5α. Plasmids were isolated and subjected to Sanger sequencing with primers JC228/229 (GeneWiz) to identify successful incorporation of the desired mutation. Plasmids were transformed into RN4220 by electroporation, re-isolated, and transformed into *S. aureus* Newman Δ*isdB*::*erm* by electroporation.

Quantification and statistical analysis

Specific statistical details for each experiment can be found in the corresponding figure legend. Data analysis and statistical tests were performed in Prism 6 (Graphpad).

Results

Parallel signatures of positive selection in primate hemoglobins at the IsdB binding interface

To investigate how natural selection has shaped hemoglobin diversity in simian primates, orthologs of the α- and β-globin genes were cloned and sequenced from primate cell lines as well as compiled from publically available databases. In total, 27 α-globin and 30 β-globin orthologs were assembled for phylogenetic analyses using the PAML and HyPhy software packages (Figure 47A, Materials and Methods), which use nonsynonymous and synonymous substitution rates to infer signatures of positive selection. Because globin genes have been shown to undergo gene conversion which can distort inferred phylogenetic relationships (379, 380), all analyses were performed using both a well-supported species tree as well as gene trees generated using PhyML. All tests detected significant evidence of positive selection acting on both α- and β-globin using both species and gene phylogenies (Appendix B). Multiple analyses repeatedly identified two sites in α- and β-globin exhibiting strong signatures of positive selection (Figure 47A). It became apparent that these rapidly-evolving sites localized to similar regions of the α- and β-globin proteins, specifically the N-terminal A helix and the hinge region between the E and F helices (Figure 47B). In fact, the two sites exhibiting signatures of selection in the α- and β-globin A helices are at homologous positions. These parallel signatures of selection between α- and β-globin could indicate that a similar selective pressure has driven this divergence between primate species. To investigate whether bacterial heme scavenging receptors could be one such selective pressure, rapidly evolving sites were mapped onto a recently solved co-crystal structure between human hemoglobin and the IsdB protein from *S. aureus* (119). Notably, all four rapidly-diverging hemoglobin residues are localized to the IsdB binding interface, in close proximity to the NEAT1 domain (Figure 47C). Together these findings indicate that primate globins have undergone rapid divergence at specific sites proximal to the binding interface of the *S. aureus* hemoglobin receptor IsdB.

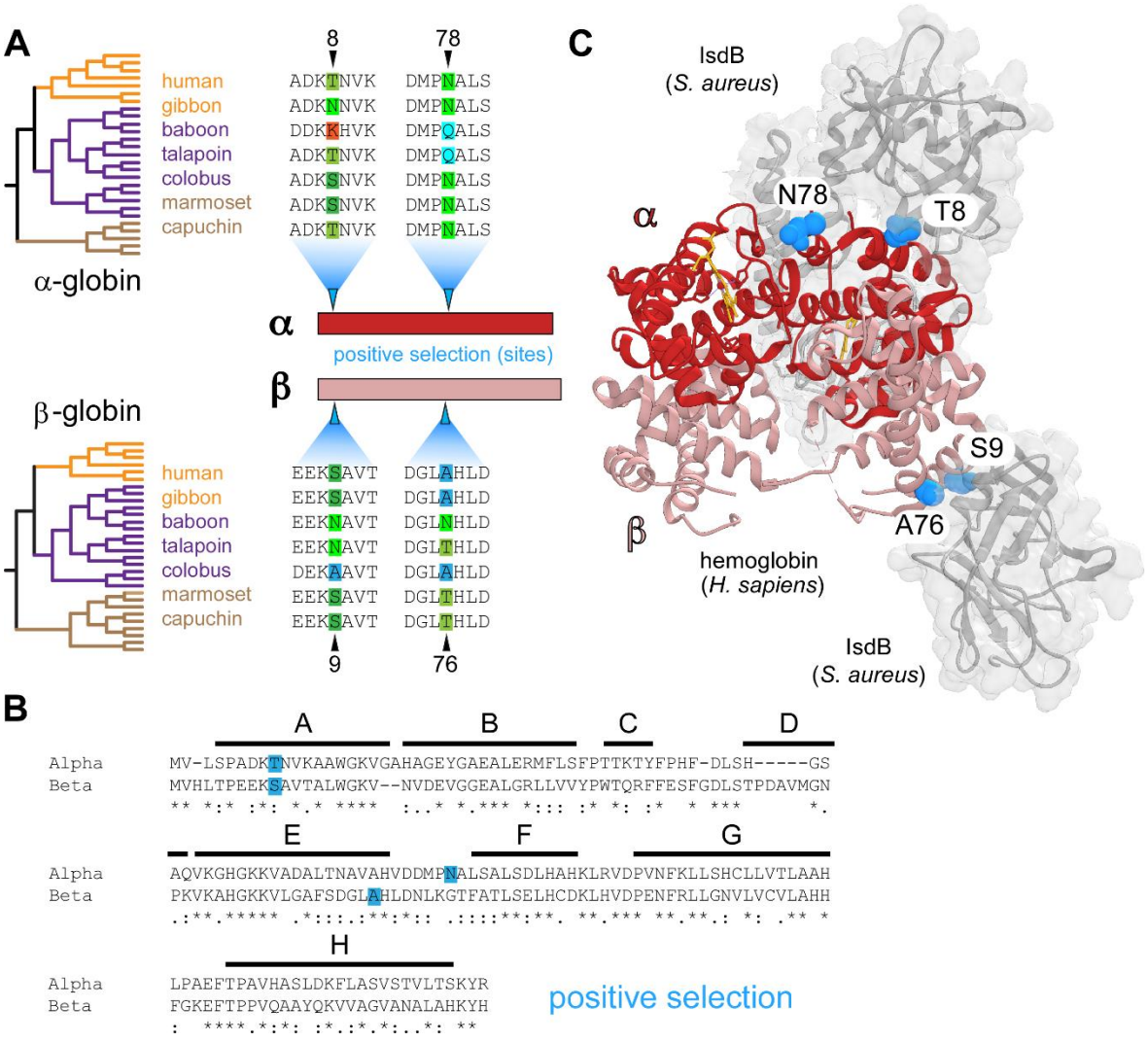

Figure 47 Parallel signatures of positive selection among primate hemoglobins at the bacterial IsdB binding interface [M.F.B]. (A) Species phylogenies for 27 α-globin and 30 β-globin orthologs analyzed (left). Alignments from representative species across hominoid (orange), Old World monkey (purple) and New World monkeys (brown) are shown, the full phylogenetic trees are displayed in Figures 3 and 4. Amino acid sites under positive selection were identified in α-globin and β-globin (blue arrows) using PAML with both species and gene trees (posterior probabilities >0.95). **(B)** Amino acid alignment of human α-globin and β-globin proteins. The position of conserved helices A-H are shown, and identity between globins is noted as conserved (*), highly similar (**:**), and similar (**.**). **(C)** The residues of α-globin (red) and β-globin (salmon) under positive selection (blue spheres) at the interface of hemoglobin capture by *Staphylococcus aureus* IsdB (gray) (PDB:5VMM).

Primate hemoglobin variation dictates *S. aureus* binding and heme-iron acquisition

To assess how hemoglobin divergence among primates impacts recognition by *S. aureus*, recombinant hemoglobin from human, white-cheeked gibbon, baboon, talapoin, and marmoset were purified, providing broad representation from our phylogenetic dataset. An established biochemical assay was used to measure binding of hemoglobin by *S. aureus*, in which *S. aureus* cells recognize recombinant human hemoglobin as well as hemoglobin purified from blood in an IsdB-dependent manner (Figure 48). *S. aureus* exhibited significantly reduced binding of baboon and marmoset hemoglobin to the cell surface (Figure 50 and Figure 51). It was noted that binding patterns do not strictly match predictions based on host phylogeny, suggesting discrete large-effect substitutions in hemoglobin may contribute disproportionately to recognition by *S. aureus*. I next determined the ability of primate hemoglobins to support growth of *S. aureus* as the sole iron source. Consistent with whole-cell binding data, hemoglobins that were bound by *S. aureus* with low affinity were unable to support optimal bacterial growth, indicating that the capability to bind hemoglobin is a measure of the ability to utilize hemoglobin as an iron source (Figure 50B and Figure 52). Together these results demonstrate that variation among primate globins dictates bacterial hemoglobin capture and heme-dependent growth.

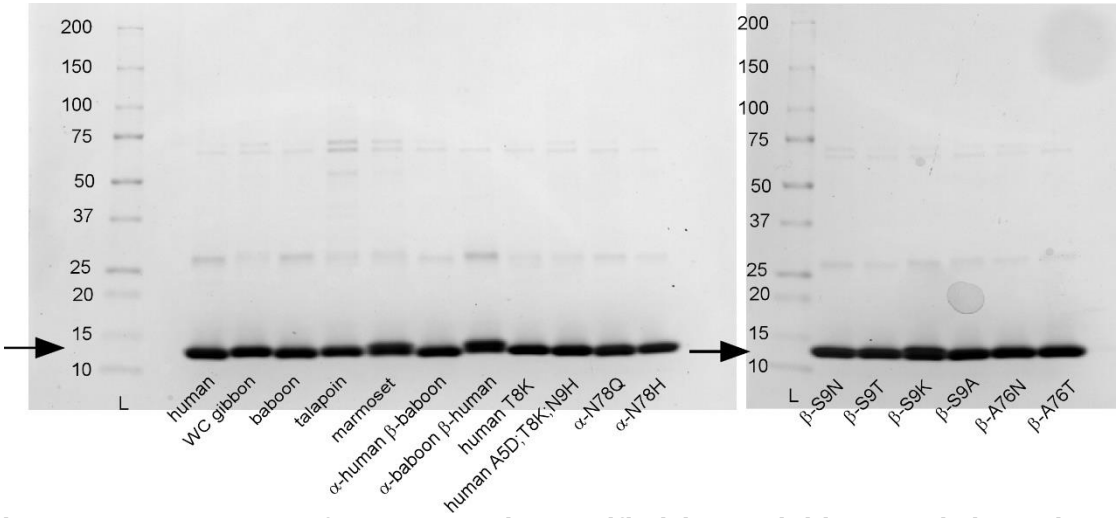

Figure 48 SDS-PAGE of representative purified hemoglobins used throughout this study. One microgram of hemoglobin was subjected to SDS-PAGE (4-20% gradient) and stained with Imperial Protein Stain. Molecular weight markers are indicated, with arrow showing hemoglobin band. High molecular weight bands may be contamination or unresolved dimers and tetramers.

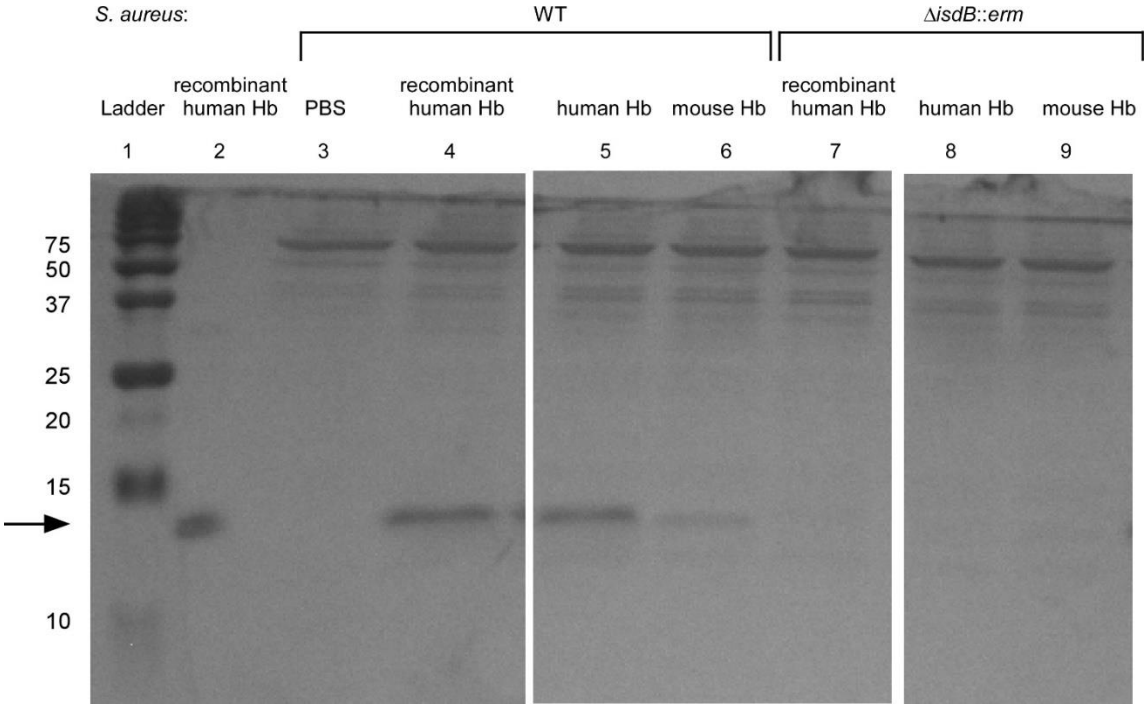

Figure 49 The whole cell hemoglobin (Hb) binding assay allows for IsdB-dependent, species-specific quantification of bound recombinant Hb. A representative silver-stained SDS-PAGE gel used to assess binding of hemoglobin to the surface of *S. aureus*. 100 ng of purified recombinant Hb was loaded (lane 2) to demonstrate apparent molecular weight in this gel; the 15 kDa marker is marked, with an arrow indicating hemoglobin. The apparent hemoglobin band is specific to Hb, as it is not visible when *S. aureus* is incubated with PBS alone (lane 3). *S. aureus* binds human hemoglobin purified recombinantly from *E. coli* (lane 4) as well as Hb purified from blood (lane 5). Binding of Hb purified from mouse blood (lane 6) is significantly diminished, as first reported in (94). Binding of Hb is dependent on IsdB, as demonstrated in lanes 7-9, where the same hemoglobins were incubated with *S. aureus* lacking *isdB*. An approximately equivalent amount of *S. aureus* was used, as demonstrated by equal loading of non-Hb specific bands across the top of the gel.

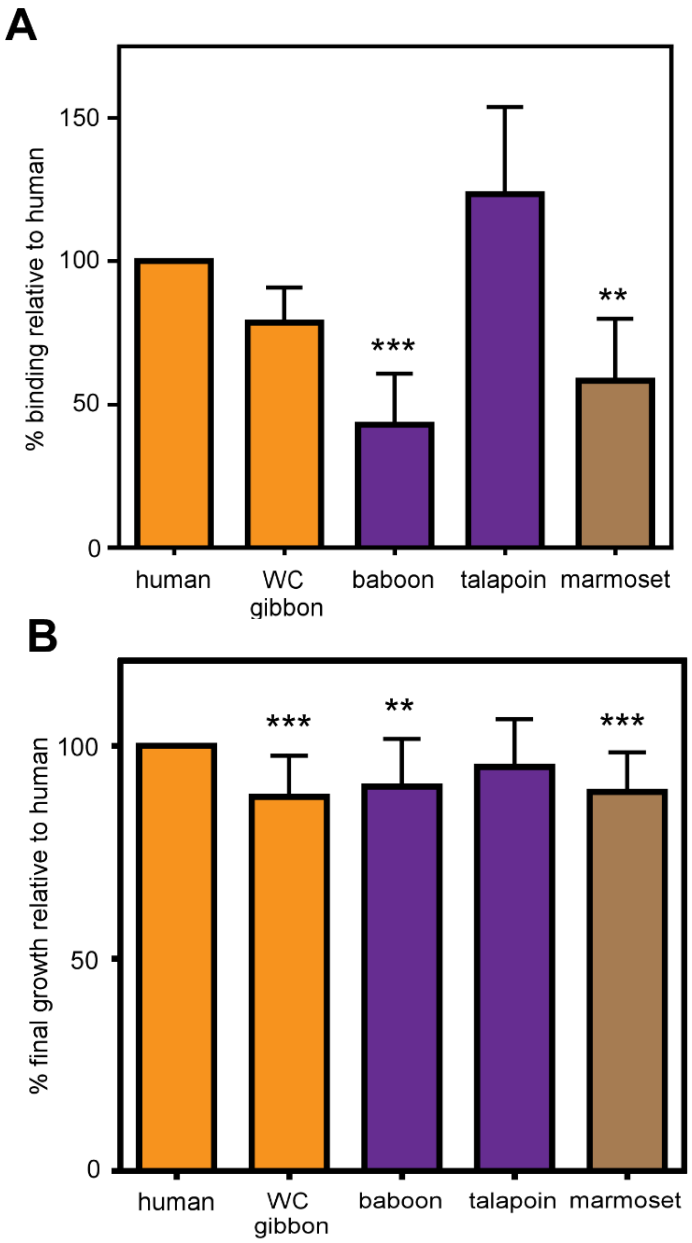

Figure 50 Primate hemoglobin variation dictates *S. aureus* binding and heme-iron acquisition [A.J.F]. (A) *S. aureus* binding of recombinant hemoglobin of various primate species. Iron-starved *S. aureus* wildtype was incubated with purified recombinant hemoglobin from representative species across hominoid (orange), Old World monkey (purple) and New World monkeys (brown). Hemoglobin bound to the surface of *S. aureus* was eluted and analyzed by SDS-PAGE; relative hemoglobin abundance was measured by densitometry analysis (Image J) and compared to human hemoglobin for each replicate. **(B)** Growth of *S. aureus* in iron-deplete medium with 2.5 µg/ml of purified recombinant hemoglobin as the sole iron source. Shown is the final growth yield of *S. aureus* after 48 hours. Growth of each replicate is compared to growth using human hemoglobin. For A, graphed are the means of two independent experiments in biological triplicate; for B, graphed are the means of three independent experiments with 2-3 biological replicates; +/- SEM, ** $p<0.005$; *** $p<0.0005$ by two-way ANOVA with Sidak correction for multiple comparisons comparing transformed (percent value) data.

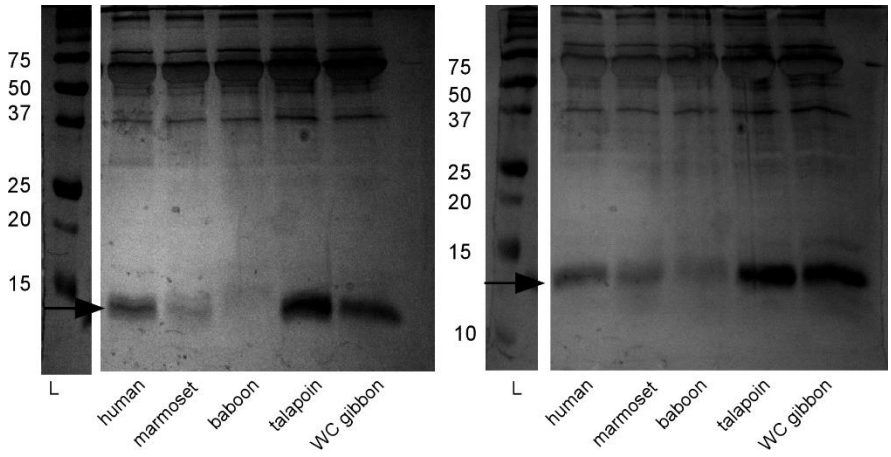

Figure 51 Representative silver stained SDS-PAGE gel of hemoglobin binding assay shown in Figure 50 [A.J.F.]. Each gel represents a biological replicate from independent binding assays. Molecular weight markers are indicated, with arrow showing hemoglobin band.

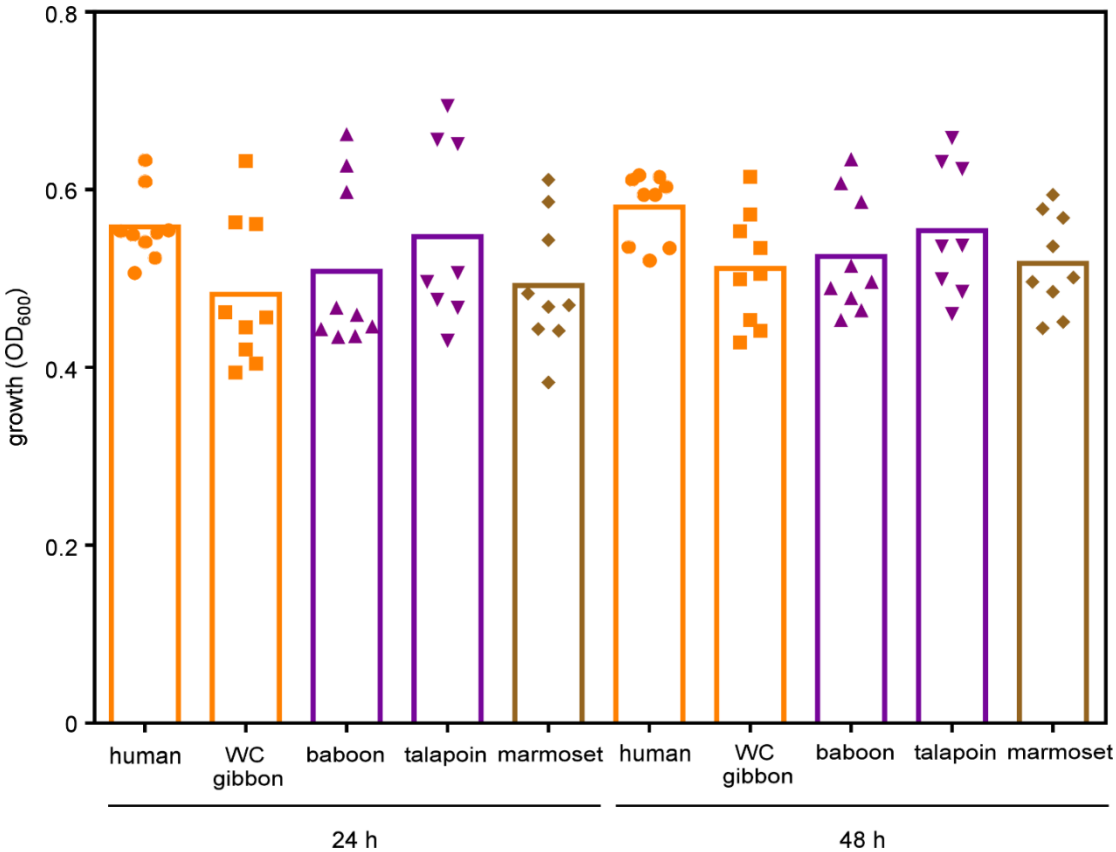

Figure 52 Growth of *S. aureus* using primate hemoglobin as the sole iron source [A.J.F.]. Graphed are the OD_{600} values at 24 and 48 h post inoculation with *S. aureus* wildtype of iron-deplete medium containing hemoglobin of various primate species. Each dot is a single biological replicate from three independent experiments, with one replicate missing for talapoin.

Species-specific diversity in α-globin restricts heme scavenging by *S. aureus*

The identification of rapidly evolving sites at the IsdB binding interface in both α-globin and β-globin suggest that both globin subunits may contribute to *S. aureus* species-specific hemoglobin capture. I therefore exploited the enhanced binding of human hemoglobin relative to baboon to examine the role of each globin subunit in this biochemical interaction. The ability of *S. aureus* to bind chimeric hemoglobins was measured, which revealed that both globins contribute to species-specificity (Figure 53A and Figure 54A), as chimeras containing either human α- or β-globin were bound more effectively than baboon hemoglobin. However, α-globin appears to have a greater effect on human-specific capture, as the α-human β-baboon chimera was bound significantly better than α-baboon β-human. Focusing on phylogenetic variation at the protein binding interface, α-globin T8 and N78 are both proximal to the NEAT1 domain of IsdB (Figure 53B, C). Mutagenesis of the N-terminal alpha helix of human α-globin revealed that substituting the Thr residue of human with the Lys residue of baboon at position 8 reduced binding by *S. aureus* (Figure 53D and Figure 54). Additionally, substituting A5D, T8K, and N9H in human α-globin, which converts this seven amino acid region (Figure 53B) to that of baboon, leaves *S. aureus* binding nearly indistinguishable from that of baboon hemoglobin. These results demonstrate that the N-terminal helix of α-globin makes a major contribution to human-specific hemoglobin recognition by *S. aureus*. Next, the relative importance of the rapidly evolving N78 residue in α-globin was assessed, which lies N-terminal to the sixth alpha helix (Figure 53B). Substitution of N78 to glutamine (present in baboon, talapoin, and other Old World primates) or to histidine, reduced binding of human hemoglobin (Figure 54E and Figure 55D). Thus, substitutions at multiple residues in α-globin that exhibit signatures of repeated positive selection are sufficient to disrupt the ability of *S. aureus* to recognize human hemoglobin.

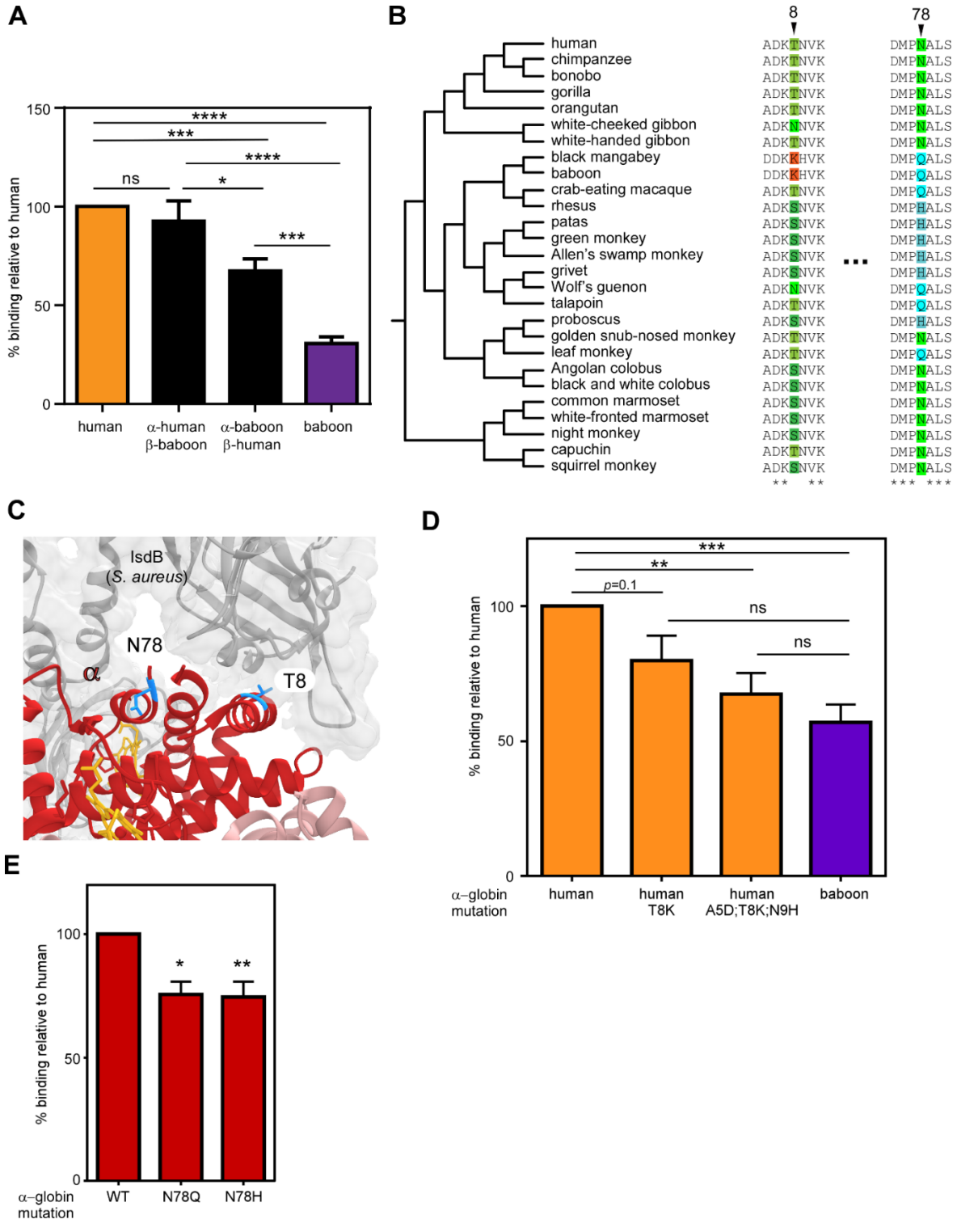
A
150
100
50
0
% binding relative to human
****
***
****
ns
*
***
human
α-human β-baboon
α-baboon β-human
baboon
B
8
78
human
chimpanzee
bonobo
gorilla
orangutan
white-cheeked gibbon
white-handed gibbon
black mangabey
baboon
crab-eating macaque
rhesus
patas
green monkey
Allen's swamp monkey
grivet
Wolf's guenon
talapoin
proboscus
golden snub-nosed monkey
leaf monkey
Angolan colobus
black and white colobus
common marmoset
white-fronted marmoset
night monkey
capuchin
squirrel monkey
ADKTNVK DMPNALS
ADKTNVK DMPNALS
ADKTNVK DMPNALS
ADKTNVK DMPNALS
ADKTNVK DMPNALS
ADKNNVK DMPNALS
ADKTNVK DMPNALS
DDKKHVK DMPQALS
DDKKHVK DMPQALS
ADKTNVK DMPQALS
ADKSNVK DMPHALS
ADKSNVK DMPHALS
ADKSNVK DMPHALS
ADKSNVK DMPHALS
ADKNNVK DMPQALS
ADKTNVK DMPQALS
ADKSNVK DMPHALS
ADKTNVK DMPNALS
ADKTNVK DMPQALS
ADKSNVK DMPNALS
ADKSNVK DMPNALS
ADKSNVK DMPNALS
ADKSNVK DMPNALS
ADKTNVK DMPNALS
ADKSNVK DMPNALS
** **
*** ***
C
IsdB
(S. aureus)
N78
α
T8
D
100
50
0
% binding relative to human
***
**
p=0.1
ns
ns
α–globin mutation
human
human T8K
human A5D;T8K;N9H
baboon
E
100
50
0
% binding relative to human
*
**
α–globin mutation
WT
N78Q
N78H

Figure 53 Species-specific diversity in α-globin restricts heme scavenging by *S. aureus* [M.F.B: panel B]. (A) Iron-starved *S. aureus* wildtype was incubated with purified recombinant hemoglobin and bound hemoglobin was quantified. **(B)** Species phylogenies and sequence alignments surrounding positions exhibiting signatures of positive selection in α-globin. **(C)** Residues 8 and 78 of human α-globin (red) interact closely with IsdB (gray) (PDB:5VMM). **(D)** Iron-starved *S. aureus* wildtype was incubated with purified recombinant hemoglobin, including mutagenized human hemoglobin, and bound hemoglobin was quantified. (E) Iron-starved *S. aureus* wildtype was incubated with purified recombinant hemoglobin, including mutagenized human hemoglobin, and bound hemoglobin was quantified. For A graphed are the means of 3 independent experiments with 2-3 biological replicates, for D, graphed are the means of 6 independent experiments with 2-3 biological replicates for E, graphed are the means of 2 independent experiments with 3 biological replicates +/- SEM, ns: no significance, * $p<0.05$, ** $p<0.005$; *** $p<0.0005$ by two-way ANOVA with Sidak correction for multiple comparisons comparing transformed (percent value) data.

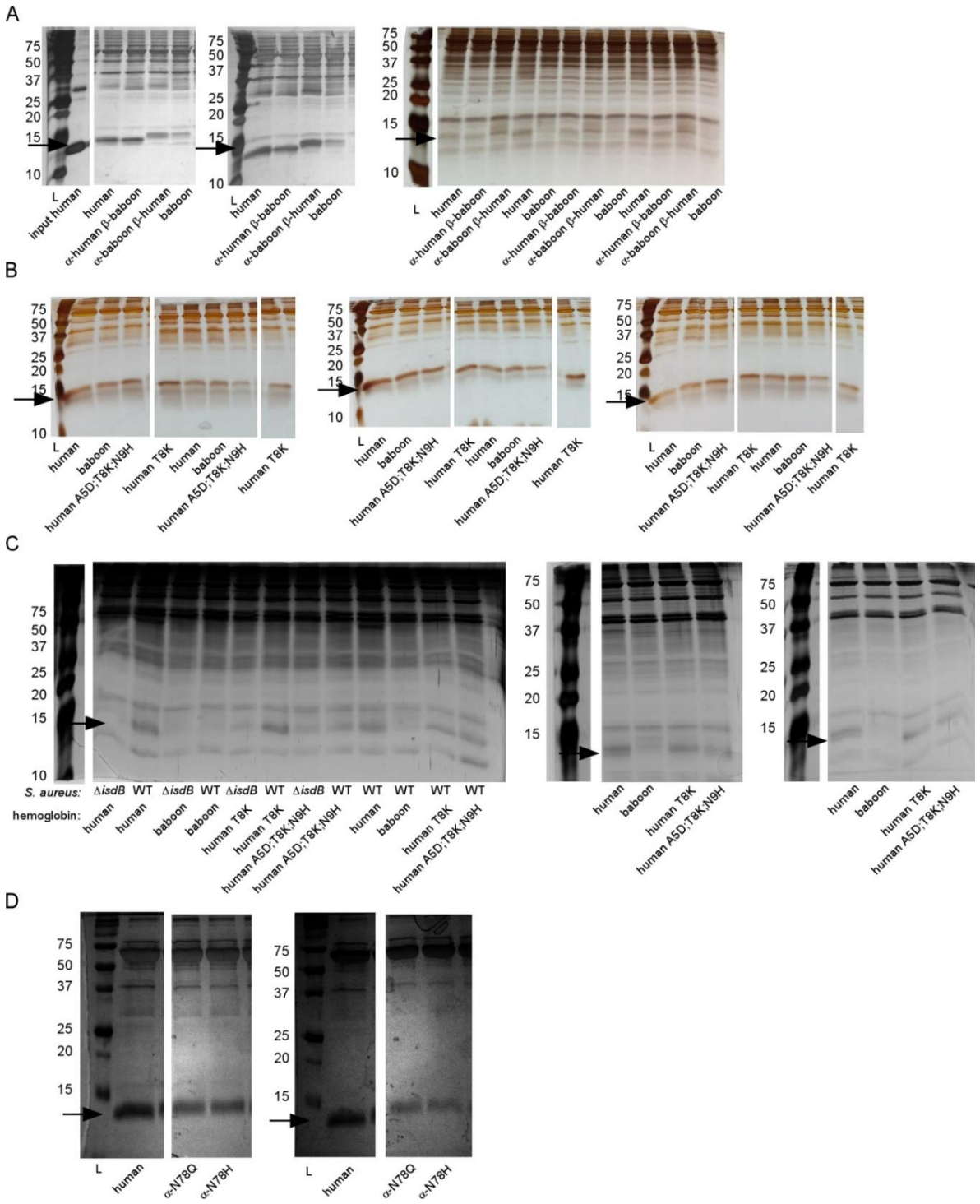

Figure 54 Representative silver stained SDS-PAGE gel of hemoglobin binding assay shown in Figure 53 [A.J.F.: panel D]. **(A)** corresponds to Figure 53A, **(B-C)** correspond to Figure 53D where **(C)** shows results of experiments using OD_{600} unit of 1 instead of 2 used throughout, and **(D)** corresponds to figure 53E. Each gel represents a biological replicate from independent binding assays. Molecular weight markers are indicated, with arrow showing hemoglobin band.

β-globin divergence contributes to *S. aureus* hemoglobin binding

S. aureus was capable of binding α-baboon β-human chimeric hemoglobin with higher affinity than baboon hemoglobin (Figure 53A), signifying that β-globin also contributes to *S. aureus* species-specific hemoglobin capture. Therefore, the contribution of rapidly evolving residues in β-globin to this binding interaction were investigated (Figure 55A). Both S9 and A76 interact closely with the NEAT1 domain of IsdB (Figure 55B). The effect of substituting human β-globin S9 and A76 with residues found in other primate species analyzed in this work was systematically tested, which revealed that A76 is particularly important for binding by *S. aureus* (Figure 55C and Figure 56). Notably, baboon and human β-globin differ at both positions 9 and 76, suggesting that these residues may contribute to the inability of IsdB to bind baboon hemoglobin. These differences might also explain the binding affinity between human hemoglobin and the α-human β-baboon chimera, observed in Figure 53A. As for α-globin, no single residue substitution improved binding by *S. aureus* IsdB, consistent with the hypothesis that IsdB has specifically adapted to bind human hemoglobin. Taken together with earlier data, residues at the IsdB interface of both α-globin and β-globin contribute to recognition of hemoglobin by *S. aureus*. This is consistent with the NEAT1 domain of multiple IsdB monomers engaging in hemoglobin capture by binding both α- and β-globins, as observed in the reported co-crystal structure (119).

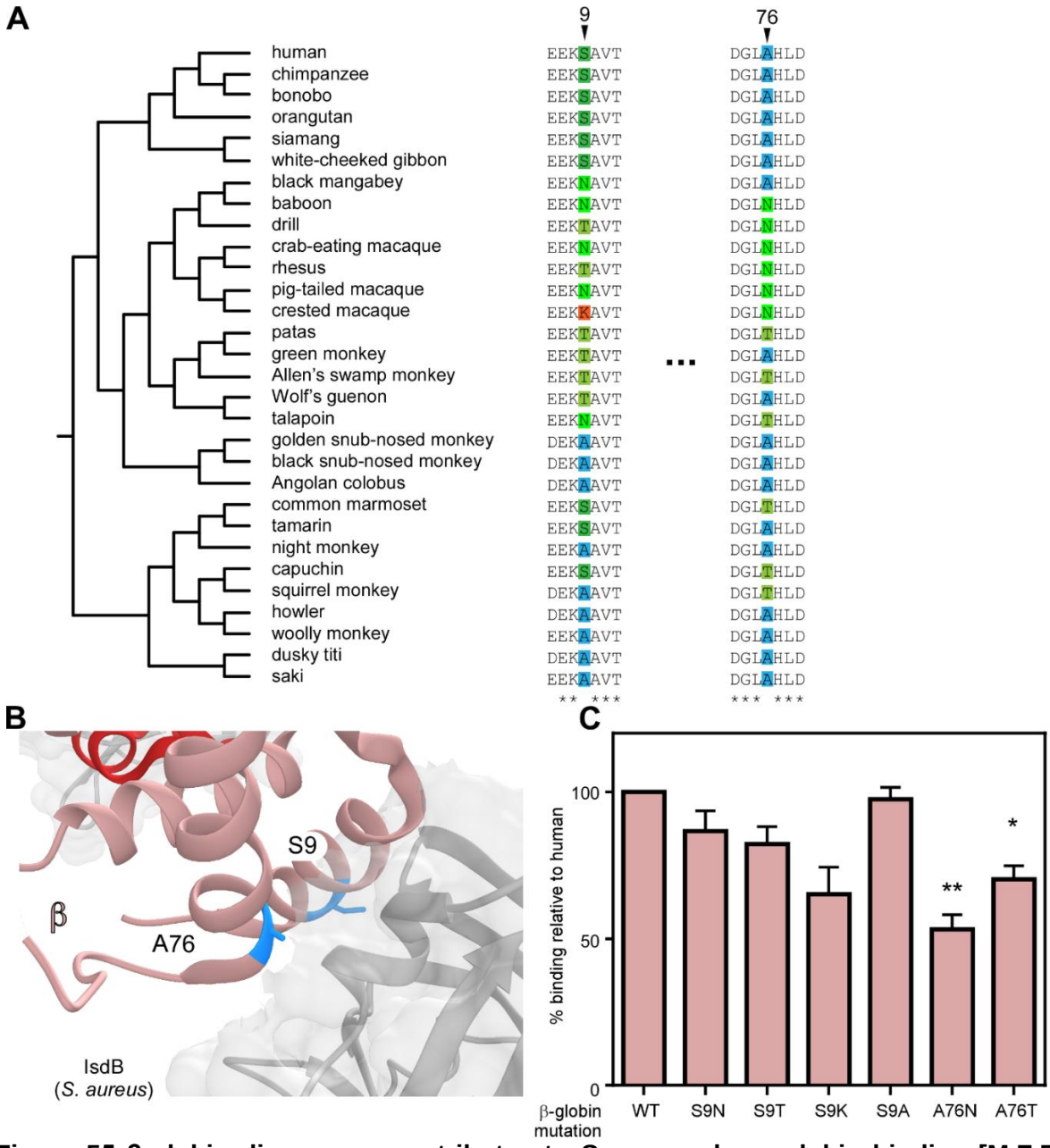

Figure 55 β-globin divergence contributes to *S. aureus* hemoglobin binding [M.F.B: panel A]. **(A)** Species phylogenies and sequence alignments surrounding positions exhibiting signatures of positive selection in β-globin. **(B)** Residues 9 and 76 of human β-globin (salmon) interact closely with IsdB (gray) (PDB:5VMM). **(C)** Iron-starved *S. aureus* wildtype was incubated with purified recombinant human hemoglobin or variants of human hemoglobin encoding variants in β-globin, and bound hemoglobin was quantified. Graphed are the means of four independent experiments with 3 biological replicates +/- SEM, * $p<0.05$; ** $p<0.005$ by two-way ANOVA with Sidak correction for multiple comparisons comparing transformed (percent value) data

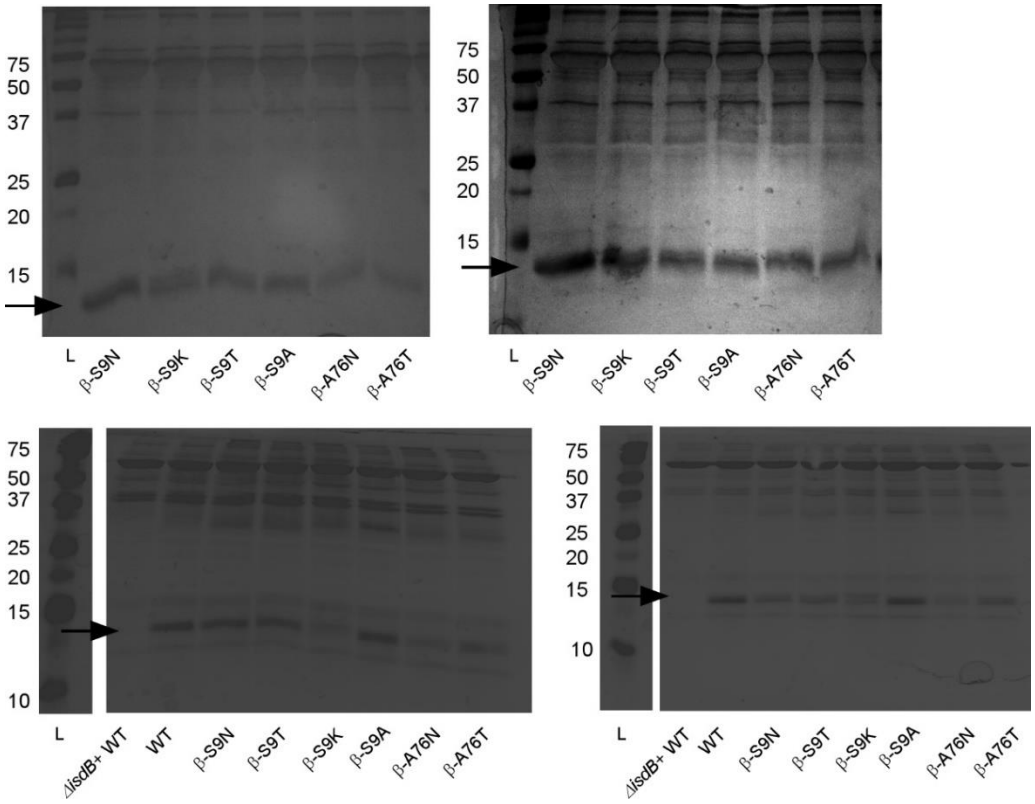

Figure 56 Representative silver stained SDS-PAGE gel of hemoglobin binding assay shown in Figure 55 [A.J.F. in part]. Each gel represents a biological replicate from independent binding assays. Molecular weight markers are indicated, with arrow showing hemoglobin band.

IsdB diversity among related staphylococcal strains impacts primate-specific hemoglobin capture

Given the observed differences in *S. aureus* binding between diverse primate hemoglobins, I considered how genetic variation in IsdB might impact this interaction. The IsdB NEAT1 subdomain Q162R-S170T is critical for hemoglobin recognition and is completely conserved among more than three thousand *S. aureus* clinical isolates (95). Therefore, IsdB variation among congeneric *S. argenteus* and *S. schweitzeri* was assessed. These recently diverged taxa (Figure 57A) are both primate-associated and, unlike most other staphylococci, encode IsdB. I measured the ability of IsdB from *S. argenteus* and *S. schweitzeri* to bind hemoglobin by expressing them ectopically in *S. aureus* lacking the native *isdB* gene. Consistent with their overall high sequence identity, *S. schweitzeri* and *S. argenteus* IsdB bind primate hemoglobin with a similar pattern of species preference as *S. aureus* (Figure 57B and Figure 58). However, both the IsdB of *S. schweitzeri* and *S. argenteus* display reduced binding of talapoin hemoglobin, and *S. argenteus* IsdB does not bind marmoset hemoglobin significantly less than human hemoglobin. These data indicate that variation among IsdB impacts species-specific hemoglobin capture.

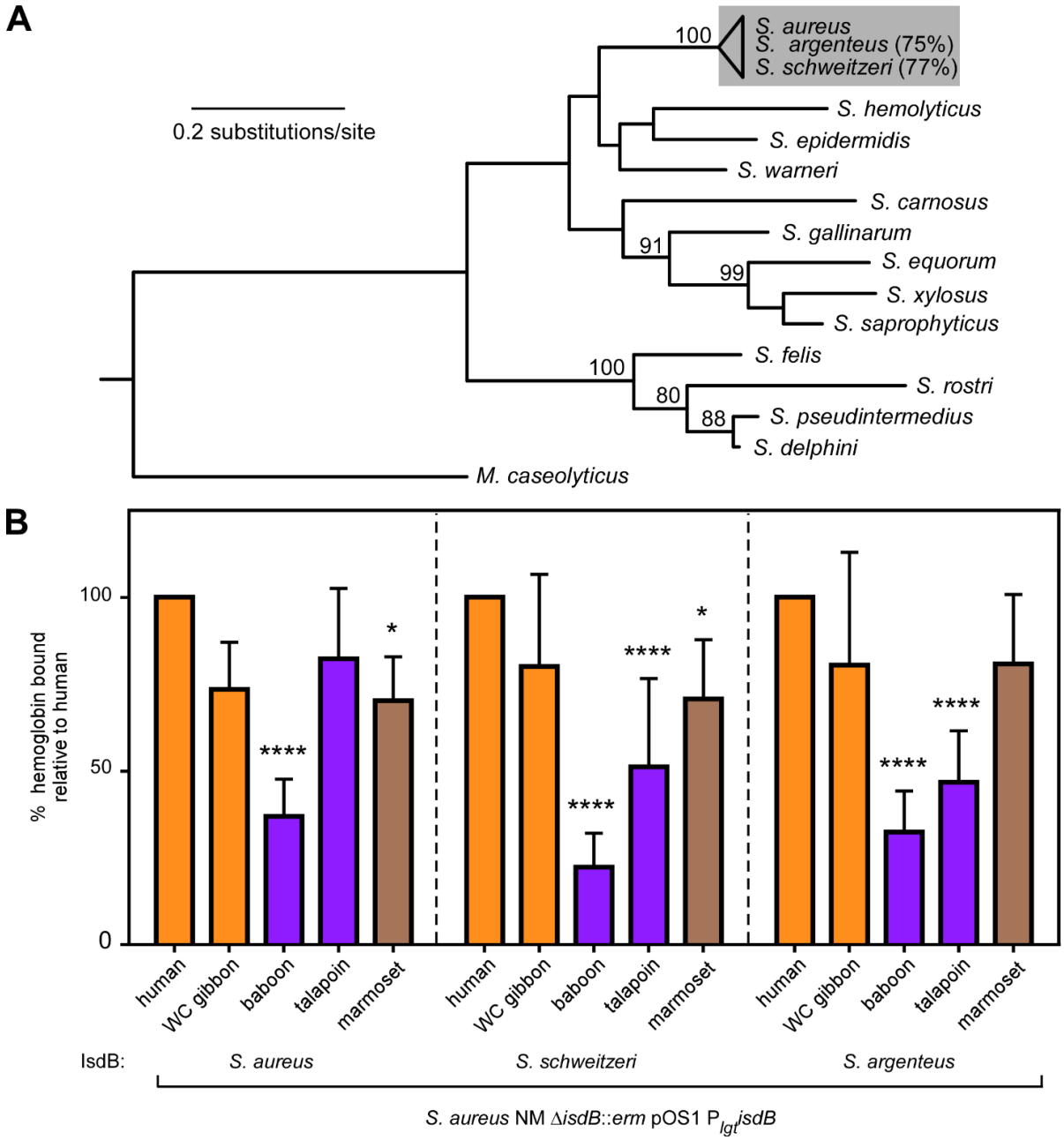

Figure 57 IsdB diversity among related staphylococcal strains impacts primate-specific hemoglobin capture [M.F.B.: panel A]. (A) Maximum likelihood phylogeny of the DNA gyrase A protein from representative staphylococci generated using PhyML. *M. caseolyticus* was included as an outgroup. The similarity of IsdB in *S. argenteus* and *S. schweitzeri* relative to *S. aureus* is shown at right. Bootstrap values above 80 are indicated. **(B)** *S. aureus* lacking native *isdB* but encoding constitutively expressed plasmid-borne *isdB* variants were incubated with purified recombinant hemoglobin, from hominoid (orange), Old World monkey (purple) and New World monkeys (brown) and bound hemoglobin was quantified. Graphed are the means of three independent experiments with 3 biological replicates +/- SEM, * $p<0.05$; **** $p<0.0001$ by two-way ANOVA with Sidak correction for multiple comparisons, comparing transformed (percent value) data.

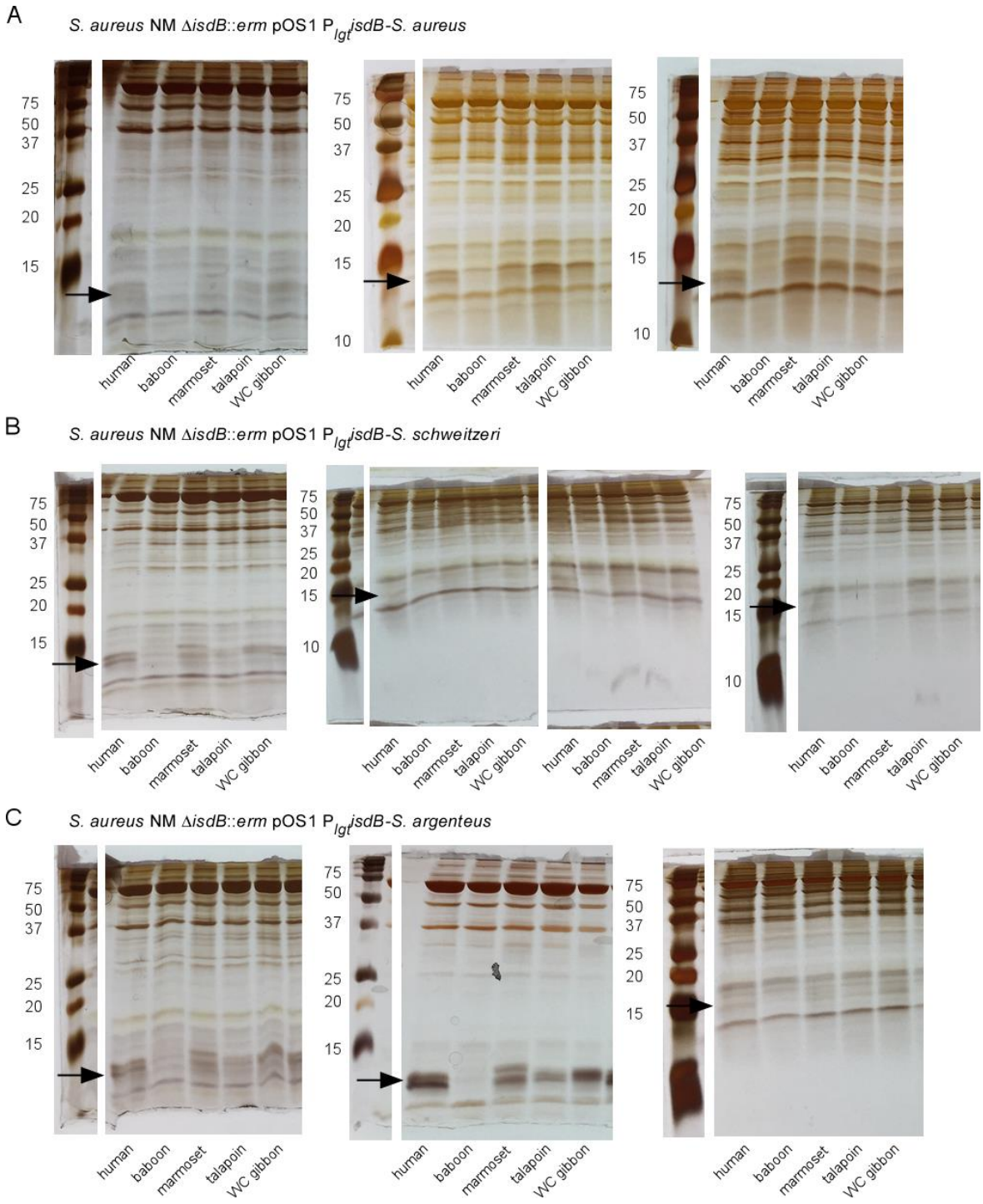

Figure 58 Representative silver stained SDS-PAGE gel of hemoglobin binding assay shown in Figure 57. Each gel represents a biological replicate from independent binding assays. Molecular weight markers are indicated, with arrow showing hemoglobin band.

IsdB NEAT1 domain diversity among staphylococci modulates human hemoglobin recognition

Closer examination of the Q162R-S170T region of IsdB NEAT1 revealed variation between related staphylococci, but no variation in the critical heme-binding region of NEAT2 (Figure 59A). This region of NEAT1 closely interacts with the N-terminal helices of either α-globin and β-globin, in close proximity to both discrete sites bearing signatures of adaptive evolution in α-globin and β-globin (Figure 59B). To determine the functional consequences of variation in this NEAT1 domain, Q162 and S170T were mutagenized in *S. aureus* IsdB to mimic the sequence of *S. schweitzeri* and *S. argenteus*. These residues are not expected to disrupt IsdB tertiary structure, as they already exist in related IsdB proteins. Variations at both of these positions reduced affinity for human hemoglobin, showing that in the context of *S. aureus* IsdB, Q162 and S170 are required for high affinity hemoglobin binding (Figure 59C and Figure 60). Additionally, mutagenized IsdB failed to fully support the growth of *S. aureus* using human hemoglobin as the sole iron source (Figure 59D), which supports the conclusion that this NEAT1 subdomain of *S. aureus* has evolved for optimal binding and utilization of human hemoglobin.

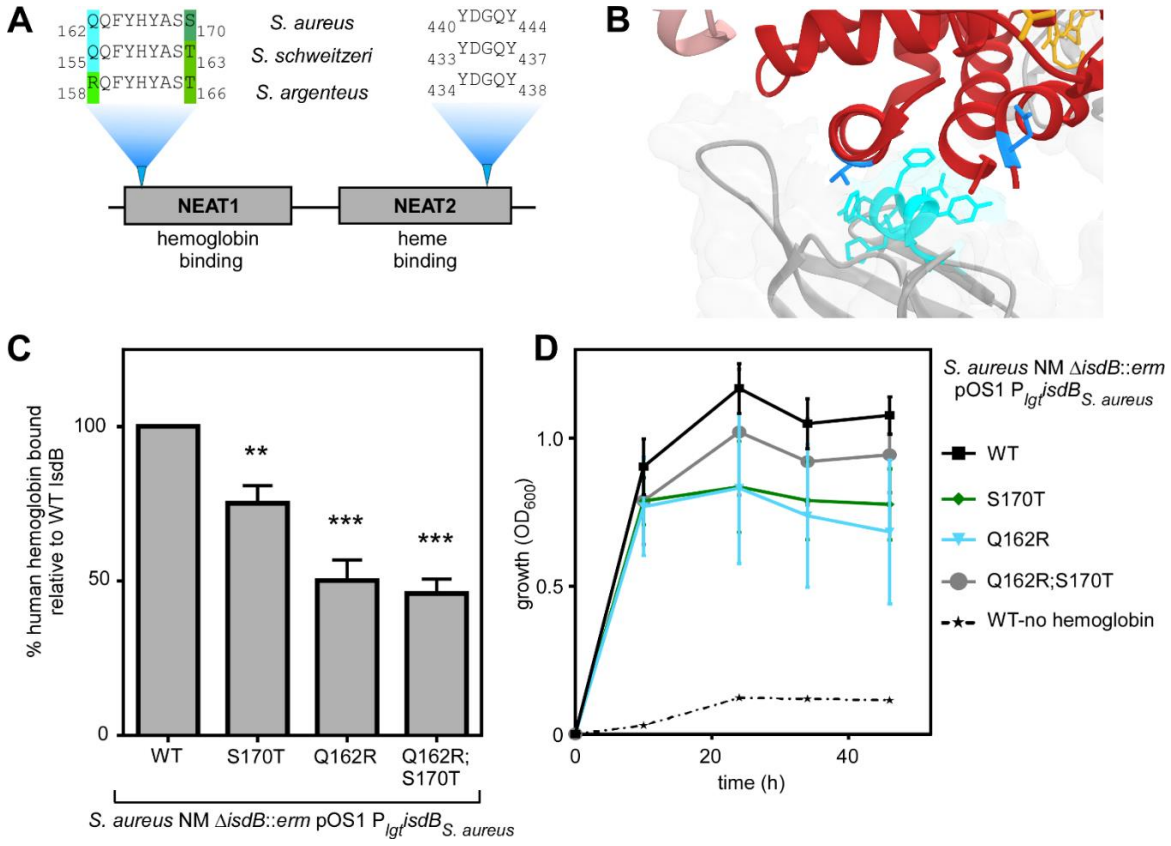

Figure 59 IsdB NEAT1 domain diversity among staphylococci modulates human hemoglobin recognition. (A) An alignment of the NEAT1 subdomain critical for hemoglobin binding shows variation among staphylococcal IsdB, while no variation is observed for the NEAT2 subdomain required for heme binding. **(B)** The Q162-S170 subdomain of NEAT1 (cyan) is proximal to helices containing T8 and N78 of α-globin (red). **(C)** *S. aureus* lacking native *isdB* but encoding constitutively expressed plasmid-borne *S. aureus isdB* variants were incubated with purified recombinant human hemoglobin and bound hemoglobin was quantified. **(D)** Growth of *S. aureus* lacking native *isdB* but encoding constitutively expressed plasmid-borne *S. aureus isdB* variants using hemoglobin as the sole iron source was monitored over time. For C, graphed are the means of three independent experiments with 3 biological replicates +/- SEM, ** $p<0.005$, *** $p<0.0005$ by two-way ANOVA with Sidak correction for multiple comparisons, comparing transformed (percent value) data. For D, graphed are the results of two independent experiments with six biological replicates each +/- standard deviation.

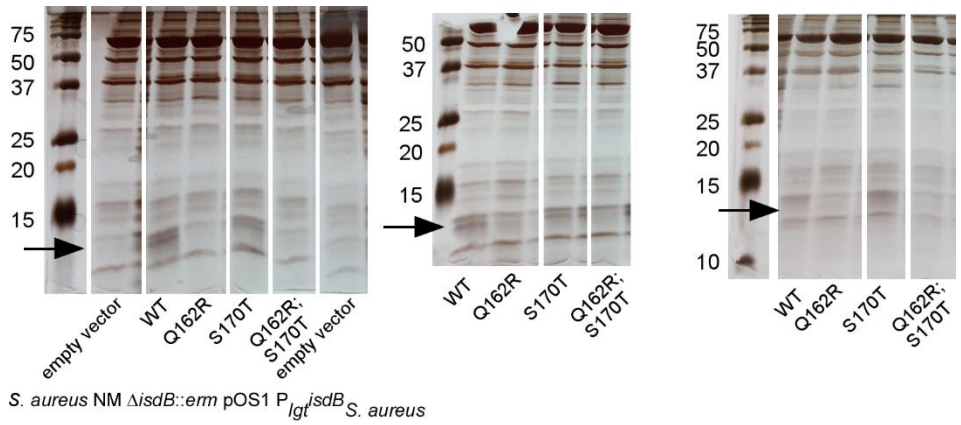

Figure 60 Representative silver stained SDS-PAGE gel of hemoglobin binding assay shown in Figure 59. Each gel represents a biological replicate from independent binding assays. Molecular weight markers are indicated, with arrow showing hemoglobin band.

Discussion

In this work we report that recurrent positive selection acting on primate α- and β-globin proteins restricts hemoglobin binding and nutrient acquisition by pathogenic *S. aureus*. Estimations of divergence in the *Staphylococcus* genus have been lacking, however the Kloos hypothesis (381) contends that staphylococci have coevolved with their mammalian hosts over long evolutionary timescales. In support of this concept, primate-specificity among staphylococci has been reported including *S. aureus*, *S. epidermidis*, and *S. warneri*, as well as avian (*S. gallinarum*), equine (*S. equorum*), and other taxa. Indeed, it has been proposed that the canine-associated *S. pseudointermedius* diverged from *S. aureus* simultaneously with the divergence of Primate and Carnivora orders (382). Most staphylococci are commensal organisms, while *S. aureus* is uniquely adapted to infect deep tissue and cause disease. As such, the IsdB system is only encoded by *S. aureus* and closely related primate-associated staphylococci. By narrowing our analysis of hemoglobin evolution to primates, we are thus able to assess specific biological features of primate-associated staphylococci.

An outstanding question in the study of *S. aureus* evolution has been determining the selective pressures responsible for human-specific virulence factors. *S. aureus* asymptomatically colonizes the anterior nares of approximately one third of the human population, yet is capable of causing a wide range of invasive diseases. While some bacterial colonization factors have been implicated in pathogenesis, many virulence factors have evolved highly specific targets that are not obviously involved in nasal colonization (383). As such, we cannot definitively conclude that IsdB evolution has been driven by selection during invasive disease. It is also likely that variation across IsdB of *S. aureus*, *S. argenteus*, and *S. schweitzeri* may be the results of antigenic variation to evade the immune system. By focusing

on the hemoglobin binding pocket of IsdB, we have been able to pinpoint critical variation for hemoglobin specificity.

Our phylogenetic analyses revealed strikingly parallel signatures of positive selection between the α- and β-globin genes across primates. In particular, rapidly evolving sites in the α- and β-globin A-helices are predicted to be homologous based on predicted protein alignments. Our results suggest that these correlations reflect selection in response to NEAT domain-containing bacterial receptors like IsdB with conserved globin binding sites. A well-established body of literature has shown that other selective pressures play an important role in patterns of hemoglobin polymorphism and divergence across vertebrates, including adaptation to high altitude and malaria resistance (368, 372). It is therefore possible that signatures of selection detected in our study have been driven by pressures other than nutritional immunity. Nonetheless, our empirical results demonstrate that variation in hemoglobins at discrete sites has important functional consequences for bacterial iron acquisition.

Previous studies have illustrated how mutations in hemoglobin coding or regulatory regions can have highly deleterious effects on heme binding, oxygen affinity, and protein stability (384, 385). In addition to aforementioned sickle-cell alleles, dozens of hemoglobin mutations in humans have been reported that contribute to genetic disease, including anemia and thalassemia (386). Thus, despite identifying particular sites that are highly divergent among primates, much of the globin gene content is constrained due to purifying selection. In future work it would be useful to determine how variation among primate globins impacts other biochemical functions, including as heme binding and oxygen affinity. Such insights could improve our fundamental understanding of hemoglobin biology and the mechanisms underlying human hemoglobinopathies.

In conclusion, this work illustrates how rapid, site-specific hemoglobin variation restricts heme acquisition by the prominent human pathogen *S. aureus*. These findings provide a fundamental new perspective on vertebrate globin evolution, highlighting nutritional immunity as a selective pressure that could strongly impact divergence and natural selection. Future studies will assist in illuminating how these combinations of adaptive mutations contribute to hemoglobin function and host physiology. Understanding the genetic and molecular determinants of bacterial pathogenicity is critical for developing new antimicrobial treatment strategies, particularly as major pathogens like *S. aureus* continue to develop resistance to existing antibiotics. Combining comparative genetics with molecular

experimentation in turn provides not only a historical perspective of host-microbe evolutionary conflict but also mechanistic insights on modern human infectious disease.

CHAPTER VI

SUMMARY

Conclusions

Investigation into the physiology that supports the pathogenesis of *Staphylococcus aureus* in recent years has yielded a consensus that metabolism and virulence are highly interconnected and research can no longer study one without the other. In this thesis, I investigated alterations in Fe-S cluster and heme cofactor biosyntheses, as well as heme uptake, in order to understand critical staphylococcal processes that contributed to pathogenesis.

Previous work in our laboratory had identified a small molecule, ‘882, that displayed two activities in *S. aureus*: activation of heme biosynthesis and inhibition of anaerobic growth. Extensive structure activity relationship studies chemically separated the two activities, confirming that ‘882 had two distinct targets in the cell (109). A genetic selection strategy identified CgoX as the enzyme activated by ‘882 to increase heme synthesis (110, 111), while our genetic and biochemical approaches identified SufC as the target of ‘882 which induced toxicity when grown in the absence of respiration (312). Inhibition of SufC led to disrupted Fe-S cluster synthesis, which has pleiotropic effects in the cell (Chapter II). We fortuitously worked with strain Newman, which encodes a constitutive active virulence program through SaeS; this constitutive activity of SaeS is required for the toxicity of ‘882, as the dual metabolic drains of Fe-S cluster inhibition and excess virulence factor production inhibits growth in the energy-limited conditions of anaerobic growth and fermentation (Chapter II). Together, this work connected metabolism, essential cofactor synthesis, and control of the staphylococcal virulence program, consistent with other reports that pathogens must balance energy production and virulence to cause disease.

There are many parallels between Fe-S cluster biogenesis and heme synthesis. Both require intracellular iron to form cofactors, both cofactors are required for the function of critical energy production, and *S. aureus* specific data on the regulation of biogenesis is lacking. Additionally, disruption of either is costly to virulence (97, 98, 283), While Fe-S cluster biogenesis is essential for growth; the metabolic flexibility of *S. aureus* allows heme synthesis to be dispensable, albeit costly. *S. aureus* can use fermentation to derive energy from carbon sources in the absence of an active heme-dependent respiratory chain, which enable our studies of heme synthesis. In this work, I genetically identified heme synthesis genes required

for heme biosynthesis, with two key findings: (i) neither of the two annotated glutamate-1-semialdehyde-2,1-amniomutase genes are required for heme synthesis, and (ii) the *cgoX* gene encoding coproporphyrinogen III oxidase is required for both anaerobic and aerobic heme synthesis (Chapter III).

Work in Chapter IV aimed to illuminate a major gap in knowledge highlighted by recent research in accurately describing the unique properties of terminal heme synthesis in *S. aureus*. Paired with a lack of understanding of the biochemical properties of heme synthesis is the lack of information concerning regulation of heme synthesis. Combining genetics with quantitative mass spectrometry, I found that abundance of GtrR is regulated in response to intracellular heme and the membrane protein HemX. In the absence of HemX-mediated regulation, excess heme is synthesized which consumes iron and thus disrupts iron homeostasis, activates the heme stress response, and therefore identifies GtrR as a key regulatory node in *S. aureus* heme synthesis. The nature of this regulation remains shrouded and will be explored further in Future Directions (below).

Finally turning to heme acquisition by *S. aureus*, work in this thesis has uncovered rapid evolution at the interface of human hemoglobin and the hemoglobin receptor IsdB (Chapter V). This work helps to fill the gap in knowledge first identified by Pishchany and colleagues (94): the molecular mechanism by which *S. aureus* prefers human hemoglobin relative to the laboratory mouse, and how this preference has evolved. We find that primate hemoglobin has undergone rapid evolution at parallel positions in α- and β-globins, which localize to the binding interface of IsdB (Chapter V). *S. aureus* IsdB binds human hemoglobin the best, which is consistent with *S. aureus* having evolved to be a human-specific commensal and pathogen. Mutagenesis of the rapidly evolving hemoglobin residues disrupts binding by *S. aureus*, further underscoring this particular binding interface to the host-pathogen interaction. To further support our hypothesis, we identified variation in the hemoglobin binding pocket of IsdB in closely related species of *Staphylococcus* which reduced binding of human hemoglobin when recreated in *S. aureus* IsdB. Together our work suggests that the IsdB-hemoglobin binding interface has been the site of repeated bouts of evolution driven by IsdB. Mutations in hemoglobin of primate ancestors of humans that would disrupt the interface would be selected for in the population owing to resistance to *S. aureus* infection. Mutations in IsdB would be rapidly selected for and this evolutionary arms race would continue until the present state: modern *S. aureus* IsdB has evolved to best bind modern human hemoglobin.

In sum, this work identified the protein target of a small molecule to uncover the unique connection between virulence and Fe-S metabolism, discovered a heme synthesis regulatory

process, and described evolution at the interface of heme acquisition. The findings that HemX and heme regulate GtrR abundance to control heme synthesis have led to further investigations and many outstanding questions, discussed below.

Future directions

Potential for a *S. aureus* heme chaperone

Investigation into the potential of NWMN_1486 acting as an oxygen-independent coproporphyrinogen III oxidase (Chapter III), which was ruled out on the basis that CgoX performs this function aerobically and anaerobically (Figure 22), led to the hypothesis that NWMN_1486 is a heme chaperone. The comparison between NWMN_1486 and *E. coli* HemN (Figure 21) identifies two critical differences: NWMN_1486 lacks the first 47 amino acids required for substrate recognition and the catalytic CxxxCxxCxC radical SAM motif. Indeed, these missing features define a sub-clade of the HemN protein family whose members include recently defined heme chaperones in *L. lactis* and *E. coli* (315, 316). Biochemical evidence supports a model that these NWMN_1486 homologs bind heme and may deliver it to heme dependent enzymes. Based on our laboratory's genetic tools for studying heme homeostasis in *S. aureus*, an exciting future direction would be to confirm that NWMN_1486 is a heme chaperone based on biochemical characteristics, then study the impact on heme homeostasis of a heme chaperone. The contribution of NWMN_1486 to bNOS, KatA, and QoxABCD/CydABC enzymes can be quantified by measuring nitric oxide production, catalase activity, and respiration, respectively. Targeted detection of interactions would be assessed using the biomolecular fluorescence complementation using split fluorophores (387) to detect *in vivo* interactions between NWMN_1486 and potential partners. These would include the heme uptake system (IsdF, IsdG, IsdI), terminal heme synthesis (ChdC), respiratory enzymes (Qox, Cyd, and Nir proteins), bNOS, KatA, heme efflux (HrtA), and proteins which might regulate heme homeostasis (GtrR and HemX). Unbiased immunoprecipitations of NWMN_1486 paired with mass spectrometry could identify interactions that would illuminate the function of a staphylococcal heme chaperone.

An integrated model for heme homeostasis in *S. aureus*

Evidence for a heme chaperone (above), new insights from literature, and a series of experiments mentioned below support a model for integrated heme homeostasis in *S. aureus* that coordinates heme acquisition, synthesis, efflux, and utilization. Chapter IV of this work set out to define regulation of heme biosynthesis based on the simple hypothesis that heme synthesis is regulated to ensure sufficient heme is available but excess is not made,

preventing heme toxicity. Experiments in Chapter IV identified regulation based on intracellular heme availability, and that excess heme activates the HssRS-HrtAB heme stress response. It is likely, therefore, that these new findings fit into a larger coordinated heme homeostatic pathway that coordinates all aspects of heme. Recent studies by other groups have found intersections at heme uptake. Siderophore based iron acquisition is repressed when host heme is present, ensuring that the Isd mediated heme-iron source is utilized during infection (133). Secondly, the IsdG heme oxygenase was found to bind CpfC to inhibit heme synthesis (388). This study suggests that when host heme is available, heme synthesis is inhibited, either to prevent excess heme buildup or to prevent costly heme synthesis when other sources are available. This finding also adds support to the model that host heme can be incorporated into *S. aureus* hemoproteins. Further evidence for interactions between Isd heme uptake and heme utilization exist in a yeast-two-hybrid experiment in which IsdI was found to interact with the heme-dependent enzyme Hmp (data not shown).

Additional experiments conducted in our laboratory support a model of integrated heme homeostasis. In support of HssRS responding to endogenous heme, various conditions have been found to activate HssRS in the absence of exogenous heme: small molecule activation of heme synthesis (109-111), genetic dysregulation of heme synthesis (Chapter IV;(389)) ; and deletion of hemoproteins (induction of HrtAB was found in Δ*qoxB cydB*; not shown) suggesting that HssRS-HrtAB can respond to changes in intracellular heme conditions absent of host heme. I would predict that measuring P_{hrt} induction would find activation of HssRS when other hemoproteins are deleted (*bNOS*, *katA*, for example) while over-expression of hemoproteins would reduce P_{hrt} induction in a Δ*hemX* mutant, which synthesizes excess heme. If the model for a heme chaperone (above) is correct, a heme chaperone mutant might synthesize excess heme to overcome the absence of the heme chaperone, resulting in HssRS activation.

Ongoing investigations into the heme chaperone, IsdI-Hmp interactions, and a genetic selection for heme homeostasis (below) will contribute new findings to the hypothesis of an integrated heme homeostatic network that modulates synthesis based on availability of host heme, requirement for hemoproteins, and available synthesized heme to connect synthesis with uptake, efflux, and utilization.

Regulatory heme binding by GtrR

Based on data in Chapter IV, which show that GtrR levels increase in heme-deficient strains, and that recombinant GtrR can bind heme *in vitro*, I propose a model in which one

layer of GtrR regulation is based on binding of excess heme to reduce GtrR levels through proteolysis or another post-translational mechanism. Efforts are underway to determine the heme-binding residues in GtrR by alanine mutagenesis of potential heme-coordinated residues (Lys, His, Tyr, Ser, Val, Asp, Ile, and Glu) in both the pOS1 P_{lgt}*gtrR* and pOS1 P_{lgt}*gtrR-hemX* plasmids encoded by the Δ*gtrR-hemX* mutant. Utilizing the heme adaptation assay (Figure 32) in which Δ*gtrR-hemX* pOS1 P_{lgt}*gtrR* is heme adapted because of excess GtrR, but Δ*gtrR-hemX* pOS1 P_{lgt}*gtrR-hemX* is not heme adapted, mutagenized GtrR will be evaluated for enhanced or reduced heme toxicity sensitivity in the presence or absence of *hemX* to identify mutations that impact GtrR levels. Interesting mutants will be recreated in a plasmid encoding *gtrR* for recombinant protein expression, purified to homogeneity, and evaluated for heme binding using the Soret shift assay (Figure 25). This strategy should identify amino acids required for heme-dependent regulation. Additionally, the crystal structure of GtrR is an ongoing effort with the laboratory of Borden Lacy to further GtrR; amino acids identified here will be mapped to the crystal structure. Mutations that truncate GtrR to prevent dimerization have been created (stop codon inserted at R312 and G340). Taken together these integrated strategies should determine the contribution of heme binding to GtrR regulation, mutants incapable of binding excess heme can be used to probe how GtrR levels change in response to heme-deficiency and will allow for the genetic dissection of HemX-dependent and –independent regulation.

Genetic selection for disrupted heme homeostasis

For an unbiased approach to uncover genes required for heme homeostasis, I developed a genetic selection in which kanamycin resistance is induced by HssRS. Using allelic exchange, *ahp-A3* encoding kanamycin resistance was inserted in the chromosome in the place of the *hrtAB* genes (see Chapter IV Materials and Methods). This strain *hrtAB*::*kan* is sensitive to kanamycin unless exogenous heme is used to activate HssRS (Figure 61A). Any disruption of heme homeostasis which increases HssS activation by endogenous heme would result in activation of P_{hrt}*kan* and can be selected for by plating hrtAB::kan on kanamycin in the absence of exogenous heme. Kanamycin resistant mutants will be screened for (i) stable kanamycin resistance and (ii) activation of a second P_{hrt} promoter, encoded in pOS1 P_{hrt}*xylE* before being subject to whole genome sequencing. I expect this strategy will select for mutations in known genes: activating mutations in HssRS, mutations that inactivate HemX, or mutations that reduce regulation of GtrR will all result in kanamycin resistance (Figure 61B). Outside of these expected hits, I predict that this untargeted approach will identify novel gene

products involved in coordinating heme synthesis. This approach will uncover mechanisms by which GtrR is regulated, by which HemX functions, and add to our understanding of heme homeostasis as described above.

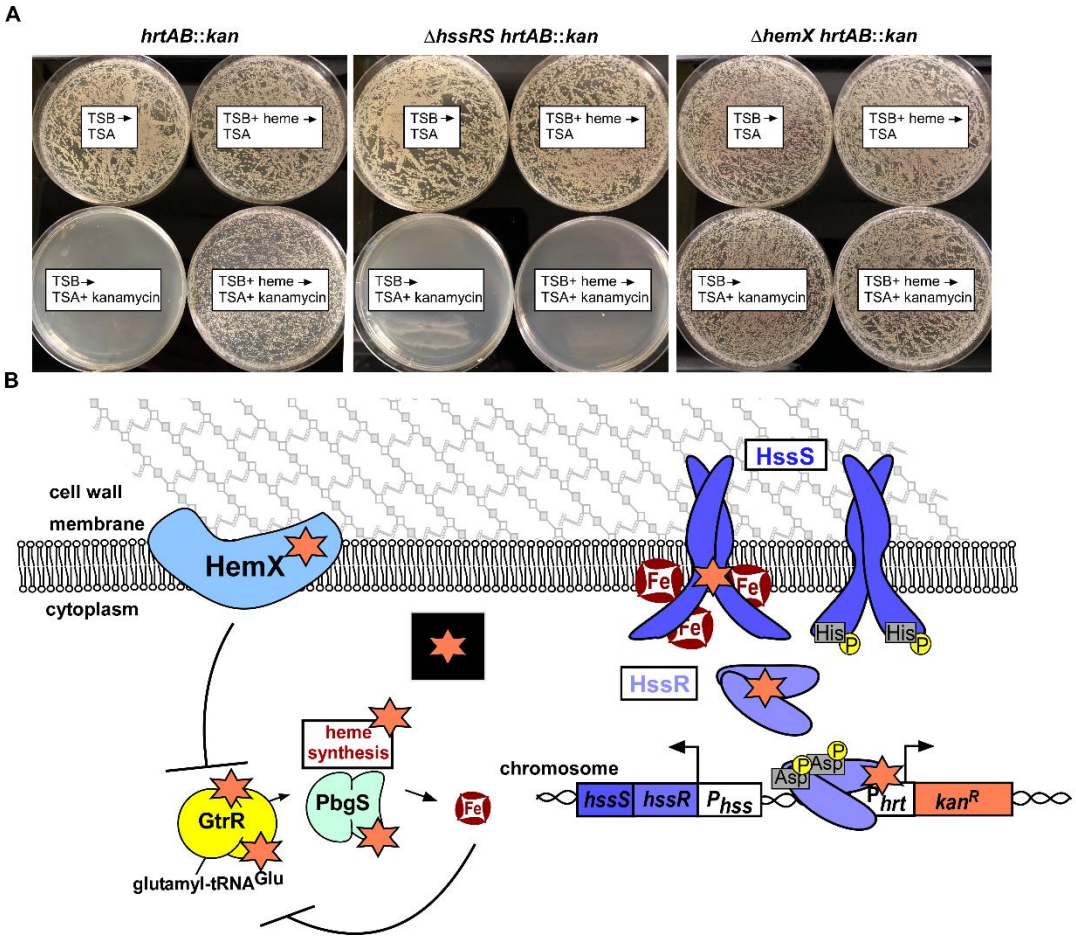

Figure 61 A genetic selection strategy to study heme homeostasis. (A) *hrtAB*::*kan* demonstrates heme-induced kanamycin resistance [left], which is dependent on HssRS [middle]. As a proof of principle, inactivation of *hemX* results in constitutive kanamycin resistance [right]. **(B)** A schematic of the *hrtAB*::*kan* strain which expresses kanamycin resistance when HssRS is induced. Mutations upstream of HssS activation (stars) could activate HssS in the absence of exogenous heme to induce kanamycin resistance.

REFERENCES

1. Monack DM. Stanley Falkow (1934–2018). Cell Host Microbe. 2018;23(6):697-88.
2. Wertheim HFL, Vos MC, Ott A, van Belkum A, Voss A, Kluytmans JAJW, et al. Risk and outcome of nosocomial *Staphylococcus aureus* bacteraemia in nasal carriers versus non-carriers. The Lancet. 2004;364(9435):703-5.
3. Tong SY, Davis JS, Eichenberger E, Holland TL, Fowler VG, Jr. *Staphylococcus aureus* infections: epidemiology, pathophysiology, clinical manifestations, and management. Clin Microbiol Rev. 2015;28(3):603-61.
4. Global Priority List of Antibiotic-resistant Bacteria to Guide Research, Discovery, and Development of New Antibiotics. World Health Organization: 2017.
5. Vitko NP, Grosser MR, Khatri D, Lance TR, Richardson AR. Expanded glucose import capability affords *Staphylococcus aureus o*ptimized glycolytic flux during infection. mBio. 2016;7(3).
6. Palmer LD, Skaar EP. Transition metals and virulence in bacteria. Annu Rev Genet. 2016;50:67-91.
7. Hammer ND, Skaar EP. Molecular mechanisms of *Staphylococcus aureus* iron acquisition. Annu Rev Microbiol. 2011;65:129-47.
8. Kelliher JL, Radin JN, Grim KP, Parraga Solorzano PK, Degnan PH, Kehl-Fie TE. Acquisition of the phosphate transporter NptA enhances *Staphylococcus aureus* pathogenesis by improving phosphate uptake in divergent environments. Infect Immun. 2018;86(1).
9. Kaiser JC, Omer S, Sheldon JR, Welch I, Heinrichs DE. Role of BrnQ1 and BrnQ2 in branched-chain amino acid transport and virulence in *Staphylococcus aureus*. Infect Immun. 2015;83(3):1019-29.
10. Shelver D, Kerby RL, He Y, Roberts GP. CooA, a CO-sensing transcription factor from *Rhodospirillum rubrum*, is a CO-binding heme protein. Proc Natl Acad Sci USA. 1997;94(21):11216-20.
11. Faller M, Matsunaga M, Yin S, Loo JA, Guo F. Heme is involved in microRNA processing. Nat Struct Mol Biol. 2007;14(1):23-9.
12. Bonyhady RE, Hendry IA, Hill CE, McLennan IS. Effects of haemin on neurones derived from the neural crest. Dev Neurosci. 1982;5(2-3):125-9.
13. Chen JJ, London IM. Hemin enhances the differentiation of mouse 3T3 cells to adipocytes. Cell. 1981;26(1 Pt 1):117-22.
14. Posey JE, Gherardini FC. Lack of a role for iron in the Lyme disease pathogen. Science. 2000;288:1651-4.
15. Archibald F. *Lactobacillus plantarum*, an organism not requiring iron. FEMS Microbiol Lett. 1983;19:29-32.
16. Kessler D, Leibrecht I, Knappe J. Pyruvate-formate-lyase-deactivase and acetyl-CoA reductase activities of *Escherichia coli* reside on a polymeric protein particle encoded by *adhE*. FEBS Lett. 1991;281(1-2):59-63.
17. Yamamoto I, Saiki T, Liu SM, Ljungdahl LG. Purification and properties of NADP-dependent formate dehydrogenase from *Clostridium thermoaceticum*, a tungsten-selenium-iron protein. J Biol Chem. 1983;258(3):1826-32.
18. Peters JW, Lanzilotta WN, Lemon BJ, Seefeldt LC. X-ray crystal structure of the Fe-only hydrogenase (CpI) from *Clostridium pasteurianum* to 1.8 angstrom resolution. Science. 1998;282(5395):1853-8.
19. Johnson DC, Dean DR, Smith AD, Johnson MK. Structure, function, and formation of biological iron-sulfur clusters. Annu Rev Biochem. 2005;74:247-81.
20. Shomura Y, Yoon KS, Nishihara H, Higuchi Y. Structural basis for a [4Fe-3S] cluster in the oxygen-tolerant membrane-bound [NiFe]-hydrogenase. Nature. 2011;479(7372):253-6.

21. Nagashima S, Nakasako M, Dohmae N, Tsujimura M, Takio K, Odaka M, et al. Novel non-heme iron center of nitrile hydratase with a claw setting of oxygen atoms. Nat Struct Biol. 1998;5(5):347-51.
22. Weinberg ED. Nutritional immunity: host's attempt to withold iron from microbial invaders. JAMA. 1975;231(1):39-41.
23. Weinberg ED. Iron and susceptibility to infectious disease. Science. 1974;184(4140):952-6.
24. Cassat JE, Skaar EP. Iron in infection and immunity. Cell Host Microbe. 2013;13(5):509-19.
25. Hood MI, Skaar EP. Nutritional immunity: transition metals at the pathogen-host interface. Nat Rev Microbiol. 2012;10(8):525-37.
26. Juttukonda LJ, Skaar EP. Manganese homeostasis and utilization in pathogenic bacteria. Mol Microbiol. 2015;97(2):216-28.
27. Zackular JP, Chazin WJ, Skaar EP. Nutritional immunity: S100 proteins at the host-pathogen interface. J Biol Chem. 2015;290(31):18991-8.
28. Wriston JC, Jr., Lack L, Shemin D. The mechanism of porphyrin formation; further evidence on the relationship of the citric acid cycle and porphyrin formation. J Biol Chem. 1955;215(2):603-11.
29. Kikuchi G, Kumar A, Talmage P, Shemin D. The enzymatic synthesis of delta-aminolevulinic acid. J Biol Chem. 1958;233(5):1214-9.
30. Hamza I, Dailey HA. One ring to rule them all: trafficking of heme and heme synthesis intermediates in the metazoans. Biochim Biophys Acta. 2012;1823(9):1617-32.
31. Omura T, Sato R. The carbon monoxide-binding pigment of liver microsomes. I. evidence for its hemoprotein nature. J Biol Chem. 1964;239:2370-8.
32. Rieske JS. Composition, structure, and function of complex III of the respiratory chain. Biochim Biophys Acta. 1976;456(2):195-247.
33. Bridges K, PA S. Disorders of iron metabolism. New York: J.B. Lippincott Company; 1995.
34. Everse J, Hsia N. The toxicities of native and modified hemoglobins. Free Radic Biol Med. 1997;22(6):1075-99.
35. Anzaldi LL, Skaar EP. Overcoming the heme paradox: heme toxicity and tolerance in bacterial pathogens. Infect Immun. 2010;78(12):4977-89.
36. Smith A, McCulloh RJ. Hemopexin and haptoglobin: allies against heme toxicity from hemoglobin not contenders. Front Physiol. 2015;6:187.
37. Schaer DJ, Buehler PW. Cell-free hemoglobin and its scavenger proteins: new disease models leading the way to targeted therapies. Cold Spring Harb Perspect Med. 2013;3(6).
38. Jeney V, Balla J, Yachie A, Varga Z, Vercellotti GM, Eaton JW, et al. Pro-oxidant and cytotoxic effects of circulating heme. Blood. 2002;100(3):879-87.
39. Tolosano E, Altruda F. Hemopexin: structure, function, and regulation. DNA Cell Biol. 2002;21(4):297-306.
40. Balla G, Jacob HS, Eaton JW, Belcher JD, Vercellotti GM. Hemin: a possible physiological mediator of low density lipoprotein oxidation and endothelial injury. Arterioscler Thromb. 1991;11(6):1700-11.
41. Lin H, McFaul SJ, Brady JC, Everse J. The mechanism of peroxidase-mediated cytotoxicity. II. Role of the heme moiety. Proc Soc Exp Biol Med. 1988;187(1):7-13.
42. Stauff DL, Skaar EP. *Bacillus anthracis* HssRS signalling to HrtAB regulates haem resistance during infection. Mol Microbiol. 2009;72(3):763-78.
43. Dailey HA, Gerdes S, Dailey TA, Burch JS, Phillips JD. Noncanonical coproporphyrin-dependent bacterial heme biosynthesis pathway that does not use protoporphyrin. Proc Natl Acad Sci USA. 2015;112(7):2210-5.

44. Beale SI, Gough SP, Granick S. Biosynthesis of delta-aminolevulinic acid from the intact carbon skeleton of glutamic acid in greening barley. Proc Natl Acad Sci U S A. 1975;72(7):2719-23.
45. Hoober JK, Kahn A, Ash DE, Gough S, Kannangara CG. Biosynthesis of delta-aminolevulinate in greening barley leaves. IX. Structure of the substrate, mode of gabaculine inhibition, and the catalytic mechanism of glutamate 1-semialdehyde aminotransferase. Carlsberg Res Commun. 1988;53(11-25).
46. Kannangara CG, Gough SP, Bruyant P, Hoober JK, Kahn A, von Wettstein D. tRNA(Glu) as a cofactor in delta-aminolevulinate biosynthesis: steps that regulate chlorophyll synthesis. Trends Biochem Sci. 1988;13(4):139-43.
47. Hansson M, Rutberg L, Schroder I, Hederstedt L. The *Bacillus subtilis hemAXCDBL* gene cluster, which encodes enzymes of the biosynthetic pathway from glutamate to uroporphyrinogen III. J Bacteriol. 1991;173(8):2590-9.
48. Louie GV, Brownlie PD, Lambert R, Cooper JB, Blundell TL, Wood SP, et al. Structure of porphobilinogen deaminase reveals a flexible multidomain polymerase with a single catalytic site. Nature. 1992;359(6390):33-9.
49. Bung N, Pradhan M, Srinivasan H, Bulusu G. Structural insights into *E. coli* porphobilinogen deaminase during synthesis and exit of 1-hydroxymethylbilane. PLoS Comput Biol. 2014;10(3):e1003484.
50. Jordan PM. The biosynthesis of tetrapyrroles. Neuberger AaVD, L.L.M., editor. New York, NY: Elsevier; 1991 1991. 309 p.
51. Dailey HA, Dailey TA, Gerdes S, Jahn D, Jahn M, O'Brian MR, et al. Prokaryotic heme biosynthesis: multiple pathways to a common essential product. Microbiol Mol Biol Rev. 2017;81(1):81:e00048-16.
52. Hansson M, Hederstedt L. Cloning and characterization of the *Bacillus subtilis hemEHY* gene cluster, which encodes protoheme IX biosynthetic enzymes. J Bacteriol. 1992;174(24):8081-93.
53. Leeper FJ. The biosynthesis of porphyrins, chlorophylls, and vitamin B12. Nat Prod Rep. 1987;4(4):441-69.
54. Bali S, Lawrence AD, Lobo SA, Saraiva LM, Golding BT, Palmer DJ, et al. Molecular hijacking of siroheme for the synthesis of heme and d1 heme. Proc Natl Acad Sci USA. 2011;108(45):18260-5.
55. Bali S, Palmer DJ, Schroeder S, Ferguson SJ, Warren MJ. Recent advances in the biosynthesis of modified tetrapyrroles: the discovery of an alternative pathway for the formation of heme and heme d 1. Cell Mol Life Sci. 2014;71(15):2837-63.
56. Troup B, Hungerer C, Jahn D. Cloning and characterization of the *Escherichia coli* hemN gene encoding the oxygen-independent coproporphyrinogen III oxidase. J Bacteriol. 1995;177(11):3326-31.
57. Seehra JS, Jordan PM, Akhtar M. Anaerobic and aerobic coproporphyrinogen III oxidases of *Rhodopseudomonas spheroides*. Mechanism and stereochemistry of vinyl group formation. Biochem J. 1983;209(3):709-18.
58. Boynton TO, Daugherty LE, Dailey TA, Dailey HA. Identification of *Escherichia coli* HemG as a novel, menadione-dependent flavodoxin with protoporphyrinogen oxidase activity. Biochemistry. 2009;48(29):6705-11.
59. Kobayashi K, Masuda T, Tajima N, Wada H, Sato N. Molecular phylogeny and intricate evolutionary history of the three isofunctional enzymes involved in the oxidation of protoporphyrinogen IX. Genome Biol Evol. 2014;6(8):2141-55.
60. Porra RJ, Falk JE. The enzymic conversion of coproporphyrinogen 3 into protoporphyrin 9. Biochem J. 1964;90(1):69-75.

61. Camadro JM, Labbe P. Purification and properties of ferrochelatase from the yeast *Saccharomyces cerevisiae*. Evidence for a precursor form of the protein. J Biol Chem. 1988;263(24):11675-82.
62. Lobo SA, Scott A, Videira MA, Winpenny D, Gardner M, Palmer MJ, et al. *Staphylococcus aureus* haem biosynthesis: characterisation of the enzymes involved in final steps of the pathway. Mol Microbiol. 2015;97(3):472-87.
63. Hansson M, Gustafsson MC, Kannangara CG, Hederstedt L. Isolated *Bacillus subtilis* HemY has coproporphyrinogen III to coproporphyrin III oxidase activity. Biochim Biophys Acta. 1997;1340(1):97-104.
64. Mayfield JA, Hammer ND, Kurker RC, Chen TK, Ojha S, Skaar EP, et al. The chlorite dismutase (HemQ) from *Staphylococcus aureus* has a redox-sensitive heme and is associated with the small colony variant phenotype. J Biol Chem. 2013;288(32):23488-504.
65. Dailey HA, Gerdes S. HemQ: An iron-coproporphyrin oxidative decarboxylase for protoheme synthesis in Firmicutes and Actinobacteria. Arch Biochem Biophys. 2015;574:27-35.
66. Dailey TA, Boynton TO, Albetel AN, Gerdes S, Johnson MK, Dailey HA. Discovery and Characterization of HemQ: an essential heme biosynthetic pathway component. J Biol Chem. 2010;285(34):25978-86.
67. Celis AI, Streit BR, Moraski GC, Kant R, Lash TD, Lukat-Rodgers GS, et al. Unusual peroxide-dependent, heme-transforming reaction catalyzed by HemQ. Biochemistry. 2015;54(26):4022-32.
68. Jahn D, Michelsen U, Soll D. Two glutamyl-tRNA reductase activities in *Escherichia coli*. J Biol Chem. 1991;266(4):2542-8.
69. Javor GT, Febre EF. Enzymatic basis of thiol-stimulated secretion of porphyrins by *Escherichia coli*. J Bacteriol. 1992;174(3):1072-5.
70. Wang LY, Brown L, Elliott M, Elliott T. Regulation of heme biosynthesis in *Salmonella typhimurium*: activity of glutamyl-tRNA reductase (HemA) is greatly elevated during heme limitation by a mechanism which increases abundance of the protein. J Bacteriol. 1997;179(9):2907-14.
71. Wang L, Elliott M, Elliott T. Conditional stability of the HemA protein (glutamyl-tRNA reductase) regulates heme biosynthesis in *Salmonella typhimurium*. J Bacteriol. 1999;181(4):1211-9.
72. Jones AM, Elliott T. A purified mutant HemA protein from *Salmonella enterica* serovar Typhimurium lacks bound heme and is defective for heme-mediated regulation *in vivo*. FEMS Microbiol Lett. 2010;307(1):41-7.
73. Wang L, Wilson S, Elliott T. A mutant HemA protein with positive charge close to the N terminus is stabilized against heme-regulated proteolysis in *Salmonella typhimurium*. J Bacteriol. 1999;181(19):6033-41.
74. Zhang J, Kang Z, Ding W, Chen J, Du G. Integrated optimization of the *in vivo* heme biosynthesis pathway and the *in vitro* iron concentration for 5-aminolevulinate production. Appl Biochem Biotechnol. 2015.
75. Schroder I, Johansson P, Rutberg L, Hederstedt L. The *hemX* gene of the *Bacillus subtilis hemAXCDBL* operon encodes a membrane protein, negatively affecting the steady-state cellular concentration of HemA (glutamyl-tRNA reductase). Microbiology. 1994;140:731-40.
76. Hungerer C, Troup B, Romling U, Jahn D. Regulation of the *hemA* gene during 5-aminolevulinic acid formation in *Pseudomonas aeruginosa*. J Bacteriol. 1995;177(6):1435-43.
77. Krieger R, Rompf A, Schobert M, Jahn D. The *Pseudomonas aeruginosa hemA* promoter is regulated by Anr, Dnr, NarL and Integration Host Factor. Mol Genet Genomics. 2002;267(3):409-17.

78. Ye RW, Tao W, Bedzyk L, Young T, Chen M, Li L. Global gene expression profiles of *Bacillus subtilis* grown under anaerobic conditions. J Bacteriol. 2000;182(16):4458-65.
79. Ji CJ, Kim JH, Won YB, Lee YE, Choi TW, Ju SY, et al. *Staphylococcus aureus* PerR Is a hypersensitive hydrogen peroxide sensor using iron-mediated histidine oxidation. J Biol Chem. 2015;290(33):20374-86.
80. Ravcheev DA, Best AA, Tintle N, Dejongh M, Osterman AL, Novichkov PS, et al. Inference of the transcriptional regulatory network in *Staphylococcus aureus* by integration of experimental and genomics-based evidence. J Bacteriol. 2011;193(13):3228-40.
81. Frunzke J, Gatgens C, Brocker M, Bott M. Control of heme homeostasis in *Corynebacterium glutamicum* by the two-component system HrrSA. J Bacteriol. 2011;193(5):1212-21.
82. Bibb LA, Kunkle CA, Schmitt MP. The ChrA-ChrS and HrrA-HrrS signal transduction systems are required for activation of the *hmuO* promoter and repression of the hemA promoter in *Corynebacterium diphtheriae*. Infect Immun. 2007;75(5):2421-31.
83. Bibb LA, Schmitt MP. The ABC transporter HrtAB confers resistance to hemin toxicity and is regulated in a hemin-dependent manner by the ChrAS two-component system in *Corynebacterium diphtheriae*. J Bacteriol. 2010;192(18):4606-17.
84. Mancini S, Imlay JA. The induction of two biosynthetic enzymes helps *Escherichia coli* sustain heme synthesis and activate catalase during hydrogen peroxide stress. Mol Microbiol. 2015;96(4):744-63.
85. Marino M, Ramos HC, Hoffmann T, Glaser P, Jahn D. Modulation of anaerobic energy metabolism of *Bacillus subtilis* by *arfM* (*ywiD*). J Bacteriol. 2001;183(23):6815-21.
86. Hippler B, Homuth G, Hoffmann T, Hungerer C, Schumann W, Jahn D. Characterization of *Bacillus subtilis hemN*. J Bacteriol. 1997;179(22):7181-5.
87. Homuth G, Rompf A, Schumann W, Jahn D. Transcriptional control of *Bacillus subtilis hemN* and *hemZ*. J Bacteriol. 1999;181(19):5922-9.
88. Chen L, Keramati L, Helmann JD. Coordinate regulation of *Bacillus subtilis* peroxide stress genes by hydrogen peroxide and metal ions. Proc Natl Acad Sci USA. 1995;92(18):8190-4.
89. Rompf A, Hungerer C, Hoffmann T, Lindenmeyer M, Romling U, Gross U, et al. Regulation of *Pseudomonas aeruginosa hemF* and *hemN* by the dual action of the redox response regulators Anr and Dnr. Mol Microbiol. 1998;29(4):985-97.
90. Sander A, Kretzer S, Bredt W, Oberle K, Bereswill S. Hemin-dependent growth and hemin binding of *Bartonella henselae*. FEMS Microbiol Lett. 2000;189(1):55-9.
91. Baureder M, Hederstedt L. Heme proteins in lactic acid bacteria. Adv Microb Physiol. 2013;62:1-43.
92. Frankenberg L, Brugna M, Hederstedt L. *Enterococcus faecalis* heme-dependent catalase. Journal of Bacteriology. 2002;184(22):6351-6.
93. Biberstein EL, Mini PD, Gills MG. Action of *Haemophilus* cultures on δ-aminolevulinic acid. J Bacteriol. 1963;86:814-9.
94. Pishchany G, McCoy AL, Torres VJ, Krause JC, Crowe JE, Jr., Fabry ME, et al. Specificity for human hemoglobin enhances *Staphylococcus aureus* infection. Cell Host Microbe. 2010;8(6):544-50.
95. Pishchany G, Sheldon JR, Dickson CF, Alam MT, Read TD, Gell DA, et al. IsdB-dependent hemoglobin binding is required for acquisition of heme by *Staphylococcus aureus*. J Infect Dis. 2014;209(11):1764-72.
96. Skaar EP, Humayun M, Bae T, DeBord KL, Schneewind O. Iron-source preference of *Staphylococcus aureus* infections. Science. 2004;305:1626-8.
97. Hammer ND, Reniere ML, Cassat JE, Zhang Y, Hirsch AO, Hood MI, et al. Two heme-dependent terminal oxidases power *Staphylococcus aureus* organ-specific colonization of the vertebrate host. mBio. 2013;4(4):e00241-13.

98. Hammer ND, Cassat JE, Noto MJ, Lojek LJ, Chadha AD, Schmitz JE, et al. Inter- and intraspecies metabolite exchange promotes virulence of antibiotic-resistant *Staphylococcus aureus*. Cell Host Microbe. 2014;16(4):531-7.
99. von Eiff C, Heilmann C, Proctor RA, Woltz C, Peters G, Gotz F. A site-directed *Staphylococcus aureus hemB* mutant is a small-colony variant which persists intracellularly. J Bacteriol. 1997;179(15):4706-12.
100. Balwit JM, van Langevelde P, Vann JM, Proctor RA. Gentamicin-resistant menadione and hemin auxotrophic *Staphylococcus aureus* persist within cultured endothelial cells. J Infect Dis. 1994;170(4):1033-7.
101. Proctor RA, von Eiff C, Kahl BC, Becker K, McNamara P, Herrmann M, et al. Small colony variants: a pathogenic form of bacteria that facilitates persistent and recurrent infections. Nat Rev Microbiol. 2006;4(4):295-305.
102. Sadowska B, Bonar A, von Eiff C, Proctor RA, Chmiela M, Rudnicka W, et al. Characteristics of *Staphylococcus aureus*, isolated from airways of cystic fibrosis patients, and their small colony variants. FEMS Immunol Med Microbiol. 2002;32(3):191-7.
103. Painter KL, Strange E, Parkhill J, Bamford KB, Armstrong-James D, Edwards AM. *Staphylococcus aureus* adapts to oxidative stress by producing H2O2-resistant small-colony variants via the SOS response. Infect Immun. 2015;83(5):1830-44.
104. Almiron M, Martinez M, Sanjuan N, Ugalde RA. Ferrochelatase is present in *Brucella abortus* and is critical for its intracellular survival and virulence. Infect Immun. 2001;69(10):6225-30.
105. Skurnik D, Roux D, Aschard H, Cattoir V, Yoder-Himes D, Lory S, et al. A comprehensive analysis of in vitro and in vivo genetic fitness of *Pseudomonas aeruginosa* using high-throughput sequencing of transposon libraries. PLoS Pathog. 2013;9(9):e1003582.
106. Palace SG, Proulx MK, Lu S, Baker RE, Goguen JD. Genome-wide mutant fitness profiling identifies nutritional requirements for optimal growth of *Yersinia pestis* in deep tissue. mBio. 2014;5(4).
107. Wang N, Ozer EA, Mandel MJ, Hauser AR. Genome-wide identification of *Acinetobacter baumannii* genes necessary for persistence in the lung. mBio. 2014;5(3):e01163-14.
108. Cummins J, Casey PG, Joyce SA, Gahan CG. A mariner transposon-based signature-tagged mutagenesis system for the analysis of oral infection by *Listeria monocytogenes*. PLoS One. 2013;8(9):e75437.
109. Dutter BF, Mike LA, Reid PR, Chong KM, Ramos-Hunter SJ, Skaar EP, et al. Decoupling activation of heme biosynthesis from anaerobic toxicity in a molecule active in *Staphylococcus aureus*. ACS Chem Biol. 2016.
110. Mike LA, Dutter BF, Stauff DL, Moore JL, Vitko NP, Aranmolate O, et al. Activation of heme biosynthesis by a small molecule that is toxic to fermenting *Staphylococcus aureus*. Proc Natl Acad Sci USA. 2013;110(20):9206-8211.
111. Surdel MC, Horvath DJ, Jr., Lojek LJ, Fullen AR, Simpson J, Dutter BF, et al. Antibacterial photosensitization through activation of coproporphyrinogen oxidase. Proc Natl Acad Sci U S A. 2017;pii: 201700469.
112. Jensen J. The effect of heme on tetrapyrrol synthesis in a heme requiring *Staphylococcus aureus*. Biochem Biophys Res Commun. 1962;8(4):271-7.
113. Mazmanian SK, Skaar EP, Gaspar AH, Humayun M, Gornicki P, Jelenska J, et al. Passage of heme-iron across the envelope of *Staphylococcus aureus*. Science. 2003;299:906-9.
114. Spaan AN, Reyes-Robles T, Badiou C, Cochet S, Boguslawski KM, Yoong P, et al. *Staphylococcus aureus* targets the Duffy Antigen Receptor for Chemokines (DARC) to lyse erythrocytes. Cell Host Microbe. 2015;18(3):363-70.

115. Grigg JC, Vermeiren CL, Heinrichs DE, Murphy ME. Haem recognition by a *Staphylococcus aureus* NEAT domain. Mol Microbiol. 2007;63(1):139-49.
116. Sharp KH, Schneider S, Cockayne A, Paoli M. Crystal structure of the heme-IsdC complex, the central conduit of the Isd iron/heme uptake system in *Staphylococcus aureus*. J Biol Chem. 2007;282(14):10625-31.
117. Fonner BA, Tripet BP, Eilers BJ, Stanisich J, Sullivan-Springhetti RK, Moore R, et al. Solution structure and molecular determinants of hemoglobin binding of the first NEAT domain of IsdB in *Staphylococcus aureus*. Biochemistry. 2014;53(24):3922-33.
118. Torres VJ, Pishchany G, Humayun M, Schneewind O, Skaar EP. *Staphylococcus aureus* IsdB is a hemoglobin receptor required for heme iron utilization. J Bacteriol. 2006;188(24):8421-9.
119. Bowden CFM, Chan ACK, Li EJW, Arrieta AL, Eltis LD, Murphy MEP. Structure-function analyses reveal key features in *Staphylococcus aureus* IsdB-associated unfolding of the heme-binding pocket of human hemoglobin. J Biol Chem. 2018;293(1):177-90.
120. Dryla A, Gelbmann D, Von Gabain A, Nagy E. Identification of a novel iron regulated staphylococcal surface protein with haptoglobin-haemoglobin binding activity. Molecular Microbiology. 2003;49(1):37-53.
121. Pilpa RM, Robson SA, Villareal VA, Wong ML, Phillips M, Clubb RT. Functionally distinct NEAT (NEAr Transporter) domains within the *Staphylococcus aureus* IsdH/HarA protein extract heme from methemoglobin. J Biol Chem. 2009;284(2):1166-76.
122. Muryoi N, Tiedemann MT, Pluym M, Cheung J, Heinrichs DE, Stillman MJ. Demonstration of the iron-regulated surface determinant (Isd) heme transfer pathway in *Staphylococcus aureus*. J Biol Chem. 2008;283(42):28125-36.
123. Mazmanian SK, Ton-That H, Su K, Schneewind O. An iron-regulated sortase anchors a class of surface protein during *Staphylococcus aureus* pathogenesis. Proc Natl Acad Sci USA. 2002;99(4):2293-8.
124. Beveridge J. Ultrastructure of Gram-positive cell walls. In: Fishetti V, Novick R, JJ F, Portnoy D, Rood J, editors. Gram-positive Pathogens. 2nd ed. Washington, D.C.: ASM Press; 2000. p. 3-10.
125. Zhu H, Xie G, Liu M, Olson JS, Fabian M, Dooley DM, et al. Pathway for heme uptake from human methemoglobin by the iron-regulated surface determinants system of *Staphylococcus aureus*. J Biol Chem. 2008;283(26):18450-60.
126. Reniere ML, Torres VJ, Skaar EP. Intracellular metalloporphyrin metabolism in Staphylococcus aureus. Biometals. 2007;20(3-4):333-45.
127. Skaar EP, Gaspar AH, Schneewind O. IsdG and IsdI, heme-degrading enzymes in the cytoplasm of *Staphylococcus aureus*. J Biol Chem. 2004;279(1):436-43.
128. Lee WC, Reniere ML, Skaar EP, Murphy ME. Ruffling of metalloporphyrins bound to IsdG and IsdI, two heme-degrading enzymes in *Staphylococcus aureus*. J Biol Chem. 2008;283(45):30957-63.
129. Reniere ML, Ukpabi GN, Harry SR, Stec DF, Krull R, Wright DW, et al. The IsdG-family of haem oxygenases degrades haem to a novel chromophore. Mol Microbiol. 2010;75(6):1529-38.
130. Wu R, Skaar EP, Zhang R, Joachimiak G, Gornicki P, Schneewind O, et al. *Staphylococcus aureus* IsdG and IsdI, heme-degrading enzymes with structural similarity to monooxygenases. J Biol Chem. 2005;280(4):2840-6.
131. Reniere ML, Skaar EP. *Staphylococcus aureus* haem oxygenases are differentially regulated by iron and haem. Mol Microbiol. 2008;69(5):1304-15.
132. Farrand AJ, Reniere ML, Ingmer H, Frees D, Skaar EP. Regulation of host hemoglobin binding by the *Staphylococcus aureus* Clp proteolytic system. J Bacteriol. 2013;195(22):5041-50.

133. Laakso HA, Marolda CL, Pinter TB, Stillman MJ, Heinrichs DE. A heme-responsive regulator controls synthesis of Staphyloferrin B in *Staphylococcus aureus*. J Biol Chem. 2016;291(1):29-40.
134. Cheng AG, Kim HK, Burts ML, Krausz T, Schneewind O, Missiakas DM. Genetic requirements for *Staphylococcus aureus* abscess formation and persistence in host tissues. FASEB J. 2009;23(10):3393-404.
135. Visai L, Yanagisawa N, Josefsson E, Tarkowski A, Pezzali I, Rooijakkers SH, et al. Immune evasion by *Staphylococcus aureus* conferred by iron-regulated surface determinant protein IsdH. Microbiology. 2009;155(Pt 3):667-79.
136. Maresso AW, Garufi G, Schneewind O. *Bacillus anthracis* secretes proteins that mediate heme acquisition from hemoglobin. PLoS Pathog. 2008;4(8):e1000132.
137. Fabian M, Solomaha E, Olson JS, Maresso AW. Heme transfer to the bacterial cell envelope occurs via a secreted hemophore in the Gram-positive pathogen *Bacillus anthracis*. J Biol Chem. 2009;284(46):32138-46.
138. Honsa ES, Fabian M, Cardenas AM, Olson JS, Maresso AW. The five near-iron transporter (NEAT) domain anthrax hemophore, IsdX2, scavenges heme from hemoglobin and transfers heme to the surface protein IsdC. J Biol Chem. 2011;286(38):33652-60.
139. Honsa ES, Owens CP, Goulding CW, Maresso AW. The near-iron transporter (NEAT) domains of the anthrax hemophore IsdX2 require a critical glutamine to extract heme from methemoglobin. J Biol Chem. 2013;288(12):8479-90.
140. Maresso AW, Chapa TJ, Schneewind O. Surface protein IsdC and Sortase B are required for heme-iron scavenging of *Bacillus anthracis*. J Bacteriol. 2006;188(23):8145-52.
141. Balderas MA, Nobles CL, Honsa ES, Alicki ER, Maresso AW. Hal Is a *Bacillus anthracis* heme acquisition protein. J Bacteriol. 2012;194(20):5513-21.
142. Gaspar AH, Marraffini LA, Glass EM, Debord KL, Ton-That H, Schneewind O. *Bacillus anthracis* sortase A (SrtA) anchors LPXTG motif-containing surface proteins to the cell wall envelope. J Bacteriol. 2005;187(13):4646-55.
143. Tarlovsky Y, Fabian M, Solomaha E, Honsa E, Olson JS, Maresso AW. A *Bacillus anthracis* S-layer homology protein that binds heme and mediates heme delivery to IsdC. J Bacteriol. 2010;192(13):3503-11.
144. Skaar EP, Gaspar AH, Schneewind O. *Bacillus anthracis* IsdG, a heme-degrading monooxygenase. J Bacteriol. 2006;188(3):1071-80.
145. Gat O, Zaide G, Inbar I, Grosfeld H, Chitlaru T, Levy H, et al. Characterization of *Bacillus anthracis* iron-regulated surface determinant (Isd) proteins containing NEAT domains. Mol Microbiol. 2008;70(4):983-99.
146. Carlson PE, Jr., Carr KA, Janes BK, Anderson EC, Hanna PC. Transcriptional profiling of *Bacillus anthracis* Sterne (34F2) during iron starvation. PLoS One. 2009;4(9):e6988.
147. Farrand AJ, Haley KP, Lareau NM, Heilbronner S, McLean JA, Foster T, et al. An iron-regulated autolysin remodels the cell wall to facilitate heme acquisition in *Staphylococcus lugdunensis*. Infect Immun. 2015;83(9):3578-89.
148. Haley KP, Janson EM, Heilbronner S, Foster TJ, Skaar EP. *Staphylococcus lugdunensis* IsdG liberates iron from host heme. J Bacteriol. 2011;193(18):4749-57.
149. Zapotoczna M, Heilbronner S, Speziale P, Foster TJ. Iron-regulated surface determinant (Isd) proteins of *Staphylococcus lugdunensis*. J Bacteriol. 2012;194(23):6453-67.
150. Malmirchegini GR, Sjodt M, Shnitkind S, Sawaya MR, Rosinski J, Newton SM, et al. Novel mechanism of hemin capture by Hbp2, the hemoglobin-binding hemophore from *Listeria monocytogenes*. J Biol Chem. 2014;289(50):34886-99.
151. Xiao Q, Jiang X, Moore KJ, Shao Y, Pi H, Dubail I, et al. Sortase independent and dependent systems for acquisition of haem and haemoglobin in *Listeria monocytogenes*. Mol Microbiol. 2011;80(6):1581-97.

152. Dahesh S, Nizet V, Cole JN. Study of streptococcal hemoprotein receptor (Shr) in iron acquisition and virulence of M1T1 group A streptococcus. Virulence. 2012;3(7):566-75.
153. Ouattara M, Cunha EB, Li X, Huang YS, Dixon D, Eichenbaum Z. Shr of group A streptococcus is a new type of composite NEAT protein involved in sequestering haem from methaemoglobin. Mol Microbiol. 2010;78(3):739-56.
154. Ouattara M, Pennati A, Devlin DJ, Huang YS, Gadda G, Eichenbaum Z. Kinetics of heme transfer by the Shr NEAT domains of Group A Streptococcus. Arch Biochem Biophys. 2013;538(2):71-9.
155. Schmitt MP. Utilization of host iron sources by *Corynebacterium diphtheriae*: identification of a gene whose product is homologous to eukaryotic heme oxygenases and is required for acquisition of iron from heme and hemoglobin. J Bacteriol. 1997;179(3):838-45.
156. Drazek ES, Hammack CA, Schmitt MP. *Corynebacterium diphtheriae* genes required for acquisition of iron from haemin and haemoglobin are homologous to ABC haemin transporters. Mol Microbiol. 2000;36(1):68-84.
157. Thompson JM, Jones HA, Perry RD. Molecular characterization of the hemin uptake locus (*hmu*) from *Yersinia pestis* and analysis of hmu mutants for hemin and hemoprotein utilization. Infect Immun. 1999;67(8):3879-92.
158. Allen CE, Schmitt MP. HtaA is an iron-regulated hemin binding protein involved in the utilization of heme iron in *Corynebacterium diphtheriae*. J Bacteriol. 2009;191(8):2638-48.
159. Allen CE, Schmitt MP. Novel hemin binding domains in the *Corynebacterium diphtheriae* HtaA protein interact with hemoglobin and are critical for heme iron utilization by HtaA. J Bacteriol. 2011;193(19):5374-85.
160. Draganova EB, Akbas N, Adrian SA, Lukat-Rodgers GS, Collins DP, Dawson JH, et al. Heme binding by *Corynebacterium diphtheriae* HmuT: function and heme environment. Biochemistry. 2015;54(43):6598-609.
161. Kunkle CA, Schmitt MP. Analysis of a DtxR-regulated iron transport and siderophore biosynthesis gene cluster in *Corynebacterium diphtheriae*. J Bacteriol. 2005;187(2):422-33.
162. Kunkle CA, Schmitt MP. Analysis of the *Corynebacterium diphtheriae* DtxR regulon: identification of a putative siderophore synthesis and transport system that is similar to the *Yersinia* high-pathogenicity island-encoded yersiniabactin synthesis and uptake system. J Bacteriol. 2003;185(23):6826-40.
163. Allen CE, Burgos JM, Schmitt MP. Analysis of novel iron-regulated, surface-anchored hemin-binding proteins in *Corynebacterium diphtheriae*. J Bacteriol. 2013;195(12):2852-63.
164. Allen CE, Schmitt MP. Utilization of host iron sources by *Corynebacterium diphtheriae*: multiple hemoglobin-binding proteins are essential for the use of iron from the hemoglobin-haptoglobin complex. J Bacteriol. 2015;197(3):553-62.
165. Noinaj N, Guillier M, Barnard TJ, Buchanan SK. TonB-dependent transporters: regulation, structure, and function. Annu Rev Microbiol. 2010;64:43-60.
166. Letoffe S, Deniau C, Wolff N, Dassa E, Delepelaire P, Lecroisey A, et al. Haemophore-mediated bacterial haem transport: evidence for a common or overlapping site for haem-free and haem-loaded haemophore on its specific outer membrane receptor. Mol Microbiol. 2001;41(2):439-50.
167. Letoffe S, Nato F, Goldberg ME, Wandersman C. Interactions of HasA, a bacterial haemophore, with haemoglobin and with its outer membrane receptor HasR. Mol Microbiol. 1999;33(3):546-55.
168. Smith AD, Wilks A. Differential contributions of the outer membrane receptors PhuR and HasR to heme acquisition in *Pseudomonas aeruginosa*. J Biol Chem. 2015;290(12):7756-66.
169. Oglesby-Sherrouse AG, Vasil ML. Characterization of a heme-regulated non-coding RNA encoded by the *prrF* locus of *Pseudomonas aeruginosa*. PLoS One. 2010;5(4):e9930.

170. Reinhart AA, Powell DA, Nguyen AT, O'Neill M, Djapgne L, Wilks A, et al. The *prrF*-encoded small regulatory RNAs are required for iron homeostasis and virulence of *Pseudomonas aeruginosa*. Infect Immun. 2015;83(3):863-75.
171. Lansky IB, Lukat-Rodgers GS, Block D, Rodgers KR, Ratliff M, Wilks A. The cytoplasmic heme-binding protein (PhuS) from the heme uptake system of *Pseudomonas aeruginosa* is an intracellular heme-trafficking protein to the delta-regioselective heme oxygenase. J Biol Chem. 2006;281(19):13652-62.
172. Block DR, Lukat-Rodgers GS, Rodgers KR, Wilks A, Bhakta MN, Lansky IB. Identification of two heme-binding sites in the cytoplasmic heme-trafficking protein PhuS from *Pseudomonas aeruginosa* and their relevance to function. Biochemistry. 2007;46(50):14391-402.
173. O'Neill MJ, Bhakta MN, Fleming KG, Wilks A. Induced fit on heme binding to the *Pseudomonas aeruginosa* cytoplasmic protein (PhuS) drives interaction with heme oxygenase (HemO). Proc Natl Acad Sci USA. 2012;109(15):5639-44.
174. Tripathi S, O'Neill MJ, Wilks A, Poulos TL. Crystal structure of the *Pseudomonas aeruginosa* cytoplasmic heme binding protein, Apo-PhuS. J Inorg Biochem. 2013;128:131-6.
175. Lee MJ, Schep D, McLaughlin B, Kaufmann M, Jia Z. Structural analysis and identification of PhuS as a heme-degrading enzyme from *Pseudomonas aeruginosa*. J Mol Biol. 2014;426(9):1936-46.
176. O'Neill MJ, Wilks A. The *P. aeruginosa* heme binding protein PhuS is a heme oxygenase titratable regulator of heme uptake. ACS Chem Biol. 2013;8(8):1794-802.
177. Marvig RL, Damkiaer S, Khademi SM, Markussen TM, Molin S, Jelsbak L. Within-host evolution of *Pseudomonas aeruginosa* reveals adaptation toward iron acquisition from hemoglobin. mBio. 2014;5(3):e00966-14.
178. Granick S, Gilder H. The Porphyrin requirements of *Haemophilus influenzae* and some functions of the vinyl and propionic acid side chains of heme. J Gen Physiol. 1946;30(1):1-13.
179. Stull TL. Protein sources of heme for *Haemophilus influenzae*. Infect Immun. 1987;55(1):148-53.
180. Cope LD, Thomas SE, Hrkal Z, Hansen EJ. Binding of heme-hemopexin complexes by soluble HxuA protein allows utilization of this complexed heme by *Haemophilus influenzae*. Infect Immun. 1998;66(9):4511-6.
181. Cope LD, Yogev R, Muller-Eberhard U, Hansen EJ. A gene cluster involved in the utilization of both free heme and heme:hemopexin by *Haemophilus influenzae* type b. J Bacteriol. 1995;177(10):2644-53.
182. Baelen S, Dewitte F, Clantin B, Villeret V. Structure of the secretion domain of HxuA from *Haemophilus influenzae*. Acta Crystallogr Sect F Struct Biol Cryst Commun. 2013;69(Pt 12):1322-7.
183. Fournier C, Smith A, Delepelaire P. Haem release from haemopexin by HxuA allows *Haemophilus influenzae* to escape host nutritional immunity. Mol Microbiol. 2011;80(1):133-48.
184. Cope LD, Love RP, Guinn SE, Gilep A, Usanov S, Estabrook RW, et al. Involvement of HxuC outer membrane protein in utilization of hemoglobin by *Haemophilus influenzae*. Infect Immun. 2001;69(4):2353-63.
185. Morton DJ, Seale TW, Madore LL, VanWagoner TM, Whitby PW, Stull TL. The haem-haemopexin utilization gene cluster (hxuCBA) as a virulence factor of *Haemophilus influenzae*. Microbiology. 2007;153(Pt 1):215-24.
186. Morton DJ, Madore LL, Smith A, Vanwagoner TM, Seale TW, Whitby PW, et al. The heme-binding lipoprotein (HbpA) of *Haemophilus influenzae*: role in heme utilization. FEMS Microbiol Lett. 2005;253(2):193-9.

187. Morton DJ, Seale TW, Bakaletz LO, Jurcisek JA, Smith A, VanWagoner TM, et al. The heme-binding protein (HbpA) of *Haemophilus influenzae* as a virulence determinant. Int J Med Microbiol. 2009;299(7):479-88.
188. Morton DJ, VanWagoner TM, Seale TW, Whitby PW, Stull TL. Differential utilization by *Haemophilus influenzae* of haemoglobin complexed to the three human haptoglobin phenotypes. FEMS Immunol Med Microbiol. 2006;46(3):426-32.
189. Morton DJ, Van Wagoner TM, Seale TW, Whitby PW, Stull TL. Utilization of myoglobin as a heme source by *Haemophilus influenzae* requires binding of myoglobin to haptoglobin. FEMS Microbiol Lett. 2006;258(2):235-40.
190. Morton DJ, Smith A, VanWagoner TM, Seale TW, Whitby PW, Stull TL. Lipoprotein e (P4) of *Haemophilus influenzae*: role in heme utilization and pathogenesis. Microbes Infect. 2007;9(8):932-9.
191. Morton DJ, Smith A, Ren Z, Madore LL, VanWagoner TM, Seale TW, et al. Identification of a haem-utilization protein (Hup) in *Haemophilus influenzae*. Microbiology. 2004;150(Pt 12):3923-33.
192. Morton DJ, Seale TW, Vanwagoner TM, Whitby PW, Stull TL. The *dppBCDF* gene cluster of *Haemophilus influenzae*: role in heme utilization. BMC Res Notes. 2009;2:166.
193. LaCross NC, Marrs CF, Gilsdorf JR. Otitis media associated polymorphisms in the hemin receptor HemR of nontypeable *Haemophilus influenzae*. Infect Genet Evol. 2014;26:47-57.
194. Vogel AR, Szelestey BR, Raffel FK, Sharpe SW, Gearinger RL, Justice SS, et al. SapF-mediated heme-iron utilization enhances persistence and coordinates biofilm architecture of *Haemophilus*. Front Cell Infect Microbiol. 2012;2:42.
195. Whitby PW, VanWagoner TM, Seale TW, Morton DJ, Stull TL. Comparison of transcription of the *Haemophilus influenzae* iron/heme modulon genes *in vitro* and *in vivo* in the chinchilla middle ear. BMC Genomics. 2013;14:925.
196. Xie J, Juliao PC, Gilsdorf JR, Ghosh D, Patel M, Marrs CF. Identification of new genetic regions more prevalent in nontypeable *Haemophilus influenzae* otitis media strains than in throat strains. J Clin Microbiol. 2006;44(12):4316-25.
197. Hariadi NI, Zhang L, Patel M, Sandstedt SA, Davis GS, Marrs CF, et al. Comparative profile of heme acquisition genes in disease-causing and colonizing nontypeable *Haemophilus influenzae* and *Haemophilus haemolyticus*. J Clin Microbiol. 2015;53(7):2132-7.
198. Seale TW, Morton DJ, Whitby PW, Wolf R, Kosanke SD, VanWagoner TM, et al. Complex role of hemoglobin and hemoglobin-haptoglobin binding proteins in *Haemophilus influenzae* virulence in the infant rat model of invasive infection. Infect Immun. 2006;74(11):6213-25.
199. Morton DJ, Bakaletz LO, Jurcisek JA, VanWagoner TM, Seale TW, Whitby PW, et al. Reduced severity of middle ear infection caused by nontypeable *Haemophilus influenzae* lacking the hemoglobin/hemoglobin-haptoglobin binding proteins (Hgp) in a chinchilla model of otitis media. Microb Pathog. 2004;36(1):25-33.
200. Lewis LA, Gray E, Wang YP, Roe BA, Dyer DW. Molecular characterization of *hpuAB*, the haemoglobin-haptoglobin-utilization operon of *Neisseria meningitidis*. Mol Microbiol. 1997;23(4):737-49.
201. Lewis LA, Dyer DW. Identification of an iron-regulated outer membrane protein of *Neisseria meningitidis* involved in the utilization of hemoglobin complexed to haptoglobin. J Bacteriol. 1995;177(5):1299-306.
202. Zhu W, Hunt DJ, Richardson AR, Stojiljkovic I. Use of heme compounds as iron sources by pathogenic neisseriae requires the product of the *hemO* gene. J Bacteriol. 2000;182(2):439-47.

203. Zhu W, Wilks A, Stojiljkovic I. Degradation of heme in gram-negative bacteria: the product of the *hemO* gene of Neisseriae is a heme oxygenase. J Bacteriol. 2000;182(23):6783-90.
204. Lewis LA, Sung MH, Gipson M, Hartman K, Dyer DW. Transport of intact porphyrin by HpuAB, the hemoglobin-haptoglobin utilization system of *Neisseria meningitidis*. J Bacteriol. 1998;180(22):6043-7.
205. Kumar P, Sannigrahi S, Tzeng YL. The *Neisseria meningitidis* ZnuD zinc receptor contributes to interactions with epithelial cells and supports heme utilization when expressed in *Escherichia coli*. Infect Immun. 2012;80(2):657-67.
206. Chen CJ, Elkins C, Sparling PF. Phase variation of hemoglobin utilization in *Neisseria gonorrhoeae*. Infect Immun. 1998;66(3):987-93.
207. Rohde KH, Dyer DW. Analysis of haptoglobin and hemoglobin-haptoglobin interactions with the *Neisseria meningitidis* TonB-dependent receptor HpuAB by flow cytometry. Infect Immun. 2004;72(5):2494-506.
208. Rohde KH, Gillaspy AF, Hatfield MD, Lewis LA, Dyer DW. Interactions of haemoglobin with the Neisseria meningitidis receptor HpuAB: the role of TonB and an intact proton motive force. Mol Microbiol. 2002;43(2):335-54.
209. Wong CT, Xu Y, Gupta A, Garnett JA, Matthews SJ, Hare SA. Structural analysis of haemoglobin binding by HpuA from the *Neisseriaceae* family. Nat Commun. 2015;6:10172.
210. Stojiljkovic I, Larson J, Hwa V, Anic S, So M. HmbR outer membrane receptors of pathogenic *Neisseria* spp.: iron-regulated, hemoglobin-binding proteins with a high level of primary structure conservation. J Bacteriol. 1996;178(15):4670-8.
211. Richardson AR, Stojiljkovic I. HmbR, a hemoglobin-binding outer membrane protein of *Neisseria meningitidis*, undergoes phase variation. J Bacteriol. 1999;181(7):2067-74.
212. Mokry DZ, Nadia-Albete A, Johnson MK, Lukat-Rodgers GS, Rodgers KR, Lanzilotta WN. Spectroscopic evidence for a 5-coordinate oxygenic ligated high spin ferric heme moiety in the *Neisseria meningitidis* hemoglobin binding receptor. Biochim Biophys Acta. 2014;1840(10):3058-66.
213. Sebastian S, Agarwal S, Murphy JR, Genco CA. The gonococcal Fur regulon: identification of additional genes involved in major catabolic, recombination, and secretory pathways. J Bacteriol. 2002;184(14):3965-74.
214. Zhao S, Montanez GE, Kumar P, Sannigrahi S, Tzeng YL. Regulatory role of the MisR/S two-component system in hemoglobin utilization in *Neisseria meningitidis*. Infect Immun. 2010;78(3):1109-22.
215. Harrison OB, Bennett JS, Derrick JP, Maiden MC, Bayliss CD. Distribution and diversity of the haemoglobin-haptoglobin iron-acquisition systems in pathogenic and non-pathogenic *Neisseria*. Microbiology. 2013;159(Pt 9):1920-30.
216. Harrison OB, Evans NJ, Blair JM, Grimes HS, Tinsley CR, Nassif X, et al. Epidemiological evidence for the role of the hemoglobin receptor, MmbR, in meningococcal virulence. J Infect Dis. 2009;200(1):94-8.
217. Lucidarme J, Findlow J, Chan H, Feavers IM, Gray SJ, Kaczmarski EB, et al. The distribution and 'in vivo' phase variation status of haemoglobin receptors in invasive meningococcal serogroup B disease: genotypic and phenotypic analysis. PLoS One. 2013;8(9):e76932.
218. Fowler VG, Jr., Proctor RA. Where does a *Staphylococcus aureus* vaccine stand? Clin Microbiol Infect. 2014;20 Suppl 5:66-75.
219. Kuklin NA, Clark DJ, Secore S, Cook J, Cope LD, McNeely T, et al. A novel *Staphylococcus aureus* vaccine: iron surface determinant B induces rapid antibody responses in rhesus macaques and specific increased survival in a murine *S. aureus* sepsis model. Infect Immun. 2006;74(4):2215-23.

220. McNeely TB, Shah NA, Fridman A, Joshi A, Hartzel JS, Keshari RS, et al. Mortality among recipients of the Merck V710 *Staphylococcus aureus* vaccine after postoperative *S. aureus* infections: an analysis of possible contributing host factors. Hum Vaccin Immunother. 2014;10(12):3513-6.
221. Pancari G, Fan H, Smith S, Joshi A, Haimbach R, Clark D, et al. Characterization of the mechanism of protection mediated by CS-D7, a monoclonal antibody to *Staphylococcus aureus* iron regulated surface determinant B (IsdB). Front Cell Infect Microbiol. 2012;2:36.
222. Ebert T, Smith S, Pancari G, Clark D, Hampton R, Secore S, et al. A fully human monoclonal antibody to *Staphylococcus aureus* iron regulated surface determinant B (IsdB) with functional activity *in vitro* and *in vivo*. Hum Antibodies. 2010;19(4):113-28.
223. Parish T, Schaeffer M, Roberts G, Duncan K. HemZ is essential for heme biosynthesis in *Mycobacterium tuberculosis*. Tuberculosis (Edinb). 2005;85(3):197-204.
224. Owens CP, Chim N, Goulding CW. Insights on how the *Mycobacterium tuberculosis* heme uptake pathway can be used as a drug target. Future Med Chem. 2013;5(12):1391-403.
225. Tullius MV, Harmston CA, Owens CP, Chim N, Morse RP, McMath LM, et al. Discovery and characterization of a unique mycobacterial heme acquisition system. Proc Natl Acad Sci U S A. 2011;108(12):5051-6.
226. Barber MF, Elde NC. Nutritional immunity. Escape from bacterial iron piracy through rapid evolution of transferrin. Science. 2014;346(6215):1362-6.
227. Barber MF, Elde NC. Buried treasure: evolutionary perspectives on microbial Iron piracy. Trends Genet. 2015;31(11):627-36.
228. Chou AC, Fitch CD. Mechanism of hemolysis induced by ferriprotoporphyrin IX. J Clin Invest. 1981;68(3):672-7.
229. Schmitt TH, Frezzatti WA, Jr., Schreier S. Hemin-induced lipid membrane disorder and increased permeability: a molecular model for the mechanism of cell lysis. Arch Biochem Biophys. 1993;307(1):96-103.
230. Van Heyningen WE. Inhibition of aerobic sporing bacilli by haematin. Nature. 1948;162(4107):114.
231. Fernandez A, Lechardeur D, Derre-Bobillot A, Couve E, Gaudu P, Gruss A. Two coregulated efflux transporters modulate intracellular heme and protoporphyrin IX availability in *Streptococcus agalactiae*. PLoS Pathog. 2010;6(4):e1000860.
232. Stauff DL, Torres VJ, Skaar EP. Signaling and DNA-binding activities of the *Staphylococcus aureus* HssR-HssS two-component system required for heme sensing. J Biol Chem. 2007;282(36):26111-21.
233. Rasmussen AW, Alexander HL, Perkins-Balding D, Shafer WM, Stojiljkovic I. Resistance of *Neisseria meningitidis* to the toxic effects of heme iron and other hydrophobic agents requires expression of *ght*. J Bacteriol. 2005;187(15):5214-23.
234. Wyckoff EE, Lopreato GF, Tipton KA, Payne SM. Shigella dysenteriae ShuS promotes utilization of heme as an iron source and protects against heme toxicity. J Bacteriol. 2005;187(16):5658-64.
235. Imlay JA, Chin SM, Linn S. Toxic DNA damage by hydrogen peroxide through the Fenton reaction in vivo and in vitro. Science. 1988;240(4852):640-2.
236. Imlay JA, Linn S. DNA damage and oxygen radical toxicity. Science. 1988;240(4857):1302-9.
237. Wakeman CA, Hammer ND, Stauff DL, Attia AS, Anzaldi LL, Dikalov SI, et al. Menaquinone biosynthesis potentiates haem toxicity in *Staphylococcus aureus*. Mol Microbiol. 2012;86(6):1376-92.
238. Wakeman CA, Stauff DL, Zhang Y, Skaar EP. Differential activation of *Staphylococcus aureus* heme detoxification machinery by heme analogues. J Bacteriol. 2014;196(7):1335-42.

239. Nitzan Y, Wexler HM, Finegold SM. Inactivation of anaerobic bacteria by various photosensitized porphyrins or by hemin. Curr Microbiol. 1994;29(3):125-31.
240. Stojiljkovic I, Kumar V, Srinivasan N. Non-iron metalloporphyrins: potent antibacterial compounds that exploit haem/Hb uptake systems of pathogenic bacteria. Mol Microbiol. 1999;31(2):429-42.
241. Nir U, Ladan H, Malik Z, Nitzan Y. *In vivo* effects of porphyrins on bacterial DNA. J Photochem Photobiol B. 1991;11(3-4):295-306.
242. Putker F, Grutsch A, Tommassen J, Bos MP. Ght protein of *Neisseria meningitidis* is involved in the regulation of lipopolysaccharide biosynthesis. J Bacteriol. 2014;196(4):780-9.
243. Stauff DL, Bagaley D, Torres VJ, Joyce R, Anderson KL, Kuechenmeister L, et al. *Staphylococcus aureus* HrtA is an ATPase required for protection against heme toxicity and prevention of a transcriptional heme stress response. J Bacteriol. 2008;190(10):3588-96.
244. Torres VJ, Stauff DL, Pishchany G, Bezbradica JS, Gordy LE, Iturregui J, et al. A *Staphylococcus aureus* regulatory system that responds to host heme and modulates virulence. Cell Host Microbe. 2007;1(2):109-19.
245. Lechardeur D, Cesselin B, Liebl U, Vos MH, Fernandez A, Brun C, et al. Discovery of intracellular heme-binding protein HrtR, which controls heme efflux by the conserved HrtB-HrtA transporter in *Lactococcus lactis*. J Biol Chem. 2012;287(7):4752-8.
246. Joubert L, Derre-Bobillot A, Gaudu P, Gruss A, Lechardeur D. HrtBA and menaquinones control haem homeostasis in *Lactococcus lactis*. Mol Microbiol. 2014;93(4):823-33.
247. Mike LA, Choby JE, Brinkman PR, Olive LQ, Dutter BF, Ivan SJ, et al. Two-component system cross-regulation integrates *Bacillus anthracis* response to heme and cell envelope stress. PLoS Pathog. 2014;10(3):e1004044.
248. Hagman KE, Pan W, Spratt BG, Balthazar JT, Judd RC, Shafer WM. Resistance of *Neisseria gonorrhoeae* to antimicrobial hydrophobic agents is modulated by the *mtrRCDE* efflux system. Microbiology. 1995;141 (Pt 3):611-22.
249. Stojiljkovic I, Hantke K. Transport of haemin across the cytoplasmic membrane through a haemin-specific periplasmic binding-protein-dependent transport system in *Yersinia enterocolitica*. Mol Microbiol. 1994;13(4):719-32.
250. Suits MD, Pal GP, Nakatsu K, Matte A, Cygler M, Jia Z. Identification of an *Escherichia coli* O157:H7 heme oxygenase with tandem functional repeats. Proc Natl Acad Sci USA. 2005;102(47):16955-60.
251. Ouellet YH, Ndiaye CT, Gagne SM, Sebilo A, Suits MD, Jubinville E, et al. An alternative reaction for heme degradation catalyzed by the *Escherichia coli* O157:H7 ChuS protein: Release of hematinic acid, tripyrrole and Fe(III). J Inorg Biochem. 2016;154:103-13.
252. Kaur AP, Wilks A. Heme inhibits the DNA binding properties of the cytoplasmic heme binding protein of *Shigella dysenteriae* (ShuS). Biochemistry. 2007;46(11):2994-3000.
253. Al Jubair T, Singh B, Fleury C, Blom AM, Morgelin M, Thunnissen MM, et al. *Haemophilus influenzae* stores and distributes hemin by using protein E. Int J Med Microbiol. 2014;304(5-6):662-8.
254. Negari S, Sulpher J, Pacello F, Ingrey K, Battistoni A, Lee BC. A role for *Haemophilus ducreyi* Cu,ZnSOD in resistance to heme toxicity. Biometals. 2008;21(3):249-58.
255. Sheldon JR, Heinrichs DE. Recent developments in understanding the iron acquisition strategies of gram positive pathogens. FEMS Microbiol Rev. 2015;39(4):592-630.
256. Hammer ND, Schurig-Briccio LA, Gerdes SY, Gennis RB, Skaar EP. CtaM is required for menaquinol oxidase aa3 function in *Staphylococcus aureus*. mBio. 2016;7(4):e00823-16.
257. Celis AI, Gauss GH, Streit BR, Shisler K, Moraski GC, Rodgers KR, et al. Structure-based mechanism for oxidative decarboxylation reactions mediated by amino acids and heme propionates in coproheme decarboxylase (HemQ). J Am Chem Soc. 2017;139(5):1900-11.

258. Goncalves VL, Nobre LS, Vicente JB, Teixeira M, Saraiva LM. Flavohemoglobin requires microaerophilic conditions for nitrosative protection of *Staphylococcus aureus*. FEBS Lett. 2006;580(7):1817-21.
259. Flack CE, Zurek OW, Meishery DD, Pallister KB, Malone CL, Horswill AR, et al. Differential regulation of staphylococcal virulence by the sensor kinase SaeS in response to neutrophil-derived stimuli. Proc Natl Acad Sci U S A. 2014;111(19):E2037-45.
260. Sun F, Li C, Jeong D, Sohn C, He C, Bae T. In the *Staphylococcus aureus* two-component system sae, the response regulator SaeR binds to a direct repeat sequence and DNA binding requires phosphorylation by the sensor kinase SaeS. J Bacteriol. 2010;192(8):2111-27.
261. Palazzolo-Ballance AM, Reniere ML, Braughton KR, Sturdevant DE, Otto M, Kreiswirth BN, et al. Neutrophil microbicides induce a pathogen survival response in community-associated methicillin-resistant *Staphylococcus aureus*. J Immunol. 2008;180(1):500-9.
262. Jeong DW, Cho H, Jones MB, Shatzkes K, Sun F, Ji Q, et al. The auxiliary protein complex SaePQ activates the phosphatase activity of sensor kinase SaeS in the SaeRS two-component system of *Staphylococcus aureus*. Mol Microbiol. 2012;86(2):331-48.
263. Murima P, McKinney JD, Pethe K. Targeting bacterial central metabolism for drug development. Chem Biol. 2014;21(11):1423-32.
264. Vitko NP, Spahich NA, Richardson AR. Glycolytic dependency of high-level nitric oxide resistance and virulence in *Staphylococcus aureus*. mBio. 2015;6(2).
265. Wilde AD, Snyder DJ, Putnam NE, Valentino MD, Hammer ND, Lonergan ZR, et al. Bacterial hypoxic responses reaveld as critical determinants of the host-pathogen outcome by TnSeq analysis of *Staphylococcus aureus* invasive infection. PLoS Pathog. 2015;11(12):e1005341.
266. Friedman DB, Stauff DL, Pishchany G, Whitwell CW, Torres VJ, Skaar EP. *Staphylococcus aureus* redirects central metabolism to increase iron availability. PLoS Pathog. 2006;2(8):e87.
267. Mashruwala AA, Pang YY, Rosario-Cruz Z, Chahal HK, Benson MA, Mike LA, et al. Nfu facilitates the maturation of iron-sulfur proteins and participates in virulence in *Staphylococcus aureus*. Mol Microbiol. 2015;95(3):383-409.
268. Kennedy MC, Emptage MH, Dreyer JL, Beinert H. The role of iron in the activation-inactivation of aconitase. J Biol Chem. 1983;258(18):11098-105.
269. Flint DH, Emptage MH, Finnegan MG, Fu W, Johnson MK. The role and properties of the iron-sulfur cluster in *Escherichia coli* dihydroxy-acid dehydratase. J Biol Chem. 1993;268(20):14732-42.
270. Yan F, LaMarre JM, Rohrich R, Wiesner J, Jomaa H, Mankin AS, et al. RlmN and Cfr are radical SAM enzymes involved in methylation of ribosomal RNA. J Am Chem Soc. 2010;132(11):3953-64.
271. Sun F, Ji Q, Jones MB, Deng X, Liang H, Frank B, et al. AirSR, a [2Fe-2S] cluster-containing two-component system, mediates global oxygen sensing and redox signaling in *Staphylococcus aureus*. J Am Chem Soc. 2012;134(1):305-14.
272. Selbach BP, Chung AH, Scott AD, George SJ, Cramer SP, Dos Santos PC. Fe-S cluster biogenesis in Gram-positive bacteria: SufU is a zinc-dependent sulfur transfer protein. Biochemistry. 2014;53(1):152-60.
273. Rosario-Cruz Z, Chahal HK, Mike LA, Skaar EP, Boyd JM. Bacillithiol has a role in Fe-S cluster biogenesis in *Staphylococcus aureus*. Mol Microbiol. 2015;98(2):218-42.
274. Mashruwala AA, Bhatt S, Poudel S, Boyd ES, Boyd JM. The DUF59 containing protein SufT is involved in the maturation of iron-sulfur (FeS) proteins during conditions of high FeS cofactor demand in *Staphylococcus aureus*. PLoS Genet. 2016;12(8):e1006233.
275. <PNAS-2013-Mike-8206-11.pdf>.

276. Dutter BF, Mike LA, Reid PR, Chong KM, Ramos-Hunter SJ, Skaar EP, et al. Decoupling activation of heme biosynthesis from anaerobic toxicity in a molecule active in *Staphylococcus aureus*. ACS Chem Biol. 2016;DOI:10.1021/acschembio.5b00934.
277. Duthie EL, Lisa L. Staphylococcal coagulase: mode of action and antigenicity. J Gen Microbiol. 1952;6:95-107.
278. Kennedy AD, Otto M, Braughton KR, Whitney AR, Chen L, Mathema B, et al. Epidemic community-associated methicillin-resistant *Staphylococcus aureus*: recent clonal expansion and diversification. Proc Natl Acad Sci U S A. 2008;105(4):1327-32.
279. Fey PD, Endres JL, Yajjala VK, Widhelm TJ, Boissy RJ, Bose JL, et al. A genetic resource for rapid and comprehensive phenotype screening of nonessential *Staphylococcus aureus* genes. mBio. 2013;4(1):e00537-12.
280. Kreiswirth BN, Lofdahl S, Betley MJ, O'Reilly M, Schlievert PM, Bergdoll MS, et al. The toxic shock syndrome exotoxin structural gene is not detectably transmitted by a prophage. Nature. 1983;305(5936):709-12.
281. Luong TT, Sau K, Roux C, Sau S, Dunman PM, Lee CY. *Staphylococcus aureus* ClpC divergently regulates capsule via *sae* and *codY* in strain Newman but activates capsule via codY in strain UAMS-1 and in strain Newman with repaired *saeS*. J Bacteriol. 2011;193(3):686-94.
282. Benson MA, Lilo S, Nygaard T, Voyich JM, Torres VJ. Rot and SaeRS cooperate to activate expression of the staphylococcal superantigen-like exoproteins. J Bacteriol. 2012;194(16):4355-65.
283. Mashruwala AA, Pang YY, Rosario-Cruz Z, Chahal HK, Benson MA, Mike LA, et al. Nfu facilitates the maturation of iron-sulfur proteins and participates in virulence in *Staphylococcus aureus*. Mol Microbiol. 2015;95(3):383-409.
284. Schneewind O, Model P, Fischetti VA. Sorting of protein A to the staphylococcal cell wall. Cell. 1992;70(2):267-81.
285. Malone CL, Boles BR, Lauderdale KJ, Thoendel M, Kavanaugh JS, Horswill AR. Fluorescent reporters for *Staphylococcus aureus*. J Microbiol Methods. 2009;77(3):251-60.
286. Forsyth RA, Haselbeck RJ, Ohlsen KL, Yamamoto RT, Xu H, Trawick JD, et al. A genome-wide strategy for the identification of essential genes in *Staphylococcus aureus*. Mol Microbiol. 2002;43(6):1387-400.
287. Olson ME, King JM, Yahr TL, Horswill AR. Sialic acid catabolism in *Staphylococcus aureus*. J Bacteriol. 2013;195(8):1779-88.
288. Ham AJ, Caprioli RM, Gross ML. Proteolytic Digestion Protocols The Encylopedia of Mass Spectrometry. 2: Elsevier; 2005.
289. Zhang B, Chambers MC, Tabb DL. Proteomic parsimony through bipartite graph analysis improves accuracy and transparency. J Proteome Res. 2007;6(9):3549-57.
290. Boyd JM, Sondelski JL, Downs DM. Bacterial ApbC protein has two biochemical activities that are required for *in vivo* function. J Biol Chem. 2009;284(1):110-8.
291. Olson BJ, Markwell J. Assays for determination of protein concentration. Curr Protoc Protein Sci. 2007;Chapter 3:Unit 3 4.
292. Fuchs S, Pane-Farre J, Kohler C, Hecker M, Engelmann S. Anaerobic gene expression in *Staphylococcus aureus*. J Bacteriol. 2007;189(11):4275-89.
293. Kennedy MC, Emptage MH, Dreyer JL, Beinert H. The role of iron in the activation-inactivation of aconitase. J Biol Chem. 1983;258(18):11098-105.
294. Adhikari RP, Novick RP. Regulatory organization of the staphylococcal *sae* locus. Microbiology. 2008;154(Pt 3):949-59.
295. Parsons JB, Broussard TC, Bose JL, Rosch JW, Jackson P, Subramanian C, et al. Identification of a two-component fatty acid kinase responsible for host fatty acid incorporation by *Staphylococcus aureus*. Proc Natl Acad Sci U S A. 2014;111(29):10532-7.

296. Feng J, Michalik S, Varming AN, Andersen JH, Albrecht D, Jelsbak L, et al. Trapping and proteomic identification of cellular substrates of the ClpP protease in *Staphylococcus aureus*. J Proteome Res. 2013;12(2):547-58.
297. Jeong DW, Cho H, Lee H, Li C, Garza J, Fried M, et al. Identification of the P3 promoter and distinct roles of the two promoters of the SaeRS two-component system in *Staphylococcus aureus*. J Bacteriol. 2011;193(18):4672-84.
298. Tanaka S, Matsushita Y, Yoshikawa A, Isono K. Cloning and molecular characterization of the gene *rimL* which encodes an enzyme acetylating ribosomal protein L12 of *Escherichia coli* K12. Mol Gen Genet. 1989;217(2-3):289-93.
299. Boyd ES, Thomas KM, Dai Y, Boyd JM, Outten FW. Interplay between oxygen and Fe-S cluster biogenesis: insights from the Suf pathway. Biochemistry. 2014;53(37):5834-47.
300. Bose JL, Daly SM, Hall PR, Bayles KW. Identification of the *Staphylococcus aureus vfrAB* operon, a novel virulence factor regulatory locus. Infect Immun. 2014;82(5):1813-22.
301. Sabirova JS, Hernalsteens JP, De Backer S, Xavier BB, Moons P, Turlej-Rogacka A, et al. Fatty acid kinase A is an important determinant of biofilm formation in *Staphylococcus aureus* USA300. BMC Genomics. 2015;16(1):861.
302. Frees D, Savijoki K, Varmanen P, Ingmer H. Clp ATPases and ClpP proteolytic complexes regulate vital biological processes in low GC, Gram-positive bacteria. Mol Microbiol. 2007;63(5):1285-95.
303. Sturm A, Heinemann M, Arnoldini M, Benecke A, Ackermann M, Benz M, et al. The cost of virulence: retarded growth of *Salmonella* Typhimurium cells expressing type III secretion system 1. PLoS Pathog. 2011;7(7):e1002143.
304. Fuchs S, Pane-Farre J, Kohler C, Hecker M, Engelmann S. Anaerobic gene expression in *Staphylococcus aureus*. J Bacteriol. 2007;189(11):4275-89.
305. Crain AV, Broderick JB. Pyruvate formate-lyase and its activation by pyruvate formate-lyase activating enzyme. J Biol Chem. 2014;289(9):5723-9.
306. Hentze MW, Argos P. Homology between IRE-BP, a regulatory RNA-binding protein, aconitase, and isopropylmalate isomerase. Nucleic Acids Res. 1991;19(8):1739-40.
307. Campbell EA, Korzheva N, Mustaev A, Murakami K, Nair S, Goldfarb A, et al. Structural mechanism for rifampicin inhibition of bacterial RNA polymerase. Cell. 2001;104(6):901-12.
308. Lill R. Function and biogenesis of iron-sulphur proteins. Nature. 2009;460(7257):831-8.
309. Rouault TA. Biogenesis of iron-sulfur clusters in mammalian cells: new insights and relevance to human disease. Dis Model Mech. 2012;5(2):155-64.
310. Elliott T, Avissar YJ, Rhie GE, Beale SI. Cloning and sequence of the *Salmonella typhimurium hemL* gene and identification of the missing enzyme in *hemL* mutants as glutamate-1-semialdehyde aminotransferase. J Bacteriol. 1990;172(12):7071-84.
311. Bae T, Schneewind O. Allelic replacement in *Staphylococcus aureus* with inducible counter-selection. Plasmid. 2006;55(1):58-63.
312. Choby JE, Mike LA, Mashruwala AA, Dutter BF, Dunman PM, Sulikowski GA, et al. A small-molecule inhibitor of iron-sulfur cluster assembly uncovers a link between virulence regulation and metabolism in *Staphylococcus aureus*. Cell Chem Biol. 2016;23(11):1351-61.
313. Murphy KC, Campellone KG, Poteete AR. PCR-mediated gene replacement in *Escherichia coli*. Gene. 2000;246(1-2):321-30.
314. Bubeck Wardenburg J, Williams WA, Missiakas D. Host defenses against *Staphylococcus aureus* infection require recognition of bacterial lipoproteins. Proc Natl Acad Sci U S A. 2006;103(37):13831-6.
315. Abicht HK, Martinez J, Layer G, Jahn D, Solioz M. *Lactococcus lactis* HemW (HemN) is a haem-binding protein with a putative role in haem trafficking. Biochem J. 2012;442(2):335-43.

316. Haskamp V, Karrie S, Mingers T, Barthels S, Alberge F, Magalon A, et al. The radical SAM protein HemW is a heme chaperone. J Biol Chem. 2018;293(7):2558-72.
317. Choby JE, Skaar EP. Heme synthesis and acquisition in bacterial pathogens. J Mol Biol. 2016;428(17):3408-28.
318. Klevens RM, Morrison MA, Nadle J, Petit S, Gershman K, Ray S, et al. Invasive methicillin-resistant *Staphylococcus aureus* infections in the United States. JAMA. 2007;298(15):1763-71.
319. Cosgrove K, Coutts G, Jonsson IM, Tarkowski A, Kokai-Kun JF, Mond JJ, et al. Catalase (KatA) and alkyl hydroperoxide reductase (AhpC) have compensatory roles in peroxide stress resistance and are required for survival, persistence, and nasal colonization in *Staphylococcus aureus*. J Bacteriol. 2007;189(3):1025-35.
320. Mogen AB, Carroll RK, James KL, Lima G, Silva D, Culver JA, et al. *Staphylococcus aureus* nitric oxide synthase (saNOS) modulates aerobic respiratory metabolism and cell physiology. Mol Microbiol. 2017;105(1):139-57.
321. van Sorge NM, Beasley FC, Gusarov I, Gonzalez DJ, von Kockritz-Blickwede M, Anik S, et al. Methicillin-resistant *Staphylococcus aureus* bacterial nitric-oxide synthase affects antibiotic sensitivity and skin abscess development. J Biol Chem. 2013;288(9):6417-26.
322. Beale SI, Castelfranco PA. 14 C incorporation from exogenous compounds into -aminolevulinic acid by greening cucumber cotyledons. Biochem Biophys Res Commun. 1973;52(1):143-9.
323. Schon A, Krupp G, Gough S, Berry-Lowe S, Kannangara CG, Soll D. The RNA required in the first step of chlorophyll biosynthesis is a chloroplast glutamate tRNA. Nature. 1986;322(6076):281-4.
324. Moser J, Schubert WD, Beier V, Bringemeier I, Jahn D, Heinz DW. V-shaped structure of glutamyl-tRNA reductase, the first enzyme of tRNA-dependent tetrapyrrole biosynthesis. EMBO J. 2001;20(23):6583-90.
325. Chen J, Yoong P, Ram G, Torres VJ, Novick RP. Single-copy vectors for integration at the SaPI1 attachment site for *Staphylococcus aureus*. Plasmid. 2014;76C:1-7.
326. Kehl-Fie TE, Chitayat S, Hood MI, Damo S, Restrepo N, Garcia C, et al. Nutrient metal sequestration by calprotectin inhibits bacterial superoxide defense, enhancing neutrophil killing of *Staphylococcus aureus*. Cell Host Microbe. 2011;10(2):158-64.
327. Attia AS, Benson MA, Stauff DL, Torres VJ, Skaar EP. Membrane damage elicits an immunomodulatory program in *Staphylococcus aureus*. PLoS Pathog. 2010;6(3):e1000802.
328. Bose JL, Fey PD, Bayles KW. Genetic tools to enhance the study of gene function and regulation in *Staphylococcus aureus*. Applied and environmental microbiology. 2013;79(7):2218-24.
329. Kiedrowski MR, Crosby HA, Hernandez FJ, Malone CL, McNamara JO, II, Horswill AR. *Staphylococcus aureus* Nuc2 is a functional, surface-attached extracellular nuclease. PLoS One. 2014;9(4):e95574.
330. Guzman LM, Belin D, Carson MJ, Beckwith J. Tight regulation, modulation, and high-level expression by vectors containing the arabinose PBAD promoter. J Bacteriol. 1995;177(14):4121-30.
331. Shevchenko A, Wilm M, Vorm O, Mann M. Mass spectrometric sequencing of proteins silver-stained polyacrylamide gels. Anal Chem. 1996;68(5):850-8.
332. Gerber SA, Rush J, Stemman O, Kirschner MW, Gygi SP. Absolute quantification of proteins and phosphoproteins from cell lysates by tandem MS. Proc Natl Acad Sci U S A. 2003;100(12):6940-5.
333. MacLean B, Tomazela DM, Shulman N, Chambers M, Finney GL, Frewen B, et al. Skyline: an open source document editor for creating and analyzing targeted proteomics experiments. Bioinformatics. 2010;26(7):966-8.

334. Zhao A, Fang Y, Chen X, Zhao S, Dong W, Lin Y, et al. Crystal structure of *Arabidopsis* glutamyl-tRNA reductase in complex with its stimulator protein. Proc Natl Acad Sci USA. 2014;111(18):6630-5.
335. Waterhouse A, Bertoni M, Bienert S, Studer G, Tauriello G, Gumienny R, et al. SWISS-MODEL: homology modelling of protein structures and complexes. Nucleic Acids Res. 2018;46(W1):W296-W303.
336. Kardon JR, Yien YY, Huston NC, Branco DS, Hildick-Smith GJ, Rhee KY, et al. Mitochondrial ClpX activates a key enzyme for heme biosynthesis and erythropoiesis. Cell. 2015;161(4):858-67.
337. Vitko NP, Richardson AR. Laboratory maintenance of methicillin-resistant *Staphylococcus aureus* (MRSA). Curr Protoc Microbiol. 2013;Chapter 9:Unit 9C 2.
338. Blaxter M, Mann J, Chapman T, Thomas F, Whitton C, Floyd R, et al. Defining operational taxonomic units using DNA barcode data. Philosophical transactions of the Royal Society of London Series B, Biological sciences. 2005;360(1462):1935-43.
339. Jones M, Ghoorah A, Blaxter M. jMOTU and Taxonerator: turning DNA Barcode sequences into annotated operational taxonomic units. PLoS One. 2011;6(4):e19259.
340. Overbeek R, Begley T, Butler RM, Choudhuri JV, Chuang HY, Cohoon M, et al. The subsystems approach to genome annotation and its use in the project to annotate 1000 genomes. Nucleic Acids Res. 2005;33(17):5691-702.
341. Overbeek R, Olson R, Pusch GD, Olsen GJ, Davis JJ, Disz T, et al. The SEED and the Rapid Annotation of microbial genomes using Subsystems Technology (RAST). Nucleic Acids Res. 2014;42(Database issue):D206-14.
342. Ciccarelli FD, Doerks T, von Mering C, Creevey CJ, Snel B, Bork P. Toward automatic reconstruction of a highly resolved tree of life. Science. 2006;311(5765):1283-7.
343. Thompson JD, Higgins DG, Gibson TJ. CLUSTAL W: improving the sensitivity of progressive multiple sequence alignment through sequence weighting, position-specific gap penalties and weight matrix choice. Nucleic Acids Res. 1994;22(22):4673-80.
344. Krogh A, Larsson B, von Heijne G, Sonnhammer EL. Predicting transmembrane protein topology with a hidden Markov model: application to complete genomes. J Mol Biol. 2001;305(3):567-80.
345. Johansson P, Hederstedt L. Organization of genes for tetrapyrrole biosynthesis in Gram-positive bacteria. Microbiology. 1999;145 (Pt 3):529-38.
346. Schroder I, Hederstedt L, Kannangara CG, Gough P. Glutamyl-tRNA reductase activity in *Bacillus subtilis* is dependent on the *hemA* gene product. Biochem J. 1992;281 (Pt 3):843-50.
347. Schlag S, Fuchs S, Nerz C, Gaupp R, Engelmann S, Liebeke M, et al. Characterization of the oxygen-responsive NreABC regulon of *Staphylococcus aureus*. J Bacteriol. 2008;190(23):7847-58.
348. Overbeek R, Fonstein M, D'Souza M, Pusch GD, Maltsev N. The use of gene clusters to infer functional coupling. Proc Natl Acad Sci U S A. 1999;96(6):2896-901.
349. Chang W, Small DA, Toghrol F, Bentley WE. Global transcriptome analysis of *Staphylococcus aureus* response to hydrogen peroxide. J Bacteriol. 2006;188(4):1648-59.
350. Horsburgh MJ, Clements MO, Crossley H, Ingham E, Foster SJ. PerR controls oxidative stress resistance and iron storage proteins and is required for virulence in *Staphylococcus aureus*. Infect Immun. 2001;69(6):3744-54.
351. Kinkel TL, Roux CM, Dunman PM, Fang FC. The *Staphylococcus aureus* SrrAB two-component system promotes resistance to nitrosative stress and hypoxia. mBio. 2013;4(6):e00696-13.
352. Mader U, Nicolas P, Depke M, Pane-Farre J, Debarbouille M, van der Kooi-Pol MM, et al. *Staphylococcus aureus* transcriptome architecture: from laboratory to infection-mimicking conditions. PLoS Genet. 2016;12(4):e1005962.

353. Girvan HM, Munro AW. Heme sensor proteins. J Biol Chem. 2013;288(19):13194-203.
354. Apitz J, Nishimura K, Schmied J, Wolf A, Hedtke B, van Wijk KJ, et al. Posttranslational control of ALA synthesis includes GluTR degradation by Clp protease and stabilization by GluTR-binding protein. Plant physiology. 2016;170(4):2040-51.
355. Schade AL, Caroline L. Raw Hen Egg White and the Role of Iron in Growth Inhibition of *Shigella dysenteriae, Staphylococcus aureus, Escherichia coli and Saccharomyces cerevisiae*. Science. 1944;100(2584):14-5.
356. Malachowa N, Whitney AR, Kobayashi SD, Sturdevant DE, Kennedy AD, Braughton KR, et al. Global changes in *Staphylococcus aureus* gene expression in human blood. PLoS One. 2011;6(4):e18617.
357. Grigg JC, Vermeiren CL, Heinrichs DE, Murphy ME. Heme coordination by *Staphylococcus aureus* IsdE. J Biol Chem. 2007;282(39):28815-22.
358. Daugherty MD, Malik HS. Rules of engagement: molecular insights from host-virus arms races. Annu Rev Genet. 2012;46:677-700.
359. Hughes AL, Nei M. Pattern of nucleotide substitution at major histocompatibility complex class I loci reveals overdominant selection. Nature. 1988;335(6186):167-70.
360. Hamilton WD, Axelrod R, Tanese R. Sexual reproduction as an adaptation to resist parasites (a review). Proc Natl Acad Sci U S A. 1990;87(9):3566-73.
361. Yang Z, Bielawski JP. Statistical methods for detecting molecular adaptation. Trends in ecology & evolution. 2000;15(12):496-503.
362. Nei M, Gojobori T. Simple methods for estimating the numbers of synonymous and nonsynonymous nucleotide substitutions. Molecular biology and evolution. 1986;3(5):418-26.
363. Demogines A, Farzan M, Sawyer SL. Evidence for ACE2-utilizing coronaviruses (CoVs) related to severe acute respiratory syndrome CoV in bats. J Virol. 2012;86(11):6350-3.
364. Sawyer SL, Wu LI, Emerman M, Malik HS. Positive selection of primate TRIM5alpha identifies a critical species-specific retroviral restriction domain. Proc Natl Acad Sci U S A. 2005;102(8):2832-7.
365. Elde NC, Child SJ, Geballe AP, Malik HS. Protein kinase R reveals an evolutionary model for defeating viral mimicry. Nature. 2009;457(7228):485-9.
366. Enard D, Cai L, Gwennap C, Petrov DA. Viruses are a dominant driver of protein adaptation in mammals. eLife. 2016;5.
367. Barber MF, Kronenberg Z, Yandell M, Elde NC. Antimicrobial functions of lactoferrin promote genetic conflicts in ancient primates and modern humans. PLoS Genet. 2016;12(5):e1006063.
368. Storz JF, Moriyama H. Mechanisms of hemoglobin adaptation to high altitude hypoxia. High Alt Med Biol. 2008;9(2):148-57.
369. Galen SC, Natarajan C, Moriyama H, Weber RE, Fago A, Benham PM, et al. Contribution of a mutational hot spot to hemoglobin adaptation in high-altitude Andean house wrens. Proc Natl Acad Sci U S A. 2015;112(45):13958-63.
370. Natarajan C, Hoffmann FG, Weber RE, Fago A, Witt CC, Storz JF. Predictable convergence in hemoglobin function has unpredictable molecular underpinnings. Science. 2016;354(6310):336-9.
371. Storz JF, Sabatino SJ, Hoffmann FG, Gering EJ, Moriyama H, Ferrand N, et al. The molecular basis of high-altitude adaptation in deer mice. PLoS Genet. 2007;3(3):e45.
372. Ferreira A, Marguti I, Bechmann I, Jeney V, Chora A, Palha NR, et al. Sickle hemoglobin confers tolerance to *Plasmodium* infection. Cell. 2011;145(3):398-409.
373. Villarreal DM, Phillips CL, Kelley AM, Villarreal S, Villaloboz A, Hernandez P, et al. Enhancement of recombinant hemoglobin production in *Escherichia coli* BL21(DE3) containing the *Plesiomonas shigelloides* heme transport system. Applied and environmental microbiology. 2008;74(18):5854-6.

374. Perelman P, Johnson WE, Roos C, Seuanez HN, Horvath JE, Moreira MA, et al. A molecular phylogeny of living primates. PLoS Genet. 2011;7(3):e1001342.
375. Guindon S, Dufayard JF, Lefort V, Anisimova M, Hordijk W, Gascuel O. New algorithms and methods to estimate maximum-likelihood phylogenies: assessing the performance of PhyML 3.0. Systematic biology. 2010;59(3):307-21.
376. Delport W, Poon AF, Frost SD, Kosakovsky Pond SL. Datamonkey 2010: a suite of phylogenetic analysis tools for evolutionary biology. Bioinformatics. 2010;26(19):2455-7.
377. Pond SL, Frost SD, Muse SV. HyPhy: hypothesis testing using phylogenies. Bioinformatics. 2005;21(5):676-9.
378. Pettersen EF, Goddard TD, Huang CC, Couch GS, Greenblatt DM, Meng EC, et al. UCSF Chimera--a visualization system for exploratory research and analysis. Journal of computational chemistry. 2004;25(13):1605-12.
379. Spritz RA, DeRiel JK, Forget BG, Weissman SM. Complete nucleotide sequence of the human delta-globin gene. Cell. 1980;21(3):639-46.
380. Hardison RC. Evolution of hemoglobin and its genes. Cold Spring Harb Perspect Med. 2012;2(12):a011627.
381. Kloos WE. Natural populations of the genus *Staphylococcus*. Annu Rev Microbiol. 1980;34:559-92.
382. Wright JS, 3rd, Traber KE, Corrigan R, Benson SA, Musser JM, Novick RP. The *agr* radiation: an early event in the evolution of staphylococci. J Bacteriol. 2005;187(16):5585-94.
383. van Belkum A, Melles DC, Nouwen J, van Leeuwen WB, van Wamel W, Vos MC, et al. Co-evolutionary aspects of human colonisation and infection by *Staphylococcus aureus*. Infect Genet Evol. 2009;9(1):32-47.
384. Weatherall D, Akinyanju O, Fucharoen S, Olivieri N, Musgrove P. Inherited Disorders of Hemoglobin. In: Jamison DT, Breman JG, Measham AR, Alleyne G, Claeson M, Evans DB, et al., editors. Disease Control Priorities in Developing Countries. 2nd ed. Washington (DC): Oxford University Press and The World Bank; 2006. p. 663-80.
385. Stamatoyannopoulos G. The molecular basis of hemoglobin disease. Annu Rev Genet. 1972;6:47-70.
386. Thom CS, Dickson CF, Gell DA, Weiss MJ. Hemoglobin variants: biochemical properties and clinical correlates. Cold Spring Harb Perspect Med. 2013;3(3):a011858.
387. Miller KE, Kim Y, Huh WK, Park HO. Bimolecular fluorescence complementation (BiFC) analysis: advances and recent applications for genome-wide interaction studies. J Mol Biol. 2015;427(11):2039-55.
388. Videira MAM, Lobo SAL, Silva LSO, Palmer DJ, Warren MJ, Prieto M, et al. *Staphylococcus aureus* haem biosynthesis and acquisition pathways are linked through haem monooxygenase IsdG. Mol Microbiol. 2018.
389. Choby JE, Grunenwald CM, Celis AI, Gerdes SY, DuBois JL, Skaar EP. *Staphylococcus aureus* HemX modulates glutamyl-tRNA reductase abundance To regulate heme biosynthesis. mBio. 2018;9(1).

APPENDIX A

TABLES ASSOCIATED WITH CHAPTER II

Appendix A Table 1. Microarray data comparing NM +'882 and Δ*saeRS*+'882 anaerobically*†

NM Locus ID	USA300 Locus ID	fold change	gene name	description
Protein synthesis				
NWMN_1175	SAUSA300_1158	-2.48	-	conserved hypothetical protein
NWMN_1497	SAUSA300_1554	-3.24	-	conserved hypothetical protein TIGR00253, RNA binding protein
NWMN_1957	**SAUSA300_2002**	**-2.12**	**rimJ**	**ribosomal-protein-alanine acetyltransferase, putative**
NWMN_2022	SAUSA300_2072	-2.21	prfA	peptide chain release factor 1
NWMN_2146	SAUSA300_2198	-2.15	rpsC/rplF	ribosomal protein L6
NWMN_2147	SAUSA300_2199	-2.12	rplV	ribosomal protein L22
NWMN_2150	SAUSA300_2202	-2.65	rplW	ribosomal protein L23
Nucleic Acid				
NWMN_0249	SAUSA300_0307	-3.24	-	acid phosphatase5-nucleotidase, lipoprotein e(P4) family
Co-factor Synthesis				
NWMN_0553	SAUSA300_0572	-2.1	mvk/mvaK1	mevalonate kinase
NWMN_0554	SAUSA300_0573	-2.37	mvaD	mevalonate diphosphate decarboxylase
NWMN_0926	SAUSA300_0959	-2.03	fmt	Synthesizes THF and F-met-tRNA
Cell signaling				
NWMN_0484	between SAUSA300_0700/ 0701	-2.11	ctsR	conserved hypothetical protein: repressor of class III stress genes homologue
NWMN_1130	**SAUSA300_1113**	**-2.08**	**pknB**	**serine/threonine-protein kinase**
NWMN_1852	**SAUSA300_1895**	**-2.13**	**-**	**nitric-oxide synthase, oxygenase subunit; converts Arg to citrulline to make NO**
Energy Production				
NWMN_0071	SAUSA300_0129	3.6	-	acetoin reductase
NWMN_0171	SAUSA300_0229	5.05	-	propionate CoA-transferase, putative;
NWMN_1616	**SAUSA300_1669**	**2.13**	**-**	**aminotransferase, class V**
NWMN_1617	**SAUSA300_1670**	**2.16**	**serA**	**D-3-phosphoglycerate dehydrogenase**
NWMN_2110	**SAUSA300_2165**	**-5.67**	**budA1**	**alpha-acetolactate decarboxylase; converts pyruvate to acetoin**
NWMN_2111	SAUSA300_2166	-4.16	budB	acetolactate synthase, catabolic
NWMN_2499	SAUSA300_2537	4.61	ldh	L-lactate dehydrogenase 2
Cell Envelope				
NWMN_0193	**SAUSA300_0253**	**-2.59**	**scdA**	**cell wall synthesis**
NWMN_1145	SAUSA300_1128	-2.01	-	cell division protein FtsY, putative; FtsY recognizes signal peptide for secretion
NWMN_1342	**SAUSA300_1324**	**-2.92**	**-**	**membrane protein, putative**
NWMN_1309	SAUSA300_1291	2.95	hipO	peptidase, M20/M25/M40 family
NWMN_1310	SAUSA300_1292	3.09	alr2	alanine racemase family protein, pyridoxal 5'phosphate dependent
Amino acid metabolism				
Cys/Met				
NWMN_0011	**SAUSA300_0012**	**2.6**	**-**	**homoserine O-acetyltransferase, putative**
NWMN_0348	**SAUSA300_0357**	**2.82**	**metE**	**5-methyltetrahydropteroyltriglutamate--homocysteine methyltransferase (metE)**
NWMN_0351	SAUSA300_0360	2.08	-	trans-sulfuration enzyme family protein
NWMN_0426	SAUSA300_0435	3.28	-	ABC transporter, ATP-binding protein; predicted to transport methionine
NWMN_0427	**SAUSA300_0436**	**3.19**	**-**	**ABC transporter, permease protein**
NWMN_0428	SAUSA300_0437	3.04	-	ABC transporter, substrate-binding protein
NWMN_2021	**SAUSA300_2071**	**-2.13**	**-**	**SAM-dependent modification methylase, HemK family**
Asp				
NWMN_1239	**SAUSA300_1224**	**2.05**	**thrA**	**aspartate kinase**
NWMN_1241	**SAUSA300_1226**	**2.39**	**hom**	**homoserine dehydrogenase**
NWMN_1242	**SAUSA300_1227**	**2.71**	**thrC**	**threonine synthase**
NWMN_1243	SAUSA300_1228	2.89	thrB	homoserine kinase
Lys				
NWMN_1305	**SAUSA300_1286**	**2.18**	**asd**	**aspartate-semialdehyde dehydrogenase**
NWMN_1306	SAUSA300_1287	2.39	dapA	dihydrodipicolinate synthase
NWMN_1307	SAUSA300_1288	2.65	dapB	dihydrodipicolinate reductase
NWMN_1308	SAUSA300_1289	2.74	dapD	2,3,4,5-tetrahydropyridine-2,6-dicarboxylate N-succinyltransferase
Val, Leu, Ile				
NWMN_1960	**SAUSA300_2005**	**4.45**	**ilvD**	**dihydroxy-acid dehydratase**
NWMN_1961	SAUSA300_2006	4.48	ilvB	acetolactate synthase, large subunit, biosynthetic type
NWMN_1963	SAUSA300_2008	4.94	ilvC	ketol-acid reductoisomerase
NWMN_1964	SAUSA300_2009	4.64	leuA	2-isopropylmalate synthase

NWMN_1965	SAUSA300_2010	4.85	leuB	3-isopropylmalate dehydrogenase
NWMN_1966	SAUSA300_2011	4.27	leuC	3-isopropylmalate dehydratase, large subunit
NWMN_1967	SAUSA300_2012	3.97	leuD	3-isopropylmalate dehydratase, small subunit
NWMN_1968	SAUSA300_2013	2.56	ilvA2	threonine dehydratase
Glu				
NWMN_0145	**SAUSA300_0202**	**2.33**	**-**	**peptide ABC transporter, permease protein**
NWMN_0147	SAUSA300_0204	2.29	ggt	gamma-glutamyltranspeptidase; releases cysteine from glutathione
NWMN_0436	SAUSA300_0445	2.42	gltB	glutamate synthase, large subunit
NWMN_0437	SAUSA300_0446	2.72	gltD	glutamate synthase, small subunit
His				
NWMN_0692	**SAUSA300_0708**	**2.68**	**hisC**	**histidinol-phosphate aminotransferase**
Transport				
NWMN_0856	**SAUSA300_0887**	**2.43**	**oppB**	**oligopeptide ABC transporter, permease protein**
NWMN_0857	SAUSA300_0888	2.27	oppC	oligopeptide ABC transporter, permease protein
NWMN_0858	SAUSA300_0889	2.47	oppD	oligopeptide ABC transporter, ATP-binding protein
NWMN_0859	SAUSA300_0890	2.86	oppF	oligopeptide ABC transporter, ATP-binding protein
NWMN_0860	SAUSA300_0891	2.69	oppA	oligopeptide ABC transporter, oligopeptide-binding protein
NWMN_2303	**SAUSA300_2349**	**-2.27**	**-**	**formate/nitrite transporter family protein**
NWMN_2500	SAUSA300_2538	2.32	-	amino acid permease
NWMN_2581	**SAUSA300_2616**	**2.75**	**-**	**cobalt transport family protein**
NWMN_2582	SAUSA300_2617	3.67	-	ABC transporter, ATP-binding protein
NWMN_2584	SAUSA300_2619	3.61	-	conserved hypothetical protein
Virulence factors and exoproteins				
NWMN_0362	SAUSA300_0370	68.74	-	staphylococcal enterotoxin, putative
NWMN_0388	SAUSA300_0395	12.85	ssl1nm	exotoxin 3, putative
NWMN_0389	SAUSA300_0396	23.62	ssl2nm/ set7	exotoxin 1, putative
NWMN_0390	SAUSA300_0397	7.81	ssl3nm	exotoxin 8
NWMN_0392	SAUSA300_0399	5.48	ssl5nm	exotoxin 3
NWMN_0393	SAUSA300_0400	5.81	ssl6nm	exotoxin
NWMN_0395	SAUSA300_0402	21.35	ssl8nm	exotoxin 12
NWMN_0396	SAUSA300_0403	29.33	ssl9nm	exotoxin 5, putative
NWMN_0397	SAUSA300_0404	14.54	ssl10	exotoxin 4, putative
NWMN_0758	SAUSA300_0774	53.71	empbp/ ssp	secretory extracellular matrix and plasma binding protein
NWMN_1067	SAUSA300_1053	60.29	-	hypothetical protein, formyl peptide receptor-like 1 inhibitory protein
NWMN_1246	**SAUSA300_1232**	**2.25**	**katA**	**catalase**
NWMN_1075	SAUSA300_1059	14.62	-	exotoxin 1, putative
NWMN_1076	SAUSA300_1060	22.31	-	exotoxin 4, putative
NWMN_1077	SAUSA300_1061	69.11	-	exotoxin 3, putative
NWMN_1872	SAUSA300_1917	137.5	map	map protein, authentic frameshift
NWMN_1926	SAUSA300_1973	64.33	hlb	phospholipase C
NWMN_2318	SAUSA300_2365	94.07	hlgA	gamma-hemolysin, component A
NWMN_2320	**SAUSA300_2367**	**135.74**	**hlgC**	**gamma hemolysin, component C**
NWMN_2321	SAUSA300_2368	47.03	hlgB	gamma hemolysin, component B
Hypothetical				
NWMN_0150	**SAUSA300_0207**	**2.45**	**-**	**M23/M37 peptidase domain protein**
NWMN_0206	**SAUSA300_0266**	**-2.5**	**-**	**hypothetical protein**
NWMN_0402	SAUSA300_0409	114.43	-	hypothetical protein
NWMN_0896	SAUSA300_0929	2.1	-	hypothetical protein
NWMN_2370	**SAUSA300_2417**	**2.39**	**-**	**transporter, putative**
NWMN_2579	**SAUSA300_2614**	**2.06**	**-**	**hypothetical protein**
NWMN_2608	**SAUSA300_2642**	**-2.71**	**-**	**conserved hypothetical protein**
***bold indicates genes for which the corresponding NARSA mutant allele was transduced into NM**				
†transcript fold change in NM +'882 relative to *ΔsaeRS*+'882				

Appendix A-Table 2. Proteomic results of protein abundance changes in NM WT treated with 20 μM '882 relative to DMSO[1]

Protein (accession number)	'882 peptides[2]	DMSO peptides[2]	t-test	fold-change	Locus	NM locus ID	Product Name
gi|151221945	120	193	3.51E-05	1.6083	*prsA*	NWMN_1733	peptidyl-prolyl cis/trans-isomerase
gi|151220665	185	97	8.21E-05	-1.9072	*metS*	NWMN_0453	methionyl-tRNA synthetase
gi|151221286	34	66	8.92E-05	1.9412	-	NWMN_1074	hypothetical protein NWMN_1074
gi|151220882	42	15	9.89E-05	-2.8	*nagA*	NWMN_0670	N-acetylglucosamine-6-phosphate deacetylase
gi|151221298	284	148	0.000101162	-1.9189	-	NWMN_1086	hypothetical protein NWMN_1086
gi|151221814	112	55	0.000108276	-2.0364	-	NWMN_1602	proline dipeptidase-like protein
gi|151221378	152	777	0.000124937	5.1118	*rpsB*	NWMN_1166	30S ribosomal protein S2
gi|151221577	184	89	0.000157226	-2.0674	*asnC*	NWMN_1365	asparaginyl-tRNA synthetase
gi|151220323	26	7	0.000177551	-3.7143	-	NWMN_0111	heme-degrading monooxygenase IsdI
gi|151221350	7	25	0.000219511	3.5714	-	NWMN_1138	fatty acid biosynthesis transcriptional regulator
gi|151220765	25	8	0.000274562	-3.125	*mvaK1*	NWMN_0553	mevalonate kinase
gi|151221480	118	233	0.000352366	1.9746	*parC*	NWMN_1268	DNA topoisomerase IV subunit A
gi|151221001	151	98	0.000381207	-1.5408	*sufB*	NWMN_0789	FeS assembly protein SufB
gi|151220621	6	17	0.000388171	2.8333	*lpl6nm*	NWMN_0409	staphylococcal tandem lipoprotein
gi|151222473	16	1	0.000447238	-16	-	NWMN_2261	ABC transporter ATP-binding protein
gi|151221781	391	198	0.000470873	-1.9747	*tig*	NWMN_1569	trigger factor
gi|151221893	263	186	0.000485872	-1.414	*pckA*	NWMN_1681	phosphoenolpyruvate carboxykinase
gi|151222821	47	159	0.000499214	3.383	-	NWMN_2609	chromosome partioning ParB family protein
gi|151221315	322	187	0.000525274	-1.7219	*ileS*	NWMN_1103	isoleucyl-tRNA synthetase
gi|151222723	24	48	0.000608185	2	-	NWMN_2511	hypothetical protein NWMN_2511
gi|151221053	99	48	0.000740347	-2.0625	*cdr*	NWMN_0841	coenzyme A disulfide reductase
gi|151222358	107	307	0.000767274	2.8692	*rpsC*	NWMN_2146	30S ribosomal protein S3
gi|151222347	69	318	0.000798972	4.6087	*rpsE*	NWMN_2135	30S ribosomal protein S5
gi|151221385	161	92	0.000849973	-1.75	*proS*	NWMN_1173	prolyl-tRNA synthetase
gi|151222221	262	858	0.000913352	3.2748	*atpA*	NWMN_2009	F0F1 ATP synthase subunit alpha
gi|151222721	22	57	0.000940196	2.5909	-	NWMN_2509	choline dehydrogenase
gi|151222398	55	26	0.000942743	-2.1154	-	NWMN_2186	acyl-CoA dehydrogenase-related protein
gi|151221947	139	234	0.000988493	1.6835	-	NWMN_1735	hypothetical protein NWMN_1735
gi|151220881	32	64	0.001026183	2	*fruA*	NWMN_0669	fructose specific permease
gi|151221427	16	4	0.001057565	-4	-	NWMN_1215	hypothetical protein NWMN_1215
gi|151222459	35	23	0.001057565	-1.5217	*idi*	NWMN_2247	isopentenyl pyrophosphate isomerase
gi|151220693	349	185	0.001059972	-1.8865	-	NWMN_0481	pyridoxal biosynthesis lyase PdxS
gi|151222266	53	22	0.001158554	-2.4091	-	NWMN_2054	haloacid dehalogenase-like hydrolase
gi|151221390	196	754	0.001194869	3.8469	*infB*	NWMN_1178	translation initiation factor IF-2
gi|151221838	320	159	0.001220027	-2.0126	*acs*	NWMN_1626	acetyl-CoA synthetase
gi|151220217	335	879	0.001278516	2.6239	*gyrA*	NWMN_0005	DNA gyrase A subunit

gi|151220675	298	217	0.00128691	-1.3733	*prs*	NWMN_0463	ribose-phosphate pyrophosphokinase
gi|151221795	297	816	0.001290135	2.7475	*polA*	NWMN_1583	DNA polymerase I
gi|151221789	40	22	0.001292978	-1.8182	*dnaI*	NWMN_1577	primosomal protein DnaI
gi|151221065	60	31	0.001297077	-1.9355	-	NWMN_0853	3-oxoacyl-(acyl carrier protein) synthase III
gi|151220939	201	422	0.001323433	2.0995	*uvrA*	NWMN_0727	excinuclease ABC subunit A
gi|151220681	4	12	0.001323897	3	*divIC*	NWMN_0469	cell-division initiation protein
gi|151221703	22	6	0.001323897	-3.6667	*comEB*	NWMN_1491	competence protein ComEB required for DNA binding and uptake
gi|151220987	236	706	0.001326405	2.9915	-	NWMN_0775	hypothetical protein NWMN_0775
gi|151221499	201	347	0.001376803	1.7264	*femB*	NWMN_1287	methicillin resistance expression factor FemB
gi|151221323	44	22	0.001473119	-2	*pyrB*	NWMN_1111	aspartate carbamoyltransferase catalytic subunit
gi|151220659	42	112	0.001508079	2.6667	-	NWMN_0447	hypothetical protein NWMN_0447
gi|151222650	150	349	0.001539661	2.3267	*poxB*	NWMN_2438	pyruvate oxidase
gi|151220725	463	182	0.001574935	-2.544	-	NWMN_0513	chaperone protein HchA
gi|151222352	57	124	0.001779752	2.1754	*rplE*	NWMN_2140	50S ribosomal protein L5
gi|151221372	83	175	0.001854005	2.1084	*topA*	NWMN_1160	DNA topoisomerase I
gi|151221645	115	276	0.001854908	2.4	*efp*	NWMN_1433	elongation factor P
gi|151220933	289	1600	0.002008593	5.5363	-	NWMN_0721	sigma 54 modulation protein
gi|151222474	11	1	0.002110646	-11	-	NWMN_2262	hypothetical protein NWMN_2262
gi|151220327	351	50	0.002205477	-7.02	-	NWMN_0115	hypothetical protein NWMN_0115
gi|151221870	181	72	0.002269462	-2.5139	*putA*	NWMN_1658	proline dehydrogenase
gi|151221141	63	75	0.002278426	1.1905	*qoxB*	NWMN_0929	quinol oxidase polypeptide I QoxB
gi|151222219	706	1372	0.002291477	1.9433	*atpD*	NWMN_2007	F0F1 ATP synthase subunit beta
gi|151221082	400	219	0.002293937	-1.8265	-	NWMN_0870	oligoendopeptidase F
gi|151220954	372	127	0.002314277	-2.9291	*pgk*	NWMN_0742	phosphoglycerate kinase
gi|151222223	97	263	0.002397959	2.7113	*atpF*	NWMN_2011	F0F1 ATP synthase subunit B
gi|151221643	68	117	0.002449811	1.7206	*accC*	NWMN_1431	acetyl-CoA carboxylase biotin carboxylase subunit
gi|151222268	282	177	0.002473311	-1.5932	*glmS*	NWMN_2056	glucosamine--fructose-6-phosphate aminotransferase
gi|151220694	49	34	0.002570261	-1.4412	-	NWMN_0482	glutamine amidotransferase subunit PdxT
gi|151222055	14	29	0.002570261	2.0714	*pcrA*	NWMN_1843	ATP-dependent DNA helicase
gi|151221406	72	126	0.002659609	1.75	*recA*	NWMN_1194	recombinase A
gi|151222220	40	101	0.002765088	2.525	*atpG*	NWMN_2008	F0F1 ATP synthase subunit gamma
gi|151222084	59	112	0.002771281	1.8983	*map*	NWMN_1872	MHC class II analog protein
gi|151222797	539	232	0.002826024	-2.3233	-	NWMN_2585	hypothetical protein NWMN_2585
gi|151221709	15	2	0.002890007	-7.5	-	NWMN_1497	hypothetical protein NWMN_1497
gi|151221805	152	87	0.002890007	-1.7471	*pfk*	NWMN_1593	6-phosphofructokinase
gi|151221716	38	67	0.002915557	1.7632	-	NWMN_1504	hypothetical protein NWMN_1504
gi|151220867	162	357	0.002961871	2.2037	-	NWMN_0655	MarR family regulatory protein
gi|151221021	61	152	0.003000305	2.4918	-	NWMN_0809	hypothetical protein NWMN_0809
gi|151220711	47	254	0.003044078	5.4043	*rplK*	NWMN_0499	50S ribosomal protein L11

gi|151220712	64	123	0.003061925	1.9219	*rplA*	NWMN_0500	50S ribosomal protein L1
gi|151220579	14	5	0.003125589	-2.8	-	NWMN_0367	phosphoglycerate mutase family protein
gi|151221519	20	11	0.003125589	-1.8182	*dapB*	NWMN_1307	dihydrodipicolinate reductase
gi|151222130	2	11	0.003125589	5.5	-	NWMN_1918	phage anti repressor
gi|151222349	49	85	0.003125589	1.7347	*rplF*	NWMN_2137	50S ribosomal protein L6
gi|151220947	18	43	0.00334135	2.3889	-	NWMN_0735	hypothetical protein NWMN_0735
gi|151221420	82	36	0.003436385	-2.2778	*glpK*	NWMN_1208	glycerol kinase
gi|151220404	138	200	0.003441777	1.4493	-	NWMN_0192	glycosyl transferase group 2 family protein
gi|151221872	36	5	0.003441777	-7.2	*ribA*	NWMN_1660	riboflavin biosynthesis protein
gi|151221641	39	15	0.003448385	-2.6	*nusB*	NWMN_1429	transcription antitermination protein NusB
gi|151221253	199	73	0.00348785	-2.726	*isdA*	NWMN_1041	iron-regulated heme-iron binding protein IsdA
gi|151222070	200	517	0.003502201	2.585	-	NWMN_1858	aldehyde dehydrogenase
gi|151220763	232	156	0.003601086	-1.4872	*eutD*	NWMN_0551	phosphotransacetylase
gi|151221452	60	30	0.003602233	-2	*metL*	NWMN_1240	homoserine dehydrogenase
gi|151220219	94	38	0.003792218	-2.4737	*hutH*	NWMN_0007	histidine ammonia-lyase
gi|151220733	40	21	0.003862848	-1.9048	-	NWMN_0521	hydrolase, haloacid dehalogenase-like protein
gi|151222140	20	82	0.004099666	4.1	*lukS*	NWMN_1928	leukocidin/hemolysin toxin subunit S
gi|151221485	71	31	0.004300386	-2.2903	*msrA*	NWMN_1273	methionine sulfoxide reductase A
gi|151222243	115	64	0.004361708	-1.7969	*pyrG*	NWMN_2031	CTP synthetase
gi|151220721	1828	891	0.004457132	-2.0516	*fus*	NWMN_0509	elongation factor G
gi|151220593	273	171	0.004465448	-1.5965	*guaA*	NWMN_0381	GMP synthase
gi|151220637	57	21	0.004493713	-2.7143	*metB*	NWMN_0425	cystathionine gamma-synthase
gi|151221379	1117	593	0.004722975	-1.8836	*tsf*	NWMN_1167	elongation factor Ts
gi|151221162	445	160	0.004932672	-2.7813	-	NWMN_0950	phosphoenolpyruvate-protein phosphatase
gi|151220685	282	559	0.004945259	1.9823	*ftsH*	NWMN_0473	ATP-dependent metalloprotease FtsH
gi|151221301	37	62	0.005023998	1.6757	*mraW*	NWMN_1089	S-adenosyl-methyltransferase MraW
gi|151222320	50	24	0.005179626	-2.0833	-	NWMN_2108	HAD family hydrolase
gi|151221761	12	1	0.005328128	-12	*rplU*	NWMN_1549	50S ribosomal protein L21
gi|151220999	113	62	0.005329977	-1.8226	*sufS*	NWMN_0787	cysteine desulfurase SufS subfamily protein
gi|151220634	32	15	0.005784564	-2.1333	-	NWMN_0422	hypothetical protein NWMN_0422
gi|151222274	105	69	0.005820687	-1.5217	*glmM*	NWMN_2062	phosphoglucosamine-mutase
gi|151221756	17	29	0.005820687	1.7059	*ruvA*	NWMN_1544	Holliday junction DNA helicase RuvA
gi|151221815	115	61	0.006107227	-1.8852	*ald*	NWMN_1603	alanine dehydrogenase
gi|151220378	10	37	0.006107227	3.7	*coa*	NWMN_0166	staphylocoagulase precursor
gi|151221252	35	8	0.006107227	-4.375	*isdB*	NWMN_1040	iron-regulated heme-iron binding protein IsdB
gi|151221720	39	11	0.006122257	-3.5455	*accB*	NWMN_1508	acetyl-CoA carboxylase, biotin carboxyl carrier protein
gi|151221740	19	82	0.006219215	4.3158	-	NWMN_1528	hypothetical protein NWMN_1528
gi|151221328	47	16	0.006340451	-2.9375	*pyrE*	NWMN_1116	orotate phosphoribosyltransferase
gi|151221867	92	376	0.006427365	4.087	-	NWMN_1655	staphylococcal accessory regulator Rot

gi|151220401	139	80	0.006721869	-1.7375	*ispD*	NWMN_0189	2-C-methyl-D-erythritol 4-phosphate cytidylyltransferase
gi|151221261	40	17	0.006777398	-2.3529	*pheS*	NWMN_1049	phenylalanyl-tRNA synthetase subunit alpha
gi|151222607	34	18	0.007182329	-1.8889	*gtaB*	NWMN_2395	UTP-glucose-1-phosphate uridyltransferase
gi|151221308	460	801	0.007404485	1.7413	*ftsZ*	NWMN_1096	cell division protein FtsZ
gi|151221334	42	89	0.00743653	2.119	*priA*	NWMN_1122	primosomal protein N'
gi|151222808	46	22	0.007467447	-2.0909	-	NWMN_2596	N-acetyltransferase family protein
gi|151221410	12	2	0.007490434	-6	*porA*	NWMN_1198	pyruvate flavodoxin ferredoxin oxidoreductase, alpha subunit
gi|151221476	9	4	0.007490434	-2.25	-	NWMN_1264	hypothetical protein NWMN_1264
gi|151222139	19	39	0.007490434	2.0526	*lukF*	NWMN_1927	leukocidin/hemolysin toxin subunit F
gi|151222497	14	9	0.007490434	-1.5556	-	NWMN_2285	hypothetical protein NWMN_2285
gi|151222023	3	13	0.007490434	4.3333	-	NWMN_1811	phage anti-repressor
gi|151220226	62	103	0.007640728	1.6613	*rplI*	NWMN_0014	50S ribosomal protein L9
gi|151221624	113	59	0.007760254	-1.9153	*zwf*	NWMN_1412	glucose-6-phosphate 1-dehydrogenase
gi|151220827	13	20	0.007762603	1.5385	-	NWMN_0615	hypothetical protein NWMN_0615
gi|151220894	22	8	0.007762603	-2.75	*pabA*	NWMN_0682	para-aminobenzoate synthase component II
gi|151221745	48	21	0.007875643	-2.2857	*hisS*	NWMN_1533	histidyl-tRNA synthetase
gi|151221397	15	28	0.007966202	1.8667	*ftsK*	NWMN_1185	DNA translocase FtsK/SpoIIIE family protein
gi|151221831	3	15	0.008049893	5	-	NWMN_1619	PTS system, N-acetylglucosamine-specific IIBC component
gi|151222133	99	190	0.008089287	1.9192	-	NWMN_1921	phage cI-like repressor
gi|151221160	128	290	0.008095296	2.2656	-	NWMN_0948	hypothetical protein NWMN_0948
gi|151221191	259	182	0.008104933	-1.4231	*pycA*	NWMN_0979	pyruvate carboxylase
gi|151220953	1456	1005	0.008152054	-1.4488	*gapA*	NWMN_0741	glyceraldehyde 3-phosphate dehydrogenase 1
gi|151221638	78	250	0.008169004	3.2051	*ahrC*	NWMN_1426	arginine repressor
gi|151221731	151	64	0.008258683	-2.3594	*alaS*	NWMN_1519	alanyl-tRNA synthetase
gi|151222284	108	45	0.008801167	-2.4	-	NWMN_2072	hypothetical protein NWMN_2072
gi|151220813	652	1172	0.008813809	1.7975	-	NWMN_0601	hypothetical protein NWMN_0601
gi|151221652	304	115	0.0089689	-2.6435	*gcvPA*	NWMN_1440	glycine dehydrogenase subunit 1
gi|151221816	747	448	0.009096334	-1.6674	-	NWMN_1604	universal stress protein family protein
gi|151220344	61	30	0.009121205	-2.0333	*ipdC*	NWMN_0132	indole-3-pyruvate decarboxylase
gi|151221012	49	24	0.009140759	-2.0417	-	NWMN_0800	hydrolase
gi|151220268	82	147	0.009201503	1.7927	*sarH1*	NWMN_0056	accessory regulator A-like protein
gi|151220793	33	60	0.009307737	1.8182	-	NWMN_0581	iron compound ABC transporter, iron compound-binding protein
gi|151220544	41	20	0.009337848	-2.05	-	NWMN_0332	NADH-dependent FMN reductase
gi|151221127	157	97	0.009411161	-1.6186	*memB*	NWMN_0915	naphthoate synthase
gi|151220351	87	127	0.009436154	1.4598	*hsdR*	NWMN_0139	type-I restriction-modification system restriction endonuclease subunit
gi|151221780	79	119	0.009662137	1.5063	*clpX*	NWMN_1568	ATP-dependent protease ATP-binding subunit ClpX
gi|151222422	112	47	0.009799436	-2.383	-	NWMN_2210	formate dehydrogenase-like protein

gi|151222823	51	21	0.009813833	-2.4286	*gidA*	NWMN_2611	tRNA uridine 5-carboxymethylaminomethyl modification enzyme GidA
gi|151222407	181	486	0.010006124	2.6851	*sarR*	NWMN_2195	staphylococcal accessory regulator R
gi|151220955	321	212	0.010046876	-1.5142	*tpiA*	NWMN_0743	triosephosphate isomerase
gi|151220648	17	4	0.01005971	-4.25	*gltB*	NWMN_0436	glutamate synthase, large subunit
gi|151221481	9	29	0.01011969	3.2222	-	NWMN_1269	sodium:alanine symporter family protein
gi|151221517	59	37	0.010127315	-1.5946	*asd*	NWMN_1305	aspartate semialdehyde dehydrogenase
gi|151222054	84	142	0.010142733	1.6905	*lig*	NWMN_1842	DNA ligase, NAD-dependent
gi|151220734	103	23	0.010177401	-4.4783	-	NWMN_0522	hypothetical protein NWMN_0522
gi|151221847	63	32	0.010255349	-1.9688	-	NWMN_1635	hypothetical protein NWMN_1635
gi|151222260	162	76	0.010304362	-2.1316	-	NWMN_2048	hypothetical protein NWMN_2048
gi|151221884	774	445	0.010350876	-1.7393	-	NWMN_1672	putative translaldolase
gi|151221490	127	88	0.010547909	-1.4432	-	NWMN_1278	hypothetical protein NWMN_1278
gi|151220333	25	10	0.010636628	-2.5	-	NWMN_0121	formate dehydrogenase
gi|151220216	207	375	0.010919323	1.8116	*gyrB*	NWMN_0004	DNA gyrase B subunit
gi|151221395	204	134	0.010978961	-1.5224	*pnpA*	NWMN_1183	polynucleotide phosphorylase/polyadenylase
gi|151221343	17	7	0.011056493	-2.4286	-	NWMN_1131	hypothetical protein NWMN_1131
gi|151221813	83	43	0.011056493	-1.9302	-	NWMN_1601	metallo-beta-lactamase superfamily protein
gi|151220730	22	6	0.011354999	-3.6667	-	NWMN_0518	hypothetical protein NWMN_0518
gi|151220397	90	34	0.011446913	-2.6471	-	NWMN_0185	2-C-methyl-D-erythritol 4-phosphate cytidylyltransferase
gi|151221348	149	98	0.011639195	-1.5204	-	NWMN_1136	hypothetical protein NWMN_1136
gi|151221807	30	80	0.011825976	2.6667	*accD*	NWMN_1595	acetyl-CoA carboxylase subunit beta
gi|151221942	54	122	0.011872451	2.2593	-	NWMN_1730	hypothetical protein NWMN_1730
gi|151220236	96	174	0.011930492	1.8125	-	NWMN_0024	hypothetical protein NWMN_0024
gi|151221938	97	45	0.012026824	-2.1556	-	NWMN_1726	RNAIII-activating protein TRAP
gi|151221368	357	173	0.012224495	-2.0636	*sucD*	NWMN_1156	succinyl-CoA synthetase subunit alpha
gi|151222749	30	74	0.012296869	2.4667	*isaB*	NWMN_2537	immunodominant antigen B
gi|151221828	33	18	0.012348477	-1.8333	-	NWMN_1616	aminotransferase, class V
gi|151221856	235	115	0.012568373	-2.0435	-	NWMN_1644	dipeptidase PepV
gi|151220717	1321	2382	0.012698763	1.8032	*rpoC*	NWMN_0505	DNA-directed RNA polymerase subunit beta'
gi|151220325	566	365	0.012892338	-1.5507	*aldA*	NWMN_0113	aldehyde dehydrogenase-like protein
gi|151220291	38	61	0.012939917	1.6053	-	NWMN_0079	hypothetical protein NWMN_0079
gi|151220640	47	75	0.012950548	1.5957	-	NWMN_0428	ABC transporter, substrate-binding protein
gi|151220570	113	190	0.013005517	1.6814	-	NWMN_0358	single-strand DNA-binding family protein
gi|151222740	30	10	0.013011949	-3	*estA*	NWMN_2528	tributyrin esterase
gi|151221125	54	14	0.013011949	-3.8571	*memD*	NWMN_0913	2-succinyl-6-hydroxy-2,4-cyclohexadiene-1- carboxylic acid synthase
gi|151220821	11	5	0.0132356	-2.2	*tagB*	NWMN_0609	teichoic acid biosynthesis protein B
gi|151222032	17	41	0.0132356	2.4118	-	NWMN_1820	hypothetical protein NWMN_1820
gi|151222598	86	181	0.013442364	2.1047	-	NWMN_2386	hypothetical protein NWMN_2386

gi|151221937	46	20	0.013501854	-2.3	*hemE*	NWMN_1725	uroporphyrinogen decarboxylase
gi|151220713	27	85	0.013610614	3.1481	*rplJ*	NWMN_0501	50S ribosomal protein L10
gi|151221479	53	93	0.013771647	1.7547	*parE*	NWMN_1267	DNA topoisomerase IV subunit B
gi|151221800	812	500	0.014039412	-1.624	*citZ*	NWMN_1588	citrate synthase
gi|151220319	7	18	0.014172595	2.5714	*capM*	NWMN_0107	capsular polysaccharide biosynthesis protein CapM
gi|151221852	14	3	0.014172595	-4.6667	-	NWMN_1640	hypothetical protein NWMN_1640
gi|151221518	39	28	0.014172595	-1.3929	*dapA*	NWMN_1306	dihydrodipicolinate synthase
gi|151222470	51	122	0.014203042	2.3922	*tcaR*	NWMN_2258	teicoplanin resistance operon transcriptional regulator TcaR
gi|151220569	58	107	0.014361861	1.8448	*rpsF*	NWMN_0357	30S ribosomal protein S6
gi|151220251	27	14	0.014720594	-1.9286	-	NWMN_0039	hypothetical protein NWMN_0039
gi|151221341	18	5	0.014720594	-3.6	-	NWMN_1129	hypothetical protein NWMN_1129
gi|151220859	263	792	0.01509707	3.0114	-	NWMN_0647	hypothetical protein NWMN_0647
gi|151221399	37	14	0.015274813	-2.6429	-	NWMN_1187	hypothetical protein NWMN_1187
gi|151220907	64	30	0.01530106	-2.1333	-	NWMN_0695	hypothetical protein NWMN_0695
gi|151220486	136	219	0.015352974	1.6103	-	NWMN_0274	hypothetical protein NWMN_0274
gi|151221214	136	219	0.015352974	1.6103	-	NWMN_1002	hypothetical protein NWMN_1002
gi|151222018	136	219	0.015352974	1.6103	-	NWMN_1806	hypothetical protein NWMN_1806
gi|151220349	24	43	0.015465343	1.7917	-	NWMN_0137	transcriptional regulator
gi|151220902	19	50	0.015657535	2.6316	-	NWMN_0690	osmoprotectant ABC transporter, ATP-binding protein
gi|151221811	22	31	0.015799848	1.4091	-	NWMN_1599	CBS domain-containing protein
gi|151220480	2	11	0.015799848	5.5	-	NWMN_0268	phage anti-repressor protein
gi|151220896	14	5	0.015799848	-2.8	*pabC*	NWMN_0684	4-amino-4-deoxychorismate lyase
gi|151221070	37	55	0.015799848	1.4865	*oppD*	NWMN_0858	oligopeptide transport ATP-binding protein
gi|151221100	32	14	0.015799848	-2.2857	*murE*	NWMN_0888	UDP-N-acetylmuramoylalanyl-D-glutamate--L-lysine ligase
gi|151222708	31	16	0.016010966	-1.9375	*panB*	NWMN_2496	3-methyl-2-oxobutanoate hydroxymethyltransferase
gi|151220402	90	37	0.016044187	-2.4324	-	NWMN_0190	hypothetical protein NWMN_0190
gi|151222669	6	14	0.01613009	2.3333	-	NWMN_2457	cation-transporting ATPase E1-E2 family protein
gi|151222680	9	5	0.01613009	-1.8	-	NWMN_2468	acetyltransferase, GNAT family protein
gi|151222438	33	7	0.01660851	-4.7143	-	NWMN_2226	hypothetical protein NWMN_2226
gi|151220844	78	33	0.016649338	-2.3636	-	NWMN_0632	hypothetical protein NWMN_0632
gi|151221407	47	107	0.016729656	2.2766	-	NWMN_1195	phosphodiesterase
gi|151221458	986	706	0.016746882	-1.3966	*katA*	NWMN_1246	catalase
gi|151222397	53	78	0.016777901	1.4717	-	NWMN_2185	iron compound ABC transporter, iron compound-binding protein
gi|151221421	305	616	0.01693016	2.0197	*glpD*	NWMN_1209	aerobic glycerol-3-phosphate dehydrogenase
gi|151222230	56	17	0.016965564	-3.2941	-	NWMN_2018	hypothetical protein NWMN_2018
gi|151221812	191	407	0.017292431	2.1309	-	NWMN_1600	universal stress protein family protein
gi|151221629	359	259	0.017345406	-1.3861	*gnd*	NWMN_1417	6-phosphogluconate dehydrogenase
gi|151220831	71	42	0.017388558	-1.6905	-	NWMN_0619	hypothetical protein NWMN_0619
gi|151222197	51	34	0.017540467	-1.5	-	NWMN_1985	ATP-dependent RNA helicase DEAD box family protein

gi|151221653	137	95	0.017547374	-1.4421	*gcvT*	NWMN_1441	glycine cleavage system aminomethyltransferase T
gi|151222671	44	20	0.017641016	-2.2	-	NWMN_2459	D-lactate dehydrogenase
gi|151220331	39	24	0.017947913	-1.625	-	NWMN_0119	hypothetical protein NWMN_0119
gi|151220228	146	109	0.018185682	-1.3394	*purA*	NWMN_0016	adenylosuccinate synthetase
gi|151220687	1121	729	0.019387291	-1.5377	-	NWMN_0475	cysteine synthase-like protein
gi|151221793	42	19	0.019416074	-2.2105	*coaE*	NWMN_1581	dephospho-CoA kinase
gi|151221627	21	31	0.019441768	1.4762	*marR*	NWMN_1415	maltose operon transcriptional repressor
gi|151222739	32	42	0.019441768	1.3125	-	NWMN_2527	hypothetical protein NWMN_2527
gi|151220658	12	2	0.019441768	-6	*tmk*	NWMN_0446	thymidylate kinase
gi|151222559	60	40	0.019441768	-1.5	*opuCA*	NWMN_2347	glycine betaine/L-proline transport ATP-binding subunit
gi|151222718	169	120	0.019617515	-1.4083	-	NWMN_2506	hypothetical protein NWMN_2506
gi|151221979	751	304	0.019697083	-2.4704	-	NWMN_1767	ThiJ/PfpI family protein
gi|151221863	132	82	0.019987658	-1.6098	*leuS*	NWMN_1651	leucyl-tRNA synthetase
gi|151221869	59	82	0.020277578	1.3898	-	NWMN_1657	hypothetical protein NWMN_1657
gi|151221151	63	32	0.02074071	-1.9688	*purM*	NWMN_0939	phosphoribosylaminoimidazole synthetase
gi|151222673	46	18	0.021267756	-2.5556	*crtN*	NWMN_2461	squalene synthase
gi|151220923	21	12	0.021311641	-1.75	-	NWMN_0711	hypothetical protein NWMN_0711
gi|151222465	18	9	0.021311641	-2	-	NWMN_2253	drug resistance transporter EmrB/QacA subfamily protein
gi|151221788	299	246	0.021797036	-1.2154	*thrS*	NWMN_1576	threonyl-tRNA synthetase
gi|151221618	133	220	0.022010296	1.6541	-	NWMN_1406	iron uptake regulatory protein
gi|151221039	338	273	0.022311467	-1.2381	*rocD*	NWMN_0827	ornithine--oxo-acid transaminase
gi|151220676	17	36	0.022948261	2.1176	*rplY*	NWMN_0464	50S ribosomal protein L25/general stress protein Ctc
gi|151222429	45	108	0.023086213	2.4	-	NWMN_2217	phosphosugar-binding transcriptional regulator RpiR family protein
gi|151221646	260	161	0.023132649	-1.6149	-	NWMN_1434	proline dipeptidase
gi|151220660	10	2	0.023215158	-5	*holB*	NWMN_0448	DNA polymerase III delta subunit
gi|151220789	8	40	0.023215158	5	*adh1*	NWMN_0577	alcohol dehydrogenase
gi|151221268	19	11	0.023215158	-1.7273	*mutS2*	NWMN_1056	recombination and DNA strand exchange inhibitor protein
gi|151222551	2	10	0.023215158	5	-	NWMN_2339	hypothetical protein NWMN_2339
gi|151221412	19	11	0.023215158	-1.7273	-	NWMN_1200	hypothetical protein NWMN_1200
gi|151222337	37	94	0.023240291	2.5405	*rplQ*	NWMN_2125	50S ribosomal protein L17
gi|151220686	51	24	0.023245708	-2.125	*hslO*	NWMN_0474	Hsp33-like chaperonin
gi|151221024	117	63	0.023245708	-1.8571	*ampA*	NWMN_0812	cytosol aminopeptidase
gi|151220889	739	1588	0.023714348	2.1488	-	NWMN_0677	hypothetical protein NWMN_0677
gi|151221148	99	64	0.02371943	-1.5469	*purQ*	NWMN_0936	phosphoribosylformylglycinamidine synthase I
gi|151221995	14	31	0.023911192	2.2143	-	NWMN_1783	phage major tail protein
gi|151222272	55	38	0.023911192	-1.4474	*mtlD*	NWMN_2060	mannitol-1-phosphate 5-dehydrogenase
gi|151220838	11	1	0.024110111	-11	-	NWMN_0626	hypothetical protein NWMN_0626
gi|151220858	16	26	0.024110111	1.625	-	NWMN_0646	hypothetical protein NWMN_0646
gi|151221152	35	25	0.024110111	-1.4	*purN*	NWMN_0940	phosphoribosylglycinamide formyltransferase

gi|151222681	119	18	0.024577562	-6.6111	-	NWMN_2469	immunodominant antigen A
gi|151222053	61	87	0.024764921	1.4262	*camS*	NWMN_1841	CamS sex pheromone cAM373 precursor
gi|151222588	25	18	0.024896163	-1.3889	-	NWMN_2376	hypothetical protein NWMN_2376
gi|151221473	11	18	0.024896163	1.6364	-	NWMN_1261	glycine betaine transporter 1
gi|151220728	116	81	0.024896163	-1.4321	*ilvE*	NWMN_0516	branched-chain amino acid aminotransferase
gi|151221472	13	6	0.024896163	-2.1667	*mscL*	NWMN_1260	large-conductance mechanosensitive channel
gi|151221742	21	14	0.024896163	-1.5	-	NWMN_1530	hypothetical protein NWMN_1530
gi|151222161	14	21	0.024896163	1.5	*scrR*	NWMN_1949	sucrose operon repressor
gi|151222173	13	6	0.024896163	-2.1667	*ilvB*	NWMN_1961	acetolactate synthase large subunit
gi|151221843	288	596	0.024942029	2.0694	-	NWMN_1631	hypothetical protein NWMN_1631
gi|151222753	15	4	0.025386448	-3.75	-	NWMN_2541	mannose-6-phosphate isomerase
gi|151221131	24	13	0.025386448	-1.8462	-	NWMN_0919	aminotransferase, class I
gi|151221817	255	164	0.025422803	-1.5549	*ackA*	NWMN_1605	acetate kinase
gi|151220242	17	4	0.025481481	-4.25	-	NWMN_0030	hypothetical protein NWMN_0030
gi|151221784	14	1	0.025481481	-14	*rplT*	NWMN_1572	50S ribosomal protein L20
gi|151220674	55	29	0.025481481	-1.8966	*glmU*	NWMN_0462	UDP-N-acetylglucosamine pyrophosphorylase
gi|151220441	70	163	0.0256229	2.3286	-	NWMN_0229	hypothetical protein NWMN_0229
gi|151220853	35	58	0.025644709	1.6571	-	NWMN_0641	hypothetical protein NWMN_0641
gi|151220335	58	17	0.025697274	-3.4118	-	NWMN_0123	hypothetical protein NWMN_0123
gi|151220403	27	15	0.025721421	-1.8	-	NWMN_0191	hypothetical protein NWMN_0191
gi|151221693	9	3	0.025721421	-3	*prmA*	NWMN_1481	ribosomal protein L11 methylase
gi|151221707	18	6	0.025721421	-3	-	NWMN_1495	hypothetical protein NWMN_1495
gi|151222028	12	0	0.025721421	--	-	NWMN_1816	hypothetical protein NWMN_1816
gi|151222034	15	3	0.025721421	-5	*vraR*	NWMN_1822	DNA-binding response regulator VraR
gi|151222235	18	12	0.025721421	-1.5	*tdk*	NWMN_2023	thymidine kinase
gi|151220533	52	90	0.025946556	1.7308	-	NWMN_0321	oxidoreductase family protein
gi|151221326	222	173	0.026110988	-1.2832	*carB*	NWMN_1114	carbamoyl phosphate synthase large subunit
gi|151221834	79	39	0.026536326	-2.0256	*tyrS*	NWMN_1622	tyrosyl-tRNA synthetase
gi|151222361	32	48	0.026997302	1.5	*rplB*	NWMN_2149	50S ribosomal protein L2
gi|151221104	23	39	0.026997302	1.6957	*htrA*	NWMN_0892	serine protease HtrA
gi|151221237	14	30	0.026997302	2.1429	-	NWMN_1025	phage major tail protein
gi|151221594	2180	3560	0.027053617	1.633	-	NWMN_1382	DNA-binding protein HU
gi|151222255	330	209	0.027091194	-1.5789	-	NWMN_2043	hypothetical protein NWMN_2043
gi|151222158	166	448	0.027213759	2.6988	*agrA*	NWMN_1946	staphylococcal accessory gene regulator A
gi|151221806	57	109	0.027476558	1.9123	*accA*	NWMN_1594	acetyl-CoA carboxylase carboxyltransferase subunit alpha
gi|151221426	7	22	0.028460203	3.1429	-	NWMN_1214	hypothetical protein NWMN_1214
gi|151221013	34	6	0.028658204	-5.6667	-	NWMN_0801	D-isomer specific 2-hydroxyacid dehydrogenase
gi|151220863	31	62	0.02876031	2	-	NWMN_0651	hypothetical protein NWMN_0651
gi|151220804	25	43	0.028768335	1.72	-	NWMN_0592	site-specific recombinase

gi|151220745	378	281	0.028865914	-1.3452	-	NWMN_0533	hypothetical protein NWMN_0533
gi|151222634	71	38	0.029010766	-1.8684	-	NWMN_2422	D-lactate dehydrogenase
gi|151220610	137	251	0.030034749	1.8321	*hsdM*	NWMN_0398	type I restriction-modification system, methyltransferase subunit
gi|151221892	87	47	0.030272878	-1.8511	*metK*	NWMN_1680	S-adenosylmethionine synthetase
gi|151222604	27	9	0.030319669	-3	-	NWMN_2392	hypothetical protein NWMN_2392
gi|151222238	321	568	0.030328107	1.7695	-	NWMN_2026	aldehyde dehydrogenase family protein
gi|151222679	36	13	0.030337364	-2.7692	-	NWMN_2467	O-acetyltransferase OatA
gi|151221912	134	245	0.030367536	1.8284	*hsdM*	NWMN_1700	type I restriction-modification system, methyltransferase subunit
gi|151221050	62	41	0.030510813	-1.5122	*rexA*	NWMN_0838	exonuclease RexA
gi|151220705	39	68	0.031000144	1.7436	-	NWMN_0493	hypothetical protein NWMN_0493
gi|151221663	52	33	0.031125634	-1.5758	*glk*	NWMN_1451	glucokinase
gi|151221680	358	718	0.031396071	2.0056	*glyS*	NWMN_1468	glycyl-tRNA synthetase
gi|151221596	47	17	0.031824836	-2.7647	*engA*	NWMN_1384	GTP-binding protein EngA
gi|151220716	772	1076	0.032007992	1.3938	*rpoB*	NWMN_0504	DNA-directed RNA polymerase subunit beta
gi|151221205	154	262	0.032238532	1.7013	-	NWMN_0993	hypothetical protein NWMN_0993
gi|151221523	38	21	0.032505371	-1.8095	*lysA*	NWMN_1311	diaminopimelate decarboxylase
gi|151221405	30	16	0.032532525	-1.875	*cinA*	NWMN_1193	competence/damage-inducible protein
gi|151221563	93	52	0.032546532	-1.7885	-	NWMN_1351	hypothetical protein NWMN_1351
gi|151222433	17	5	0.032677923	-3.4	-	NWMN_2221	haloacid dehalogenase-like hydrolase
gi|151221181	14	26	0.032677923	1.8571	-	NWMN_0969	hypothetical protein NWMN_0969
gi|151221750	11	2	0.033471745	-5.5	*recJ*	NWMN_1538	single-stranded-DNA-specific exonuclease RecJ
gi|151221989	2	11	0.033471745	5.5	-	NWMN_1777	hypothetical protein NWMN_1777
gi|151220875	19	10	0.033471745	-1.9	-	NWMN_0663	hypothetical protein NWMN_0663
gi|151220746	28	18	0.034109423	-1.5556	-	NWMN_0534	hypothetical protein NWMN_0534
gi|151222029	113	70	0.03413741	-1.6143	*pepS*	NWMN_1817	aminopeptidase PepS
gi|151221651	198	101	0.03439011	-1.9604	*gcvPB*	NWMN_1439	glycine dehydrogenase subunit 2
gi|151221846	74	61	0.034415859	-1.2131	-	NWMN_1634	FtsK/SpoIIIE (DNA translocase stage III) family protein
gi|151222663	7	14	0.035168453	2	-	NWMN_2451	MmpL efflux pump
gi|151221548	59	93	0.035186827	1.5763	-	NWMN_1336	hypothetical protein NWMN_1336
gi|151222755	44	74	0.035262876	1.6818	-	NWMN_2543	N-acetylmuramoyl-L-alanine amidase
gi|151222391	42	89	0.035307924	2.119	*modA*	NWMN_2179	molybdenum ABC transporter, periplasmic molybdate-binding protein
gi|151221537	267	429	0.035486781	1.6067	*sucB*	NWMN_1325	dihydrolipoamide succinyltransferase
gi|151222049	412	191	0.035565471	-2.1571	*gatB*	NWMN_1837	aspartyl/glutamyl-tRNA amidotransferase subunit B
gi|151221946	59	95	0.035874451	1.6102	-	NWMN_1734	3'-5' exoribonuclease YhaM
gi|151221169	57	31	0.035955539	-1.8387	*def*	NWMN_0957	peptide deformylase
gi|151221723	43	68	0.036190628	1.5814	*greA*	NWMN_1511	transcription elongation factor GreA
gi|151222525	266	437	0.03629684	1.6429	-	NWMN_2313	amino acid ABC transporter, amino acid-binding protein
gi|151222277	153	61	0.036731704	-2.5082	-	NWMN_2065	arginase

gi|151221388	88	33	0.036952847	-2.6667	*nusA*	NWMN_1176	transcription elongation factor NusA
gi|151222063	48	33	0.037590112	-1.4545	*nadC*	NWMN_1851	nicotinate phosphoribosyltransferase
gi|151220587	99	202	0.03760864	2.0404	-	NWMN_0375	hypothetical protein NWMN_0375
gi|151222338	625	406	0.037932441	-1.5394	*rpoA*	NWMN_2126	DNA-directed RNA polymerase subunit alpha
gi|151222527	746	436	0.037948342	-1.711	*gpmA*	NWMN_2315	2,3-bisphosphoglycerate-dependent phosphoglycerate mutase
gi|151221051	701	471	0.038291218	-1.4883	-	NWMN_0839	fumarylacetoacetate hydrolase family protein
gi|151222159	34	16	0.038306255	-2.125	-	NWMN_1947	hypothetical protein NWMN_1947
gi|151222024	35	17	0.038306255	-2.0588	-	NWMN_1812	phage repressor
gi|151221507	101	45	0.038514275	-2.2444	*pepF*	NWMN_1295	oligoendopeptidase F
gi|151222265	41	120	0.038968806	2.9268	-	NWMN_2053	SAP domain-containing protein
gi|151222342	67	75	0.039020527	1.1194	*infA*	NWMN_2130	translation initiation factor IF-1
gi|151221683	11	3	0.039020527	-3.6667	-	NWMN_1471	cytidine deaminase
gi|151222369	24	1	0.039161395	-24	-	NWMN_2157	GCN5-related N-acetyltransferase
gi|151221347	61	134	0.03973141	2.1967	-	NWMN_1135	hypothetical protein NWMN_1135
gi|151221521	31	12	0.039778363	-2.5833	*hipO*	NWMN_1309	hippurate hydrolase
gi|151222244	69	87	0.039941968	1.2609	*rpoE*	NWMN_2032	DNA-directed RNA polymerase subunit delta
gi|151221150	56	42	0.040545533	-1.3333	*purF*	NWMN_0938	amidophosphoribosyltransferase
gi|151222709	24	11	0.040642089	-2.1818	*panE*	NWMN_2497	2-dehydropantoate 2-reductase
gi|151222079	162	360	0.04096118	2.2222	-	NWMN_1867	ABC transporter ATP-binding protein
gi|151220895	53	32	0.041150473	-1.6563	*pabB*	NWMN_0683	anthranilate/para-aminobenzoate synthase component I
gi|151221515	124	61	0.041419765	-2.0328	-	NWMN_1303	ABC transporter ATP-binding protein
gi|151220729	39	15	0.04179468	-2.6	-	NWMN_0517	haloacid dehalogenase-like hydrolase
gi|151221072	53	92	0.042400297	1.7358	-	NWMN_0860	hypothetical protein NWMN_0860
gi|151220800	1641	2248	0.042565657	1.3699	*sarA*	NWMN_0588	staphylococcal accessory regulator A
gi|151221079	225	450	0.043079419	2	*spxA*	NWMN_0867	transcriptional regulator Spx
gi|151222523	23	41	0.04324409	1.7826	-	NWMN_2311	amino acid ABC transporter, ATP-binding protein
gi|151220592	513	382	0.043943631	-1.3429	*guaB*	NWMN_0380	inosine-5'-monophosphate dehydrogenase
gi|151222071	137	101	0.044491833	-1.3564	-	NWMN_1859	hypothetical protein NWMN_1859
gi|151222447	55	33	0.044619278	-1.6667	*hutG*	NWMN_2235	formimidoylglutamase
gi|151221774	63	35	0.04465345	-1.8	*hemB*	NWMN_1562	delta-aminolevulinic acid dehydratase
gi|151221040	512	336	0.045090505	-1.5238	*gudB*	NWMN_0828	NAD-specific glutamate dehydrogenase
gi|151220940	59	31	0.045343299	-1.9032	*hprK*	NWMN_0728	HPr kinase/phosphorylase
gi|151222703	74	26	0.045770336	-2.8462	-	NWMN_2491	hypothetical protein NWMN_2491
gi|151222692	193	112	0.046002431	-1.7232	-	NWMN_2480	hydrolase
gi|151220850	45	65	0.04606216	1.4444	-	NWMN_0638	hypothetical protein NWMN_0638
gi|151222350	39	59	0.04606216	1.5128	*rpsH*	NWMN_2138	30S ribosomal protein S8
gi|151221798	52	122	0.046255938	2.3462	*phoP*	NWMN_1586	alkaline phosphatase synthesis transcriptional regulatory protein
gi|151221773	99	55	0.04629759	-1.8	*hemL*	NWMN_1561	glutamate-1-semialdehyde aminotransferase

gi|151221186	58	34	0.046476751	-1.7059	-	NWMN_0974	GTP-binding protein TypA
gi|151220784	66	28	0.046479363	-2.3571	-	NWMN_0572	aldo/keto reductase family protein
gi|151221273	178	280	0.04666274	1.573	*sdhA*	NWMN_1061	succinate dehydrogenase flavoprotein subunit
gi|151221566	29	13	0.047420656	-2.2308	-	NWMN_1354	hypothetical protein NWMN_1354
gi|151221970	4	8	0.047420656	2	-	NWMN_1758	ABC transporter ATP-binding protein
gi|151222077	11	7	0.047420656	-1.5714	-	NWMN_1865	hypothetical protein NWMN_1865
gi|151220756	20	47	0.048074518	2.35	*ung*	NWMN_0544	uracil-DNA glycosylase
gi|151221676	172	284	0.048332922	1.6512	*sigA*	NWMN_1464	RNA polymerase sigma factor RpoD
gi|151222611	78	92	0.048811551	1.1795	*fnbA*	NWMN_2399	fibronectin binding protein A precursor
gi|151220692	10	24	0.048811551	2.4	-	NWMN_0480	GntR family regulatory protein
gi|151221173	901	508	0.049235597	-1.7736	*pdhC*	NWMN_0961	branched-chain alpha-keto acid dehydrogenase subunit E2
gi|151221118	42	63	0.049741244	1.5	-	NWMN_0906	glycosyl transferase, group 1 family protein
gi|151221149	221	114	0.049750673	-1.9386	*purL*	NWMN_0937	phosphoribosylformylglycinamidine synthase II
gi|151221578	39	57	0.049948092	1.4615	-	NWMN_1366	DnaQ family exonuclease

[1]for peptides with calculated *p* value <0.05

[2]the sum of peptides detected in three biological replicates

APPENDIX B

TABLES ASSOCIATED WITH CHAPTER V

Appendix B Table 1 PAML Dataset									
Model	**Tree length**	**lnL**	**dN/dS**	**Statistical inference**	**Amino acid site**	**Posterior probability**	**dN/dS (+/- error)**	**2d**	**p-value**
Hemoglobin alpha (HBA) Tree: species (27 species)									
M1	0.85769	-1199.0014	0.1829						
M2	0.89659	-1191.5734	0.2901	Naïve Empirical Bayes	8T	1.000**	4.55		
					19A	0.737	3.616		
					78N	0.959*	4.404		
				Bayes Empirical Bayes	8T	0.999**	4.516+-1.363		
					19A	0.787	3.650+-1.769		
					78N	0.963*	4.358+-1.461	14.855998	0.000594376
M7	0.8883	-1199.5302	0.212						
M8	0.90418	-1191.9496	0.2981	Naïve Empirical Bayes	8T	1.000**	4.541		
					19A	0.79	3.786		
					78N	0.972*	4.444		
				Bayes Empirical Bayes	8T	1.000**	3.557+-1.088		
					19A	0.959*	3.427+-1.174		
					25G	0.715	2.678+-1.561		
					71A	0.706	2.563+-1.378		
					78N	0.996**	3.544+-1.097	15.161196	0.000510256
Model	**Tree length**	**lnL**	**dN/dS**	**Statistical inference**	**Amino acid site**	**Posterior probability**	**dN/dS (+/- error)**	**2d**	**p-value**
Hemoglboin alpha (HBA) Gene: species (27 species)									
M1	0.77035	-1153.8583	0.2026						
M2	0.79051	-1151.7888	0.2518	Naïve Empirical Bayes	8T	0.967*	3.969		
				Bayes Empirical Bayes	8T	0.960*	2.882+-1.590		
					19A	0.605	1.914+-1.161		
					21A	0.522	1.786+-1.215		
					25G	0.567	1.925+-1.341	2.069454	0.126254698
M7	0.77202	-1154.0221	0.2106						
M8	0.78543	-1152.289	0.2722	Naïve Empirical Bayes	8T	1.000**	1.595		
					12A	0.998**	1.591		
					15G	0.82	1.314		
					18G	0.952*	1.52		
					19A	1.000**	1.595		
					21A	0.993**	1.585		
					23E	0.999**	1.593		
					24Y	0.845	1.354		
					25G	0.994**	1.586		
					57G	0.998**	1.592		
					64D	0.909	1.454		
					67T	1.000**	1.595		
					68N	1.000**	1.595		
					71A	0.999**	1.594		
					78N	1.000**	1.595		
					82A	0.958*	1.531		
					113L	0.973*	1.552		
					116E	0.975*	1.557		
				Bayes Empirical Bayes	8T	0.996**	2.037+-0.714		
					12A	0.638	1.387+-0.698		
					19A	0.918	1.906+-0.726		
					21A	0.803	1.707+-0.812		
					23E	0.729	1.550+-0.719		
					24Y	0.524	1.158+-0.923		
					25G	0.826	1.753+-0.814		
					57G	0.677	1.453+-0.705		
					67T	0.836	1.740+-0.698		
					68N	0.83	1.728+-0.696		
					71A	0.77	1.625+-0.726		
					78N	0.85	1.767+-0.701		
					113L	0.54	1.202+-0.741		
					116E	0.555	1.229+-0.743	1.733127	0.176730907
Model	**Tree length**	**lnL**	**dN/dS**	**Statistical inference**	**Amino acid site**	**Posterior probability**	**dN/dS (+/- error)**	**2d**	**p-value**
Hemoglobin beta (HBB) Tree: species (30 species)									
M1	1.02343	-1355.5177							
M2	1.0674	-1342.483		Naïve Empirical Bayes	5P	0.549	2.56		
					6E	0.601	2.71		
					9S	1.000**	3.844		
					13A	0.679	2.93		
					43E	0.94	3.675		
					50T	0.896	3.55		
					76A	0.999**	3.841		
					87T	0.709	3.016		
					125P	0.916	3.604		
				Bayes Empirical Bayes	5P	0.528	2.537+-1.556		
					6E	0.571	2.662+-1.544		
					9S	1.000**	4.163+-0.944		
					13A	0.646	2.909+-1.540		
					43E	0.915	3.823+-1.179		
					50T	0.887	3.763+-1.286		
					76A	0.999**	4.160+-0.949		

					87T	0.677	3.016+-1.530		
					125P	0.919	3.904+-1.239	26.069494	2.18314E-06
M7	0.96435	-1354.4734							
M8	1.06678	-1342.6481		Naïve Empirical Bayes	5P	0.805	2.96		
					6E	0.886	3.203		
					9S	1.000**	3.543		
					13A	0.919	3.299		
					43E	0.997**	3.534		
					50T	0.981*	3.485		
					56G	0.531	2.141		
					76A	1.000**	3.543		
					87T	0.93	3.334		
					125P	0.976*	3.471		
				Bayes Empirical Bayes	5P	0.748	2.983+-1.479		
					6E	0.833	3.271+-1.300		
					9S	1.000**	3.849+-0.676		
					13A	0.877	3.426+-1.191		
					43E	0.991**	3.817+-0.731		
					50T	0.972*	3.759+-0.841		
					76A	1.000**	3.849+-0.677		
					87T	0.894	3.487+-1.142		
					125P	0.972*	3.760+-0.852	23.650616	7.31702E-06
Model	**Tree length**	**lnL**	**dN/dS**	**Statistical inference**	**Amino acid site**	**Posterior probability**	**dN/dS (+/- error)**	**2d**	**p-value**
Hemoglobin beta (HBB) Tree: gene (30 species)									
M1	0.88184	-1280.4927	0.1544						
M2	0.89868	-1274.4497	0.2662	Naïve Empirical Bayes	5P	0.942	2.414		
					6E	0.965*	2.448		
					9S	0.998**	2.499		
					13A	0.965*	2.449		
					21D	0.728	2.065		
					22E	0.574	1.569		
					43E	0.964*	2.447		
					50T	0.885	2.323		
					56G	0.904	2.357		
					76A	0.986*	2.481		
					87T	0.968*	2.454		
					104R	0.774	2.144		
					125P	0.979*	2.47		
				Bayes Empirical Bayes	5P	0.707	2.480+-1.116		
					6E	0.811	2.730+-1.050		
					9S	0.994**	3.179+-0.795		
					13A	0.808	2.719+-1.048		
					43E	0.771	2.608+-1.055		
					50T	0.515	1.995+-1.170		
					56G	0.545	2.082+-1.100		
					76A	0.928	3.018+-0.910		
					87T	0.827	2.768+-1.033		
					125P	0.915	3.009+-0.962	12.086108	0.002374297
M7	0.94438	-1281.2449	0.2						
M8	0.89947	-1274.3967	0.2664	Naïve Empirical Bayes	5P	0.984*	2.483		
					6E	0.997**	2.512		
					9S	1.000**	2.519		
					13A	0.997**	2.512		
					21D	0.656	1.743		
					22E	0.577	1.551		
					43E	0.999**	2.516		
					50T	0.9	2.294		
					56G	0.965*	2.439		
					76A	1.000**	2.518		
					87T	0.997**	2.513		
					104R	0.737	1.926		
					125P	0.997**	2.512		
				Bayes Empirical Bayes	5P	0.844	2.716+-1.064		
					6E	0.934	2.956+-0.855		
					9S	0.999**	3.123+-0.636		
					13A	0.934	2.955+-0.854		
					43E	0.93	2.940+-0.851		
					50T	0.569	1.938+-1.354		
					56G	0.693	2.294+-1.230		
					76A	0.984*	3.087+-0.693		
					87T	0.943	2.979+-0.830		
					125P	0.968*	3.050+-0.760	13.696394	0.001061368

NOTE: amino acid numbering is based on removal of N-terminal methionine

Phylogenetic analysis by maximum likelihood (PAML) performed using simian primate sequences (Figure 3B). Analysis was performed using both conserved species and maximum likelihood gene trees (see Materials and Methods for additional details).

Appendix B Table 2

Hemoglobin alpha (HBA) data

Test	Codon	a	b-	Pr[b=b-]	b+	Pr[b=b+]	p-value	q-value					
MEME	18	0	0	0.910193	14.3338	0.0898074	0.0656901	1					
	67	0	0	0.75422	18.392	0.24578	0.0574455	1					
	68	0.00798137	0.00730452	0.816103	26.2233	0.183897	0.0430483	1					
FEL	4												
	23												
	43												
	44												
	50												
	55												
	72												
	81												
	84												
	102												
	111												
	114												
	116												
	124												
	131												
	71												
SLAC	43												
	50												
	72												
	84												
	102												
	111												
REL	8												
	12												
	19												
	67												
	68												
	71												
	78												
	113												
	4												
	26												
	43												
	44												
	50												
	55												
	66												
	72												
	81												
	83												
	84												
	88												
	101												
	102												
	105												
	108												
	111												
	114												
	124												
	130												
	131												

Test (cont'd)	Codon (cont'd)	dS	dN	dN/dS	dN-dS	Normalized dN-dS	p-value	E[dS]	E[dN]	Normalized E[dN-dS]	Posterior Probability	Bayes Factor	Selection
MEME	18												episodic purifying
	67												episodic purifying
	68												episodic purifying
FEL	4	2.93937	0	0		-11.1833	0.0471894						negative
	23	45.1096	2.10936	0.047		-163.602	0.0488065						negative

	43	94.7368	0	0		-360.442	0.000109565						negative
	44	6.09185	0	0		-23.1775	0.0159847						negative
	50	15.0581	0	0		-57.2909	0.0149202						negative
	55	3.56477	0	0		-13.5628	0.0392927						negative
	72	32.555	0	0		-123.861	0.0101873						negative
	81	2.76418	0	0		-10.5168	0.085434						negative
	84	25.2724	0	0		-96.153	0.00988594						negative
	102	32.555	0	0		-123.861	0.00899011						negative
	111	7.46451	0	0		-28.4	0.00617556						negative
	114	2.58747	0	0		-9.84445	0.098816						negative
	116	73.6674	1.42197	0.019		-274.87	0.0357135						negative
	124	2.79306	0	0		-10.6267	0.0846156						negative
	131	2.89817	0	0		-11.0266	0.0417009						negative
	71	3.16E-15	3.84127	1.21461E+15		14.6148	0.0920853						negative
SLAC	43				-8.99446	-34.2205	0.00823006						negative
	50				-4.49723	-17.1103	0.0907197						negative
	72				-4.49723	-17.1103	0.0907197						negative
	84				-4.49723	-17.1103	0.0907197						negative
	102				-4.49723	-17.1103	0.0907197						negative
	111				-3.67189	-13.9701	0.037037						negative
REL	8							1.02514	2.85362	1.82848	1	5.19E+12	positive
	12							0.710751	2.84953	2.13878	0.999442	1583.68	positive
	19							1.86895	2.85362	0.984669	0.999999	1.59E+06	positive
	67							0.696934	2.85347	2.15654	0.99998	45098	positive
	68							0.847512	2.85342	2.0059	0.999967	2.67E+04	positive
	71							0.671969	2.85351	2.18154	0.999986	62309.9	positive
	78							1.83124	2.85362	1.02238	1	6.03E+08	positive
	113							0.76883	2.84829	2.07946	0.999212	1122.21	positive
	4							1.86914	0.076952	-1.79219	0.993884	183.703	negative
	26							1.86913	0.0786563	-1.79047	0.993275	166.983	negative
	43								1.86914	0.0652868	-1.80385	0.998029	negative
	44								1.86914	0.0769634	-1.79217	0.993879	negative
	50								1.869	0.0702911	-1.7987	0.996245	negative
	55								1.86914	0.0783505	-1.79079	0.993385	negative
	66								1.86913	0.0844826	-1.78464	0.991197	negative
	72								1.86905	0.0701687	-1.79888	0.996292	negative
	81								1.86914	0.0709109	-1.79823	0.996035	negative
	83								1.86913	0.0844826	-1.78464	0.991197	negative
	84								1.86911	0.0639924	-1.80512	0.998483	negative
	88								1.86914	0.0786405	-1.7905	0.993281	negative
	101								1.86914	0.0847781	-1.78436	0.991092	negative
	102								1.86909	0.0640284	-1.80507	0.998468	negative
	105								1.8687	0.0854985	-1.7832	0.990823	negative
	108								1.86914	0.0717289	-1.79741	0.995743	negative
	111								1.86914	0.0786363	-1.7905	0.993283	negative
	114								1.86913	0.0769662	-1.79216	0.993878	negative
	124								1.86914	0.0709103	-1.79823	0.996035	negative
	130								1.86914	0.0786363	-1.7905	0.993282	negative
	131								1.86914	0.0709099	-1.79823	0.996035	negative

Hemoglobin beta (HBB) data

Test	Codon	a	b-	Pr[b=b-]	b+	Pr[b=b+]	p-value	q-value					
MEME	5	0	0	0.87038	18.7966	0.12962	0.0310067	1					
	13	0	0	1.00E-09	2.69248	1	0.0877052	1					
	56	0	0	0.823708	10.1067	0.176292	0.0611889	1					
	76	0	0	0.14923	6.26513	0.85077	0.0223575	1					
	125	1.34367	0.00574856	0.876098	22.6673	0.123902	0.0861075	1					
FEL	13												
	76												
	2												
	7												
	8												
	11												
	12												
	17												
	19												
	21												
	34												

	38												
	42												
	46												
	64												
	66												
	68												
	73												
	80												
	83												
	84												
	87												
	97												
	98												
	100												
	102												
	108												
	111												
	118												
	121												
	124												
	132												
	141												
	142												
REL	5												
	9												
	13												
	43												
	50												
	56												
	76												
	104												
	125												
	0												
	2												
	4												
	7												
	8												
	10												
	12												
	17												
	27												
	30												
	36												
	38												
	40												
	44												
	49												
	51												
	53												
	55												
	57												
	59												
	61												
	62												
	63												
	65												
	66												
	68												
	70												
	72												
	77												
	80												
	82												
	84												
	86												
	89												
	92												
	93												

	95												
	97												
	100												
	102												
	108												
	111												
	112												
	115												
	117												
	118												
	120												
	121												
	123												
	124												
	128												
	129												
	132												
	135												
	138												
	140												
	142												

Test (cont'd)	Codon (cont'd)	dS	dN	dN/dS	dN-dS	Normalized dN-dS	p-value	E[dS]	E[dN]	Normalized E[dN-dS]	Posterior Probability	Bayes Factor	Selection
MEME	5												
	13												
	56												
	76												
	125												
FEL	13	0	2.10144	infinite		6.58518	0.0918563						positive
	76	3.01E-15	3.94962	1.31355E+15		12.3767	0.0317138						positive
	2	7.62968	0	0		-23.9087	0.00146618						
	7	8.58608	0	0		-26.9057	0.0224143						
	8	6.1291	0	0		-19.2064	0.00349089						
	11	2.81636	0	0		-8.82548	0.0479094						
	12	7.40161	0	0		-23.194	0.000100501						
	17	9.1354	0	0		-28.6271	0.0139439						
	19	4.273	0.422265	0.099		-12.0668	0.0574594						
	21	7.84395	1.27037	0.162		-20.5993	0.0626165						
	34	2.66941	0	0		-8.36497	0.0516265						
	38	1.24566	0	0		-3.90347	0.0914441						
	42	2.11589	0	0		-6.63045	0.0851162						
	46	2.63085	0	0		-8.24413	0.0762976						
	64	2.59332	0	0		-8.12655	0.040055						
	66	5.40855	0	0		-16.9485	0.00434612						
	68	3.85901	0	0		-12.0928	0.0104218						
	73	2.01287	0	0		-6.30761	0.0901901						
	80	1.95794	0	0		-6.1355	0.0636718						
	83	2.55789	0	0		-8.01552	0.0409329						
	84	1.23056	0	0		-3.85613	0.0924171						
	87	44.0784	2.3855	0.054		-130.651	0.0158841						
	97	7.40883	0	0		-23.2166	0.00150941						
	98	2.48851	0	0		-7.79811	0.0970344						
	100	1.4271	0	0		-4.47201	0.0964693						
	102	10.0584	0	0		-31.5194	0.000125309						
	108	2.14545	0	0		-6.72307	0.0581598						
	111	8.85059	0	0		-27.7346	0.00297945						
	118	4.27332	0	0		-13.3911	0.0147849						
	121	1.50332	0	0		-4.71088	0.0964152						
	124	10.0344	0	0		-31.4441	0.000157485						
	132	1.47855	0	0		-4.63324	0.0730412						
	141	1.98623	0	0		-6.22413	0.0924969						
	142	1.96552	0	0		-6.15925	0.0777414						
REL	5							0.482549	2.11607	1.63352	0.991654	1443.55	positive
	9							1.1786	2.11769	0.939086	0.813629	53.0398	positive
	13							0.474529	2.11762	1.64309	0.994451	2177.38	positive
	43							0.833337	2.11769	1.28435	0.902322	112.232	positive
	50							0.482243	2.1176	1.63536	0.992461	1599.45	positive

	56							0.492065	2.11416	1.6221	0.988304	1026.59	positive
	76							0.486525	2.11769	1.63117	0.991405	1401.35	positive
	104							0.557437	1.79752	1.24008	0.823768	56.7903	positive
	125							0.708036	2.11403	1.406	0.932868	168.828	positive
	0							0.999999	0.0248461	-0.975153	0.999571	191.94	negative
	2							4.17485	0.0266203	-4.14823	0.999939	1360.39	negative
	4							0.482199	0.0243741	-0.457825	0.999718	291.842	negative
	7							2.24873	0.0283573	-2.22037	0.998837	70.6747	negative
	8							3.4882	0.0244914	-3.46371	0.999919	1018.98	negative
	10							0.687723	0.0268239	-0.660899	0.998663	61.4984	negative
	12							4.3394	0.0243747	-4.31503	0.999999	159988	negative
	17							2.3106	0.0247531	-2.28585	0.999757	338.923	negative
	27							0.474512	0.0268238	-0.447688	0.998585	58.1069	negative
	30							0.519849	0.0257652	-0.494084	0.999091	90.4992	negative
	36							0.482199	0.0254614	-0.456738	0.999223	105.796	negative
	38							0.65393	0.0243741	-0.629556	0.999731	305.443	negative
	40							0.519849	0.0257652	-0.494084	0.999091	90.4992	negative
	44							0.474512	0.0256345	-0.448878	0.999141	95.7564	negative
	49							0.637502	0.0258303	-0.611672	0.99909	90.4011	negative
	51							0.482199	0.0254614	-0.456738	0.999223	105.796	negative
	53							0.482199	0.026824	-0.455375	0.998588	58.2187	negative
	55							0.999999	0.0248461	-0.975153	0.999571	191.94	negative
	57							0.524688	0.0246784	-0.500009	0.999586	198.682	negative
	59							0.849545	0.0247926	-0.824752	0.999574	193.17	negative
	61							0.849545	0.0247926	-0.824752	0.999574	193.17	negative
	62							0.482199	0.026824	-0.455375	0.998588	58.2187	negative
	63							0.528371	0.0266605	-0.50171	0.998681	62.3018	negative
	65							0.849545	0.0247926	-0.824752	0.999574	193.17	negative
	66							3.36156	0.0244697	-3.33709	0.999908	898.079	negative
	68							4.10148	0.0332232	-4.06826	0.999718	292.234	negative
	70							0.474512	0.0268238	-0.447688	0.998585	58.1069	negative
	72							0.528371	0.024626	-0.503745	0.99961	211.124	negative
	77							0.524688	0.0262728	-0.498415	0.998858	72.0049	negative
	80							1.04628	0.0246847	-1.0216	0.99964	228.285	negative
	82							0.849545	0.0247926	-0.824752	0.999574	193.17	negative
	84							0.644758	0.0243772	-0.620381	0.999728	302.982	negative
	86							0.474512	0.0268238	-0.447688	0.998585	58.1069	negative
	89							0.528371	0.024626	-0.503745	0.99961	211.124	negative
	92							0.524688	0.0262728	-0.498415	0.998858	72.0049	negative
	93							0.528371	0.0265321	-0.501839	0.998741	65.2861	negative
	95							0.849545	0.0247926	-0.824752	0.999574	193.17	negative
	97							4.16567	0.0264225	-4.13924	0.99994	1365.35	negative
	100							0.748533	0.0254658	-0.723068	0.999274	113.303	negative
	102							4.32538	0.0247354	-4.30064	0.999997	31286.3	negative
	108							1.14182	0.0246859	-1.11713	0.999649	234.748	negative
	111							4.21955	0.036883	-4.18267	0.999798	406.533	negative
	112							0.528371	0.0265321	-0.501839	0.998741	65.2861	negative
	115							0.654767	0.026824	-0.627943	0.998651	60.9462	negative
	117							0.524688	0.0262728	-0.498415	0.998858	72.0049	negative
	118							2.98177	0.0283646	-2.95341	0.999218	105.215	negative
	120							0.486501	0.0241845	-0.462317	0.999801	414.314	negative
	121							0.775172	0.0261162	-0.749056	0.998995	81.8086	negative
	123							0.474512	0.024374	-0.450138	0.999718	291.283	negative
	124							4.32806	0.0254632	-4.30259	0.999996	22158.6	negative
	128							0.482199	0.026824	-0.455375	0.998588	58.2187	negative
	129							0.474512	0.0268238	-0.447688	0.998585	58.1069	negative
	132							0.761318	0.0241986	-0.737119	0.999809	431.264	negative
	135							0.716714	0.0268242	-0.689889	0.998674	61.9843	negative
	138							0.731618	0.0268241	-0.704794	0.998679	62.2416	negative
	140							0.569697	0.0268243	-0.542872	0.99862	59.5657	negative
	142							1.04851	0.026366	-1.02215	0.998972	79.9894	
NOTE: amino acid numbering is based on removal of N-terminal methionine													

APPENDIX C

HUMAN PHEWAS IDENTIFIES PATHOLOGICAL ROLE OF FACTOR X DURING *ACINETOBACTER BAUMANNII* INFECTION

Introduction

Phenome-Wide Association Studies (PheWAS) are an efficient discovery tool to identify novel associations between clinical outcomes and genotypes. PheWAS explore the association between nuclear single nucleotide polymorphisms (SNPs) and phenotypes represented in electronic health records (EHR) (1). PheWAS have successfully revealed novel SNP/phenotype associations, and have been used to explore pleiotropy (2, 3), disease heritability (4), therapeutic and adverse medication effects (5, 6), and drug repurposing opportunities (7, 8). One aim of PheWAS is to discover new applications for therapeutics by investigating clinical phenotypes of patients with variation in a known drug target.

One biological pathway attractive to drug repurposing efforts is coagulation. Coagulation plays a considerable role in hemostasis and as such perturbations to coagulation affect many disease outcomes. Additionally, work in murine models of inflammation and infection have identified many examples of the crosstalk between coagulation and immunity (9-11). Therefore, PheWAS of genes encoding coagulation proteins offers opportunity to find new diseases associated with altered coagulation and new indications for current coagulation therapeutics.

Blood-coagulation factor X (FX) is a vitamin K-dependent serine protease that functions upstream in the blood coagulation cascade. FX is synthesized in the liver and secreted into the bloodstream in an inactive form until the coagulation pathway is activated by an injury that damages blood vessels. Both the extrinsic and intrinsic pathways of coagulation initiation converge on FX, which is activated to FXa and subsequently interacts with other coagulation factors to convert prothrombin to its active form, thrombin. Thrombin converts fibrinogen into fibrin, which then forms a blood clot (12). Current treatment of bleeding disorders includes FX replacement therapy using fresh-frozen plasma, FIX plasma concentrates, and prothrombin complex concentrations (PCCs) (13). Additionally, FDA-approved therapeutics are used to inhibit FXa as anticoagulants. The specificity of these drugs has several advantages over more general anticoagulants that inhibit vitamin K. Enoxaparin binds antithrombin to irreversibly inactivate FXa (14, 15) and is used to treat deep vein thrombosis, pulmonary embolism, and for thromboprophylaxis in a variety of surgical

procedures (16). Enoxaparin is well tolerated with good bioavailability and is approved in many countries. We leveraged PheWAS to find potential links between coding variants in *F10*, the gene that encodes FX, and novel clinical phenotypes that are not currently well-treated or understood. The goal was to repurpose approved coagulation therapeutics for a new therapeutic use.

PheWAS analysis was focused on *F10* SNP rs3211783 which denotes a Gly192Arg residue substitution in the N-terminal portion of the protein. The functional effect of the FX Gly192Arg SNP is unknown. Residue 192 resides very close to the cleavage site within the activation peptide of the protein (17). Substitution of Glycine 192 to Arginine did not affect coagulation activity and catalytic activity of the enzyme as compared with wild-type (18). However, it must be noted that this was an *in vitro* study and did not explore *in vivo* effects. This study also did not explore any direct effects of the SNP on FX, focusing instead on its activated form.

FX deficiency causes bleeding disorders that can range in severity from hemorrhagic symptoms to asymptomatic. The condition can be hereditary or acquired as a result of liver disease, cancer, or infections (12). The inherited form is autosomal recessive and very rare. The homozygous and most severe hereditary forms have an incidence rate of approximately one in a million (19) and are due to polymorphisms in *F10*. Individuals with FX deficiency from the Friuli region of Italy contain a homozygous mutation in the *F10*. Affected individuals had a moderate bleeding tendency since early childhood, with epistaxis, bleeding from the gums, posttraumatic hemarthroses, and bleeding after dental extractions and other surgical procedures. Laboratory studies showed prolonged prothrombin and partial thromboplastin clotting times, and factor X activity levels between 4 to 9% of normal (20).

Acinetobacter baumannii is a Gram-negative bacterium that has emerged as a critically important pathogen with high rates of anti-microbial resistance. Owing to its ability to survive dessication, environmental extremes, and antimicrobials, *A. baumannii* is a frequent cause of hospital-acquired infections of the critically ill and is a leading cause of ventilator-associated pneumonia and burn wounds (21). Most infections are caused by strains of *A. baumannii* that are resistant to multiple classes of antibiotics which leads to treatment failures (22). *A. baumannii* are classified as a Centers for Disease Control threat “Serious” and a “Priority 1: Critical” WHO priority pathogen for antibiotic development (23). Thus, identifying novel therapeutics that might aid the ability of the immune response to limit bacterial replication during infection is an attractive goal until new antibiotics become available.

In this study, we used PheWAS to identify novel clinical phenotypes associated with a SNP in coagulation Factor X. In addition to the expected phenotypes relevant to hemostasis, the SNP was associated with altered risk for multiple types of microbial infections. Factor X deficiency was modeled in mice and found to protect from systemic *A. baumannii* infection, suggesting that in some infections, Factor X may play a pathological role during the early innate immune response. Additionally, inhibition of Factor X with an FDA-approved therapeutic reduced bacterial burden in wildtype mice following infection, serving as a proof-of-principal for the use of PheWAS in drug repurposing by identifying a potential new adjunctive treatment for *A. baumannii* infection.

Materials and methods

PheWAS Methods

The BioVU biorepository at Vanderbilt University Medical Center contains approximately 250,000 de-identified DNA samples extracted from excess patient blood samples collected during routine clinical testing that would otherwise be discarded. The specimens are linked to corresponding, longitudinal clinical and demographic data derived from the Synthetic Derivative, a de-identified EHR built for research purposes (24-26). This study leveraged data from approximately 36,000 subjects in BioVU genotyped on using the Illumina Infinium Exomechip. PheWAS was conducted using previously reported methods (1, 6, 27, 28); analysis was focused on 29,722 patients of European ancestry with Exomechip data and phenotype data in SD to achieve maximum statistical power. Our variant of focus for these studies was the *F10* missense SNP rs3211783 (Gly192Arg).

Mice

F10$^{F/F}$ mice (29) sperm was kindly provided by P. Margaratis (CHOP) and rederived in the C57BL/6J (Jackson) background by the Vanderbilt Transgenic Mouse/Embryonic Stem Cell Shared Resource and maintained as a homozygous colony in specific pathogen-free housing. Mice were genotyped according to Tai et al (29). Age- and sex-matched C57BL/6J (Jackson) were used after one week of acclimation. All infections were performed at the Vanderbilt University Medical Center under the principles and guidelines described in the Guide for the Care and Use of Laboratory Animals using Institutional Animal Care and Use Committee (IACUC)-approved protocol M1600123-00. Vanderbilt University Medical Center is an American Association for Laboratory Animal Science (AALAS)-accredited facility. The

Vanderbilt University Medical Center is registered with the Office of Laboratory Animal Welfare (OLAW), assurance number A-3227-01.

A. baumannii infection

A. baumannii strain ATCC17978 was streaked to lysogeny broth agar (LBA) from -80° stock. After 24 h at 37°C, a single colony was used to inoculate 3 ml of LB in a 15 ml aeration culture tube, and grown overnight for 16 h at 37° with shaking. 10 µl of this culture was inoculated into 10 ml of LB in a 50 ml conical tube and grown for 3.5 h at 37° with shaking. Bacteria were collected by centrifugation, washed twice in ice-cold PBS, and resuspended in ice-cold PBS to a concentration of 1-3x10^9 CFU/ml. For each infection, the inoculum was serially diluted in PBS and plated to LBA for enumeration. Mice were anaesthetized with avertin by intraperitoneal injection and subsequently injected with 100 µl of the *A. baumannii* suspension retroorbitally. For most experiments, mice were sacrificed at times noted by CO_2 asphyxiation, and organs were sterilely collected in PBS, homogenized with Next Advance Bullet Blender (Navy Lysis tubes), serially diluted in PBS, and plated to LBA for enumeration following incubation at 37° for 24 h. For survival experiments, mice were infected as above and weighted daily monitored daily for death or moribund status. Mice were sacrificed if they exhibited signs of infection (lack of grooming, hunched posture) and if they were unable to right themselves within 5 seconds of being placed on side. For infection with heat-killed bacteria, *A. baumannii* was grown and prepared as above, except resuspended in PBS to a final density of approximately 2x10^{10} CFU/ml , and then heated in a 70°C water bath for 45 minutes, cooled to room temperature, then placed on ice. A portion of the inoculum was plated to LBA to ensure no viable bacteria were detected.

Pathology and immunohistochemistry

Tissues were fixed in 10% neutral buffered formalin immediately following euthanasia of the mice. Unbiased, standardized sectioning of the liver [30] was performed and spleens were submitted whole for histological processing. Fixed tissues were routinely processed using a standard 8 hour processing cycle of graded alcohols, xylenes, and paraffin wax, embedded and sectioned at 4-5 microns, floated on a water bath, and mounted on positively charged or hydrophobic glass slides.

Hematoxylin and eosin (H&E) staining was performed on the Gemini autostainer (Thermo Fisher Scientific, Waltham, MA). Immunohistochemical (IHC) staining for thrombosis was performed using an anti-fibrinogen/fibrin (FGA) antibody on a Leica Bond-Max IHC

autostainer (Leica Biosystems Inc., Buffalo Grove, IL). All steps besides dehydration, clearing and coverslipping were performed on the Bond-Max. Slides were deparaffinized. Enzymatic-induced antigen retrieval was performed using Proteinase K (Dako, Agilent, Santa Clara, CA) for 5 minutes. Slides were incubated with anti-FGA (A0080, DAKO/Agilent Technologies, Inc, Carpinteria, CA) for 1 hour at a 1:5000 dilution. The Bond Polymer Refine Detection system was used for visualization. Slides were then dehydrated, cleared and coverslipped.

All histopathologic interpretation was conducted by a board-certified veterinary pathologist under masked conditions. Semiquantitative lesion scoring in H&E stained sections of the liver (hepatitis [31], thrombosis) and spleen (lymphocytolysis, thrombosis) was completed on a 5-point scale. Quantitation of hepatic thrombosis was performed on digitized, FGA-stained IHC slides using the Aperio ImageScope positive pixel count v9 algorithm.

Cytokine and chemokine analysis

Cytokines were quantified using Milliplex MAP Mouse Cytokine/Chemokine Magnetic Kit (Millipore #MCYTOMAG-70K-PMK; Premixed beads MCYPMK25-MAG) Multiplex Assays according to manufacturer's instructions and analyzed with a Luminex FLEXMAP 3D instrument. Tissues were removed immediately following euthanasia and were homogenized in PBS containing 1 mM phenylmethane sulfonyl fluorise (PMSF), homogenized using a Next Advance Bullet Blender (Navy Lysis tubes), and protein content was quantified by BCA (Thermo).Whole blood was collected by blind cardiac puncture following euthanasia and allowed to clot at room temperature for at least 30 minutes, then serum was collected by centrifugation at 6500 x g for 10 minutes at 4°C. All samples were stored at -80°C until analysis. Tissue samples were analyzed undiluted and cytokine values were normalized to total protein content, while diluted 1:1 in serum matrix buffer, except for samples of limited volume, which were diluted 1:2. Analyte values were corrected for dilution.

Cell population analysis by flow cytometry

Organs and blood were harvested from the mice and single cells suspensions were created from the kidney and spleen. Red blood cells were lysed from organ cell suspensions and peripheral blood followed by the introduction of a Live/Dead stain (Invitrogen, L23105) on ice for 20 min. Samples were spun, aspirated, and fixed in 4% paraformaldehyde at room temperature, and transferred onto ice for 15 min. Samples were spun, aspirated and resuspended in mouse Fc Block (BD Pharmigen, clone 2.4G2) diluted in fluorescence-activated cell sorting (FAC) media (PBS +2% FBS +0.02% NaAz) for 20 min on ice. Following

block, samples were spun, aspirated, and resuspended in FACs media containing surface markers for 20 min on ice. To stain for Tregs, samples were spun, aspirated, and resuspending in saponin permeabilization buffer (PBS +0.05% saponin +0.5% BSA) containing anti-FOXP3. Finally, samples were spun, aspirated, and resuspended in FACs media for flow cytometry. Data were collected using a BD LSRII flow cytometer with FACSDIVA software and analyzed using FlowJo.

Enoxaparin inhibitor

Seven-week old female C57BL/6J (Jackson) mice were anaesthetized with avertin by intraperitoneal injection followed by injection with 100 µl of either PBS or 1.9 mg/ml enoxaparin (Fresenius Kabi #FK562586) for final dose of approximately 10 mg/kg. Mice were then injected with 100 µl of *A. baumannii* 17978 in PBS to final inoculation of 2-3x10^8 CFU. Mice were sacrificed at 24 hpi by CO_2 asphyxiation, organs were sterilely collected in PBS, homogenized with Next Advance Bullet Blender (Navy Lysis tubes), serially diluted in PBS, and plated to LBA for enumeration following incubation at 37° for 24 h.

Results

PheWAS identifies predicted and novel disease associations with *F10* SNP.

The electronic health records of approximately 30,000 patients and their associated exome sequencing was scanned for novel associations between ICD-9 medical codes and *F10* rs3211783 (32), a SNP that results in Gly192Arg in FX (Table 1). The Gly192Arg minor allele is found in about 3% of the world population and is most abundant in those of African descent (11%) (33). Importantly, carriers of this SNP minor allele display an increased incidence compared to non-carriers of a number of hematological conditions in their EHR as indicated by odd ratios (ORs) >1 (Table 2). These phenotypes were expected based on the known function of FX in blood clotting and thus serve as validation phenotype supporting the integrity of the PheWAS results. Interestingly, PheWAS analysis here identified unexpected phenotypes regarding the liver, which is the site of FX synthesis (Table 2).

In addition to the validating phenotypes, the PheWAS analysis revealed unexpected associations between rs3211783 and a cluster of infection-related phenotypes, including postoperative infection, mycoses, and cellulitis and abscess of trunk (Table 2). Both phenotype clusters had positive ORs, indicating SNP carriers are at an increased risk of developing these conditions. To better understand the pathogens driving a subset of the

infectious phenotypes, we reviewed microbiology lab results; the cultures of the case carriers in this group had positive tests a variety of Gram-positive and Gram-negative bacterial pathogens were isolated from patients (Table 3). Based on these findings, we hypothesized that FX contributes to the innate immune response to bacterial infection and that FX might affect the ability to resist infection by a variety of pathogens.

SNP	rsID	Mutation	SIFT	PP2	Exome MAF	Variant frequency	Populations with highest MAF
Gly192Arg	rs3211783	Missense	0.31	0.195	0.14%	3%	African 11%

Table 1. Predicted consequences and minor allele frequencies (MAF) of rs3211783 based on the 1000 Genomes Project (33).

	Condition	PheWAS Code	p Value	Odds Ratio	Affected Cases	Total Cases	Controls
Expected (validating) phenotypes	Other diseases of blood and blood-forming organs	289	1.2E-03	4.65	5	481	18328
	Pernicious anemia	281.11	1.3E-02	6.41	2	195	15680
	Hematemesis	578.1	2.5E-02	5.08	2	155	20426
	Abnormality of red blood cells	289.9	3.3E-02	8.84	3	51	18328
	Polycythemia vera, secondary	289.8	1.3E-04	10.25	3	188	20349
	Condition	**PheWAS Code**	**p Value**	**Odds Ratio**	**Affected Cases**	**Total Cases**	**Controls**
Unexpected infection-related phenotypes	Mycoses	117	7.8E-07	8.62	6	278	21953
	Athlete's foot	110.12	2.3E-05	13.19	3	106	21953
	Cellulitis and abscess of trunk	681.7	2.7E-04	5.60	5	357	21003
	Tuberculosis	010	3.2E-02	8.99	2	46	21520
	Cholangitis	575.1	5.5E-03	5.24	3	221	23497
	Endocarditis	420.3	2.7E-02	4.98	2	160	23314
	Viral infection	079	3.9E-02	2.96	4	459	21250
	Condition	**PheWAS Code**	**p Value**	**Odds Ratio**	**Affected Cases**	**Total Cases**	**Controls**
Unexpected liver-related phenotypes	Primary biliary cirrhosis	571.6	2.0E-07	9.91	6	232	19711
	Other disorders of biliary tract	575.8	5.5E-04	6.05	4	251	23497
	Other biliary tract disease	575	1.6E-03	3.88	6	587	23497
	Jaundice (not of newborn)	573.5	2.0E-03	5.09	4	316	19711
	Liver replaced by transplant	573.2	2.4E-03	4.92	4	327	19711
	Other disorders of liver	573	2.7E-02	3.17	4	510	19711
	Cirrhosis of liver without mention of alcohol	571.51	2.8E-02	2.84	5	709	19711
	Chronic liver disease and cirrhosis	571	2.9E-02	2.42	7	1,149	19711
	Malignant neoplasm of liver, primary	155.1	3.9E-02	4.47	2	174	21458
	Cholangitis	575.1	5.5E-03	5.24	3	221	23497

Table 2. Phenotypes identified by PheWAS of *F10* rs3211783

Culture reports from 12 mycoses, athlete's foot, and endocarditis patients		
isolated organism(s)	**number of culture reports**	**number of subjects**
Staphylococcus coagulase *(aureus)*	23	6
Escherichia coli	12	2
Klebsiella pneumoniae	12	3
Scedosporium apiospermum	11	1
Candida albicans	8	2
Pseudomonas aeruginosa	6	1
Mycobacterium avium	5	1
Pseudomonas aeruginosa mucoid	5	1
Enterobacter cloacae	4	1
Enterobacter cloacae, Acinetobacter baumannii	4	1
Candida albicans, Scedosporium apiospermum	3	1
Pseudomonas aeruginosa non-mucoid	3	1
Pseudomonas aeruginosa, Stenotrophomonas maltophilia	3	1
Streptococcus bovis	3	1
Bacillus species not *anthracis*	2	1
Cryptococcus neoformans	2	1
Unidentified Nontuberculous *Mycobacterium*	2	1
Aspergillus flavus	1	1
Candida parapsilosis	1	1
candida, NOT *albicans,* probable *parapsilosis*	1	1
Diphtheroids aerobic	1	1
Enterococcus faecalis	1	1
Escherichia coli, Proteus mirabilis	1	1
Haemophilus influenzae, Diphtheroids aerobic	1	1
Mycobacterium	1	1
Mycobacterium simiae	1	1
Neisseria species	1	1
Probable atypical *Mycobacterium*	1	1
Proteus mirabilis	1	1
Pseudomonas aeruginosa mucoid, *Stenotrophomonas maltophilia*	1	1
Staphylococcus epidermidis	1	1
Streptococcus agalactiae (group B)	1	1
Yeast, probable *Candida glabrata*	1	1
Black text indicates Gram-positive bacteria, red indicates Gram-negative bacteria, grey is other		

Table 3. Culture reports from 12 mycoses, athlete's foot, and endocarditis patients

FX deficient mice demonstrate reduced bacterial burdens after systemic *A. baumannii* infection.

To assess the role of FX during infection, we used *A. baumannii* as a model opportunistic Gram-negative pathogen. Mice with the Friuli allele of *F10* (referred to as $F10^{F/F}$ throughout), which have reduced FX activity, were used to model the *F10* rs3211783 variant and FX-deficiency in general. As deletion of *F10* is embryonic lethal, this is a well-characterized murine model of FX-deficiency (29). Age- and sex-matched wildtype C57BL/6J and $F10^{F/F}$ mice were infected retroorbitally with *A. baumannii* to establish systemic infection. As early as 4 hours post infection (hpi), $F10^{F/F}$ mice demonstrated reduced bacterial burdens

in the blood, and at 24 hpi, less *A. baumannii* was recovered from the blood and every organ tested of *F10*$^{F/F}$ mice (Figure 1A-B). Contrary to our hypothesis, these data suggest FX is pathological during systemic *A. baumannii* infection.

Because Gram-negative bacteria can induce clotting dysregulation, including microthrombi and disseminated intravascular coagulation, we hypothesized that reduced FX activity in *F10*$^{F/F}$ mice would protect from infection-induced hypercoagulation. Histopathology of mock and infected mice at 24 hpi detected no differences between C57BL/6J and *F10*$^{F/F}$ mice, measuring liver hepatitis and thrombosis, and spleen lymphocytolysis and thrombosis (Figure 1C). To further assess *A. baumannii* induced thrombosis, liver thrombi formation was measured using immunohistochemistry against fibrin, fibrinogen, and fibrinogen fragments D and E. Again, no difference between mouse genotypes at 24 hpi was observed (Figure 1D).

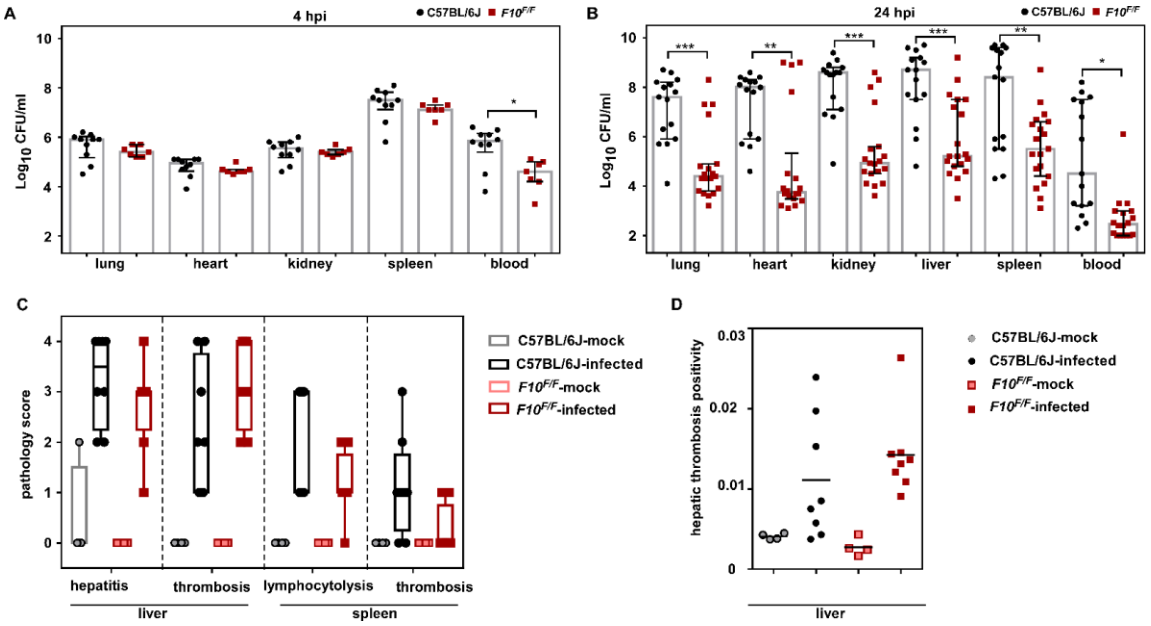

Figure 1. FX deficient mice exhibit reduced bacterial burdens after systemic *A. baumannii* infection. Approximately 3x10^8 CFU of *A. baumannii* 17978 was injected retro-orbitally. Mice were sacrificed and tissues removed at (A) 4 and (B) 24 hpi. (C-D) Mice were infected with approximately 3x10^8 CFU of *A. baumannii* 17978 retro-orbitally and sacrificed at 24 hpi. Tissue were fixed and (C) scored blindly or (D) hepatic thrombosis was quantified using anti-fibrin/fibrinogen immunohistochemistry. Each dot represents a single mouse, and data are compiled from (A) two experiments, (B) three experiments, or (C-D) one experiment. For A and B, * indicates P<0.05, **P<0.01, and ***P<0.001 by Mann-Whitney test. For C and D, no statistical difference was found by two-way ANOVA with Sidak's correction for multiple comparisons

F10$^{F/F}$ mice demonstrate reduced serum immune response to systemic *A. baumannii* infection

As no difference was observed for infection-induced coagulation, we therefore hypothesized that an altered early immune response is responsible for the difference in bacterial burdens between C57BL/6J and *F10*$^{F/F}$ mice. To test this hypothesis, cytokines and chemokines were quantified from serum at 4 and 24 hpi using a multiplexed analysis. *F10*$^{F/F}$ mice exhibited reduced levels of a variety of cytokines by 24 hpi, including both pro-inflammatory (TNF, IL6) and anti-inflammatory (IL10) cytokines (Figure 2A; Table 4). Chemokines, including the IFNG-induced CXCL10 and chemoattractants CXCL1, CXCL2, and CCL4 were reduced by 4 or 24 hpi (Figure 2B). These data suggest that C57BL/6J mice experience a rapid induction of inflammatory response to *A. baumannii*, and this induction is blunted in *F10*$^{F/F}$ mice.

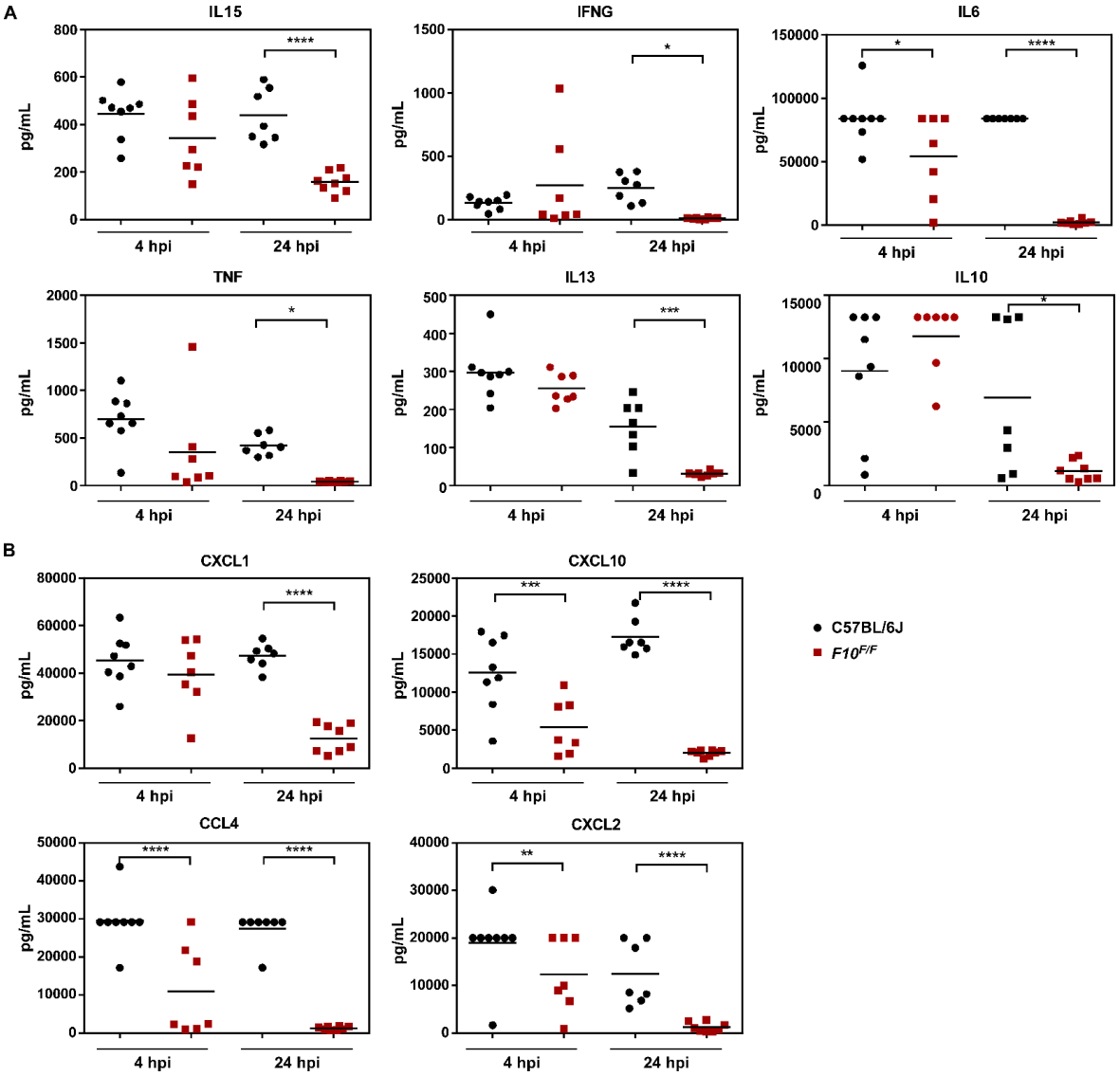

Figure 2. *F10$^{F/F}$* mice exhibit reduced inflammatory response to systemic *A. baumannii* infection. Serum (A) cytokines and (B) chemoattractants at 4 and 24 hours following retro-orbital infection with approximately 3x10^{8} CFU of *A. baumannii* 17978 were quantified by Luminex analysis. For A and B, each dot represents data from a single mouse, from two experiments. * indicates P<0.05, **P<0.01, ***P<0.001, and ****P<0.0001 by one-way ANOVA with Sidak's correction for multiple comparisons, comparing genotypes at each time point. For graphing and statistical tests, values that exceeded the limit of detection were set to the limit for each analyte.

	WT-4 hpi			*F10*$^{F/F}$-4 hpi			WT-24 hpi			*F10*$^{F/F}$-24 hpi		
Analyte	Mean	St.Dev	n	Mean	St.Dev	n	Mean	St.Dev	n	Mean	St.Dev	n
CSF2 (GM-CSF)	**327.7025**	62.08024	8	**485.3343**	633.2576	7	**314.92**	14.65961	7	**139.8075**	7.470375	8
INFG	**131.3987**	49.28693	8	**270.0657***	387.877	7	**252.3229**	110.9572	7	**10.3025**	5.887055	8
IL1A	**1426.055**	269.1899	8	**1565.874**	1382.498	7	**1628.929**	248.8949	7	**610.66***	89.3456	8
IL1B	**300.79**	136.8141	8	**276.3**	372.6778	7	**195.4514**	43.40271	7	**44.5775**	3.660827	8
IL2	**50.95375**	9.210788	8	**42.53429**	16.88327	7	**53.88857**	11.92116	7	**21.9625***	7.378582	8
IL4	**5.64625**	1.103875	8	**7.72**	6.058107	7	**6.091429**	1.672239	7	**1.9625***	0.428744	8
IL5	**93.1325**	25.05097	8	**107.4171**	48.32001	7	**114.68**	23.35679	7	**61.0375***	9.267175	8
IL6	**83708.63**	20310.59	8	**54250.36***	33562.25	7	**83778**	0	7	**2071.1***	1560.823	8
IL7	**19.98**	5.374511	8	**36.98571***	16.89109	7	**18.8**	6.819306	7	**12.5275**	3.239082	8
IL10	**18073.26**	9993.004	8	**13851.27**	12037.68	7	**23510.57**	5547.001	7	**2258.51***	1594.731	8
IL-12B	**96.81875**	24.53519	8	**55.08***	33.3248	7	**103.8571**	25.24159	7	**19.6875***	6.630544	8
IL-12 (p70)	**186.0263**	35.90669	8	**135.1543***	48.97088	7	**161.2514**	23.4808	7	**38.3025***	6.535524	8
IL13	**594.8137**	142.1335	8	**310.7972***	143.792	7	**510.3714**	80.17876	7	**62.5125***	12.13332	8
IL15	**444.51**	100.3283	8	**343.9514**	163.53	7	**438.2543**	112.3424	7	**158.2125***	43.14843	8
IL17A	**54.225**	14.38015	8	**132.2057**	146.2406	7	**62.34**	21.28257	7	**9.995**	1.986778	8
CXCL10	**12543.88**	4920.522	8	**5403.249***	3631.554	7	**17238.57**	2396.865	7	**2024.805***	386.9841	8
CXCL1	**45385.88**	11141.4	8	**39404.29**	14597.6	7	**47253.72**	5201.075	7	**12543.75***	5948.964	8
CCL2	**27695**	7126.445	8	**17280.57**	10272.27	7	**30874**	0	7	**13482.5***	3444.329	8
CCL3	**21335.75**	10605.42	8	**5453.72***	9361.949	7	**15283.71**	5151.298	7	**537.4325***	105.578	8
CCL4	**29500.88**	7123.949	8	**10942.61***	11935.94	7	**27470.29**	4507.604	7	**1307.733***	475.3569	8
CXCL2	**19013.93**	7818.556	8	**12383.54***	7729.882	7	**12400.29**	6624.862	7	**1248.693***	981.7016	8
CCL5	**3741.504**	2101.41	8	**4356.406**	5266.379	7	**6365.106**	3163.374	7	**526.2425***	148.9296	8
TNF	**699.9313**	284.0037	8	**351.8914**	504.584	7	**421.2743**	109.8479	7	**42.8925***	6.345617	8

Red text indicates compiled data includes values from the upper or lower limit of detection
* indicates statistical significance comparing *F10*$^{F/F}$ to WT within each time point by one-way ANOVA with Sidak's correction for multiple comparisons

Table 4. Total Luminex analysis of 4 and 24 hpi cytokines

Factor X activity is required for induction of rapid immune response and subsequent mortality after injection of heat-killed *A. baumannii*

The reduction in cytokine and chemokine levels in *F10*$^{F/F}$ mice at 24 hpi could be the result of either 1) correlation with reduced abundance of bloodstream *A. baumannii* or 2) an intrinsically different immune response to *A. baumannii*. To test this hypothesis, cytokines and chemokines were quantified at 24 h following injection with PBS (mock) or heat-killed *A. baumannii*. For both mouse genotypes, the presence of heat-killed *A. baumannii* induced immune signaling (Figure 3A,B; Table 5). Chemokines and cytokines previously observed to be reduced in *F10*$^{F/F}$ mice following infection compared to C57BL/6J mice were also reduced following injection with heat killed bacteria. Together, these data suggest that during *A.*

baumannii infection, the innate immune response is triggered rapidly, and this response is reduced in *F10*$^{F/F}$ mice, regardless of the abundance of viable bacteria.

Thus far, it has been established that C57BL/6J mice demonstrate a strong induction of inflammatory signaling during infection of *A. baumannii*, and at 24 hpi, bacteria burdens are increased compared to *F10*$^{F/F}$ mice across organs. We hypothesized that the inflammatory response in C57BL/6J mice is pathological during *A. baumannii* infection regardless of the ability of *A. baumannii* to replicate in organs. Therefore, heat-killed *A. baumannii* was injected into mice and survival was monitored for 8 days. C57BL/6J mice succumbed to this treatment at a greater rate compared to *F10*$^{F/F}$ mice (Figure 3C), suggesting that the inflammatory response, which requires FX activity, is pathological during systemic *A. baumannii* infection.

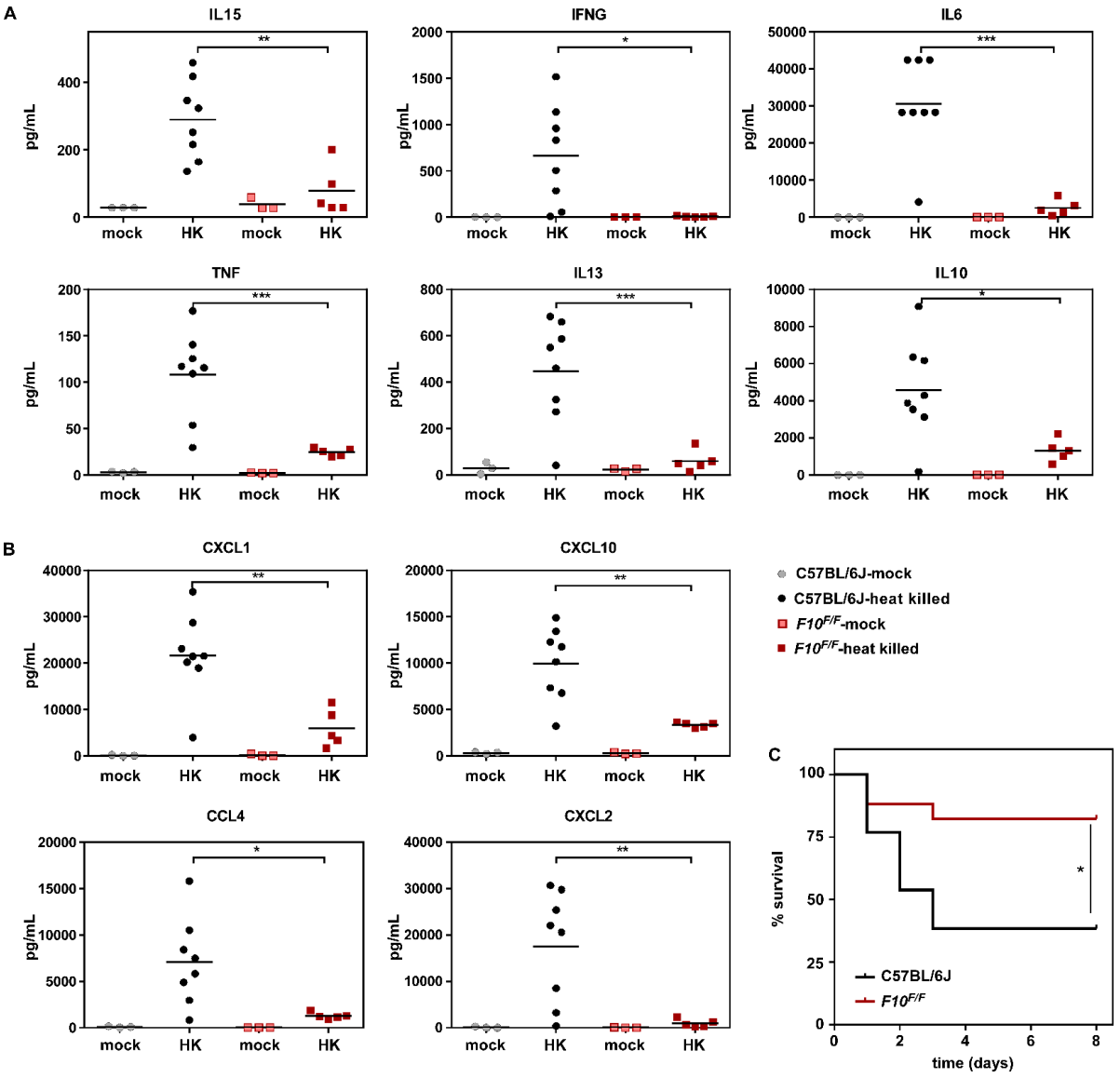

Figure 3. FX mice are protected from hyperactivated immune response and subsequent mortality after injection of heat-killed *A. baumannii.* Serum (A) cytokines and (B) chemoattractants following retro-orbital injection with PBS (mock) or approximately 1-2x10^9 CFU of heat-killed *A. baumannii* 17978 were quantified by Luminex analysis after mice were sacrificed at 24 hpi. (C) Survival of mice injected with approximately 1-2x10^9 CFU of heat-killed *A. baumannii* 17978. For A-B, each dot represents data from a single mouse, from two experiments. For A and B, * indicates P<0.05, **P<0.01, ***P<0.001, and ****P<0.0001 by one-way ANOVA with Sidak's correction for multiple comparisons, comparing genotypes within each treatment group. For graphing and statistical tests, values that exceeded the limit of detection were set to the limit for each analyte. For C data are combined from two independent experiments with n=13 for C57/BL6J and n=17 for *F10*$^{F/F}$, * indicates P<0.05 by Logrank (Mantel-Cox) Survival test.

	WT-heat-killed			*F10*$^{F/F}$-heat killed			WT-mock			*F10*$^{F/F}$-mock		
Analyte	Mean	St.Dev	n	Mean	St.Dev	n	Mean	St.Dev	n	Mean	St.Dev	n
CSF2 (GM-CSF)	**259.5875**	91.54469	8	**78.83***	53.53201	5	**8.793333**	1.060063	3	**7.74**	0	3
INFG	**662.3362**	538.0319	8	**8.668***	6.295278	5	**2.28**	1.247077	3	**1.56**	0	3
IL1A	**8036.625**	2800.238	8	**4771.8**	3182.584	5	**3106.16**	1626.119	2	**8946.667**	3128.198	3
IL1B	**131.4063**	68.8995	8	**21.81***	11.68858	5	**4.026667**	3.554678	3	**1.973333**	0.8386498	3
IL2	**127.8588**	35.05793	8	**24.23***	10.61529	5	**27.46667**	39.63065	3	**6.826667**	9.260698	3
IL4	**2.65875**	0.8803641	8	**2.596**	1.297027	5	**0.5266666**	0.1747379	3	**0.98**	1.039231	3
IL5	**72.6875**	22.64867	8	**26.592**	6.569727	5	**161.2667**	245.793	3	**20.18**	9.200586	3
IL6	**30542.38**	12765.34	8	**2535.328***	2098.501	5	**20.37333**	10.39703	3	**3.7**	2.298173	3
IL7	**12.9525**	4.833525	8	**2.964***	1.213623	5	**1.18**	0	3	**1.18**	0	3
IL10	**4574.797**	2649.544	8	**1308.91***	598.7396	5	**3.513333**	1.119345	3	**2.32**	0	3
IL-12B	**54.93625**	13.04581	8	**32.856**	39.19164	5	**14.57333**	6.223836	3	**19.21333**	7.366365	3
IL-12 (p70)	**225.0875**	89.26364	8	**33.522***	19.62103	5	**6.4**	0	3	**10.64**	4.442207	3
IL13	**447.645**	220.784	8	**59.378***	45.09955	5	**29.44**	25.70114	3	**23.39333**	6.572924	3
IL15	**289.3175**	116.5687	8	**79.41***	73.52285	5	**28.4**	0	3	**38.64**	17.7362	3
IL17A	**140.7275**	83.73083	8	**10.902***	6.713943	5	**1.08**	0	3	**1.08**	0	3
CXCL10	**9974.25**	3918.134	8	**3343.4***	258.0403	5	**316.5267**	78.18846	3	**286.5067**	92.51986	3
CXCL1	**21661.38**	8957.103	8	**5909.872***	4096.94	5	**98.44**	89.73907	3	**166.4133**	232.2218	3
CCL2	**20907.38**	10364.18	8	**6146***	2069.581	5	**59.33333**	31.76177	3	**14.91333**	4.206772	3
CCL3	**705.775**	258.1041	8	**197.22***	40.3411	4	**66.09**	57.74234	2	**36.80667**	22.34282	3
CCL4	**7088.273**	4665.535	8	**1278.752***	368.3191	5	**87.59333**	66.03769	3	**20.02**	0	3
CXCL2	**17586.15**	11917.55	8	**959.06***	854.0344	5	**117.3867**	157.9053	3	**46.86**	35.74953	3
CCL5	**1991.095**	654.0701	8	**652.026***	335.7575	5	**40.18**	32.66029	3	**50.72667**	20.53968	3
TNF	**108.4313**	46.77999	8	**24.696***	4.237556	5	**2.913333**	0.9047284	3	**2.113333**	0.3695042	3

Red text indicates compiled data includes values from the upper or lower limit of detection
* indicates statistical significance comparing ***F10***$^{F/F}$ to WT within either heat-killed or mock by one-way ANOVA with Sidak's correction for multiple comparisons

Table 5. Total Luminex analysis of mock and heat-killed cytokines at 24 hpi

F10$^{F/F}$ mice exhibit enhanced $T_{effector}$ response

To understand the cellular response to *A. baumannii* in C57BL/6J and *F10*$^{F/F}$ mice, we quantified populations of CD4+, CD8+, and CD11b+ cells in mock and infected spleen, kidney, and blood. A variety of changes were observed between infected C57BL/6J and *F10*$^{F/F}$ mice. Total blood CD11b+ cells are increased in *F10*$^{F/F}$ mice, driven by an increase in neutrophils and macrophages (Figure 4A, Figure 5A). C57BL/6J mice demonstrate a reduction in splenic neutrophils which results in neutropenia. The magnitude of this phenomenon is reduced in *F10*$^{F/F}$ mice, resulting in a greater percentage of splenic neutrophils (Figure 5A). Additionally, *F10*$^{F/F}$ mice have higher percent neutrophils in the blood during infection. On the other hand,

the percent of CD11b+ cells that stain as dendritic cells is reduced in infected *F10*$^{F/F}$ mice in the spleen and blood.

Consistent with the ability to restrict *A. baumannii* burdens during infection, *F10*$^{F/F}$ mice demonstrated a stronger induction total CD8+ cells in the spleen and increased CD8+ $T_{effector}$ cells in the spleen and kidney. concomitant with this increase in T_{eff} cells, CD8+ naive and CD4+ regulatory T cells populations were decreased (Figure 4B, Figure 5B). A similar trend was observed in CD4+ cells; spleen and kidney CD4+ T_{eff} cell populations were increases and reduced percentat goe of CD4+ T_{naive} were observed in the spleen and blood, and reduced T_{reg} cell population was incuded in the kidney (Figure 4C). Together, these differential cell populations suggest *F10*$^{F/F}$ mice are better prepared to kill *A. baumannii* and restrict bacterial replication during systemic infection.

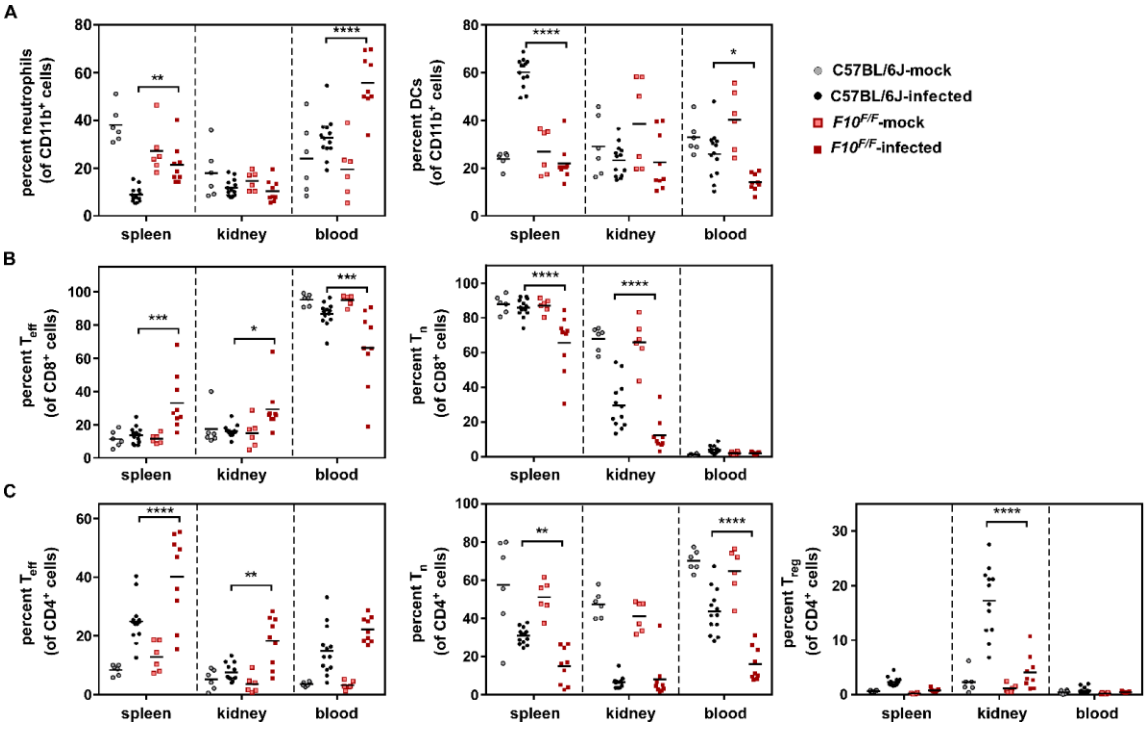

Figure 4. *F10*$^{F/F}$ mice exhibit enhanced $T_{effector}$ response. (A) CD11b+ populations, (B) CD8+ populations, and (C) CD4+ populations were quantified from spleen, kidney, and blood of mice injected with either PBS (mock) or approximately 2-3x10^8 CFU *A. baumannii* 17978 at 24 hpi using flow cytometry. For A-C, each dot represents data from a single mouse, from two experiments. * indicates P<0.05, **P<0.01, ***P<0.001, and ****P<0.0001 by two-way ANOVA with Tukey's correction for multiple comparisons.

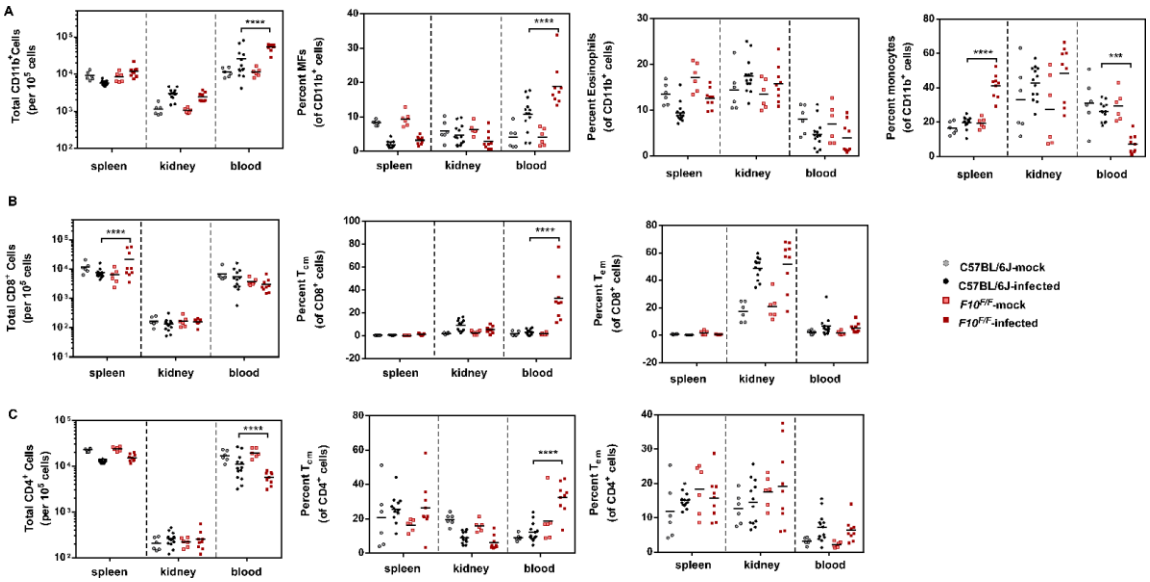

Figure 5. Additional cell population changes at 24 hpi. (A) CD11b+ populations, (B) CD8+ populations, and (C) CD4+ populations were quantified from spleen, kidney, and blood of mice injected with either PBS (mock) or approximately 2-3x10^8 CFU *A. baumannii* 17978 at 24 hpi using flow cytometry. For A-C, each dot represents data from a single mouse, from two experiments. * indicates P<0.05, **P<0.01, ***P<0.001, and ****P<0.0001 by two-way ANOVA with Tukey's correction for multiple comparisons.

Cytokines and chemokine levels are reduced in infected tissues of *F10$^{F/F}$* mice

From the serum cytokines measured in Figure 3, it was unclear whether the reduced induction of cytokines and chemokines at 24 hpi was a global change in *F10$^{F/F}$* mice, or whether tissue levels of pro-inflammatory cytokines and chemokines would be elevated in *F10$^{F/F}$* mice at 24 hpi, resulting in increased neutrophils and T_{eff} cells found in infected tissue (Figure 4). Therefore, we measured cytokines and chemokines at 24 hpi and compared levels of immune signaling molecules between PBS treated (mock) and infected C57BL/6J and *F10$^{F/F}$* mice. In general, as observed in the serum, the cytokines (Figure 6A; Table 6) and chemokines (Figure 6B) measured were reduced in tissue of infected *F10$^{F/F}$* mice. However, IL-15 levels were increased in the infected spleens of *F10$^{F/F}$* mice. In general, these data suggest that in the absence of FX activity, global innate immune is blunted during systemic *A. baumannii* infection.

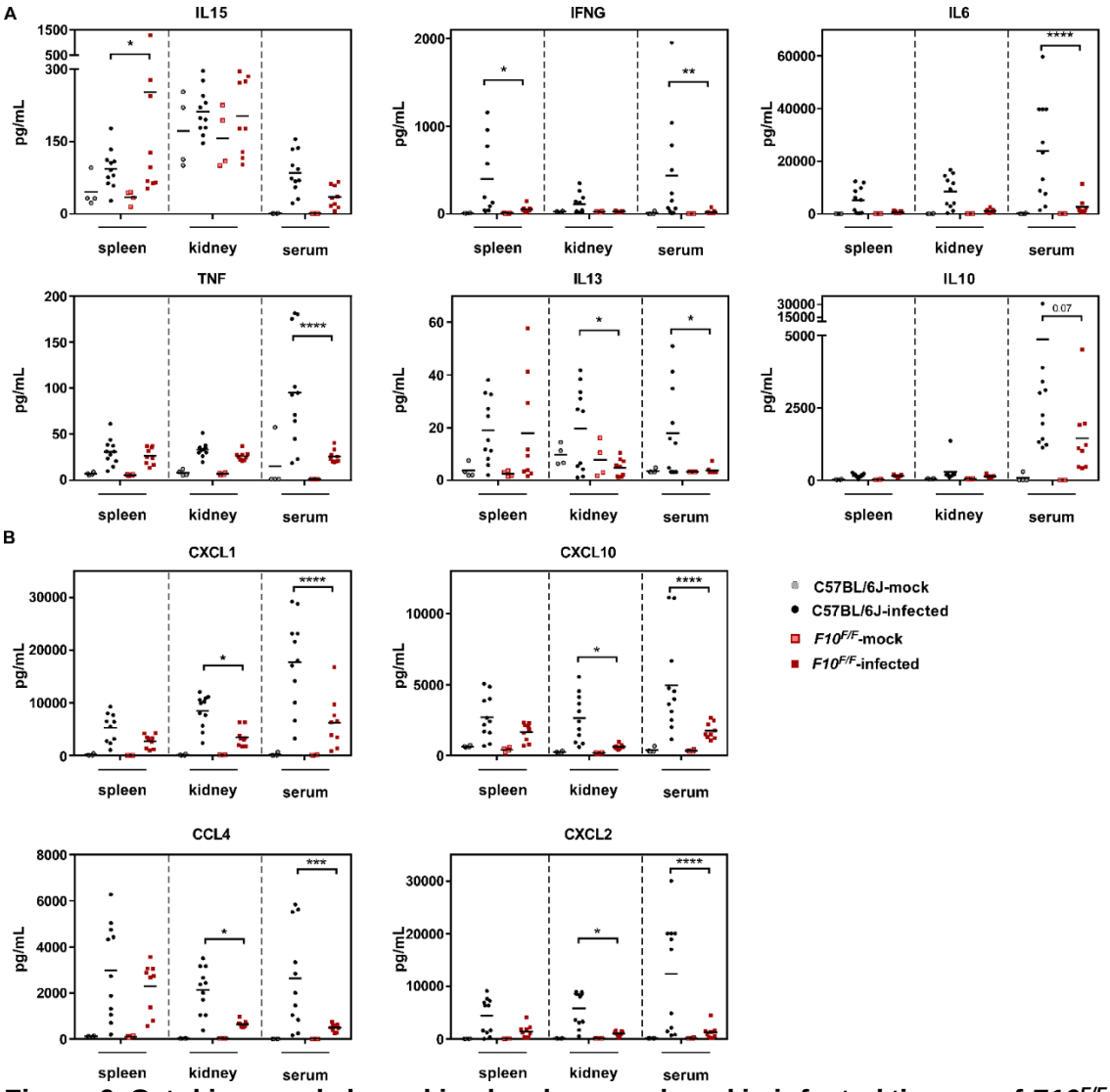

Figure 6. Cytokines and chemokine levels are reduced in infected tissues of *F10$^{F/F}$* mice
(A) cytokines and (B) chemoattractants following retro-orbital injection of PBS (mock) or approximately 2-3x10^{8} CFU of *A. baumannii* 17978 were quantified by Luminex analysis at 24 hpi from spleen, kidney, and serum. Each dot represents data from a single mouse, from two experiments. * indicates P<0.05, **P<0.01, ***P<0.001, and ****P<0.0001 by one-way ANOVA with Sidak's correction for multiple comparisons, comparing the infected group of each genotypes and tissue. For graphing and statistical tests, values that exceeded the limit of detection were set to the limit for each analyte.

	SPLEEN							
	C57BL/6J-mock		**C57BL/6J-infected**		***F10*$^{F/F}$-mock**		***F10*$^{F/F}$-infected**	
Analyte	Mean	St.Dev	Mean	St.Dev	Mean	St.Dev	Mean	St.Dev
CSF2 (GM-CSF)	**37.4**	15.8	**153.6**	118.5	**32.5**	8.9	**113.1**	42.5
INFG	**7.9**	1.5	**397.1**	429.2	**9.7**	4.7	**53.8***	37.7
IL1A	**153.5**	15.7	**3442.4**	1247.0	**122.9**	23.8	**2853.0**	1638.5
IL1B	**30.3**	6.9	**229.3**	118.9	**32.2**	9.4	**159.9**	51.2
IL2	**8.5**	3.4	**25.9**	30.4	**14.0**	11.4	**21.9**	18.3
IL4	**7.4**	3.6	**6.8**	2.0	**4.7**	1.3	**10.2**	5.7
IL5	**29.2**	38.9	**36.2**	9.8	**10.7**	5.4	**27.1**	6.5
IL6	**16.1**	9.5	**5184.6**	4907.4	**9.7**	1.6	**609.3**	477.7
IL7	**10.5**	2.4	**16.2**	5.6	**7.8**	1.9	**39.1**	58.3
IL10	**22.7**	9.7	**151.3**	69.7	**23.4**	2.5	**143.7**	35.8
IL-12B	**0.7**	0.1	**17.6**	11.8	**5.5**	7.7	**10.4**	8.7
IL-12 (p70)	**14.8**	14.1	**36.2**	14.7	**8.6**	1.7	**41.8**	19.3
IL13	**3.6**	2.6	**19.0**	12.5	**2.4**	1.0	**17.8**	20.2
IL15	**45.7**	33.7	**93.8**	40.5	**34.4**	14.2	**252.5***	393.5
IL17A	**2.9**	1.4	**128.0**	130.5	**2.4**	0.8	**46.4***	26.7
CXCL10	**638.5**	66.0	**2705.2**	1532.2	**403.4**	156.5	**1643.1**	633.2
CXCL1	**137.9**	163.2	**5253.1**	2776.6	**49.2**	7.7	**2726.3**	1282.8
CCL2	**83.9**	44.9	**3061.3**	1643.1	**49.0**	4.2	**2184.2**	721.7
CCL3	**56.9**	7.5	**2845.5**	1802.7	**44.4**	11.6	**1460.5***	688.6
CCL4	**110.6**	26.6	**2968.3**	2068.9	**106.5**	42.8	**2296.5**	1090.3
CXCL2	**59.1**	13.1	**4411.6**	3407.0	**57.6**	13.2	**1448.2**	1238.2
CCL5	**151.8**	22.7	**698.1**	466.8	**106.6**	50.7	**451.3***	233.2
TNF	**7.0**	1.6	**30.8**	14.3	**5.6**	0.7	**26.5**	9.2
	KIDNEY							
	C57BL/6J-mock		**C57BL/6J-infected**		***F10*$^{F/F}$-mock**		***F10*$^{F/F}$-infected**	
Analyte	Mean	St.Dev	Mean	St.Dev	Mean	St.Dev	Mean	St.Dev
CSF2 (GM-CSF)	**52.9**	11.9	**144.2**	119.5	**57.2**	17.4	**83.8**	24.1
INFG	**25.2**	6.1	**110.8**	114.2	**22.9**	7.0	**25.4**	9.8
IL1A	**200.7**	82.0	**343.8**	66.0	**146.4**	30.1	**268.1**	46.3
IL1B	**57.1**	26.0	**95.1**	22.1	**57.9**	29.8	**89.2**	34.4
IL2	**64.7**	13.7	**42.9**	16.1	**50.6**	10.9	**39.7**	17.7
IL4	**6.6**	4.3	**5.3**	3.0	**5.0**	2.2	**4.7**	2.7
IL5	**53.7**	39.8	**58.0**	30.9	**36.8**	9.7	**41.2**	18.0
IL6	**53.4**	54.9	**8451.0**	6128.1	**26.0**	4.7	**1078.0**	668.8
IL7	**40.2**	12.0	**38.3**	9.7	**33.4**	9.3	**35.8**	12.1
IL10	**49.2**	16.0	**289.6**	357.8	**47.8**	16.8	**125.8**	49.0

IL-12B	**72.8**	21.7	**70.8**	8.6	**45.4**	12.3	**63.6**	21.4
IL-12 (p70)	**57.0**	13.6	**54.2**	17.5	**51.2**	17.9	**47.3**	18.9
IL13	**9.7**	3.9	**19.6**	16.0	**7.8**	6.7	**4.7***	3.4
IL15	**171.5**	76.3	**211.6**	47.0	**157.1**	61.8	**202.7**	79.1
IL17A	**12.8**	3.7	**26.3**	13.1	**10.6**	3.3	**14.5**	5.2
CXCL10	**226.7**	72.6	**2641.2**	1674.5	**174.2**	45.5	**607.6***	165.6
CXCL1	**115.0**	111.9	**8437.6**	3149.4	**80.9**	15.8	**3480.7***	1760.0
CCL2	**115.1**	72.7	**6108.3**	3194.0	**73.9**	18.7	**2890.1**	778.3
CCL3	**48.6**	15.3	**630.5**	303.7	**38.6**	9.6	**261.6**	52.9
CCL4	**22.8**	2.7	**2132.4**	1007.7	**23.5**	9.1	**645.0***	148.7
CXCL2	**104.0**	32.1	**5815.6**	3303.5	**98.4**	29.5	**1025.7***	438.6
CCL5	**11.3**	1.8	**284.4**	86.4	**10.0**	2.8	**181.0**	46.2
TNF	**8.1**	3.1	**33.3**	7.8	**6.9**	1.2	**26.1**	4.9
	SERUM							
	C57BL/6J-mock		**C57BL/6J-infected**		***F10*$^{F/F}$-mock**		***F10*$^{F/F}$-infected**	
Analyte	Mean	St.Dev	Mean	St.Dev	Mean	St.Dev	Mean	St.Dev
CSF2 (GM-CSF)	**15.8**	27.3	**148.9**	150.7	**2.2**	0.0	**70.0**	40.6
INFG	**9.2**	16.4	**438.9**	609.1	**1.1**	0.3	**20.3***	21.8
IL1A	**951.4**	459.4	**482.2**	173.8	**779.6**	267.7	**347.9**	104.7
IL1B	**120.7**	238.5	**126.6**	71.7	**2.3**	0.5	**44.3**	17.8
IL2	**4.7**	8.8	**9.6**	5.7	**0.3**	0.0	**6.4**	4.9
IL4	**31.6**	61.6	**3.1**	1.2	**0.8**	0.0	**2.5**	1.5
IL5	**236.7**	435.9	**76.3**	31.1	**8.6**	2.9	**60.4**	37.9
IL6	**89.9**	172.0	**23948.1**	19002.0	**2.3**	1.7	**2720.9***	3475.7
IL7	**0.7**	0.2	**20.3**	11.2	**0.6**	0.0	**12.7**	10.3
IL10	**74.2**	146.7	**4870.8**	8673.8	**1.2**	0.3	**1450.9**	1286.1
IL-12B	**2.7**	0.6	**4.3**	3.9	**2.4**	0.0	**2.4**	0.3
IL-12 (p70)	**136.3**	269.6	**39.4**	21.9	**1.5**	0.0	**27.6**	35.5
IL13	**3.5**	0.8	**17.8**	17.3	**3.1**	0.0	**3.8***	1.5
IL15	**1.1**	0.2	**85.2**	43.2	**0.9**	0.0	**34.7**	23.0
IL17A	**11.5**	21.4	**39.6**	34.9	**1.7**	0.6	**10.8**	9.3
CXCL10	**381.0**	188.1	**4958.1**	3386.0	**324.0**	69.7	**1737.6***	566.6
CXCL1	**189.3**	316.4	**17725.4**	8573.9	**73.2**	15.6	**6255.4***	4889.8
CCL2	**97.9**	163.8	**14872.8**	7406.3	**24.9**	6.4	**5755.8***	2309.3
CCL3	**64.2**	116.5	**1023.7**	1081.3	**5.9**	0.0	**281.6**	70.9
CCL4	**7.2**	1.6	**2627.4**	2175.6	**6.4**	0.0	**494.6***	163.8
CXCL2	**145.1**	10.2	**12365.4**	10491.3	**142.2**	67.0	**1231.7***	1327.7
CCL5	**6.5**	10.7	**335.7**	186.8	**3.2**	1.6	**103.3***	44.9
TNF	**15.2**	28.1	**95.2**	60.2	**1.2**	0.0	**25.7***	7.1

Red text indicates compiled data includes values from the upper or lower limit of detection
* indicates statistical significance comparing ***F10***$^{F/F}$ to WT within either heat-killed or mock by one-way ANOVA with Sidak's correction for multiple comparisons
n=4 mock infected per genotype, 11 C57BL/6J infected and 9 *F10*$^{F/F}$ infected

Table 6. Total Luminex analysis of serum, kidney, and spleen cytokines at 24 hpi

An FDA-approved Factor Xa inhibitor reduces bacterial burdens in C57BL/6J mice

To test whether pharmacological inhibition of FXa could reduce the bacterial burdens observed in WT mice infected with *A. baumannii*, enoxaparin was administered at the time of infection and bacteria was enumerated across organs at 24 hpi. Consistent with a pathological role of FX during systemic *A. baumannii* infection, bacterial burdens were reduced in the heart, liver, and spleen of wildtype mice after a single treatment with enoxaparin (Figure 7).

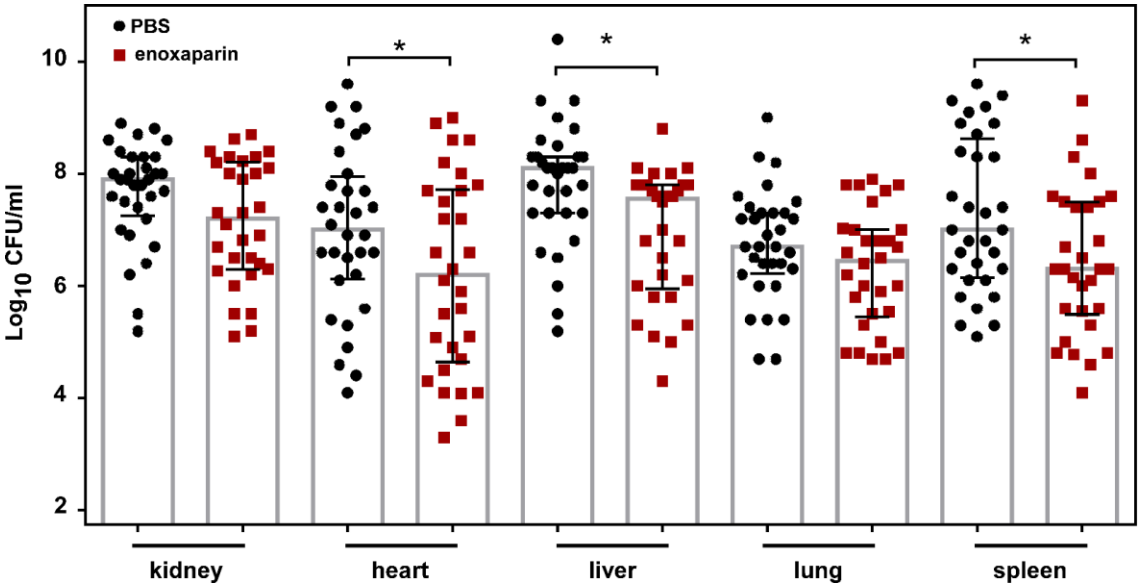

Figure 7. An FDA-approved Factor Xa inhibitor reduces bacterial burdens in WT mice. Bacterial burdens 24 hpi following infection with 2x10^8 CFU A. baumannii 17978 after treatment with PBS (vehicle) or 10 mg/kg enoxaparin, intraperitoneal, at the time of infection. Each dot represents data from a single mouse, from three experiments. * indicates P<0.05 by one-way ANOVA with Sidak's correction for multiple comparisons, comparing the infected group of each genotypes and tissue.

Discussion

In this study, we discovered associations between a polymorphism in a known drug target and novel disease phenotypes using PheWAS. Individuals with a SNP in coagulation FX demonstrated validating phenotypes of hemostatic disorders but also increases odds ratio of being hospitalized for a variety of infection-related disorders (Table 2). Consistent with a critical role of FX in innate immunity to bacterial infection, FX-deficient mice display enhanced

clearance of *A. baumannii* (Figure 1) associated with reduced induction of cytokine and chemokine production in the serum and infected organs. Heat-killed *A. baumannii* induces a strong innate response which is blunted in FX deficient mice, resulting in increased survival relative to C57BL/6J mice. Together, these data suggest FX activity is pathological during systemic *A. baumannii* infection. While the mechanism is not clear, our work suggests the interplay between FX and immune signaling is responsible, as no changes were detected between mouse genotypes when assessing pathogen-induced hypercoagulation (Figure 1). Instead, we detected widespread changes to the immune cell populations (Figures 4,5) and signaling molecules (Figure 6) that suggest *A. baumannii* induces FX-dependent widespread activation of the immune system that results in poor ability to limit replication and increased mortality as the result of immune activation (Figure 3). As a proof of principle for the use of PheWAS to drive novel therapeutic development, we found that the FDA approved FXa inhibitor enoxaparin was able to reduce bacterial burdens in C57BL/6J mice, suggesting anticoagulants might offer new treatment for Gram-negative sepsis (Figure 7).

The interplay between FX and antibacterial immunity adds to a growing body of literature suggesting FX, and coagulation more broadly, is a critical determinant of the immune response to bacterial or viral infection. For instance, Factor XII deficient mice are protected in *Klebsiella* pneumonia, but Factor XI deficient mice are more susceptible to *Klebsiella* pneumonia. Additionally, Factor XI deficient mice have increased survival in models of cecal ligation and puncture sepsis (34, 35). Interestingly, the survival advantage was partially attributed to changes in the cytokine response, where $FXI^{-/-}$ mice demonstrated reduced TNF and IL10 induction compared WT mice, as observed in this study, but increased IL6 induction, which was the opposite in our study (34). Consistent with our study, inhibition of FXa and thrombin was recently shown to improve outcomes of Gram-negative sepsis in baboons by attenuating DIC and inhibiting IL6 induction (36). Taken together, coagulation appears to be a previously overlooked contributor of the innate immune response to bacterial infection. Additionally, this work highlights the potential use of human clinical PheWAS to drive basic discovery using laboratory models and validate potential treatments.

References

1. Denny JC, Ritchie MD, Basford MA, Pulley JM, Bastarache L, Brown-Gentry K, et al. PheWAS: demonstrating the feasibility of a phenome-wide scan to discover gene-disease associations. Bioinformatics. 2010;26(9):1205-10.
2. Cronin RM, Field JR, Bradford Y, Shaffer CM, Carroll RJ, Mosley JD, et al. Phenome-wide association studies demonstrating pleiotropy of genetic variants within FTO with and without adjustment for body mass index. Frontiers in genetics. 2014;5:250.
3. Solovieff N, Cotsapas C, Lee PH, Purcell SM, Smoller JW. Pleiotropy in complex traits: challenges and strategies. Nature reviews Genetics. 2013;14(7):483-95.
4. Denny JC, Mosley JD. Disease Heritability Studies Harness the Healthcare System to Achieve Massive Scale. Cell. 2018;173(7):1568-70.
5. Choi L, Carroll RJ, Beck C, Mosley JD, Roden DM, Denny JC, et al. Evaluating statistical approaches to leverage large clinical datasets for uncovering therapeutic and adverse medication effects. Bioinformatics. 2018.
6. Jerome RN, Pulley JM, Roden DM, Shirey-Rice JK, Bastarache LA, G RB, et al. Using Human 'Experiments of Nature' to Predict Drug Safety Issues: An Example with PCSK9 Inhibitors. Drug safety. 2018;41(3):303-11.
7. Pulley JM, Shirey-Rice JK, Lavieri RR, Jerome RN, Zaleski NM, Aronoff DM, et al. Accelerating Precision Drug Development and Drug Repurposing by Leveraging Human Genetics. Assay and drug development technologies. 2017;15(3):113-9.
8. Rastegar-Mojarad M, Ye Z, Kolesar JM, Hebbring SJ, Lin SM. Opportunities for drug repositioning from phenome-wide association studies. Nature biotechnology. 2015;33(4):342-5.
9. Loof TG, Morgelin M, Johansson L, Oehmcke S, Olin AI, Dickneite G, et al. Coagulation, an ancestral serine protease cascade, exerts a novel function in early immune defense. Blood. 2011;118(9):2589-98.
10. Nickel KF, Renne T. Crosstalk of the plasma contact system with bacteria. Thromb Res. 2012;130 Suppl 1:S78-83.
11. Antoniak S. The coagulation system in host defense. Research and practice in thrombosis and haemostasis. 2018;2(3):549-57.
12. Uprichard J, Perry DJ. Factor X deficiency. Blood reviews. 2002;16(2):97-110.
13. Shapiro A. Plasma-derived human factor X concentrate for on-demand and perioperative treatment in factor X-deficient patients: pharmacology, pharmacokinetics, efficacy, and safety. Expert opinion on drug metabolism & toxicology. 2017;13(1):97-104.
14. Koda-Kimble MA, Alldredge BK. Applied therapeutics : the clinical use of drugs. 10th ed. Philadelphia: Wolters Kluwer/Lippincott Williams & Wilkins; 2013. xxxix, 2519 p. p.
15. Iqbal Z, Cohen M. Enoxaparin: a pharmacologic and clinical review. Expert opinion on pharmacotherapy. 2011;12(7):1157-70.
16. American Society of Health-System Pharmacists I. Enoxaparin Sodium 2018 [10/17/2018]. Available from: https://www.drugs.com/monograph/enoxaparin-sodium.html.
17. Venkateswarlu D, Perera L, Darden T, Pedersen LG. Structure and dynamics of zymogen human blood coagulation factor X. Biophys J. 2002;82(3):1190-206.
18. Noguchi K, Morishima Y, Takahashi S, Ishihara H, Shibano T, Murata M. Impact of nonsynonymous mutations of factor X on the functions of factor X and anticoagulant activity of edoxaban. Blood Coagul Fibrinolysis. 2015;26(2):117-22.
19. Bolton-Maggs PH, Perry DJ, Chalmers EA, Parapia LA, Wilde JT, Williams MD, et al. The rare coagulation disorders--review with guidelines for management from the United Kingdom Haemophilia Centre Doctors' Organisation. Haemophilia. 2004;10(5):593-628.
20. James HL, Girolami A, Fair DS. Molecular defect in coagulation factor XFriuli results from a substitution of serine for proline at position 343. Blood. 1991;77(2):317-23.

21. Vincent JL, Rello J, Marshall J, Silva E, Anzueto A, Martin CD, et al. International study of the prevalence and outcomes of infection in intensive care units. JAMA. 2009;302(21):2323-9.
22. Kaye KS, Pogue JM. Infections Caused by Resistant Gram-Negative Bacteria: Epidemiology and Management. Pharmacotherapy. 2015;35(10):949-62.
23. Global Priority List of Antibiotic-resistant Bacteria to Guide Research, Discovery, and Development of New Antibiotics. World Health Organization: 2017.
24. Roden DM, Pulley JM, Basford MA, Bernard GR, Clayton EW, Balser JR, et al. Development of a large-scale de-identified DNA biobank to enable personalized medicine. Clinical pharmacology and therapeutics. 2008;84(3):362-9.
25. Bowton E, Field JR, Wang S, Schildcrout JS, Van Driest SL, Delaney JT, et al. Biobanks and electronic medical records: enabling cost-effective research. Science translational medicine. 2014;6(234):234cm3.
26. Pulley J, Clayton E, Bernard GR, Roden DM, Masys DR. Principles of human subjects protections applied in an opt-out, de-identified biobank. Clinical and translational science. 2010;3(1):42-8.
27. Denny JC, Bastarache L, Ritchie MD, Carroll RJ, Zink R, Mosley JD, et al. Systematic comparison of phenome-wide association study of electronic medical record data and genome-wide association study data. Nature biotechnology. 2013;31(12):1102-10.
28. Wei WQ, Bastarache LA, Carroll RJ, Marlo JE, Osterman TJ, Gamazon ER, et al. Evaluating phecodes, clinical classification software, and ICD-9-CM codes for phenome-wide association studies in the electronic health record. PLoS One. 2017;12(7):e0175508.
29. Tai SJ, Herzog RW, Margaritis P, Arruda VR, Chu K, Golden JA, et al. A viable mouse model of factor X deficiency provides evidence for maternal transfer of factor X. J Thromb Haemost. 2008;6(2):339-45.
30. Fiebig T, Boll H, Figueiredo G, Kerl HU, Nittka S, Groden C, et al. Three-dimensional in vivo imaging of the murine liver: a micro-computed tomography-based anatomical study. PLoS One. 2012;7(2):e31179.
31. Thoolen B, Maronpot RR, Harada T, Nyska A, Rousseaux C, Nolte T, et al. Proliferative and nonproliferative lesions of the rat and mouse hepatobiliary system. Toxicologic pathology. 2010;38(7 Suppl):5S-81S.
32. ClinVar: NM_000504.3(F10):c.574G>A (p.Gly192Arg) [Internet]. National Center for Biotechnology Information. 2018 [cited 10/17/2018]. Available from: https://www.ncbi.nlm.nih.gov/clinvar/variation/311275/.
33. Flicek P, Amode MR, Barrell D, Beal K, Brent S, Chen Y, et al. Ensembl 2011. Nucleic Acids Res. 2011;39(Database issue):D800-6.
34. Bane CE, Jr., Ivanov I, Matafonov A, Boyd KL, Cheng Q, Sherwood ER, et al. Factor XI Deficiency Alters the Cytokine Response and Activation of Contact Proteases during Polymicrobial Sepsis in Mice. PLoS One. 2016;11(4):e0152968.
35. Tucker EI, Gailani D, Hurst S, Cheng Q, Hanson SR, Gruber A. Survival advantage of coagulation factor XI-deficient mice during peritoneal sepsis. J Infect Dis. 2008;198(2):271-4.
36. Schochl H, van Griensven M, Heitmeier S, Laux V, Kipman U, Roodt J, et al. Dual inhibition of thrombin and activated factor X attenuates disseminated intravascular coagulation and protects organ function in a baboon model of severe Gram-negative sepsis. Critical care. 2017;21(1):51.